

The Solar Neighborhood LV: Spectral Characterization of an Equatorial Sample of 580 K Dwarfs

HODARI-SADIKI HUBBARD-JAMES ^{1,2,*} SEBASTIAN CARRAZCO-GAXIOLA ^{2,3,*} TODD J. HENRY ^{2,*}
LEONARDO A. PAREDES ^{1,2,4,*} AZMAIN H. NIZAK ^{5,*} XAVIER LESLEY-SALDAÑA ⁶ WEI-CHUN JAO ^{2,3,*} AND
ABIGAIL ARBOGAST ¹

¹*Department of Physics and Astronomy, Agnes Scott College, Decatur, GA 30030, USA*

²*RECONS Institute, Chambersburg, PA 17201, USA*

³*Department of Physics and Astronomy, Georgia State University, Atlanta, GA 30302, USA*

⁴*Steward Observatory and Department of Astronomy, The University of Arizona, Tucson, AZ 85721, USA*

⁵*Department of Astronomy and Van Vleck Observatory, Wesleyan University, Middletown, CT 06459, USA*

⁶*Department of Astronomy, The Ohio State University, 140 West 18th Avenue, Columbus, OH 43210 USA*

(Received October 16th, 2025; Revised December 20th, 2025)

Submitted to AJ

ABSTRACT

We present a spectroscopic characterization of 580 K dwarfs within 33 pc, observed with the CHIRON echelle spectrograph (R=80,000) on the SMARTS 1.5m telescope. This volume-limited sample is part of the RKSTAR survey of ~ 4400 K dwarf primaries within 50 pc. Using Empirical SpecMatch and the diagnostic lines H α (6562.8 Å) and Li I (6707.8 Å), we derive stellar properties, activity status, and age indicators calibrated against 35 benchmark K dwarfs with ages from 20 Myr to 5 Gyr. We find that 7.4% (43 stars) exhibit signatures of youth and/or chromospheric activity: 19 stars show lithium absorption indicating ages < 1 Gyr, and 36 display H α emission. Kinematic analysis using BANYAN Σ identifies 8 additional young stars through membership in the AB Doradus moving group and the Hyades cluster, bringing the total young/active population to 8.8% (51 stars). Stellar parameters span 3600–5500 K in T_{eff} , -0.60 to $+0.55$ dex in [Fe/H], and < 10 to > 25 km s⁻¹ in $v \sin i$. A metal-poor population ([Fe/H] ≤ -0.50 dex) comprises 4% of the sample. Galactic kinematics place 80% in the thin disk and 18.4% in the thick disk, with one halo member (HD 134439). Young and active stars are predominantly thin disk members, with two thick disk exceptions. Cross-matching with NASA’s Exoplanet Archive reveals only 7.5% (44 stars) host confirmed planets as of July 2025. Our results identify 529 mature, inactive K dwarfs as prime targets for terrestrial planet searches, providing a crucial resource for exoplanet habitability studies in the solar neighborhood.

Keywords: Late-type stars (909) — Solar neighborhood (1509) — Spectroscopy (1558) — Stellar activity (1580) — Stellar ages (1581)

1. INTRODUCTION

K dwarfs, with surface temperatures between 3930–5270 K (our volume-limited sample extends this range to 3600–5500 K to ensure completeness near the K/M boundary) and masses of 0.59–0.88 M_⊙ (Henry & McCarthy 1993; Gray & Corbally 2009; Pecaute & Mamajek 2013), represent promising targets for exoplanet detection and characterization efforts. These stars constitute 11% of the solar neighborhood population (Henry & Jao 2024) and offer several

Corresponding author: Hodari-Sadiki Hubbard-James
hjames@agnesscott.edu

* Visiting Astronomer, Cerro Tololo Inter-American Observatory. CTIO is operated by AURA, Inc., under contract to the National Science Foundation.

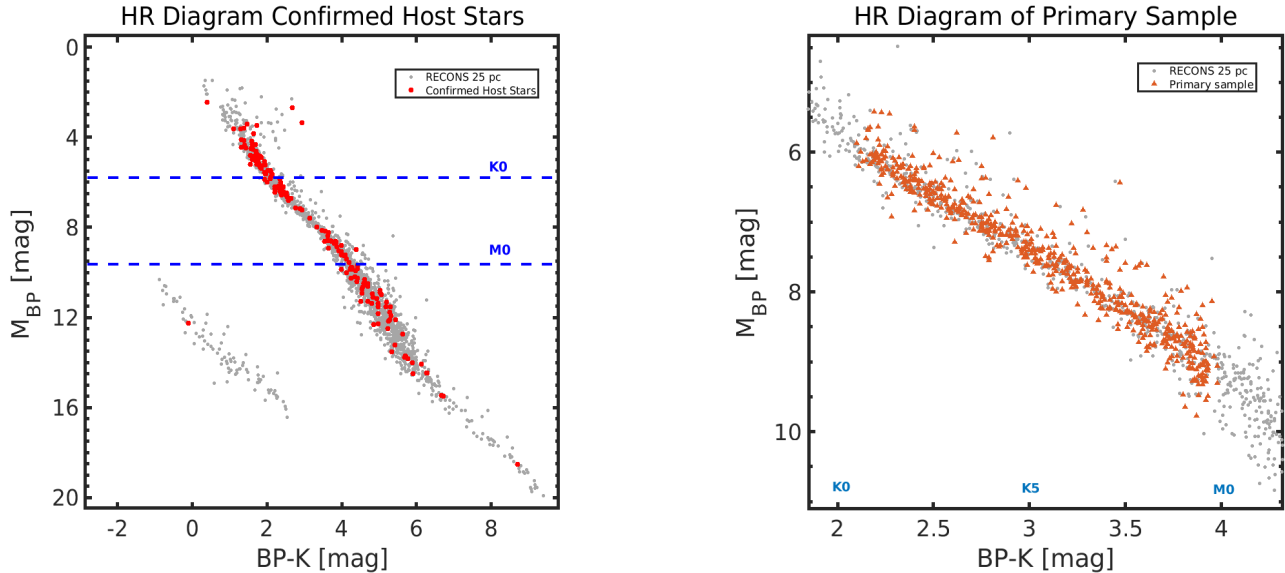


Figure 1. Left: HR diagram displaying the RECONS sample of stars within 25 pc (grey dots), with confirmed exoplanet hosts as of June 2025 from the NASA Exoplanet Archive (NASA Exoplanet Science Institute 2020) highlighted in red. Dashed blue lines indicate the K0 and M0 dwarf boundaries used to select K dwarfs for this work. Right: HR diagram showing the same 25 pc sample in grey with our 580 K dwarfs (orange triangles) from the equatorial 33.3 pc survey. The sequence of objects above the main sequence indicates young and/or unresolved multiple stars, while subdwarfs appear along the lower envelope. Magnitude data are from *Gaia* DR3 (BP) and 2MASS ($K = K_s$) with absolute magnitudes derived using *Gaia* DR3 parallaxes.

advantages over their more commonly studied counterparts. K dwarfs have longer main-sequence lifetimes than more massive F and G dwarfs, providing extended periods for planetary formation and biological evolution. Compared to M dwarfs, K dwarfs produce less extreme ultraviolet radiation and exhibit reduced flare activity, potentially offering more stable environments for atmospheric retention on orbiting planets (Cuntz & Guinan 2016; Arney 2019).

Despite these favorable characteristics, K dwarfs have been systematically underexplored in exoplanet surveys. Figure 1 illustrates this observational bias, showing that within 25 pc, mid-type K dwarfs (spectral types $\sim K3V$ – $K6V$) host significantly fewer confirmed exoplanets than comparable samples of G and M dwarfs and K dwarfs similar to those more and less massive stars. This disparity reflects survey selection effects rather than an intrinsic lack of planetary systems — relatively bright G dwarfs and early K dwarfs have been preferentially targeted due to their higher photon rates, enabling higher signal-to-noise observations, whereas late K dwarfs and M dwarfs offer larger planet-to-star size and mass ratios, facilitating transit detection for planets of a given size and resulting in larger radial velocity amplitudes for planets of a given mass (Arney 2019; Richey-Yowell et al. 2019).

Recent theoretical and observational studies have highlighted K dwarfs as potentially optimal hosts for habitable planets. Cuntz & Guinan (2016) determined that early-type K dwarfs provide the most favorable conditions for detecting biosignatures, while Arney (2019) identified a potential “K dwarf advantage” for characterizing exoplanet atmospheres. Dedicated surveys targeting nearby K dwarfs, including the RECONS K Star (RKSTAR) survey (Paredes et al. 2021; Hubbard-James et al. 2022) outlined below and the K Dwarfs Orbiting By Habitable Exoplanets (KOBEx) experiment (Lillo-Box et al. 2022), have yielded promising initial results. These efforts suggest that approximately 50% of nearby K dwarfs host stellar or substellar companions, while approximately half may contain habitable zone planets (Kunimoto & Matthews 2020; Paredes et al. 2021; Lillo-Box et al. 2022).

Central to evaluating exoplanet habitability is understanding the evolutionary state and activity level of the host star. Young and magnetically active stars produce enhanced ultraviolet emission, flares, and coronal mass ejections that can significantly impact planetary atmospheres through photoevaporation and atmospheric chemistry alteration (Segura et al. 2010; Luger & Barnes 2015). These high-energy processes are particularly problematic for terrestrial planets in habitable zones, where atmospheric stability over geologic timescales is crucial for maintaining liquid water (Ribas et al. 2005; Airapetian et al. 2020). Conversely, mature, quiescent stars provide stable radiation environments conducive to atmospheric retention and the development of detectable biosignatures (Meadows et al. 2018).

Stellar activity diagnostics, particularly the H α absorption line (6562.8 Å) and the Li I resonance line (6707.8 Å), have proven effective for identifying active and young stars across spectral types (Soderblom et al. 1993). H α emission serves as a tracer of chromospheric activity and magnetic heating, while lithium abundance provides a robust age indicator for stars younger than ~ 1 Gyr through well-understood depletion mechanisms (Soderblom 2010). These diagnostics are essential for constructing samples of optimal exoplanet host stars and understanding the relationship between stellar evolution and planetary system architecture.

In this paper, we present spectroscopic characterization of 580 K dwarfs within 33 pc, representing the largest uniform survey of high-resolution spectroscopy of nearby K dwarfs to date. Using CHIRON spectra from the SMARTS 1.5m and established spectroscopic diagnostics, we determine stellar properties, activity status, youth status, and kinematic populations to identify the most suitable targets for future exoplanet surveys. In §2, we describe the construction of our volume-limited sample and the benchmark calibration set used to establish activity and age relationships. In §3, we present the CHIRON observations and data reduction procedures, followed in §4 by our spectroscopic analysis methods, including stellar parameter determinations, activity measurements, and age evaluations. In §5, we present the results of our comprehensive spectroscopic characterization, identifying active, young, and mature stellar populations, and in §6 we analyze the kinematic properties and Galactic population membership for stars in our sample. Our results provide crucial insights into the activity status and ages of the local K dwarf population, and establish a foundation for prioritizing targets in the ongoing search for potentially habitable worlds, as discussed in §7 and §8.

2. THE RECONS K STAR (RKSTAR) PROJECT

2.1. Four K Dwarf Surveys

The RKSTAR Project is a RECONS¹ effort to survey the ~ 4400 nearest K dwarfs within 50 parsecs of the Sun, a sample constructed primarily using *Gaia* parallax and photometry measurements. The comprehensive RECONS effort includes four systematic surveys of these K dwarfs — three are for stellar companions (and in the case of the Radial Velocity Survey, orbiting brown dwarfs and planets as well), while the fourth is a characterization survey that is the focus of the results here. The four surveys are:

The **Wide Field Survey** investigates stellar companions with separations greater than $\sim 1''$, utilizing *Gaia* data (Gaia Collaboration et al. 2018, 2022) and cataloged companions from, for example, the Washington Double Star (WDS) Catalog (Mason et al. 2001). To date, the Wide Field Survey includes over 1000 stellar companions with separations of ~ 50 –30000 AU in the entire RKSTAR 50 pc sample (Johns et al. 2024).

The **Speckle Survey** reveals stellar companions with separations of ~ 0.5 –100 AU, thereby spanning distances similar to the scale of our Solar System. The primary instruments used are optical speckle cameras on 4m to 8m class telescopes, most notably the Differential Speckle Survey Instrument (Horch et al. 2009, 2021). This survey has detected over 160 stellar companions, with approximately 90 being new discoveries, with the majority of stellar companions found orbiting within 15 AU of the K dwarfs (Henry et al. 2022).

The **Radial Velocity Survey** uses the CHIRON high-resolution spectrograph on the SMARTS 1.5m telescope at CTIO to reveal companions orbiting K dwarfs that are stars, brown dwarfs, and jovian exoplanets orbiting within ~ 3 AU. This survey has resulted in the discovery of dozens of stellar companions (Johns et al. 2024). This survey is complemented by long-term work by others reporting companions with stars and brown dwarf companions at larger separations, as well as planets down to terrestrial masses.

The **Characterization Survey**, which is the main focus of the work reported in this paper, utilizes CHIRON spectra to determine the stellar properties, activity status, ages, and kinematic motions of the nearby K dwarfs. Here we report on two distinct samples of K dwarfs — a survey sample of 580 field stars within 33 pc in the equatorial region of the sky selected from the RKSTAR sample, and a benchmark comparison sample of 35 stars with reliable estimated ages (Hubbard-James et al. 2022).

2.2. Sample for this Portion of the Characterization Survey

In this paper, we report results from the initial portion of the Characterization Survey that began in 2017, focused on a sample of K dwarf primaries created using the results of *Hipparcos* and *Gaia* Data Release 2 (DR2). K dwarfs were defined to have $M_{BP} = 5.30 - 9.90$ mag and $BP - K_s = 2.00 - 4.00$ mag, where the BP photometry comes from *Gaia* and the K_s photometry comes from 2MASS. Among the ~ 4400 K dwarf systems in the full 50 pc sample,

¹ REsearch Consortium On Nearby Stars, www.recons.org

this work focuses on systems located within 33.3 pc, selected using a cutoff in parallax of 30 mas, and situated in the equatorial sky band, ranging from DEC $+30^\circ$ to -30° . This approach results in a volume-limited sample that can be targeted at most major observatories in both hemispheres.

The list was revised somewhat with *Gaia* Data Release 3 (DR3), with particular attention paid to updated parallaxes and continued vetting for earlier-type primaries that knocked out K dwarfs that were companions to more massive stars or white dwarfs that were initially more massive than the K dwarfs. The focus on systems in which the K dwarf is the primary is central to our science goals: we aim to understand systems that formed with the primary star having a mass in the K dwarf range (roughly 0.6–0.9 M_\odot). These systems remain effectively unevolved over the age of the Galaxy, representing the outcomes of formation processes without evolutionary complications. This is particularly important for characterizing multiplicity statistics, including the frequency and properties of lower-mass stellar companions, brown dwarfs, and planets around K dwarfs. K dwarfs that are secondaries in systems with more massive components are maintained in a separate list but excluded from the statistical analyses presented here, as including them would mix distinct formation scenarios and complicate interpretation of companion demographics.

Table 1 provides a summary of the sample selection process. In May 2018, 687 K dwarfs were selected based on *Gaia* DR2 parallax measurements and photometry (Gaia Collaboration et al. 2016, 2018), with a few additional stars from *Hipparcos* that were not in *Gaia* DR2. Updated parallaxes from the *Gaia* DR3 (Gaia Collaboration et al. 2022) resulted in the exclusion of 22 K dwarf systems beyond the distance cutoff of 33.3 pc. Upon closer inspection, an additional 26 K dwarfs that are secondaries to earlier spectral type stars or white dwarfs were removed. Another 50 stars were removed due to $BP - K_s$ color cuts and additional quality control measures, and a final 9 for which we could not carry out complete data analyses. This leaves the survey sample of 580 K dwarf systems that are plotted in Figure 2, where the left panel illustrates the sky distribution mapping the “bowtie” configuration that depicts the declination and distance cutoffs, whereas the right panel is the more traditional polar plot. Note the increase in population density with increasing distance out to the horizon at 33.3 pc in both plots due to the projection of larger volumes onto the two dimensional maps representing cross-sectional cuts through space.

Table 1. Summary of the Sample Selection Process for the 580 K Dwarfs

Selection Step	Number of K Dwarfs
Initial list (May 2018, <i>Gaia</i> DR2)	687
Excluded due to updated parallaxes (<i>Gaia</i> DR3)	−22
Removed due to secondary status	−26
Removed due to color cuts and quality control	−50
Removed due to incomplete data	−9
Final Survey Sample	580

A list of the 580 stars in the survey sample, along with their positions, proper motions, parallaxes, and photometry, can be found in Appendix C. Sample refinement remains ongoing, as parallaxes may be subject to minor changes in future *Gaia* Data Releases, and new K dwarfs are likely to be added because *Gaia* DR2 and DR3 may not have provided astrometric solutions in systems that are short period binaries exhibiting astrometric perturbations. Some additional stars will likely be removed to ensure only the inclusion of systems with K dwarf primaries. For example, if additional white dwarfs are discovered, those systems will be excluded from the sample because the white dwarf progenitor originally had a greater mass and was the primary star. It is important to note that systems with white dwarf primaries are valuable for age determination, so they will still be considered for age calibration work but will not be included in the statistics for K dwarf samples and their companions.

A supplementary benchmark sample of ~ 100 K dwarfs with age estimates (Hubbard-James et al. 2022) was created to provide measurements of various spectral features and space motions that can be used as guidelines for the larger survey samples. These stars were taken from moving groups, associations, or clusters, plus a handful of field stars within 25 pc that have ages determined via isochrone fitting. Table 2 lists the various subsets used to construct this benchmark sample and the estimated ages of each group. The four associations utilized here are the β Pictoris moving group (β Pic, age ~ 20 Myr), the Tucana-Horologium association (Tuc-Hor, ~ 40 Myr), the AB Doradus moving group (AB Dor, ~ 120 Myr), and the Hyades cluster (~ 750 Myr). The four field K dwarfs within 25 pc have age estimates made via model isochrone fits and have ages of 0.3–5.7 Gyr. References for the ages assigned to the groups and

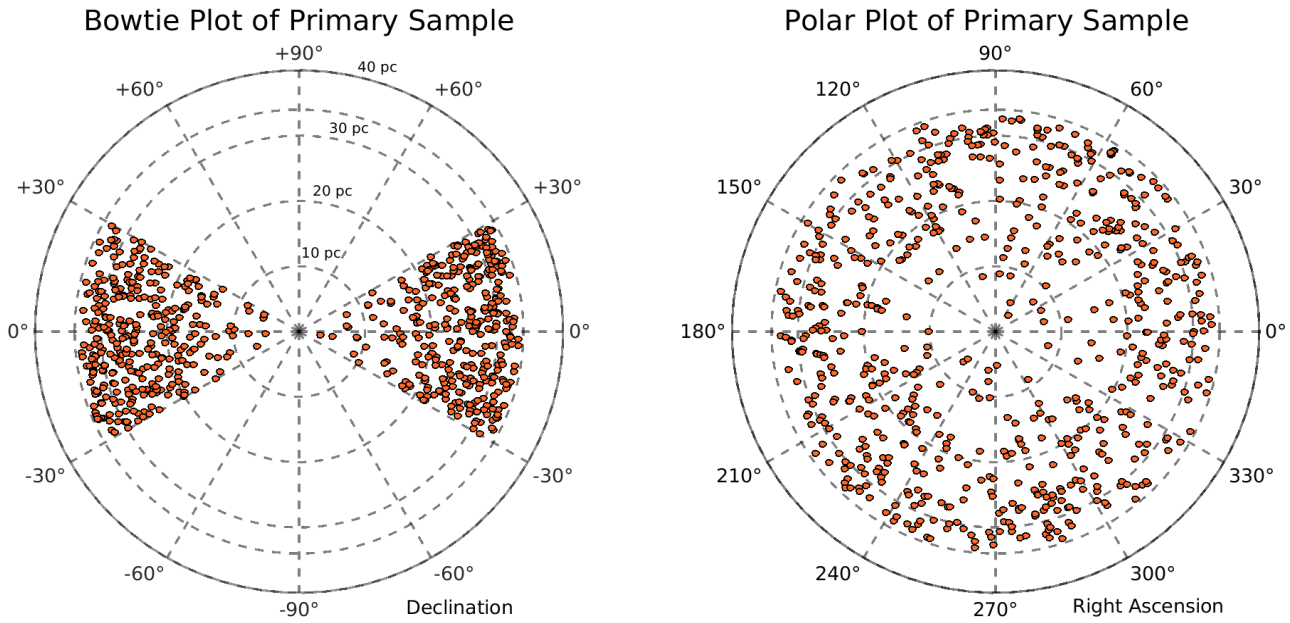


Figure 2. Left: Bowtie plot displaying declination (Dec) (circular direction) and distance (radial direction) for the survey sample of 580 K dwarfs. Right: Polar plot illustrating Right Ascension (R.A.) (circular direction) and distance (radial direction) for the survey sample of 580 K dwarfs. R.A. and Dec positions are based on J2000 coordinates, while distance values were derived from *Gaia* DR3 parallax measurements.

Table 2. Moving Groups (M.G.), Associations (Assoc.), Clusters, and Field K dwarfs in the Benchmark Sample

Group Name	RA (J2000)	DEC (J2000)	Distance (pc) ^a	Age	Members ^{b,c}	K dwarfs	Observed
β Pic M.G.	14 30	-42 00	~ 30	~ 20 Myr ^d	97	19	11
Tuc-Hor Assoc.	02 36	-52 03	~ 40	~ 40 Myr ^d	176	18	10
AB Dor M.G.	05 28	-65 26	~ 33	~ 120 Myr ^d	84	24	8
Hyades Cluster	04 26	+15 52	~ 42	~ 750 Myr ^d	177	47	10
Field K Dwarfs							
o^2 Eri	04 15 16.3	-07 39 10	5	4.3 Gyr ^e
20 Crv	11 34 29.5	-32 49 53	10	4.6 Gyr ^e
PX Vir	13 03 49.7	-05 09 43	22	0.3 Gyr ^g
ϵ Ind	22 03 21.7	-56 47 10	4	3.7–5.7 Gyr ^h

^a Distance from *Gaia* DR3

^b Membership list for β Pic, Tuc-Hor, and AB Dor: Bell et al. (2015)

^c Membership list for Hyades: Gagne et al. (2018)

^d Gagne et al. (2018)

^e Mamajek & Hillenbrand (2008)

^f Luck (2017)

^g Stanford-Moore et al. (2020)

^h Feng et al. (2019)

individual stars are noted at the end of Table 2. Additional information about this benchmark study can be found in Hubbard-James et al. (2022).

3. SPECTROSCOPIC OBSERVATIONS AND DATA PROCESSING

3.1. High-Resolution Spectra from CHIRON

The CHIRON high-resolution, cross-dispersed echelle spectrograph (Tokovinin et al. 2013; Paredes et al. 2021) at the Small and Moderate Aperture Research Telescope System (SMARTS) 1.5-m telescope at Cerro Tololo Inter-American Observatory (CTIO) was used for the spectroscopic observations secured for this research. CHIRON covers an optical wavelength range of 4150–8800Å, cross-dispersed into 59 to 62 spectral orders, depending on the selected mode, and can acquire targets as faint as $V \sim 18$ through a fiber that is 2.7'' in diameter on the sky. CHIRON has four modes that provide resolutions ranging from 28,000 to 136,000 — the choice of setup is determined by the scientific goals and the targets' brightnesses. For this work, we utilized CHIRON's slicer mode, which attains a resolution of $R = 80,000$ and offers minimal light loss with a fast 14-second CCD readout per image. CHIRON offers two wavelength calibration options: a ThAr comparison lamp and an iodine cell. In this study, we used the ThAr lamp for wavelength calibration, as it provides sufficient lines in the spectral orders needed for our science.

Observations at the 1.5-m with CHIRON are acquired by an onsite observer. Since 2017, operations have been led by RECONS team members at Georgia State, who create and manage nightly CHIRON observing queues, carry out the observing in tandem with CTIO staff, reduce the spectra using a modified pipeline based on that described in Tokovinin et al. (2013), and deliver reduced data to the world (Paredes et al. 2021). All spectroscopic data used in this study were obtained between June 2017 and March 2022. Each visit to a star consisted of acquiring a single exposure, with an integration time of 900 seconds for stars with Johnson V magnitudes brighter than 10.99 and up to 1800 seconds for fainter stars. These exposure times ensure a signal-to-noise ratio (SNR) in the spectra greater than 25 near a wavelength of 6740Å (see below), which is crucial for reliable analysis. To maintain overall data quality for the entire survey, stars with spectra having $\text{SNR} < 25$, typically due to poor sky conditions or inconsistent tracking during an observation, were placed on a re-observation list to secure reliable equivalent width measurements for spectral features of interest. The final set of spectral observations has a mean S/N of 50 at the Li I echelle order, with a standard deviation of 48. Only 44 spectra in the set have an S/N at Li I lower than 25.

Sets of bias and quartz lamp flat-field calibration frames were routinely taken before and after each observing night and used to set the background levels and correct for pixel-to-pixel variations on the CCD chip. To calibrate the wavelength scale for each spectrum, an observation was followed by a single ThAr lamp exposure with a duration of less than 1 second, which enables precise wavelength calibration of the acquired spectra. Table 11 in Appendix F provides a comprehensive list of the CHIRON observations carried out for this characterization study.

3.2. Spectra Assembly and Normalization

After the data were bias-subtracted and flat-fielded, the extracted spectra were blaze-corrected to flatten the spectra so that radial velocities, equivalent widths, and stellar properties could be derived. The first step for the blaze removal was to trim the first and last 100 pixels of the FITS flux-table file from each order. Major absorption features, such as the $H\alpha$ line (at 6563 Å) for order 38, were masked to remove their effects so that the continuum flux could be fit. Remaining points in each order were fit using a polynomial using Python's *scikit-learn* package (Pedregosa et al. 2011) with a robust linear regression to reduce the effect of outlier points when fitting the continuum flux. A sixth-degree polynomial was fit to every order of interest for this survey, except for order 40 where the Li I doublet falls, for which a seventh-order polynomial was used. The blaze removal was performed on 17 echelle orders total: 14 orders for radial velocity calculations, plus three additional orders to analyze the $H\alpha$, Li I, and Ca II IRT₂ spectral lines. Finally, the original unmasked spectral order was divided by the blaze function fit to obtain a flattened spectrum, which is then normalized to 1.00 at the mean continuum value.

Astrometric data from Gaia DR3 and the time of the middle of the exposure were used to adjust for barycentric motion at the time of the observation. The barycenter velocities and time in Julian dates for the corrections were calculated using the python's open-source package *barycorrpy*² (Kanodia & Wright 2018; Wright & Eastman 2014). A star's epoch systemic radial velocity, noted as the γ velocity here, was calculated using steps 3 to 9 of the *Radial Velocity Pipeline* described in Paredes et al. (2021). Briefly, an RV was calculated using a cross-correlation function (CCF) of the stellar spectrum with appropriate K dwarf template spectra taken from the work of Blanco-Cuadros

² <https://github.com/shbhuk/barycorrpy>

et al. (2014) and the peak location found by using a Cauchy–Lorentz function for the 14 CHIRON echelle orders numbered 10, 12, 13, 16, 17, 18, 20, 21, 22, 23, 24, 27, 30, and 35. Errors on the RVs are the standard deviations of the 14 measurements. The γ velocities were then incorporated to offset all spectra to rest wavelengths. Once the spectra are deblazed and wavelength corrected, they are ready for scientific analysis. The detailed discussion of the γ velocity results is given in §6.2 and results can be seen in Figure 10.

3.3. K Dwarf Spectral Gallery

Our spectroscopic observations enable the construction of a high-resolution activity and age spectral gallery of 580 nearby K dwarfs. We process this uniform, high-quality dataset to investigate stellar properties such as chromospheric activity, age indicators, metallicities, and surface gravities. The gallery will serve as a resource for broader astronomical studies, including exoplanet host characterization and comparative stellar astrophysics. Each spectrum was processed through the standardized pipeline described in §3.2, and as mentioned, only spectra achieving a SNR greater than 25 at 6740 Å are included. This standardized RECONS post-pipeline reduction produces a directory for each target spectrum. The output includes raw spectra, reduced files of wavelength/flux pairs in both CSV and FITS formats organized by individual stellar targets, and plot images of the selected echelle orders to aid visual confirmations. A first version of the gallery has been made publicly available³ and will continue to expand with additional spectra from the broader RKSTAR sample.

The gallery includes four key diagnostic features for each star: the Na I doublet at 5890/5896 Å (surface gravity indicator), the H α line at 6563 Å (chromospheric activity indicator), the Li I resonance line at 6708 Å (youth indicator), and the Ca II infrared triplet line at 8542 Å (chromospheric activity indicator). This paper focuses on the analysis of the H α and Li I features; future work will evaluate the Na I and Ca II triplet features when larger samples are available. Figure 16 in Appendix B showcases all 53 young, active, or otherwise unique stars from our sample, illustrating the diversity captured across a broad range of effective temperatures and metallicities. Groups A–D highlight young and active K dwarfs identified spectroscopically through H α emission and lithium absorption features. Group E features stars identified kinematically as young (Hyades cluster members) as well as peculiar systems including a newly discovered spectroscopic binary (SB2s) and a halo star.

4. SPECTRAL ANALYSIS

4.1. Stellar Parameters

For this study, we determined fundamental stellar parameters using the Python algorithm Empirical SpecMatch (ESM) developed by Yee et al. (2017). ESM derives stellar properties by comparing an input optical spectrum to a library of high-resolution ($R \sim 55,000$), high signal-to-noise ratio ($\text{SNR} > 100$) spectra of 404 well-characterized calibrator stars. These library stars were observed with the High Resolution Echelle Spectrometer (HIRES) on the 10-meter Keck telescope in Hawaii, as part of the California Planet Search. The stars’ parameters span effective temperatures (T_{eff}) from 3000 to 7000 K, metallicities ($[Fe/H]$) from -0.6 to $+0.6$ dex, stellar radii from 0.1 to 16 solar radii, and spectral types from F1 to M5. These parameters were derived through various independent methods, including interferometry, optical and near-infrared photometry, asteroseismology, and local thermal equilibrium (LTE) spectral synthesis (Yee et al. 2017). The ESM algorithm analyzes optical spectra through wavelengths 5100 to 5800 Å, all of which are covered in our CHIRON observations at a $R \sim 80,000$. This spectral range includes diagnostic features such as the magnesium b triplet (Mg I b, 5100 to 5340 Å) while avoiding telluric line contamination found between 6270 and 6310 Å. The spectral region around the Mg I b triplet is particularly diagnostic because line ratios in this region constrain effective temperature (T_{eff}), the shapes of the lines provide measures of surface gravity ($\log g$), and specific iron lines yield metallicity ($[Fe/H]$).

The algorithm operates systematically, beginning with a correction of the target star’s line-of-sight velocity to align its spectrum with reference spectra; this has already been accomplished for our spectra as described in §3.2. The algorithm then performs a bootstrapping procedure to identify the target spectrum with the library spectrum exhibiting the highest median correlation peak. ESM then conducts pairwise matching with each library spectrum, fitting for rotational broadening ($vsini$) and refining continuum normalization via cubic spline fits. The final stellar parameters are derived from a weighted linear combination of the five best-matching library spectra, using nonlinear least-squares minimization to reduce the unnormalized χ^2 statistic. ESM provides parameter uncertainties based

³ https://hodarijames.github.io/spectral_library/page1.html

on the scatter in differences between the algorithm-derived and library values of the stellar parameters. Within its calibration range, typical uncertainties for K dwarfs are ~ 100 K for T_{eff} , 0.09 dex for $[Fe/H]$, and 0.60 dex for $\log g$. These values are added in quadrature to the errors from the four individual measurements that use different sections of the spectra for each star. While we expect some correlation between these ESM parameter uncertainties and the SNR of individual spectra, ESM was designed to work robustly across a range of spectral qualities. A detailed analysis of how parameter uncertainties scale with SNR and other spectral characteristics for our sample will be presented in a future methodological paper.

An important consideration in our analysis is the limited representation of mid-K dwarfs (4200–4800 K) with high metallicities ($[Fe/H] > 0.2$ dex) in the ESM spectral library. This underrepresentation likely introduces systematic uncertainties and potentially underestimates metallicity values for stars in these ranges. Nonetheless, we include results for these stars in our analysis, but one must exercise caution when interpreting the derived parameters for stars in these temperature and metallicity ranges. Future expansions of the spectral library to include mid-K dwarfs could reduce these uncertainties.

To validate our results, we compared ESM-derived parameters for five well-studied benchmark K dwarfs against independent determinations from the PASTEL catalog (Soubiran et al. 2020), which compiles stellar parameters from multiple high-resolution spectral analyses (Table 3). Minor discrepancies observed are primarily attributable to differences in modeling approaches, line lists, and adopted stellar physics. Our ESM-derived parameters generally match those from PASTEL within the uncertainties, with the single exception among the 15 quantities determined being the $[Fe/H]$ value for σ^2 Eri for which we suspect the metallicity errors are underestimated because ESM has sparse coverage of library stars in this low metallicity region.

Table 3. Comparison of Stellar Properties from Empirical SpecMatch (ESM) and the PASTEL Catalog

Star	ESM T_{eff} (K)	PASTEL T_{eff} (K)	ESM $[Fe/H]$ (dex)	PASTEL $[Fe/H]$ (dex)	ESM $\log g$ (dex)	PASTEL $\log g$ (dex)
σ^2 Eri	5109 ± 105	5133 ± 43	-0.43 ± 0.09	-0.29 ± 0.01	4.49 ± 0.69	4.52 ± 0.02
HD 50281	4710 ± 102	4767 ± 31	$+0.03 \pm 0.09$	$+0.02 \pm 0.03$	4.54 ± 0.69	4.54 ± 0.08
20 Crv	5220 ± 110	5196 ± 23	-0.47 ± 0.10	-0.40 ± 0.02	4.54 ± 0.69	4.60 ± 0.04
PX Vir	5195 ± 113	5174 ± 63	-0.12 ± 0.17	-0.08 ± 0.03	4.56 ± 0.70	4.55 ± 0.05
ϵ Ind	4617 ± 104	4641 ± 21	-0.09 ± 0.09	-0.13 ± 0.03	4.58 ± 0.70	4.54 ± 0.22^a

^aPASTEL $\log g$ recalculated to exclude outlier value of 2.87 dex.

4.2. Activity & Youth Indicators

We selected four key spectral lines as indicators of stellar activity and youth for the K dwarf study: the Na I doublet at 5890 and 5896 Å, $H\alpha$ at 6563 Å, Li I at 6708 Å, and the Ca II infrared triplet (IRT) line at 8542 Å. This paper focuses on the $H\alpha$ and Li I lines, while future work with larger samples will incorporate the Na I and Ca II features. These lines were chosen based on their established sensitivities to surface gravity, chromospheric activity, and lithium depletion variations associated with stellar age and evolutionary status. For detailed discussions on the selection criteria, underlying physical processes, and prior usage of these lines as age and activity indicators, we refer the reader to Hubbard-James et al. (2022), and references therein. Briefly, the Na I doublet lines (5890 and 5896 Å) are sensitive to surface gravity changes, indicative of stellar evolutionary phases and corresponding age (Montes et al. 2001; Soderblom 2010). The $H\alpha$ and Ca II IRT (8542 Å) lines serve as effective tracers of chromospheric activity, which typically decreases with stellar age (Skumanich 1972; Soderblom 2010). The Li I resonance line at 6707.8 Å is strongly correlated with stellar age due to lithium depletion processes occurring early in a star’s lifetime (Soderblom et al. 1993; White et al. 2007; Lopez-Santiago et al. 2010; Binks & Jeffries 2014; Riedel et al. 2017).

4.3. Equivalent Width Measurement Methods

To quantify stellar activity and youth, we measured equivalent widths (EWs) of key spectral lines using two main approaches, depending on the shape of the observed feature. Figure 3 shows example spectra with the two methods used for various line shapes: Voigt profile fits and integration windows. Spectral line EW measurements for the $H\alpha$ and Li I lines — the two lines analyzed in this paper — are given in Appendix E.

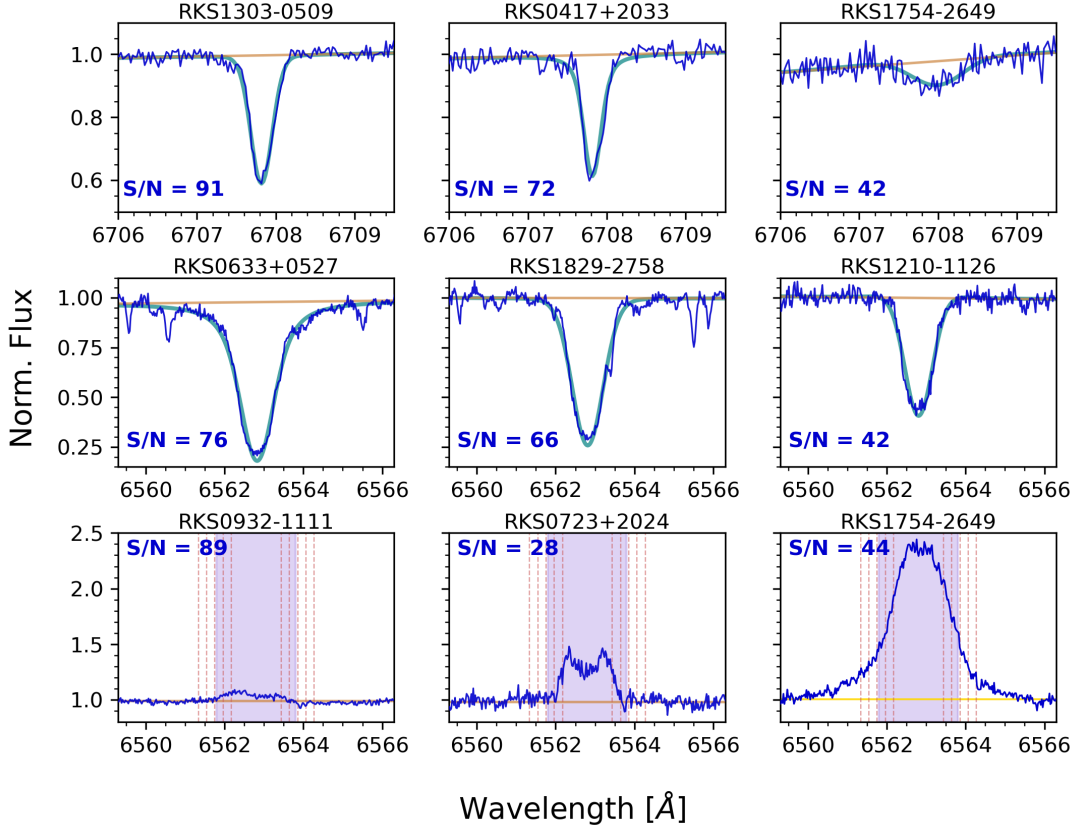


Figure 3. Examples of K dwarf spectra (blue) showing activity and age indicators with EW measurement methods. Voigt profiles (green), local continuum levels (yellow), and integration windows (purple) are shown. Top row: Li I absorption measured via Voigt fitting. Middle row: $H\alpha$ absorption measured via Voigt fitting. Bottom row: $H\alpha$ emission or filled-in profiles measured via the window method using *specutils*. Final EWs were computed by integrating flux over a nominal 2.1\AA window (purple) and four additional windows at $\pm 10\%$ and $\pm 20\%$ of the nominal width (dashed red lines).

Smooth Absorption Features: For absorption features such as the Li I line and most $H\alpha$ profiles, we used Voigt profile fitting, implemented using Python’s `scipy.optimize.curve_fit` module. This method models the spectral line with a Voigt function that accounts for both Gaussian and Lorentzian broadening. Each fit included a local linear continuum, and the EW was computed by numerically integrating the area between the fitted profile and the continuum using `numpy`. To estimate typical uncertainties in this method, we analyzed $H\alpha$ profiles in a subset of seven stars spanning the luminosities and colors of K dwarfs that had multiple high-SNR spectra. For each, we performed Voigt fits to five spectra and calculated the standard deviation of the resulting EWs. These tests showed typical errors ranging from 1 to 49 m\AA , with relative uncertainties of $\sim 1\text{--}7\%$, so we adopt a 5% error as typical for both $H\alpha$ and Li I absorption features given that they are similar in shape. These results are summarized in Table 5.

Table 4. Description of Spectral Lines and Measurement Windows

CHIRON Order	Line	Purpose Name	Lab λ (\AA)	EW Window Width (\AA)	Typical Error (\AA)
28	Na I D1	Gravity	5889.9	6.0	0.23
	Na I D2	Gravity	5895.9	5.0	0.20
38	$H\alpha$	Activity	6562.8	2.1	0.07
40	Li I	Age	6707.8	1.4	0.03
58	Ca II IRT ^a	Activity	8542.0	7.0	0.25

[a] IRT: Infrared Triplet.

RKSTAR ID	M_{BP}	$BP - K$	$\langle \text{EW H}\alpha \rangle$	$\sigma \text{EW H}\alpha$	Error	SNR at $\text{H}\alpha$
	<i>mag</i>	<i>mag</i>	\AA	\AA	%	
RKS2009+1648	5.92	2.26	1.165	0.001	0.8	92.8
RKS2125+2712	6.49	2.30	1.109	0.014	1.3	73.6
RKS0453+2214	6.93	2.75	0.844	0.049	5.8	57.4
RKS2009-0307	7.36	3.07	0.777	0.016	2.0	50.4
RKS0514+0039	7.93	3.24	0.713	0.025	3.5	43.5
RKS1729-2350	8.53	3.46	0.555	0.012	2.4	51.1
RKS1854+2844	9.00	3.83	0.420	0.030	7.1	28.7

Table 5. $\text{H}\alpha$ equivalent width (EW) data for seven K dwarfs of various luminosities and colors used to estimate the errors in EW measurements obtained with the Voigt fitting method.

Complex Features: For the subset of stars with complex $\text{H}\alpha$ profiles that cannot be reliably fit with Gaussian functions—including emission profiles, partially filled-in cores, and broader or more complex line shapes (e.g., rapidly rotating stars)—we used fixed-window integration methods. This approach provides consistent, reproducible measurements across diverse profile morphologies where defining variable window boundaries would be subjective. We carried out window-based integrations using the `specutils` package (Earl et al. 2020) with wavelength coverage as outlined in Table 4. EWs were calculated using the classical definition:

$$EW = \int_{\lambda_1}^{\lambda_2} \left(1 - \frac{F(\lambda)}{F_C} \right) d\lambda, \quad (1)$$

where $F(\lambda)$ is the observed flux, F_C is the continuum level, and λ_1 and λ_2 define the spectral window. For $\text{H}\alpha$, we calculated the continuum as the average flux in the adjacent regions 6558.4 to 6560.4 \AA and 6565.2 to 6567.2 \AA , and for the Li I line we adopted a fixed continuum of $F_C = 1$. To quantify the uncertainty arising from window placement, each EW was calculated five times: once using the nominal window and four times using windows increased or decreased by 10 and 20 percent. The final EW was the average of these five measurements, and the standard deviation was adopted as the uncertainty, systematically capturing the sensitivity of the measurement to window definition. For EWs determined using windows, a summary of the spectral lines, their central wavelengths, window spans, and typical errors is provided in Table 4.

4.4. Signal-to-Noise (SNR) Considerations

Reliable measurements of spectral line strengths depend on the SNR of each echelle order. For this study, we determined SNR individually for each of the orders containing the $\text{H}\alpha$ (order 38) and Li I (order 40) lines. We measured SNR values following the procedure established for CHIRON spectra by Tokovinin et al. (2013): calculating the ratio of the mean flux to its standard deviation across three adjacent pixels located near the blaze peak of each order, where the signal is maximized and systematic variations in the continuum are minimized. This approach provides a practical estimate of the spectral quality achieved for each observation.

To establish appropriate SNR thresholds for reliable measurements in our survey, we conducted visual inspection of spectra spanning a range of SNR values. For $\text{H}\alpha$, we found that SNR greater than 15 was sufficient for reliable measurement, which preserved 97% of the spectra taken for the survey K dwarfs. For the Li I line, distinguishing it from the nearby Fe I line at 6707.4 \AA required SNR greater than 30. This threshold was met in 83% of the spectra. EWs from spectra with orders falling below the thresholds were marked as upper limits or excluded entirely, depending on the clarity of the line shape and the reliability of the EW measurement.

4.5. Gamma Velocity Measurements and Kinematics

We derived systemic radial velocities, here called γ velocities, from the high-resolution CHIRON spectra for 572 of the 580 K dwarfs in the survey sample. 8 stars could not have their radial velocities measured due to rapid rotation or insufficient spectral quality. The methodology is described in §3.2. *Gaia* DR3 does not have values for 35 of the survey stars, and the DR3 values are generally ~ 10 times less precise than our values from CHIRON that typically have errors of 0.1–0.3 km s^{-1} , dependent on spectral quality and stellar rotation. Of course, long-term monitoring of γ velocities can reveal companions such as low-mass stars, brown dwarfs, or exoplanets, even if these companions cannot be directly imaged or observed via eclipses or transits.

We calculated the Galactic UVW space velocities for 572 stars in the survey using the `gal_uvw` function from the Python AstroLib library to provide kinematic motions for the stars. Two additional stars were excluded from this analysis because their spectroscopic binary nature (double-lined spectroscopic binaries) prevented reliable radial velocity determinations required for the kinematic calculations. This process required using our computed γ velocities combined with each star’s celestial coordinates, proper motions, and parallax-derived distances from Gaia DR3 (Gaia Collaboration et al. 2022). The resulting space velocities represent Cartesian motions aligned with Galactic coordinates, where the U axis is directed toward the Galactic center, the V axis aligns with Galactic rotation, and the W axis points toward the north Galactic pole. The calculated velocities presented in Appendix D (Table 9) are not corrected for solar motion relative to the Local Standard of Rest (LSR).

The UVW motions allow us to evaluate potential membership of our sample stars in specific moving groups or stellar associations because members typically share similar UVW motions. Furthermore, these velocities enable us to categorize our sample into the broader Galactic populations — Thin Disk, Thick Disk, and Halo — because each population exhibits characteristic kinematic properties. Thin Disk stars display relatively low random velocities and nearly circular Galactic orbits. Thick Disk stars exhibit larger velocities, particularly perpendicular to the Galactic plane, and have larger, more eccentric Galactic orbits. Halo stars, typically older and more metal-poor than disk stars, exhibit significantly higher random velocities with highly elliptical orbits and no distinct rotational preference. While kinematics alone cannot conclusively establish membership in specific associations or Galactic populations (e.g., Gagne et al. 2018; Riedel et al. 2014), these measurements combined with complementary analyses of age and metallicity provide essential context for understanding the structure, dynamics, and evolutionary history of stars in the solar neighborhood.

5. SPECTRAL CHARACTERIZATION OF K DWARFS

5.1. *Stellar Parameters Results: Temperatures, Metallicities, Surface Gravities, and Rotational Velocities*

The fundamental stellar parameters for our survey stars were derived using the Empirical SpecMatch (ESM) methodology described in § 4.1. ESM’s ability to match observed spectra to a library of well-characterized calibrator stars enables determinations of effective temperatures (T_{eff}), metallicities ($[Fe/H]$), surface gravities ($\log g$), and projected rotational velocities ($v \sin i$). These stellar parameters for the 580 survey stars are presented in Table 10 in Appendix E.

Figure 4 displays the distribution of our K dwarf sample in metallicity-temperature space. The survey stars are shown as orange plus symbols, while the 215 stars from the ESM library (Yee et al. 2017) are marked by blue dots for comparison. Our K dwarfs generally span a temperature range of 3600 to 5500 K, with two higher temperature stars at 5582K and 6177K — the latter star is a fast rotator and the temperature from ESM is likely erroneous. The stars exhibit metallicities from -0.6 to $+0.4$ dex, with one outlier near $+0.6$ dex. The histogram on the y-axis shows the metallicity distribution in 0.1 dex bins, revealing that a substantial fraction ($413/580 = 71\%$) of our sample possesses solar-like metallicities between -0.2 and $+0.2$ dex. The mean metallicity for the entire sample is -0.02 dex, confirming the predominance of solar-metallicity stars in the solar neighborhood. We adopt minimum errors of 100 K in T_{eff} , 0.09 dex in $[Fe/H]$, and 0.60 dex for $\log g$ based on Yee et al. (2017).

Notable limitations evident in Figure 4 are three regions in the ESM library with sparse coverage, including metallicities greater than $+0.4$ dex, less than -0.4 dex and at all metallicities for temperatures between 4200 and 4700 K. These gaps, highlighted by purple shaded regions, may result in systematic biases against identifying stars in these parameter spaces. For example, the scarcity of library stars with T_{eff} near 4500 K likely leads to K dwarfs being underrepresented near this temperature. Any future expansions of the ESM library should prioritize adding K dwarfs in these undersampled regions, potentially drawing from our own extensive spectroscopic dataset.

Despite these limitations, our analysis successfully characterizes a modest set of 20 (3.4%) metal-poor stars in the sample with $[Fe/H] < -0.5$ dex. These low-metallicity K dwarfs form an important subset for further work to understand Galactic stellar populations and chemical evolution. Significantly, none of these stars, nor those with metallicities of -0.4 to -0.5 dex are found to be young or active, as described in §5.3 & §5.4, highlighting a clear dichotomy between the metal-poor and chromospherically active populations.

The distribution of rotational velocities in our sample provides additional insight into the stellar population. While ESM can measure $v \sin i$ values down to the instrumental resolution limit, we report only values exceeding $v \sin i = 7$ km s $^{-1}$, following the approach of Hubbard-James et al. (2022). A robust correlation between projected rotational velocity and stellar activity emerged from our analysis — all six K dwarfs in Table 6 exhibiting $v \sin i > 5$ km s $^{-1}$

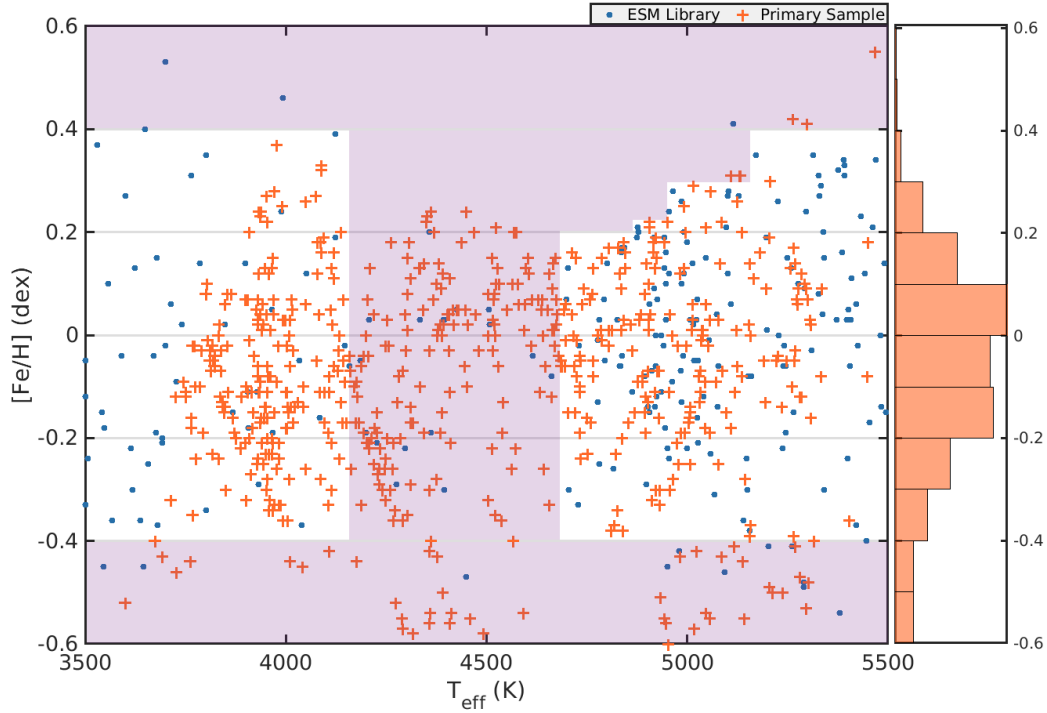


Figure 4. Distribution of $[Fe/H]$ and T_{eff} values determined via ESM for 571 of the 580 K dwarfs in our survey sample (orange plus symbols). The 215 stars within this T_{eff} & $[Fe/H]$ range from the ESM library (Yee et al. 2017) are shown as blue dots for comparison. The purple shaded regions highlight areas where the ESM library coverage is sparse, potentially affecting the reliability of derived parameters in these regions. The histogram on the y-axis shows the metallicity distribution of our sample in 0.1 dex bins, with a mean value of -0.02 dex.

also demonstrate evident chromospheric activity, as determined by their $H\alpha$ measurements (see § 5.3). These rapid rotators are AK For, BD+20 1790, HD 29697, HD 118100, HD 175742, and LQ Hya.

Interestingly, while all rapid rotators show chromospheric activity, the converse is not true: among the 26 K dwarfs identified as chromospherically active in our sample, only six showed elevated $vsini$ values. This apparent discrepancy likely results at least in part from projection effects, where stars with rotational axes nearly aligned with our line of sight may be rotating rapidly but exhibit small projected velocities (Barnes 2003). This underscores the complex relationship between stellar rotation and activity, and emphasizes the need for complementary diagnostics when characterizing stellar properties. Figure 5 illustrates the dramatic impact of rotation on spectral line profiles across two diagnostic wavelength regions, as seen in CHIRON spectra. The $H\alpha$ and Li I regions both show progressive line broadening with increasing $vsini$, from the sharp, well-defined features of the slow rotator ϵ Indi to the severely broadened and smeared lines of the extremely fast rotators LO Peg and AB Dor from our benchmark sample. This sequence demonstrates how rapid rotation can complicate spectral analysis, particularly for activity indicators like $H\alpha$ and age diagnostics like Li I.

Finally, surface gravity measurements from ESM show the expected values for main-sequence K dwarfs, with $\log g$ ranging from 4.40 to 4.85 dex for all but four of the 580 stars for which $\log g$ could be derived. We adopt a minimum error of 0.60 dex for $\log g$ measurements, based on the systematic error reported in Yee et al. (2017). To ensure no cool subgiants contaminate the sample, we vetted stars using the HR diagram with a strict cutoff at $M_G = 5.5$ mag at the bright end. Individual stars near this cutoff were examined to confirm they are main-sequence K dwarfs rather than slightly evolved objects.

The combination of the four derived stellar parameters provides a characterization of our K dwarf sample, establishing the foundation for interpretation of the measured chromospheric activity and age indicators. In Table 6 we highlight detailed spectroscopic results and derived stellar properties for 53 noteworthy K dwarfs from our survey sample, including young stars, active stars, a double-lined spectroscopic binary, and the single halo star revealed.

Table 6. Spectroscopic Results and Derived Stellar Properties of 53 K Dwarfs in the Survey Sample

RKSTAR ID	$T_{\text{eff}} \pm \sigma$	$[\text{Fe}/\text{H}] \pm \sigma$	$\log g \pm \sigma$	$v \sin i$	EW[H α]	EW[Li I]	Status	Fig 9 #s
...	(K)	(dex)	(dex)	(km s $^{-1}$)	(\AA)	(\AA)
RKS0117-1530	5302 \pm 108	-0.48 \pm 0.09	4.17 \pm 0.63	<5	0.63	0	A	...
RKS0121+2419	3942 \pm 122	+0.06 \pm 0.13	4.68 \pm 0.71	...	0.26	0	A / MG Hyades	...
RKS0252-1246	5165 \pm 103	+0.11 \pm 0.09	4.51 \pm 0.68	<5	0.92	0.21	Y+A	18
RKS0417+2033	4446 \pm 106	-0.06 \pm 0.12	4.64 \pm 0.70	<5	0.72	0.13	Y	13
RKS0430+0058	4011 \pm 102	+0.03 \pm 0.10	4.68 \pm 0.70	<5	-0.14	0	A	...
RKS0436+2707	4671 \pm 161	+0.15 \pm 0.10	4.55 \pm 0.68	<5	-0.39	0	A	...
RKS0441+2054	4572 \pm 104	-0.22 \pm 0.11	4.58 \pm 0.69	8.0	-0.18	0.06	Y+A	9
RKS0536+1119	3936 \pm 102	-0.09 \pm 0.10	4.7 \pm 0.69	<5	0.06	0	A	...
RKS0626+1845	5269 \pm 166	-0.41 \pm 0.14	4.41 \pm 0.71	<5	0.54	0	A	...
RKS0658-1259	4357 \pm 129	-0.30 \pm 0.10	4.66 \pm 0.67	<5	0.37	0.07	Y+A	10
RKS0723+2024	4285 \pm 363	-0.20 \pm 0.28	4.65 \pm 0.74	8.0	-0.55	0.16	Y+A / MG AB Dor	16
RKS0734-0653	5056 \pm 144	-0.19 \pm 0.22	4.57 \pm 0.74	<5	0.97	0.05	Y	7
RKS0739-0335	4907 \pm 113	+0.04 \pm 0.11	4.53 \pm 0.72	<5	0.52	0	A	...
RKS0819+0120	4965 \pm 120	-0.28 \pm 0.12	4.56 \pm 0.69	<5	0.85	0.12	Y+A	12
RKS0850+0751	3943 \pm 120	-0.25 \pm 0.14	4.7 \pm 0.70	<5	0.31	0	A	...
RKS0904-1554	4895 \pm 111	+0.08 \pm 0.11	4.5 \pm 0.70	<5	0.81	0.05	Y	8
RKS0907+2252	5257 \pm 113	+0.13 \pm 0.10	4.49 \pm 0.72	<5	0.83	0.12	Y+A	11
RKS0932-1111	6177 \pm 254	+0.01 \pm 0.17	4.31 \pm 0.77	27.4	-0.06	0.19	Y+A	17
RKS1000+2433	0.19	0	A	...
RKS1043-2903	5269 \pm 101	+0.14 \pm 0.10	4.51 \pm 0.69	<5	0.94	0.15	Y+A	15
RKS1121-2027	4138 \pm 111	-0.13 \pm 0.12	4.68 \pm 0.70	<5	0.29	0	A	...
RKS1205-1852	3955 \pm 108	-0.08 \pm 0.14	4.7 \pm 0.70	<5	0.25	0	A	...
RKS1303-0509	5266 \pm 113	-0.05 \pm 0.10	4.54 \pm 0.72	<5	0.97	0.14	Y	14
RKS1306+2043	4105 \pm 113	-0.19 \pm 0.14	4.68 \pm 0.70	<5	0.18	0	A	...
RKS1334-0820	4335 \pm 118	-0.10 \pm 0.17	4.65 \pm 0.68	8.1	-0.32	0.02	Y+A	1
RKS1414-1521	0.00	0	A	...
RKS1500-2905	3790 \pm 108	-0.03 \pm 0.10	4.71 \pm 0.70	<5	0.17	0	A	...
RKS1633-0933	3909 \pm 120	+0.20 \pm 0.16	4.67 \pm 0.71	<5	-0.8	0	A / MG AB Dor	...
RKS1705-0147	4835 \pm 130	+0.01 \pm 0.14	4.5 \pm 0.73	6.2	0.30	0.24	Y+A	19
RKS1716-1210	4002 \pm 110	-0.02 \pm 0.11	4.68 \pm 0.70	<5	0.45	0.05	Y	5
RKS1737-1314	0.00	0	A	...
RKS1754-2649	4249 \pm 220	-0.32 \pm 0.27	4.68 \pm 0.75	...	-2.51	0.05	Y+A	6
RKS1818-0642	4673 \pm 101	+0.02 \pm 0.10	4.58 \pm 0.70	<5	0.77	0.03	Y	2
RKS1822+0142	4129 \pm 110	-0.07 \pm 0.13	4.67 \pm 0.70	<5	-0.25	0	A	...
RKS1855+2333	5123 \pm 161	+0.01 \pm 0.14	4.54 \pm 0.73	14.8	0.02	0	A	...
RKS1910+2145	3931 \pm 110	+0.07 \pm 0.11	4.67 \pm 0.70	<5	-0.41	0.03	Y+A	4
RKS2041-2219	3953 \pm 130	-0.16 \pm 0.20	4.69 \pm 0.71	<5	-1.51	0	A	...
RKS2105-1654	3820 \pm 110	-0.05 \pm 0.11	4.7 \pm 0.70	<5	0.18	0	A	...
RKS2108-0425	4566 \pm 140	-0.40 \pm 0.15	4.6 \pm 0.73	<5	0.38	0	A	...
RKS2153+2055	5033 \pm 107	-0.07 \pm 0.11	4.56 \pm 0.70	<5	0.93	0.03	Y+A	3
RKS2308+0633	3804 \pm 108	+0.10 \pm 0.14	4.7 \pm 0.69	<5	0.08	0	A	...
RKS2335+0136	4112 \pm 101	+0.05 \pm 0.13	4.66 \pm 0.69	<5	0.24	0	A	...
RKS2348-1259	4179 \pm 113	-0.12 \pm 0.11	4.68 \pm 0.69	<5	-0.19	0	A	...
RKS0706+2358	4281 \pm 110	-0.08 \pm 0.13	4.66 \pm 0.70	<5	0.67	0	MG AB Dor	...
RKS0820+1404	4146 \pm 111	-0.09 \pm 0.11	4.67 \pm 0.69	<5	0.60	0	MG AB Dor	...
RKS0104+2607	4161 \pm 111	-0.07 \pm 0.13	4.67 \pm 0.70	<5	0.57	0	MG Hyades	...
RKS0300+0744	5058 \pm 106	+0.28 \pm 0.11	4.49 \pm 0.70	<5	0.99	0	MG Hyades	...
RKS0320+0827	4520 \pm 110	+0.08 \pm 0.12	4.6 \pm 0.72	<5	0.74	0	MG Hyades	...
RKS0322+2709	3947 \pm 111	+0.13 \pm 0.20	4.68 \pm 0.69	<5	0.42	0	MG Hyades	...
RKS0420-1445	4368 \pm 101	+0.07 \pm 0.11	4.64 \pm 0.69	<5	0.64	0	MG Hyades	...
RKS2254+2331	3931 \pm 113	+0.02 \pm 0.13	4.67 \pm 0.72	<5	0.48	0	MG Hyades	...
RKS1833-1626	4896 \pm 557	-0.19 \pm 0.53	4.56 \pm 0.77	<5	0.83	0	New SB2	...
RKS1510-1622	1.23	0	Halo	...

Columns 6 and 7 — EW[H α]: Equivalent width of the H α line at 6563 \AA . EW[Li I]: Equivalent width of the Li I line at 6707.8 \AA

In the Status column: Y = Young, A = Active, Y+A = both Youth and Active, MG = Young Moving Group, New SB2 = New spectroscopic binary, Halo = Halo star

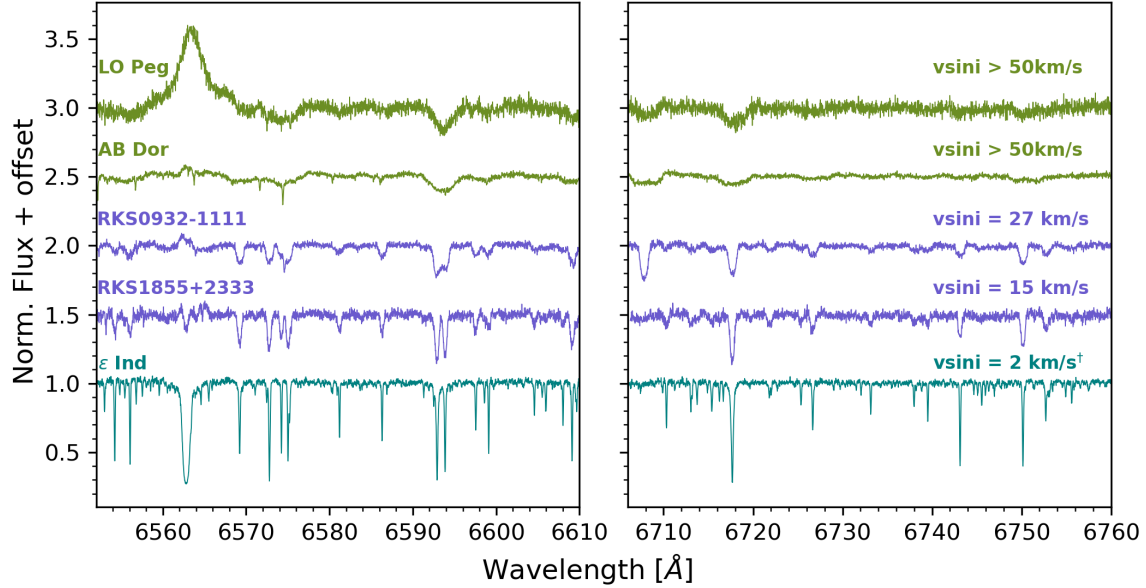


Figure 5. A sequence of spectra showing the effects of rotation on line profiles. The left panel displays a ~ 60 Å window including $H\alpha$ at 6563 Å, while the right panel shows ~ 50 Å window including Li I at 6707.8 Å and a Ca I line at 6717 Å. From bottom to top: ϵ Indi ($v \sin i < 2 \text{ km s}^{-1}$, slow rotator), RKS1855+2333 ($v \sin i = 15 \text{ km s}^{-1}$) and RKS0932-1111 ($v \sin i = 27 \text{ km s}^{-1}$) representing fast rotators from our survey sample of 580 K dwarfs, and AB Dor ($v \sin i > 50 \text{ km s}^{-1}$) and LO Peg ($v \sin i > 50 \text{ km s}^{-1}$) representing extremely fast rotators from the benchmark sample used to calibrate age and activity relationships, as described in Hubbard-James et al. (2022). The progressive line broadening and eventual smearing of spectral features with increasing rotation is clearly evident in both wavelength regions.

5.2. Quiescent $H\alpha$ Activity Level for K Dwarfs

Having established the fundamental stellar parameters for our sample, we now turn to characterizing chromospheric activity status across the K dwarf population. A critical first step in identifying active stars is establishing a baseline “quiescent” level representing the typical $H\alpha$ absorption strength for mature, inactive K dwarfs. This baseline serves as a reference against which enhanced chromospheric emission can be measured.

Figure 6 presents the relationship between $H\alpha$ EW and stellar color ($BP - K$) for the 580 K dwarfs for which we could measure values. The $H\alpha$ strength exhibits a clear dependence on color, with redder K dwarfs showing progressively weaker absorption (more negative EW values). This trend arises from the decreasing continuum flux at $H\alpha$ wavelengths in cooler stars; for a given $H\alpha$ line flux, later-type stars yield smaller equivalent widths due to their fainter continua (White et al. 2007).

Most stars fall along a quiescent population that forms a well-defined sequence in Figure 6. Through visual inspection of individual spectra, we excluded stars showing $H\alpha$ emission or core-filling from the distribution, then fit the remaining points to provide the baseline shown in solid magenta. The remaining inactive stars, including all Hyades cluster members (750 Myr Gagne et al. (2018)) from our benchmark sample, were used to derive the quiescent activity level via a polynomial:

$$\text{EW } H\alpha^{\text{quiescent}}[\text{\AA}] = 3.2638 - 1.5798 \times (BP - K) + 0.3409 \times (BP - K)^2 - 0.0307 \times (BP - K)^3 \quad (2)$$

This quiescent level, shown as the magenta line in Figure 6, effectively traces the locus of mature, inactive K dwarfs across the full range of spectral types in our sample. The excellent agreement between our fit and the Hyades members provides confidence in our characterization, as these stars represent a population old enough to have settled into chromospheric quiescence, yet young enough as a cluster to provide a reasonable age estimate.

To distinguish chromospherically active stars from the quiescent population, we establish an activity threshold shown as the solid magenta line in Figure 6. This threshold is set 0.13 Å above the typical quiescent level (i.e., more negative in EW $H\alpha$), derived from the distribution of mature field stars including Hyades members. The threshold accounts

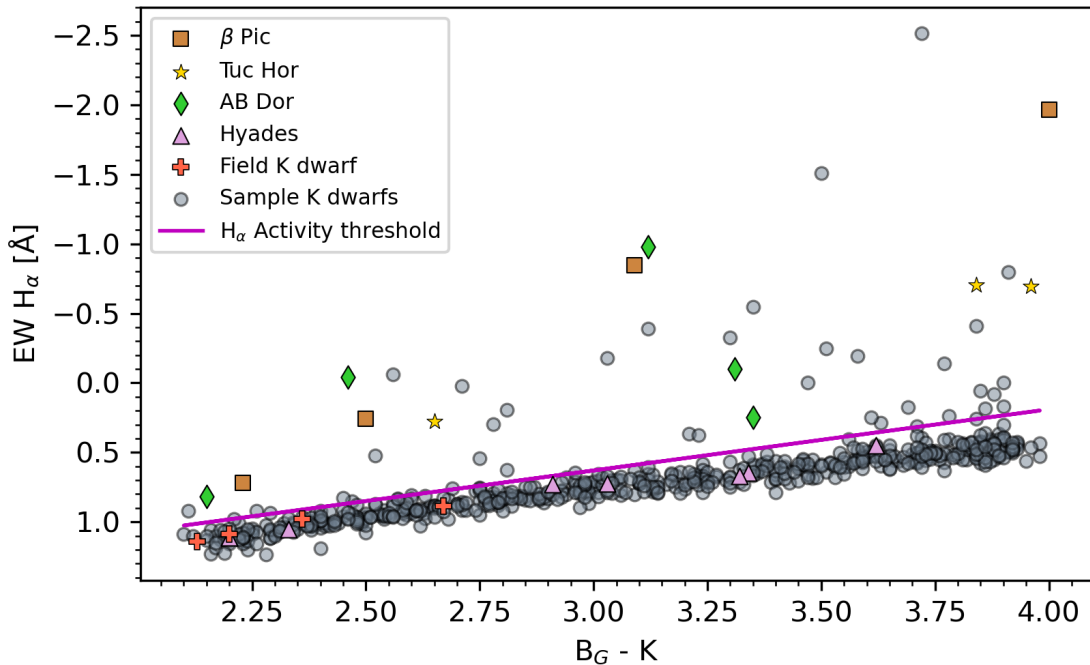


Figure 6. The equivalent width measurements for $H\alpha$ as a function of color. $EW H\alpha$ in emission is represented with negative values (toward the top of the plot). Gray circles represent 580 K dwarfs from the survey with $H\alpha$ values. The solid magenta line represents the typical quiescent level for K dwarfs, derived from the distribution of mature field stars, including Hyades members. Of the 580 K dwarfs, 36 (6.2%) stars fall above the activity threshold (magenta line) and are deemed chromospherically active, while the remaining 544 (93.8%) stars below this line are classified as calm. For comparison, K dwarfs with known ages from other methods are represented with markers other than circles: orange squares (β Pic), yellow stars (Tuc-Hor), green diamonds (AB Dor), pink triangles (Hyades), and orange crosses (mature field K dwarfs with ages of 0.3–5.7 Gyr). These comparison stars are described in Section 2 and Table 2 and serve as age calibrators.

for measurement uncertainties and intrinsic scatter in the quiescent population while providing clear separation for genuinely active stars. Stars falling above this threshold ($EW H\alpha$ more negative than the magenta line) are classified as chromospherically active and form the basis for our activity analysis in the following section.

5.3. $H\alpha$ Results: Activity

We apply the quiescent $H\alpha$ description established in the previous section to identify chromospherically active K dwarfs within our sample. This classification is essential for distinguishing mature, stable stellar environments from those with enhanced magnetic activity that could impact planetary habitability through increased variability and likely boosted high-energy radiation levels. Active stars produce elevated levels of UV and X-ray emission that may erode planetary atmospheres, alter atmospheric chemistry, and affect the potential for surface liquid water, all of which are critical factors in assessing exoplanet habitability (Richey-Yowell et al. 2019, 2022).

K dwarfs with $H\alpha$ EWs falling above the magenta line in Figure 6 (more negative EW values) are designated as chromospherically active, while those below the line are considered calm. Among the 580 stars in our sample, we find 36 (6.2%) that exhibit chromospheric activity, leaving 544 stars (93.8%) classified as calm. This relatively small fraction of active stars is consistent with the expectation that most field K dwarfs in the solar neighborhood are mature, having ages greater than approximately 1 Gyr, by which time chromospheric activity has usually declined to quiescent levels.

The spectral diversity within our active population reveals the complex nature of stellar chromospheric phenomena. Figures 7 and 8 display the $H\alpha$ and Li I spectral regions for representative active stars, illustrating a remarkable range of activity signatures. First, note that strong Li I absorption features do not necessarily imply strong $H\alpha$ emission, nor vice versa. The $H\alpha$ profiles in Figure 8 are particularly instructive, showing a clear progression of activity levels.

The uppermost spectra exhibit strong H α emission lines rising well above the continuum, characteristic of the most magnetically active stars with powerful chromospheric heating. These pure emission profiles indicate substantial non-thermal energy deposition in the chromosphere, likely from magnetic reconnection events (Cram & Mullan 1985; Hall 2008). Moving down the sequence, we observe double-peaked emission profiles, which serve as a signature of chromospheric structure where the line core forms higher in the atmosphere than the wings (Montes et al. 1997; Lopez-Santiago et al. 2010). Further down, the spectra transition to filled-in absorption profiles, where chromospheric emission partially compensates for photospheric absorption (Herbig 1985; Strassmeier et al. 1993). The spectra near the bottom of the plot show only subtle signs of activity, with H α absorption lines that are slightly weakened by modest chromospheric emission. This continuum of activity signatures demonstrates that chromospheric activity is not a binary phenomenon but rather exists along a spectrum from highly active to completely quiescent (Soderblom et al. 1993; Mamajek & Hillenbrand 2008).

In addition to H α , the Ca II infrared triplet line at 8542 Å provides a complementary diagnostic of chromospheric activity. Ca II core emission features for our sample stars can be viewed in the online spectral library⁴, which includes all four diagnostic spectral features for each star. Visual inspection of the online library clearly shows Ca II core emission in several active stars, providing independent confirmation of their chromospheric activity. While our current analysis focuses on H α as the principal activity indicator, the Ca II infrared triplet represents a valuable complementary diagnostic that will be investigated in depth when the larger sample has been observed and analyzed, to be presented in a forthcoming paper (Carrasco-Gaxiola et al., in prep).

The spectral gallery presented in Appendix B (Figures 16–20) showcases H α and Li I features for all 53 young, active, or otherwise unique stars from our sample. Most stars display H α absorption profiles with varying degrees of chromospheric filling, while Figure 19 (Group D) demonstrates prominent core emission features in four particularly active systems, with the central emission spike clearly visible in the H α panel.

The identification of chromospheric activity in 36 stars of our sample leaves 554 K dwarfs classified as chromospherically calm based on their H α measurements. This activity classification represents only one component of our comprehensive stellar characterization. While H α emission effectively identifies stars with active chromospheres, it does not distinguish between activity driven by youth versus activity maintained by other mechanisms such as close stellar companions or rapid rotation (Mamajek & Hillenbrand 2008). To address this limitation and to provide a more complete picture of stellar ages within our sample, we next examine lithium abundance as an independent indicator of stellar youth. The relationship between H α activity and lithium detection aims to reveal which of our active stars are genuinely young versus those that maintain activity through alternative mechanisms.

5.4. Lithium Results: Youth

While chromospheric activity points to stellar magnetic phenomena often associated with young stars, lithium detection provides a more definitive diagnostic for stellar youth. Lithium is destroyed by nuclear burning processes in stellar interiors, with depletion timescales directly tied to stellar mass and age (Soderblom 2010). G and K dwarfs younger than ~ 1 Gyr retain lithium at a level where spectral features can be seen, making Li I a robust age diagnostic less susceptible to confounding factors that influence activity indicators. This distinction is critical for identifying stars that are intrinsically young versus those maintaining activity through other mechanisms.

In this study, we report equivalent widths of the Li I doublet feature detected using our Voigt profile fitting methodology described in § 4. We use lithium presence as a yes/no youth indicator, classifying stars with detectable Li I as young and confirming that the features are real via visual inspection for quality control. The Hyades cluster (~ 750 Myr) provides a useful age benchmark, as K dwarfs in the Hyades show no detectable lithium and have well-determined ages from main-sequence turnoff fitting (Perryman et al. 1998), white dwarf cooling timescales (De Gennaro et al. 2009), and eclipsing binary analysis (Lebreton et al. 2001). Future papers in this series will explore quantitative age estimates using Li I depletion models (Soderblom 2010).

In the high resolution spectra provided by CHIRON, the Li I doublet at 6707.8 Å is clearly resolved from the nearby Fe I line at 6707.4 Å, eliminating line blending corrections required in previous optical lithium surveys (White et al. 2007), except for the very strongest Li I absorption features in which the weak Fe I line is then negligible. We establish a detection threshold of $\text{EW Li I} = 15 \text{ m}\text{\AA}$ for reliable lithium identification, and classify stars with $\text{EW Li I} \geq 15 \text{ m}\text{\AA}$ as young.

⁴ https://hodarijames.github.io/spectral_library/page1.html

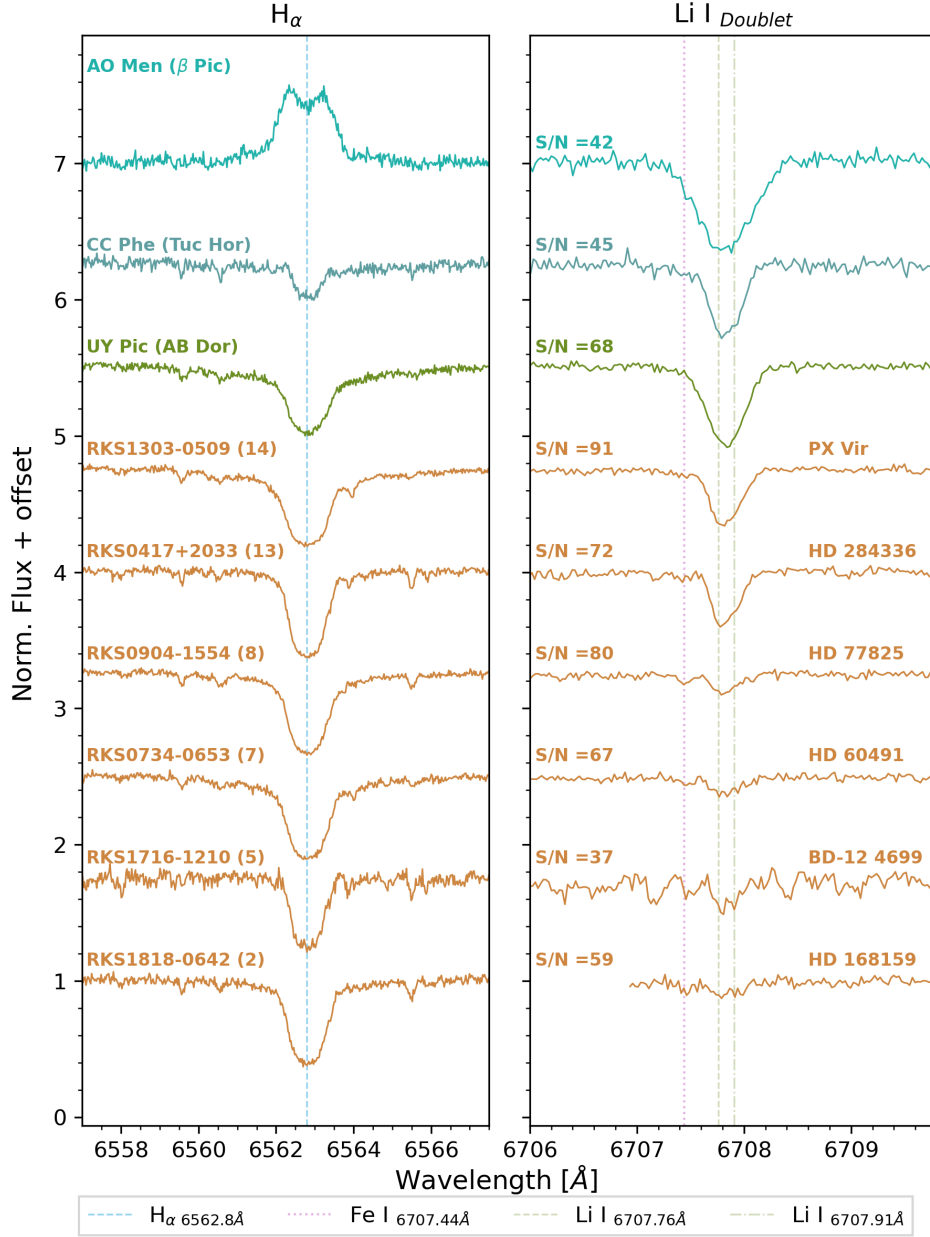


Figure 7. Panels showing the spectral regions of $H\alpha$ and Li I for K dwarfs with known ages and young K dwarfs from our analysis. Spectra in colors other than orange represent stars with known ages studied in [Hubbard-James et al. \(2022\)](#), where names from SIMBAD are given and the associated moving groups are in parentheses. Spectra in orange show six young K dwarfs from our analysis. For these spectra, the left panel includes the RKSTAR ID names and numbers used in [Figure 9](#), and the right panel includes names from SIMBAD. Vertical lines in different styles and colors show the centers of the lines of interest in the rest frame, given in the box below the main plot.

[Figure 9](#) illustrates the relationship between lithium detection and chromospheric activity, showing EW $H\alpha$ vs. EW Li I for active and/or young K dwarfs from the survey along with comparison stars of known ages from [Hubbard-James et al. \(2022\)](#). Applying our detection threshold to the complete sample of 580 K dwarfs, we identify 19 stars (3.3%) with measurable abundances of lithium. These young stars appear as purple circles in [Figure 9](#), numbered 1–19 as Li I strength increases. Red circles represent active K dwarfs from § 5.3 that do not show Li I features, while the gray histogram shows the distribution of mature quiescent stars that comprise the bulk of the population.

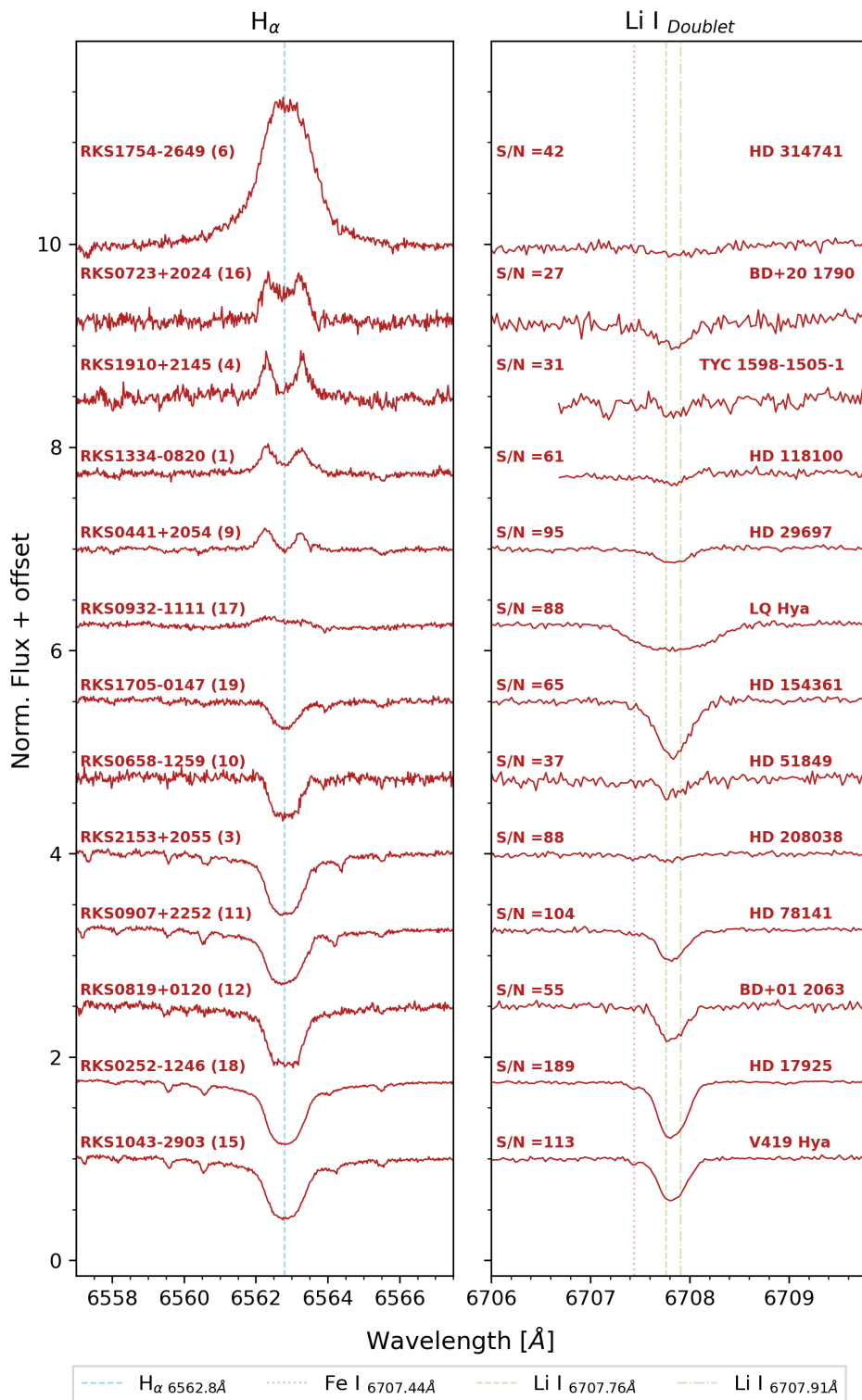


Figure 8. Panels showing the spectral regions of H α and Li I for 13 young and active K dwarfs from our analysis. The left panel includes the RKSTAR ID names and numbers used Figure 9, and the right panel includes names from SIMBAD. Vertical lines in different styles and colors show the centers of the lines of interest in the rest frame, given in the box below the main plot.

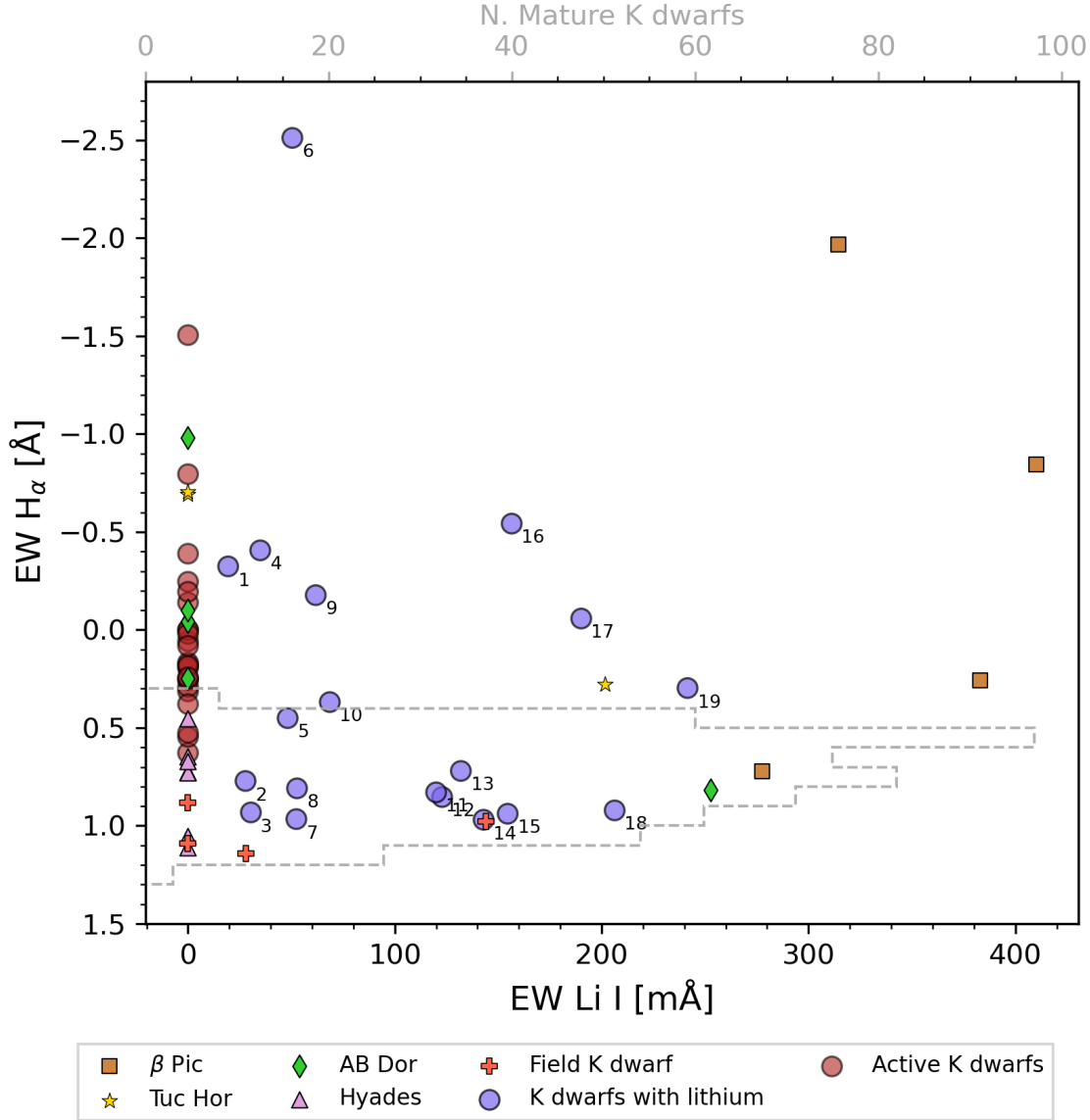


Figure 9. EW $H\alpha$ vs. EW Li I for 43 chromospherically active and/or young K dwarfs from the survey, plus K dwarfs with known ages for comparison. Circles in red represent active K dwarfs with no discernable Li I features. Circles in purple represent young K dwarfs with Li I absorption features. Numbers at the lower right of each circle are sorted from weaker to stronger EW Li I (see Table 6 for star identifications). Stars with known ages from other methods are represented with markers other than circles: orange squares (β Pic), yellow stars (Tuc-Hor), green diamonds (AB Dor), pink triangles (Hyades), and orange crosses (mature field K dwarfs with ages of 0.3–5.7 Gyr). These comparison stars are described in Section 2 and Table 2 and serve as age calibrators. PX Vir (0.3 Gyr) is the youngest field star. The overplotted histogram in gray represents the number of mature K dwarfs in our sample which have no Li I detection and weak EW $H\alpha$ relative to the activity threshold. The overplotted histogram in gray represents the numbers of mature K dwarfs in our sample with no Li I detections.

The spectral evidence for lithium detection for the 19 survey K dwarfs is displayed in Figures 7 and 8. Clear Li I absorption features are visible at 6707.8 \AA , with RKSTAR IDs and figure numbers shown in the left panels and SNR values along with names from SIMBAD in the right panels. Figure 7 shows $H\alpha$ and Li I spectral regions for 3 comparison stars with known ages from young moving groups (β Pic, Tuc-Hor, and AB Dor) (see Section 2 and Table 2) and 6 young stars in orange from our analysis that are not demonstrably active. Figure 8 presents $H\alpha$ and Li I spectral regions for 13 additional young K dwarfs that do exhibit $H\alpha$ features indicative of activity.

As mentioned previously, there is not a one-to-one correlation between $H\alpha$ and Li I EWs. Of the 19 lithium detections, 13 also exhibit chromospheric activity while 6 show lithium without significant $H\alpha$ emission. An additional 24 stars display activity without lithium, indicating older yet still magnetically active systems. In total, 43 stars (7.4%) are classified as young and/or active, leaving 537 stars (92.6%) that are mature and quiescent.

Comparisons to stars with known ages validate our methodology. Moving group K dwarfs (β Pic, Tuc-Hor, AB Dor) and Hyades members show expected lithium depletion trends. Of the 580 stars observed in the survey, PX Vir emerges as the single youngest field star (0.3 Gyr), demonstrating that isolated young K dwarfs are rare, but present, in the solar neighborhood. The 537 mature, calm stars represent prime targets for terrestrial planet searches, offering now-stable radiation environments given that their ages are likely beyond 1 Gyr.

6. KINEMATICS

6.1. *Gaia* Astrometry

Following our comprehensive spectroscopic characterization of stellar properties, activity status, and ages, we now examine the kinematic properties of our K dwarf sample to understand their dynamical context within the Galaxy. Stellar kinematics provide crucial insights into Galactic structure and evolution, as different stellar populations exhibit characteristic velocity distributions that reflect their formation histories and subsequent dynamical evolution (Freeman & Bland-Hawthorn 2002; Bland-Hawthorn & Gerhard 2016). The well-established relationships between stellar kinematics, age, and metallicity (Edvardsson et al. 1993; Nordström et al. 2004; Casagrande et al. 2011) make this analysis essential for placing our spectroscopic results in a broader Galactic context. By determining three-dimensional space motions for our sample, we can associate individual stars with moving groups, stellar associations, and broader Galactic populations, while also identifying stars with unusual motions that may indicate non-standard evolutionary histories or membership in disrupted stellar systems.

Our kinematic analysis utilizes high-precision astrometric measurements from *Gaia* Data Release 3, including celestial coordinates, proper motions ($\mu_{R.A.}$, μ_{Decl}), and trigonometric parallaxes (ϖ) (Gaia Collaboration et al. 2022). These astrometric parameters, combined with systemic radial velocities (γ_{REC}) derived from our CHIRON spectroscopic observations, enable accurate determination of UVW space velocities in the Galactic coordinate system, where U points toward the Galactic center, V aligns with Galactic rotation, and W points toward the north Galactic pole. Essential kinematic data for 572 of the 580 stars in our survey, including both *Gaia* and CHIRON radial velocity measurements ($\gamma_{Gaia_{DR3}}$ and γ_{REC}), measurement uncertainties ($\sigma_{\gamma_{REC}}$), derived UVW velocities, and population assignments are compiled in Table 9 in Appendix D. These kinematic measurements form the foundation for identifying Galactic population membership and understanding the relationships between the stellar properties characterized in § 5 and the broader context of Galactic chemical and dynamical evolution.

6.2. CHIRON γ Velocities

Using the methodology described in § 4.5, we derived systemic radial velocities (γ velocities) for 574 of the 580 K dwarfs in the survey sample. The results are given in Table 9 in Appendix D, spanning values of +116 to -133 km s^{-1} , with one additional star at $+310 \text{ km s}^{-1}$ that turns out to be a halo star. These measurements, combined with *Gaia* DR3 astrometry, provide the foundation for our kinematic analysis and enable direct comparison with space-based radial velocity determinations.

Figure 10 compares our CHIRON-derived γ velocities with corresponding measurements from *Gaia* DR3. The majority of stars (554, or 95%) follow the expected 1-to-1 correlation, validating our measurement methodology and the consistency between ground-based and space-based radial velocity determinations. The remaining 18 stars exhibit significant deviations from this relationship, marked with boxed letters ‘a’ through ‘s’ (excluding ‘i’, see below) and are identified in the Figure 10 caption. The 18 outliers represent a diverse population of stellar systems with velocity discrepancies between CHIRON and *Gaia* measurements. These are labeled as follows: [a] RKS0236-0309 (variable star), [b] RKS0258+2646 (unknown), [c] RKS0626+1845 (binary and active), [d] RKS0907+2252 (young and active), [e] RKS1108-2816 (unknown), [f] RKS1253+0645 (binary, known SB1), [g] RKS1303-0509 (young), [h] RKS1504-1835 (binary, known SB1), [j] RKS1528-0920 (binary, known SB2), [k] RKS1555+1602 (variable star), [l] RKS1605-2027 (binary, known SB2), [m] RKS1833-1626 (new SB2), [n] RKS1855+2333 (active), [o] RKS2041-2219 (active), [p] RKS2108-0425 (active), [q] RKS2119-2621 (binary, known SB1), [r] RKS2308+0633 (active), [s] RKS2345+2933 (binary, known SB1). These outliers include known binary systems observed at different orbital phases,

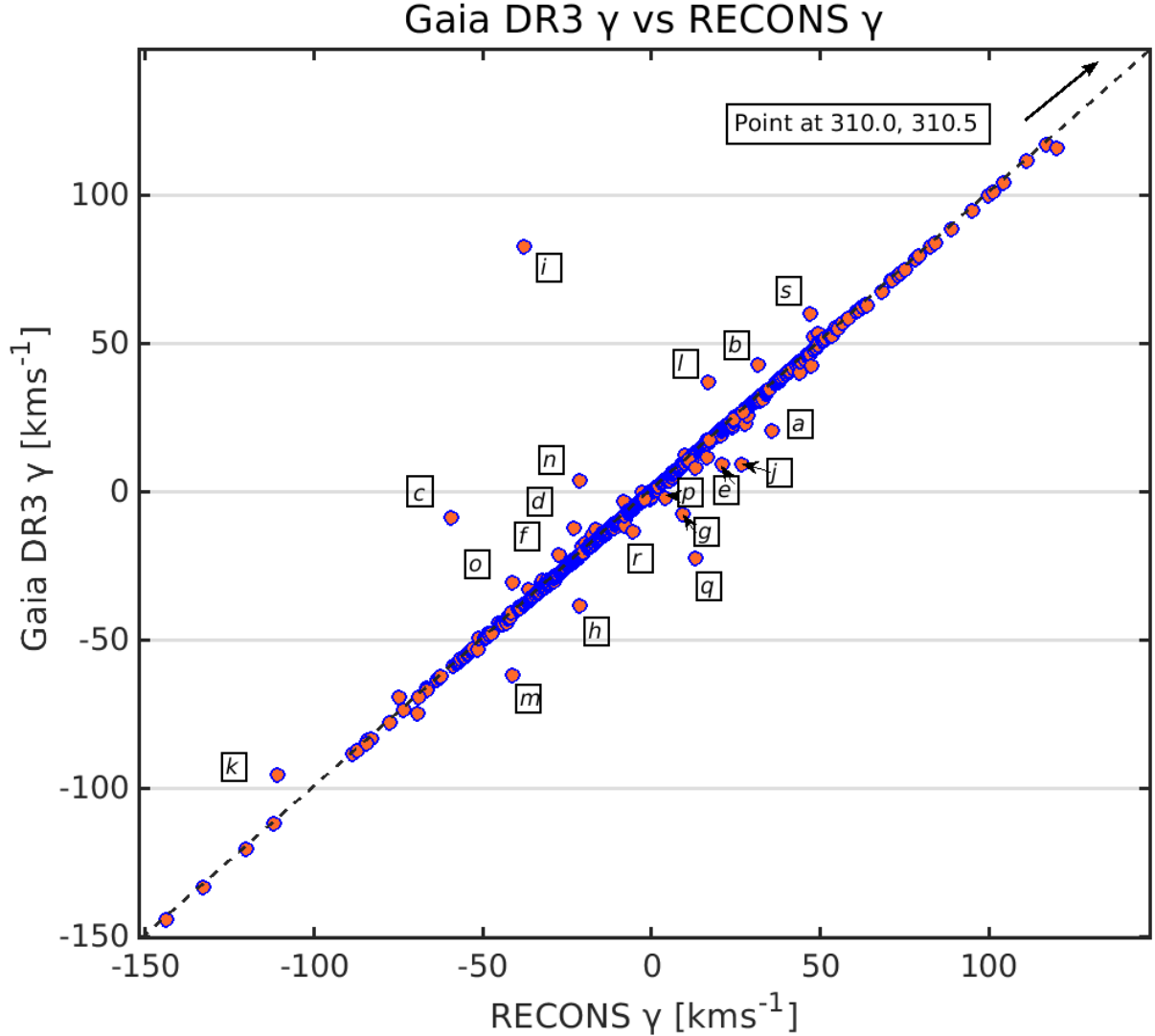


Figure 10. Comparison between our RECONS γ velocities from CHIRON observations and *Gaia* DR3 radial velocities showing an overall 1-to-1 correlation, with only 18 stars in our survey sample showing significant deviations, labeled \boxed{a} through \boxed{s} , excluding \boxed{i} . Star identifications and classifications are discussed in the text.

chromospherically active stars with activity-induced line profile variations, young stars with similar spectroscopic complications, and newly discovered spectroscopic binaries.

We include one additional notable outlier (RKS1518-1837, BD-18 4031, labeled \boxed{i}) from our broader RECONS observations that, while the K dwarf was excluded from the survey sample during quality control, provides an instructive example of radial velocity discrepancies. Among the most intriguing examples from our broader observations, this star shows a substantial radial velocity difference between our measurements and *Gaia* values. Follow-up observations revealed that this star hosts a companion in a highly eccentric orbit ($e = 0.922$) with a period of 1636 days (4.5 years), as illustrated in Figure 11. The large semi-amplitude of more than 11 km s^{-1} suggests that the companion may be a white dwarf, although the orbital inclination remains unknown, preventing a definitive determination of the mass. Thus, because the white dwarf progenitor would originally have been the more massive star in the system, this K dwarf was removed from the survey sample. This case shows how radial velocity discrepancies can reveal hidden stellar multiplicity and contribute to our understanding of the binary fraction of K dwarfs.

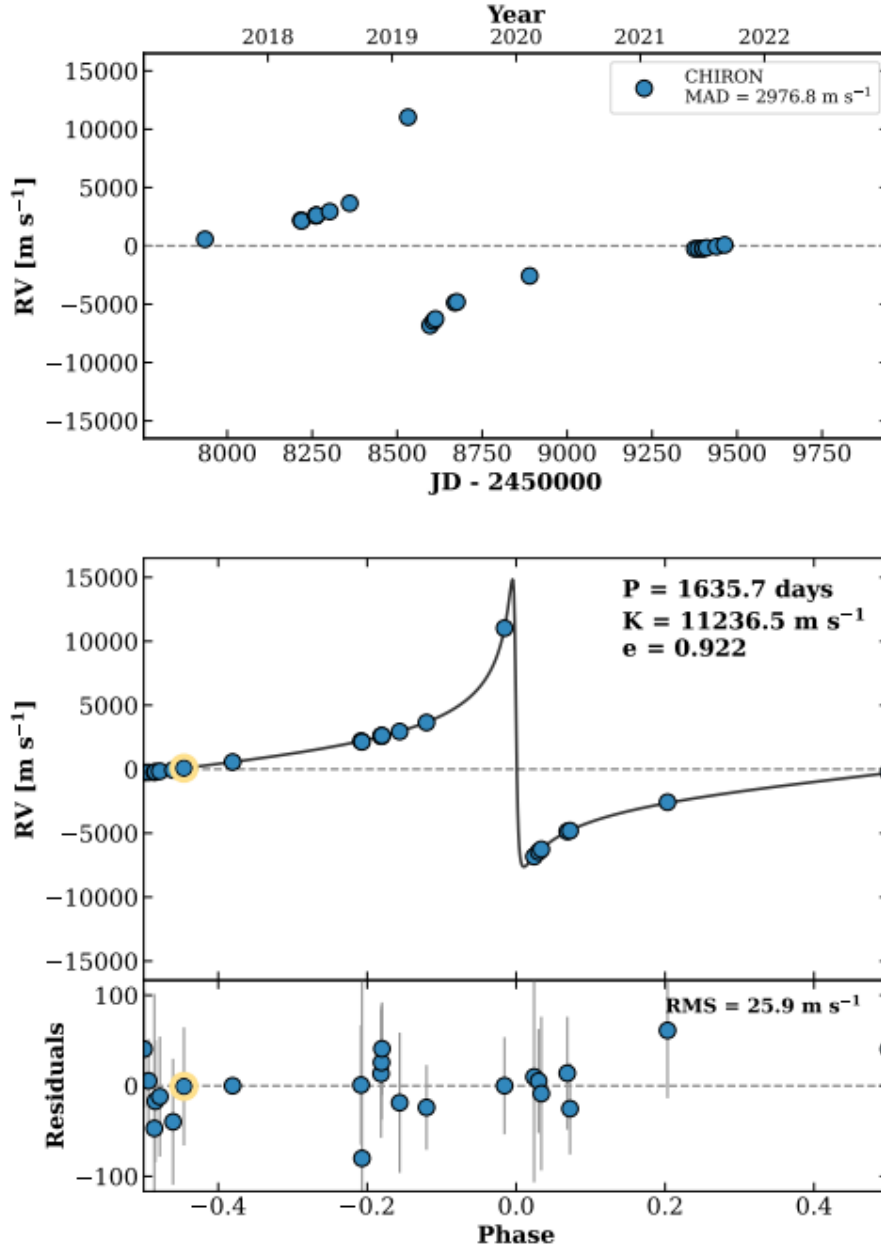


Figure 11. Radial velocity measurements of RKS1518-1837 (BD-18 4031) showing obvious variations over the 2018-2021 observing period (top panel) and phase-folded orbital solution revealing a companion in a highly elliptical orbit with eccentricity $e = 0.922$ and period of 1636 days (bottom panel). This companion is likely a white dwarf, so the K dwarf is not included in our survey sample. This system provides an instructive example of binary detection through radial velocity monitoring. The data are from Paredes (2022).

6.3. Using UVW Space Motions to Identify Young K Dwarfs

The three-dimensional space motions (UVW) for stars in our sample provide an independent method for identifying young stars through kinematic association with nearby moving groups and stellar clusters. This kinematic approach serves as a crucial complement to the spectroscopic age indicators discussed in § 5, as stellar kinematics preserve the signature of stellar formation environments even after spectroscopic youth markers have faded or become undetectable. Young stellar associations retain coherent space motions for hundreds of millions of years, allowing kinematic identification of group members that may have depleted their lithium or ceased exhibiting strong chromospheric activity (Soderblom 2010; Mamajek & Bell 2014; Gagne et al. 2018).

Figure 12 illustrates the distribution of our sample in Galactic velocity space using three diagnostic projections: V vs U , W vs U , and W vs V for 572 K dwarfs. The plots can be used to reveal stars that share common space motions with well-characterized young stellar associations, providing an age-dating method independent of stellar atmospheric diagnostics. Using established kinematic criteria and the BANYAN Σ methodology (Gagne et al. 2018), we identified 11 stars with space motions consistent with known moving groups. Our membership assignment required two criteria: (1) BANYAN Σ membership probability exceeding 95%, and (2) UVW velocities falling within 2σ of the mean group velocities, where σ represents the intrinsic velocity dispersion of each association (Riedel et al. 2014). The 2σ ellipses shown in Figure 12 visualize these kinematic boundaries and encompass approximately 95% of expected group members based on their velocity dispersions.

This approach identified seven stars exhibiting kinematics matching the Hyades cluster ($UVW = [-41, -19, -1]$ km s $^{-1}$; $\sigma = [2.0, 2.0, 2.0]$ km s $^{-1}$) and four stars showing motions consistent with the AB Doradus moving group ($UVW = [-7, -27, -13]$ km s $^{-1}$; $\sigma = [1.3, 1.2, 1.6]$ km s $^{-1}$) (Riedel et al. 2014). The UVW space motions for the stars in our sample, including moving group assignments, are provided in Table 9 in Appendix D. Remarkably, 8 of the 11 kinematically-identified young stars were *not* detected through our spectroscopic analysis described in § 5, demonstrating the complementary nature of kinematic and spectroscopic age indicators. These six Hyades members and two AB Doradus members are listed in Table 6 with the designation “Y-MG” to distinguish them from stars showing spectroscopic youth signatures. The remaining three moving group members (RKS0121+2419, RKS0723+2024, and RKS1633-0933) were independently identified as young or active through our spectroscopic analysis.

This kinematic approach effectively increases our count of young or active stars from 43 (identified spectroscopically in § 5) to 51, representing 8.8% of our survey sample and highlighting the importance of multi-faceted approaches to stellar age determination. The identification of moving group members through kinematics reveals additional young stars that have depleted their lithium or lack strong chromospheric activity signatures but retain the kinematic memory of their birth environments — such stars would be missed in lithium and activity surveys alone. These results underscore the complex relationship between stellar age, activity, and observable diagnostics, emphasizing that comprehensive stellar characterization requires both spectroscopic and kinematic analysis. The result leaves us with 529 mature and inactive K dwarfs in our sample, shown in Table 7 as 91.2% of our stars.

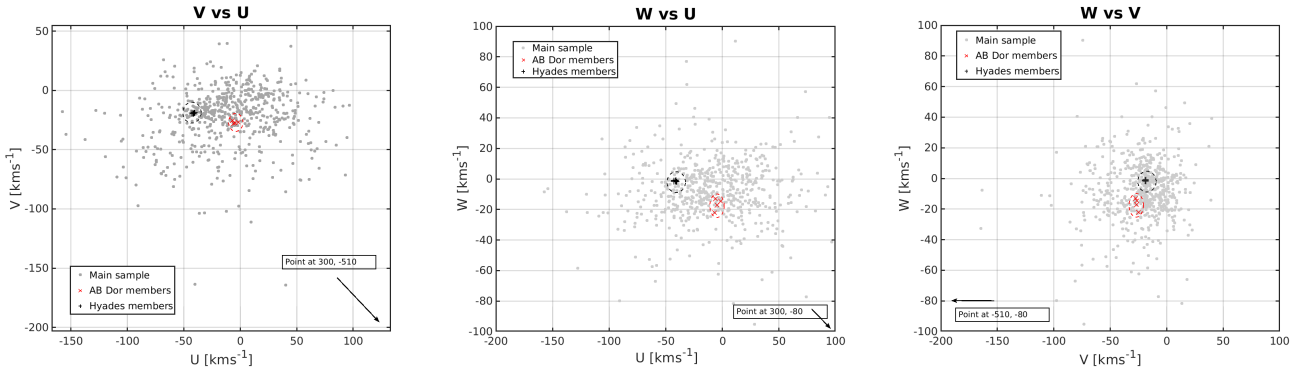


Figure 12. Galactic space motion diagrams for 572 K dwarfs showing kinematic identification of moving group members: (a) V vs U velocities, (b) W vs U velocities, and (c) W vs V velocities. Field stars are shown as grey circles, Hyades cluster members as black crosses, and AB Doradus moving group members as red Xs. The black ellipse (Hyades) and red ellipse (AB Dor) represent 2σ velocity dispersion boundaries based on the mean UVW velocities and velocity dispersions from Riedel et al. (2014). These ellipses encompass approximately 95% of expected group members. Moving group member identifications are provided in Table 6.

6.4. Identifying Galactic Populations via UVW Space Motions

We now examine the broader Galactic population structure within our K dwarf sample. This classification utilizes the UVW space motions compiled in Table 9 in Appendix D to distinguish between the primary stellar populations of the Milky Way: the thin disk, thick disk, and halo components. Each population exhibits characteristic velocity distributions that allow us to place our K dwarf sample in the context of Galactic structure and evolution.

Figure 13 presents a Toomre diagram for our characterized sample, plotting the total random velocity $\sqrt{U^2 + W^2}$ against the V component of Galactic motion. This diagnostic effectively separates stellar populations based on their kinematic properties. Dotted curves at velocities of 75 km s^{-1} and 180 km s^{-1} from [Bensby et al. \(2003\)](#) and [Hinkel et al. \(2014\)](#) provide provisional demarcations between populations. In the sample of 572 stars with UVW values, we find 464 thin disk stars (80%), 107 thick disk stars (18.4%), and 1 halo star (0.2%); these are represented graphically as squares and triangles, with the single point for the halo star well off the plot, in Figure 13. An additional 8 stars could not be reliably classified due to measurement limitations. The adjacent color bar indicates the metallicity ($[Fe/H]$) for each star, revealing the well-known metallicity-kinematics correlation.

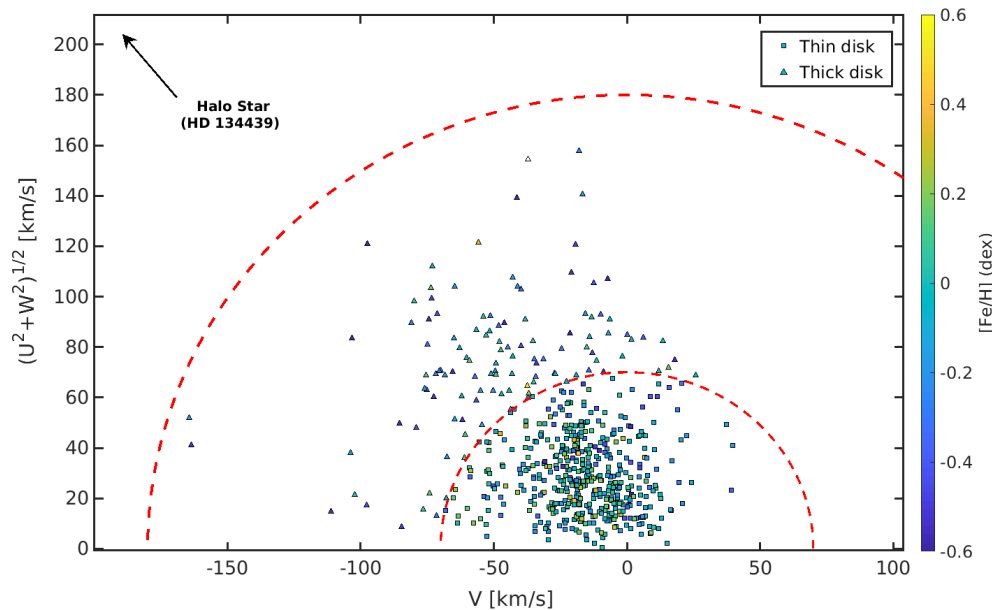


Figure 13. A Toomre diagram of 572 K dwarfs with UVW values helps distinguish Galactic populations. The dotted curves at 75 km s^{-1} and 180 km s^{-1} roughly delineate the thin disk, thick disk, and halo populations. The thin disk (squares), thick disk (triangles), and halo (off the plot) contain 464, 107, and 1 stars, respectively. The adjacent color bar indicates the metallicity ($[Fe/H]$) for each star.

The metallicity distributions of these populations, shown in Figure 14, reveal significant differences between the thin and thick disk components. Our thin disk sample has a mean $[Fe/H]$ of -0.05 dex, while the thick disk has a mean of -0.21 dex, indicating the thick disk population is approximately 30% more metal-poor. These proportions align remarkably well with previous studies: our 18.3% thick disk fraction compares favorably with the 18% reported by [Hinkel et al. \(2014\)](#) for a sample of over 2000 nearby stars, and agrees with the comparable value of $\sim 20\%$ from [Adibekyan et al. \(2013\)](#). However, our metallicity difference of ~ 0.16 dex between populations is somewhat smaller than the $0.2\text{--}0.3$ dex differences reported for nearby stars ([Feltzing et al. 2003](#); [Reddy et al. 2006](#)), and is predictably smaller than the ~ 0.5 dex differences found in studies covering larger Galactic volumes that include stars with more extreme metallicity values ([Ivezić et al. 2008](#)).

A striking result from our kinematic analysis is the strong correlation between stellar age and Galactic population membership. Combining our spectroscopic results from § 5 with the kinematic identifications from § 6.3, we identify 51 young or active K dwarfs in our sample. Of these, only two belong to the thick disk population: HD 196998 (RKS2041-2219, DG Cap) and HD 7808 (RKS0117-1530). HD 196998 is an SB1 system that exhibits radial velocity variations and was identified as active in our benchmark study ([Hubbard-James et al. 2022](#)), while HD 7808 was identified as active through our spectroscopic analysis. The remaining 49 young or active stars are thin disk members, reinforcing the expected relationship between stellar age and kinematic properties.

The most remarkable object found in our kinematic analysis is HD 134439 (RKS1510-1622, also known as LHS 53 or GJ 579.2), which appears as the lone outlier in Figure 13. This high proper motion ($\mu = 3.68'' \text{ yr}^{-1}$), high velocity

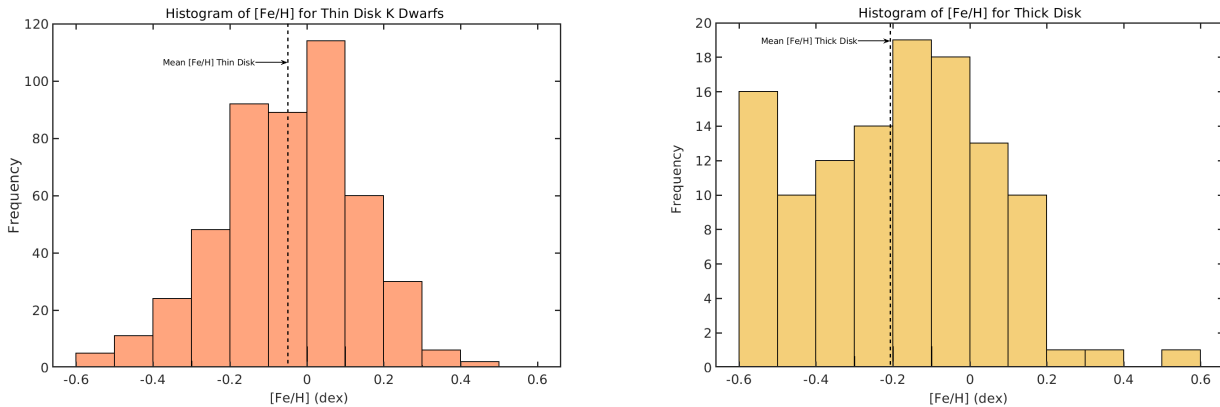


Figure 14. Histograms illustrating the $[Fe/H]$ distribution of K dwarfs in our sample in two distinct populations within the Milky Way Galaxy. The left histogram represents the thin disk population, with a mean $[Fe/H]$ value indicated by a vertical dashed line at -0.05 dex. The right histogram represents the thick disk population, with a mean $[Fe/H]$ value indicated by a vertical dashed line at -0.21 dex.

($\gamma = +310 \text{ km s}^{-1}$) K dwarf at a distance of 29.4 pc is a known metal-poor subdwarf with $[Fe/H] < -1.0$ dex, likely accreted from a disrupted dwarf galaxy (Lim et al. 2021). Its extreme kinematics place it firmly in the halo region of velocity space, making it the only halo star in our sample. As noted in § 4.1, this star exhibits a unique spectrum that falls outside the boundaries of the abridged ESM library shown in Figure 16, preventing standard stellar parameter determination and highlighting its unusual nature among nearby K dwarfs.

7. DISCUSSION

7.1. Population Summary

The combined results of our spectroscopic and dynamic analyses reveal the activity and age population characteristics of the nearby K dwarfs in unprecedented detail. Table 7 summarizes our stellar classifications. The overwhelming majority of K dwarfs in the solar neighborhood — 91.2% (529 stars) — are chromospherically quiescent (showing no $H\alpha$ excess), mature (showing no Li I feature), and are not part of a young moving group or cluster. This sample of “calm, mature” stars is an exceptional resource for future exoplanet surveys targeting potentially habitable worlds.

The remaining 8.8% (51 stars) of K dwarfs in the survey exhibit activity, have Li I absorption features, or are members of young moving groups or clusters. Of these, 24 (4.1%) are active based on $H\alpha$ measurements but do not appear to be young, and 14 (2.4%) are presumably young because they have Li I features or are members of young groups or clusters but are quiescent in $H\alpha$. A modest number of 13 stars (2.2%) show both $H\alpha$ activity and Li I absorption. This latter group demonstrates that stellar activity and age are related but not matched phenomena, with some young stars maintaining relatively quiet chromospheres while some older stars sustain magnetic activity, perhaps through mechanisms such as tidal interactions caused by close companions.

Kinematically, our sample reflects the expected Galactic population structure of the solar neighborhood as shown in Table 7, with 464 stars (80.0%) belonging to the thin disk, 107 stars (18.4%) to the thick disk, and one halo member (0.2%). The stellar properties span effective temperatures from 3600 to 5500 K and metallicities from -0.6 to $+0.4$ dex, with a mean metallicity of -0.02 dex indicative of the solar neighborhood’s composition. Notably, 413 stars (71.2%) exhibit solar-like metallicities (-0.2 to $+0.2$ dex), while 20 stars (3.4%) are metal-poor with $[Fe/H] < -0.5$ dex. The metal-poor population shows no overlap with the young or active stars, highlighting a clear separation between chemically distinct stellar populations and their evolutionary states.

7.2. Exoplanet Host Stars: Current Status and Metallicity Trends

K dwarf stars have garnered significant attention as potentially optimal hosts for habitable worlds, often termed “super-habitable” for planets, due to their favorable balance of properties: longer main-sequence lifetimes (17–70 Gyr) than solar-type stars, reduced activity compared to M dwarfs (Richey-Yowell et al. 2019), and habitable zones positioned at distances that avoid tidal locking (Kasting et al. 2014; Cuntz & Guinan 2016). As illustrated in Figure 1, K dwarfs have been systematically underexplored in exoplanet surveys compared to G and M dwarfs, making

Table 7. Population Summary of 580 K Dwarf Survey Sample

Population Category	Number	Percentage
Activity/Age Classifications:		
Mature, quiescent (calm)	529	91.2%
Active only (H α , no Li)	24	4.1%
Young only (Li or kinematic)	14	2.4%
Young and active (both)	13	2.2%
Unclassified	0	...
Galactic Populations:		
Thin disk	464	80.0%
Thick disk	107	18.4%
Halo	1	0.2%
Unclassified	8	1.4%
Metallicity:		
Metal-rich ([Fe/H] > +0.2 dex)	32	5.5%
Solar metallicity (+0.2 to -0.2 dex)	408	70.3%
Lower metallicity (< -0.2 to -0.5 dex)	111	19.1%
Metal-poor ([Fe/H] < -0.5 dex)	20	3.4%
Unclassified	9	1.6%

direct occurrence rate comparisons difficult with current data. Our comprehensive characterization of 580 nearby K dwarfs provides crucial empirical data to evaluate these claims and identify the most promising stellar hosts for future exoplanet surveys and habitability assessments.

According to the NASA Exoplanet Archive (NASA Exoplanet Science Institute 2020)⁵, as of July 2025, 44 of our 580 K dwarfs (7.5%) host a total of 72 confirmed planetary companions. Given that many of these stars have not yet been systematically searched for planets, this is certainly an underestimate of the true planetary occurrence rates around these stars. In fact, K dwarfs have been systematically overlooked in major planet-hunting surveys because they are fainter than G dwarfs at equivalent distances and less amenable to ultra-precise radial velocity measurements than M dwarfs that are observed to reveal terrestrial planets (Lillo-Box et al. 2022).

Figure 15 (top panel) reveals that exoplanet host stars are distributed across the full range of stellar metallicities in our sample, from metal-poor systems like HD 26965 and HD 96758 with $[Fe/H] = -0.4$ to metal-rich hosts such as 55 Cancri and HD 98736 with $[Fe/H] = +0.4$.⁶ While K dwarf exoplanet hosts span the complete metallicity distribution, the bottom panel of Figure 15 demonstrates that planetary mass shows a clear correlation with host star metallicity. Jupiter-mass planets ($M_p \gtrsim 1 M_{Jup}$) preferentially orbit metal-rich hosts with $[Fe/H] > 0$, consistent with the well-established giant planet-metallicity correlation (Fischer & Valenti 2005; Buchhave et al. 2014). In contrast, lower-mass planets (Neptune-mass and below) show no strong metallicity preference and are found around both metal-rich and metal-poor K dwarfs across our sample.

This differential metallicity dependence has important implications for habitability prospects. Previous studies have demonstrated that planets of various sizes form around stars with diverse metallicities, though with different formation mechanisms: terrestrial and small planets show weak or no metallicity correlations (Buchhave et al. 2012; Mann et al. 2013; Gaidos et al. 2016), while giant planet formation shows a strong preference for metal-rich environments through core accretion (Fischer & Valenti 2005; Buchhave et al. 2014). Our K dwarf sample exhibits this same pattern, with Jupiter-mass planets concentrated above $[Fe/H] > 0$ while lower-mass rocky worlds appear across the full metallicity range observed in Figure 15. This suggests that even the metal-poor K dwarfs in our sample (21 stars with $[Fe/H] \leq -0.5$ dex, comprising 3.6% of the population) could harbor terrestrial planetary systems, potentially expanding the Galactic real estate available for life beyond the metal-rich thin disk population.

⁵ <https://exoplanetarchive.ipac.caltech.edu/>

⁶ 55 Cancri hosts five confirmed planets, including 55 Cancri f in the liquid-water zone, although with $M_p \sin i = 45.8 \pm 12.7 M_{\oplus}$, this world likely lacks a solid surface conducive to surface-based life (Fischer et al. 2008).

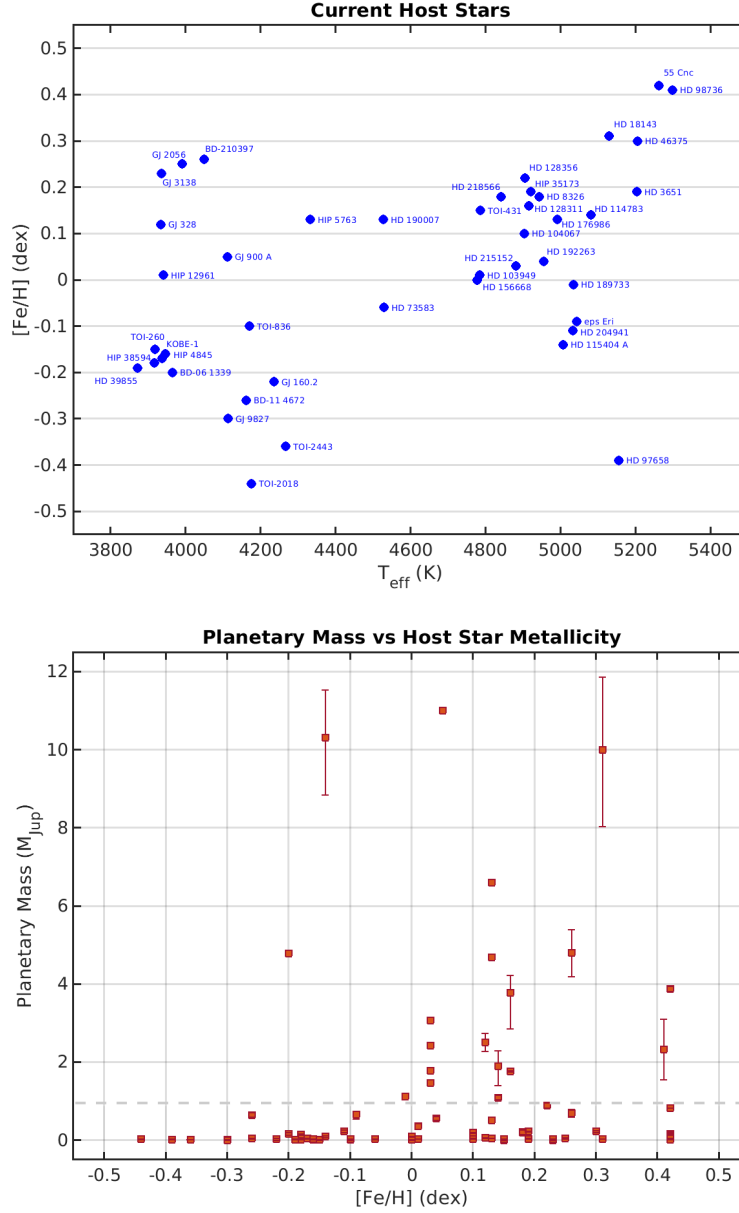


Figure 15. Exoplanet host properties for 44 nearby K dwarfs in our sample reported to have planets in the NASA Exoplanet Archive (NASA Exoplanet Science Institute 2020) as of July 2025. Top: Distribution of the 44 host stars in $[Fe/H]$ vs. T_{eff} space, with stellar parameters determined via ESM. Star names are labeled using NASA Exoplanet Archive identifiers. Bottom: Planetary mass vs. host star metallicity for the 72 planets orbiting these 44 K dwarfs. The horizontal dashed line at $M_p = 1 M_{\text{Jup}}$ marks Jupiter’s mass for reference. Error bars on planetary masses are shown where available from the NASA Exoplanet Archive.

7.3. Stellar Activity and the K Dwarf Habitability Paradigm

Recent work has raised questions about whether K dwarfs truly offer the most favorable conditions for habitable worlds. Richey-Yowell et al. (2019) conducted the first comprehensive investigation of X-ray and UV evolution in K stars, finding that these stars maintain elevated high-energy flux levels longer than previously assumed. Their follow-up spectroscopic analysis (Richey-Yowell et al. 2022) revealed that K dwarf UV emission remains nearly constant for the first 650 Myr before declining, in stark contrast to early M dwarfs, which begin UV decline after only a few hundred megayears. Most critically, they demonstrated that K dwarfs experience “rotational stalling” during their

first gigayear, maintaining rotation periods near 10 days and sustaining chromospheric and coronal activity levels comparable to young M dwarfs. This prolonged active phase appears to extend far beyond the typical timescales needed for at least initial atmospheric creation on terrestrial planets, potentially subjecting habitable zone worlds to damaging UV radiation for hundreds of millions of years longer than anticipated.

These findings suggest that the K dwarf advantage may be more nuanced than originally proposed. While K dwarfs ultimately settle into long-lived, quiescent phases ideal for hosting stable atmospheres, the extended juvenile active period may delay rather than prevent the emergence of habitable conditions. It could be that planets around K dwarfs require additional time to develop and retain thick atmospheres capable of supporting liquid water and potentially life (Airapetian et al. 2020). Thus, this delayed habitability timeline does not necessarily eliminate K dwarfs as premier planetary hosts. The extraordinary main-sequence lifetimes of K stars (17–70 Gyr) provide ample time for atmospheric recovery and the development of complex ecosystems, even if there are extended active phases. Furthermore, planets with substantial initial volatile inventories or efficient atmospheric replenishment mechanisms might maintain habitability throughout the active period (Meadows et al. 2018).

8. CONCLUSIONS

Here we present a large spectroscopic survey of nearby K dwarfs, characterizing 580 stars within 33.3 pc using high-resolution CHIRON spectra. Our comprehensive analysis of stellar properties, activity status, youth indicators, and kinematic populations yields crucial insights for prioritizing targets in the search for potentially habitable worlds around some of the most promising stellar hosts in the solar neighborhood.

One of the major outcomes of this project is the establishment of a comprehensive, high-resolution activity and age spectral gallery of 580 nearby K dwarfs⁷. This gallery represents one of the most uniform datasets of nearby K dwarfs available to the astronomical community and expands on previous work of Montes & Martin (1998) and the “Library of High-Resolution Spectra for Late-Type Stars”,⁸ as detailed in Montes (2013). The publicly available gallery provides critical resources for future studies of stellar magnetic activity cycles, Galactic chemical evolution, and the identification of optimal exoplanet host stars in the solar neighborhood.

We find that 51 (8.8%) of the K dwarfs are active and/or young based on H α emission, lithium absorption, or kinematic youth indicators. Spectra for all 51 are shown in Appendix B, with additional information about some of this sample’s most interesting members provided in the Systems Worthy of Note section (Appendix A). The remaining 529 (91.2%) stars show no spectroscopic signatures of youth or activity and do not appear to be members of young moving groups or clusters. These calm, mature stars have passed through their active juvenile phases and settled into stable, long-lived configurations ideal for maintaining planetary atmospheres over geological timescales.

Our kinematic analysis reveals that the local K dwarf population is dominated by thin disk members (464 stars, 80%), with a substantial thick disk component (107 stars, 18.4%), and one confirmed halo star. The metallicity distribution spans $[Fe/H] = -0.6$ to $+0.5$ dex, with 21 stars (3.6%) classified as metal-poor $[Fe/H] \leq -0.5$ dex. Only two of the 51 young or active stars belong to the thick disk population (HD 7808 and HD 196998), reinforcing the expected correlation between stellar age and Galactic population membership. The remaining 49 active stars are thin disk members, consistent with the younger ages of this population.

The NASA Exoplanet Archive lists 44 stars (7.5%) in the sample with reported planets, and undoubtedly more await discovery. Our K dwarf hosts span the full metallicity range sampled, from metal-poor to metal-rich systems. Importantly, while Jupiter-mass planets in our sample preferentially orbit metal-rich hosts ($[Fe/H] > 0$), lower-mass planets show no such metallicity preference, consistent with formation mechanisms that favor giant planet growth in metal-rich environments while permitting terrestrial planet formation across diverse metallicities. If this pattern holds for larger K dwarf samples, it has important implications for Galactic habitability prospects, suggesting that terrestrial planetary systems may exist around K dwarfs across diverse stellar populations, including ancient, metal-poor thick disk and halo stars. The presence of confirmed planets around both thin and thick disk K dwarfs in our sample provides initial support for this possibility.

Overall, the 529 mature, inactive K dwarfs comprise a vetted, rich list of targets for terrestrial planet detection and habitability assessment. These stars span the full range of stellar parameters in our sample: effective temperatures from 3600–5500 K, $[Fe/H]$ from -0.6 to $+0.5$ dex, and represent both thin disk and thick disk populations. This diversity ensures that future planet searches of these stars will probe planetary systems across a wide range of formation

⁷ RKSTAR Survey Activity and Age Spectral Gallery

⁸ Library of Spectra for Cool Stars (Poster 2013)

environments and stellar ages. The proximity of these targets, all within 33.3 pc, makes their planets prime candidates for detailed atmospheric characterization.

ACKNOWLEDGMENTS

We thank the dedicated staff at Cerro Tololo Inter-American Observatory, particularly Roberto Aviles and Rodrigo Hinojosa, for their expertise in executing the CHIRON observations that form the foundation of this work. We are grateful to our RECONS colleagues Andrew Couperus, Tim Johns, Aman Kar, Madison LeBlanc, and Eliot Vrijmoet for offering valuable insight along the way as this project came to fruition.

This work was supported by the National Science Foundation under grant AST-1910130. H.-S.H.-J. acknowledges support from the Georgia State University Provost's Dissertation Fellowship and the Southern Regional Education Board (SREB) Dissertation Year Award.

We have used data from the CHIRON spectrograph on the SMARTS 1.5 m telescope, which is operated as part of the SMARTS Observatory by RECONS (www.recons.org) members. This work has made use of data from the European Space Agency (ESA) mission Gaia (<https://www.cosmos.esa.int/gaia>), processed by the Gaia Data Processing and Analysis Consortium (DPAC, <https://www.cosmos.esa.int/web/gaia/dpac/consortium>). Funding for the DPAC has been provided by national institutions, in particular the institutions participating in the Gaia Multilateral Agreement. This research has made use of the NASA Exoplanet Archive (<https://exoplanetarchive.ipac.caltech.edu/>), which is operated by the California Institute of Technology, under contract with the National Aeronautics and Space Administration under the Exoplanet Exploration Program. This research has made use of the Two Micron All Sky Survey (2MASS), which is a joint project of the University of Massachusetts and the Infrared Processing and Analysis Center/California Institute of Technology, funded by the National Aeronautics and Space Administration and the National Science Foundation. This research has made use of the SIMBAD database, operated at CDS, Strasbourg, France, and NASA's Astrophysics Data System.

Facility: CTIO:1.5m (CHIRON). **Software:** *astropy* ([Astropy Collaboration et al. 2013, 2018](#)), *barycorrpy* ([Kanodia & Wright 2018](#)), *Empirical SpecMatch* ([Yee et al. 2017](#)), *matplotlib* ([Hunter 2007](#)), *SciPy* ([Virtanen et al. 2020](#)), and *TOPCAT* ([Taylor 2005](#)).

ORCID IDS

Hodari-Sadiki Hubbard-James <https://orcid.org/0000-0003-4568-2079>

Sebastian Carrazco-Gaxiola <https://orcid.org/0009-0006-9244-3707>

Todd J. Henry <https://orcid.org/0000-0002-9061-2865>

Leonardo A. Paredes <https://orcid.org/0000-0003-1324-0495>

Azmair H. Nizak <https://orcid.org/0000-0002-1457-1467>

Xavier Lesley-Saldaña <https://orcid.org/0009-0000-5136-6924>

Wei-Chun Jao <https://orcid.org/0000-0003-0193-2187>

Abigail Arbogast <https://orcid.org/0009-0004-7539-8129>

APPENDIX

A. SYSTEMS WORTHY OF NOTE

This appendix highlights a selection of the most notable and scientifically interesting systems from our sample of 51 young and/or active K dwarfs, as well as several calm stars with unique characteristics.

RKS0252-1246: [18] **HD 17925** was initially identified as a young star due to its strong Li I feature (Cayrel de Strobel & Cayrel 1989). Moreover, using the BANYAN Σ tool, this star is not linked to any specific moving group or cluster, suggesting that it is a field star.

RKS0417+2033: [13] **HD 284336** is a previously unidentified young star that we have now classified as such. Our spectral examination, evident in Figure 7, reveals a noticeable presence of the Li I absorption line, typically indicative of stellar youth. Although not characterized by high rotational speed, as per our calculated $v \sin i$ values, HD 284336 is found within the thin disk population of the galaxy, a feature worth noting. This new discovery warrants further investigation.

RKS0436+2707: **HD 283750, also known as V833 Tau or BD +26 730**, is a renowned flare star in our solar neighborhood. Its activity and status as a single-lined spectroscopic binary (SB1) with a two-day period were first noted by Hartmann et al. (1981). HD 283750 is among the most active stars in our study, exhibiting an EW[H α] of -0.34 \AA and an EW[Ca II] ratio of 0.21. Interestingly, despite its elevated activity and binary status, its γ velocity—measured by RECONS—aligns with the Gaia DR3 value, as shown by its position on the 1-to-1 line in Figure 10.

RKS0441+2054: [9] **HD 29697 or V834 Tau** is a known active star and is also one of the seven RVV K dwarfs that were analyzed with our benchmark sample. It is described in more detail in Hubbard-James et al. (2022).

RKS0658-1259: [10] **HD 51849**, identified as an active star with a stellar companion, was classified as an SB1 with a separation of $0.5''$ by Tokovinin et al. (2019). Our research exhibits evidence of both activity and youthfulness in this proximate binary system. Figure 8 reveals a minor Li I absorption line, while Figure 9 indicates that HD 51849 doesn't align with the old locus of stars.

RKS0723+2024: [16] **BD+20 1790** serves as a notable member of the AB Dor Moving Group. Recognized as a young star, it boasts an estimated age of 120 Myr. BD+20 1790 was flagged in our study as both youthful and active, as supported by spectroscopic and kinematic assessments. Notably, it displays a heightened rotational velocity with a $v \sin i$ measurement of 7.99 km s^{-1} , reported in Table 6. Its distinctive space motions further classify BD+20 1790 as a thin disk star.

RKS0734-0653: [7] **HD 60491**, categorized as a young star and potential member of the Ursa Majoris moving group by Montes et al. (2001), only meets one of the two kinematic criteria for association membership. Our analysis, as well as the BANYAN Σ tool, does not identify HD 60491 as part of any moving group. However, we do note the existence of a minor Li I absorption line in Figure 7, despite a lack of chromospheric activity at H α or Ca II.

RKS0819+0120: [12] **BD+01 2063**, acknowledged as a young star and a member of the Carina-near (estimated age ~ 200 Myr) association (Ujjwal et al. 2020), is also placed in the Carina moving group by the BANYAN Σ tool. Our analysis reveals a robust Li I absorption line, as shown in Figure 8. Additionally, we also observe chromospheric activity for this K dwarf, highlighted in Table 6.

RKS0904-1554: [8] **HD 77825**, previously identified as a young star and a member of the Castor Moving Group (estimated age 200 Myr) by Montes et al. (2001), does not correlate with any moving group or association according to the BANYAN Σ tool. Our observations depict a faint but discernible Li I absorption line as seen in Figure 7.

RKS0907+2252: [11] & [d] **HD 78141**, identified as a young star by [Stanford-Moore et al. \(2020\)](#), is estimated to be between 50-400 Myr old, as evidenced by a strong Li I signature. Our study corroborates this, depicting a profound Li I absorption feature in Figure 8. Notably, HD 78141 deviates from the 1-to-1 line in Figure 10, likely due to its classification as an SB1 star with a period of 160 days ([Griffin 2016](#)).

RKS0932-1111: [17] **LQ Hya** is a well-known young and chromospherically active K dwarf, initially reported by [Fekel et al. \(1986\)](#), and classified as a BY Draconis variable. The spectrum of LQ Hya in Figure 8 reveals not only a Li I absorption line and notably broader spectral lines compared to its K dwarf counterparts, attributable to rotational broadening. Our measurements give LQ Hya a $v \sin i$ value of 27.44 km s^{-1} .

RKS1043-2903: [15] **V419 Hya** is a recognized BY Draconis variable, with a debris disk reported by [Plavchan et al. \(2009\)](#) using data from the Spitzer Space Telescope. While our analysis categorizes V419 Hya as youthful due to a strong Li I absorption line, and minor signs of chromospheric activity as seen in Figure 8.

RKS1121-2027: **HD 98712A**, part of a known binary system, displays chromospheric activity potentially linked to its close companion as reported by [Paredes \(2022\)](#). Our study identified this K dwarf as active based on both EW[H α] and EW[Ca II] ratio tests. The absence of the Li I feature adds credence that this activity is due to the presence of a close companion and not youth.

RKS1303-0509: [14] **PX Vir** is also a member of our benchmark sample and was described in detail in [Hubbard-James et al. \(2022\)](#).

RKS1306+2043: **BD+21 2486A** is the primary component of a multi-star system comprising at least three stellar bodies. This K5V star is orbited by an M4V and an L5 star, as reported by [Gomes et al. \(2013\)](#). In our investigation, BD+21 2486A exhibited signs of chromospheric activity. However, similar to HD 98712A, this activity is likely due to the influence of nearby companions, rather than indicating stellar youth.

RKS1510-1622: **HD 134439** is uniquely characterized by its kinematic and spectroscopic properties. HD 134439 stands as the lone halo star in our sample. It is a high proper motion, metal-poor subdwarf that likely originated from a dwarf galaxy merger, exhibiting distinct kinematics that place it in the halo region of our Toomre diagram in Figure 13. Spectroscopically, as presented in Appendix B its unique attributes include the absence of prominent Fe I lines typical of K dwarfs and a much narrower Na I doublet, earning it a unique spot outside the ESM library's boundaries. Its distinguishing features underscore the rich diversity in the stellar population.

RKS1819-0156: **HD 168442 or GJ 710**, currently categorized as a calm K dwarf in our study (see Table 10), has a fascinating future in store. Projections indicate that in about 1.3 million years, this star will pass near the Sun at a distance of only 0.0636 parsecs ([Bailer-Jones 2022](#)). At such proximity, GJ 710 would shine as brightly as the most luminous planets in our sky. Additionally, its apparent motion across our sky would also be noticeable, peaking at about one arcminute per year ([de la Fuente Marcos & de la Fuente Marcos 2018](#)).

RKS1833-1626: **HD 171075** another newly uncovered SB2. The binary nature of HD 171075 is marked by distinct double-line features in the CHIRON spectra. A double-line Ca I feature at 6717 \AA , in the spectral window from 6705 to 6720 \AA , is a clear indication of its binary status. It is ensured that the light from both stars in the system is sent to the spectrograph, considering the $2.7''$ size of the fiber as projected on the sky and the significantly smaller star separation. Please refer to Appendix B for snapshot of the spectrum we observed.

RKS2041-2219: **HD 196998 or DG Cap** is a known active star and is also one of the seven RVV K dwarfs that were analyzed with our benchmark sample. As detailed in §6.4, **DG Cap** is uniquely positioned as one of two active stars from our sample within the Milky Way Galaxy's thick disk population. It is described in more detail in [Hubbard-James et al. \(2022\)](#).

B. SPECTRAL GALLERY OF SPECIAL K DWARFS

This Appendix provides a collection of 53 noteworthy K dwarfs identified during our analysis. These stars exhibit a range of interesting features, including chromospheric activity, youth indicators, metallicity differences, and binary signatures. They are categorized into five groups (A through E) based on their spectral properties. Each group contains ten stars, plotted with identical wavelength panels that highlight the H α & Li I features for consistency and comparison.

Groups A–D predominantly include young and/or chromospherically active stars, while Group E includes peculiar systems such as newly discovered spectroscopic binaries, Hyades cluster members, a candidate white dwarf companion system, and a halo star. Catalog names, RKS identifiers, and basic classifications (e.g., active, young, SB2) are annotated on each figure panel and caption.

The spectral plots provided here offer a visual resource to complement the quantitative analyses presented in the main text. Readers are encouraged to use these visualizations to explore subtle differences across the range of effective temperatures, metallicities, and stellar activity status present among the nearby K dwarf population.

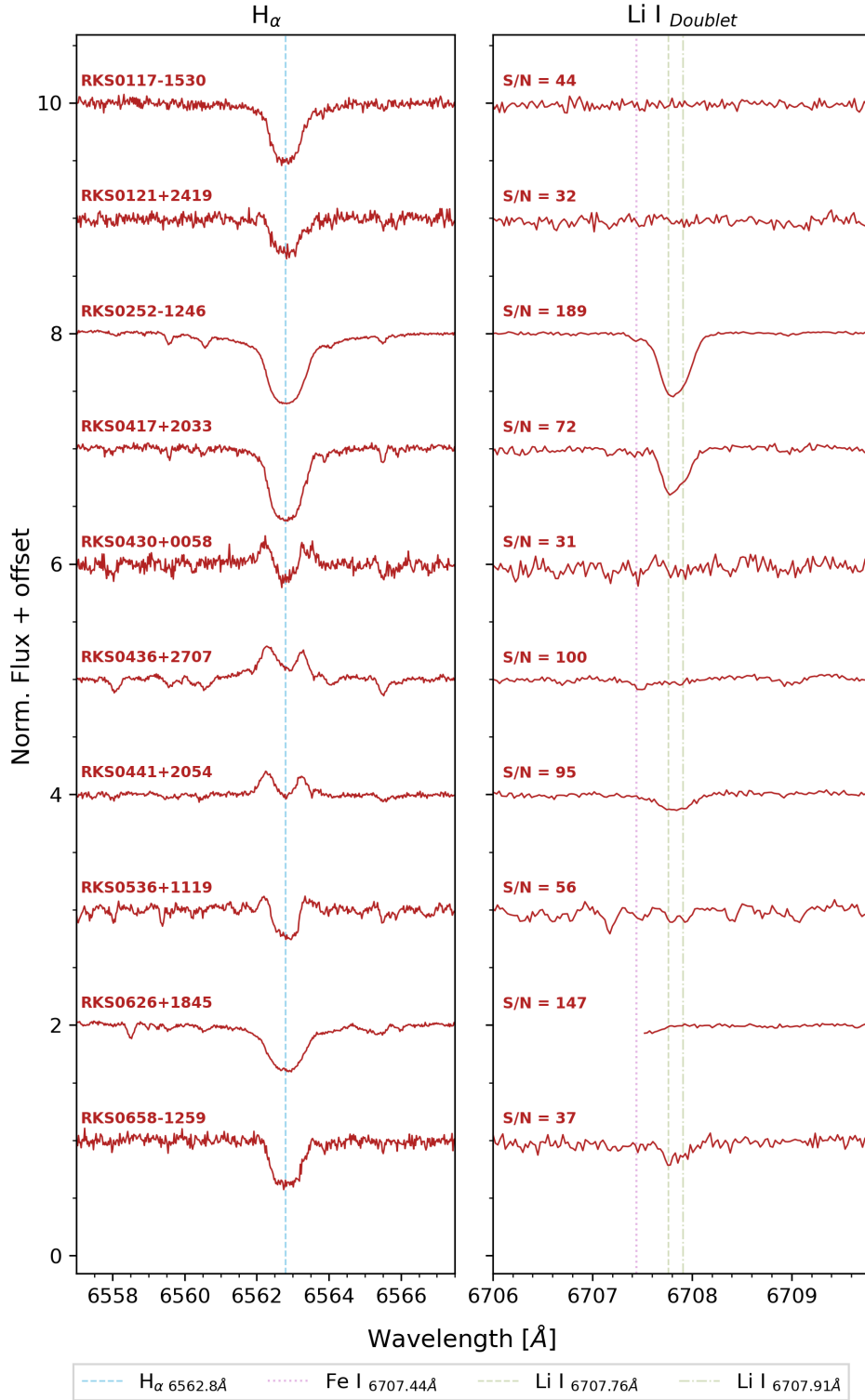


Figure 16. Group A: Spectra of young and active K dwarfs. Stars shown: RKS0117-1530 (A), RKS0121+2419 (A), RKS0252-1246 (Y+A), RKS0417+2033 (Y), RKS0430+0058 (A), RKS0436+2707 (A), RKS0441+2054 (Y+A), RKS0536+1119 (A), RKS0626+1845 (A), RKS0658-1259 (Y+A).

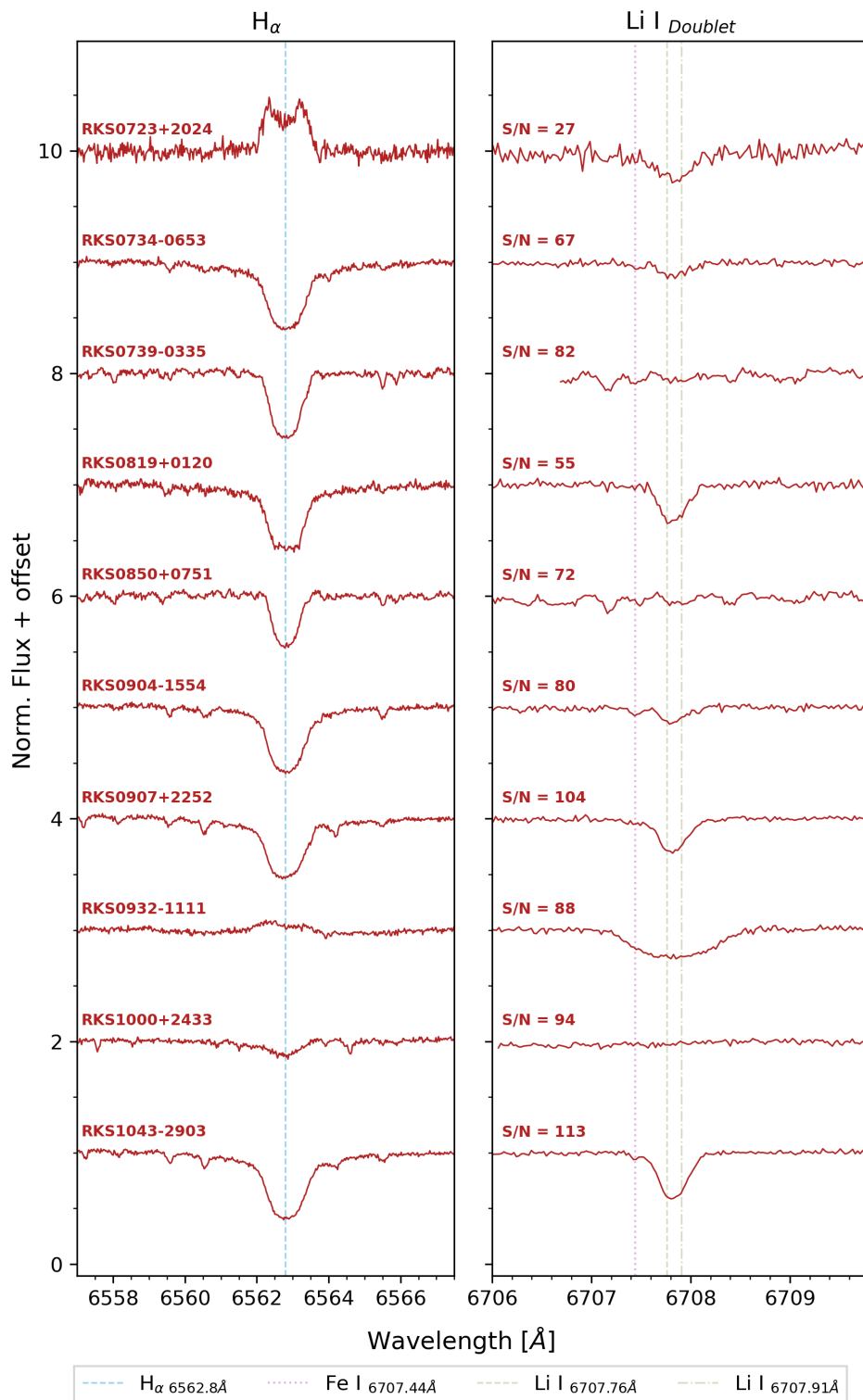


Figure 17. Group B: Spectra of young and active K dwarfs. Stars shown: RKS0723+2024 (Y+A), RKS0734-0653 (Y), RKS0739-0335 (A), RKS0819+0120 (Y+A), RKS0850+0751 (A), RKS0904-1554 (Y), RKS0907+2252 (Y+A), RKS0932-1111 (Y+A), RKS1000+2433 (A), RKS1043-2903 (Y+A).

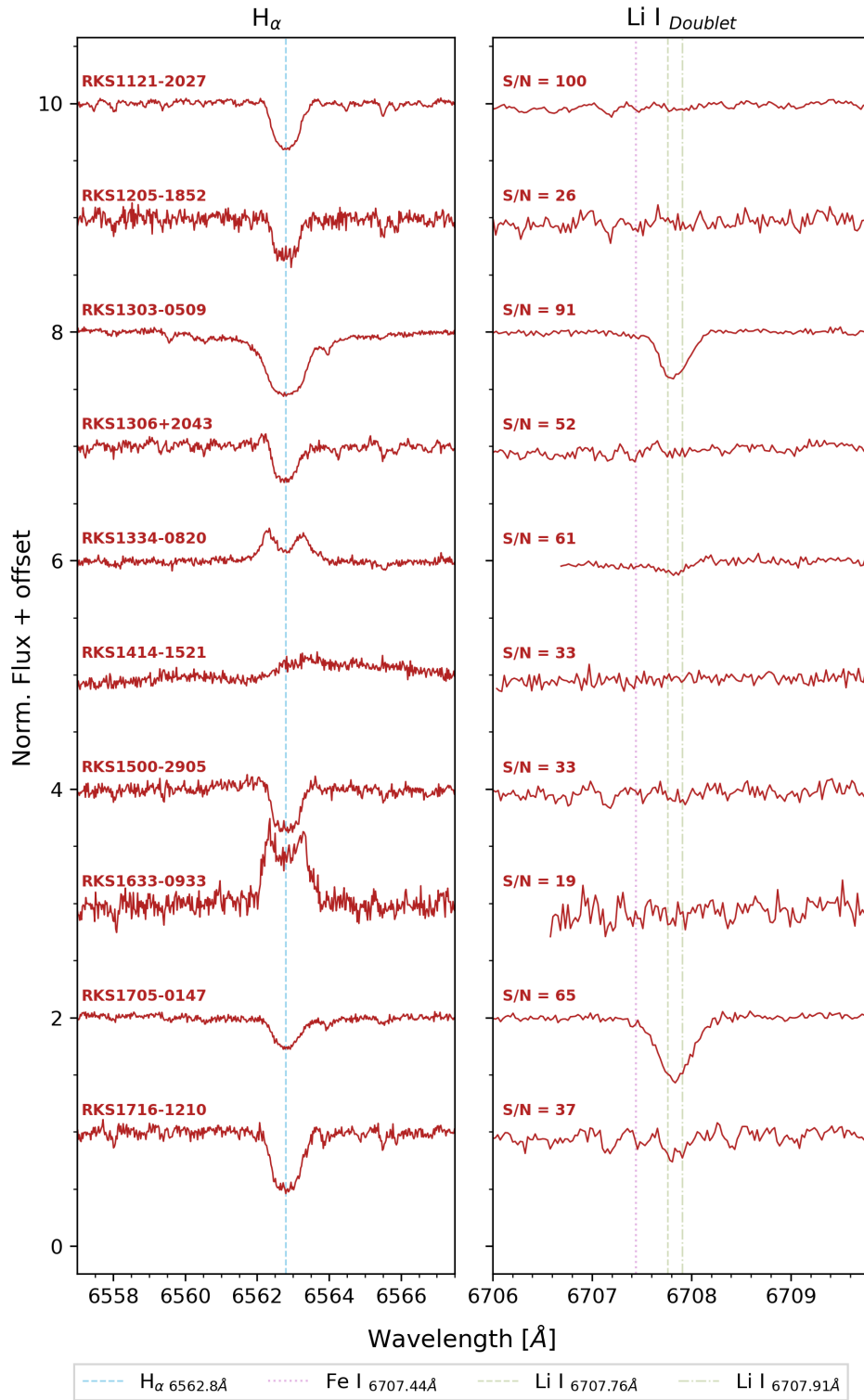


Figure 18. Group C: Spectra of young and active K dwarfs. Stars shown: RKS1121-2027 (A), RKS1205-1852 (A), RKS1303-0509 (Y), RKS1306+2043 (A), RKS1334-0820 (Y+A), RKS1414-1521 (A), RKS1500-2905 (A), RKS1633-0933 (A), RKS1705-0147 (Y+A), RKS1716-1210 (Y).

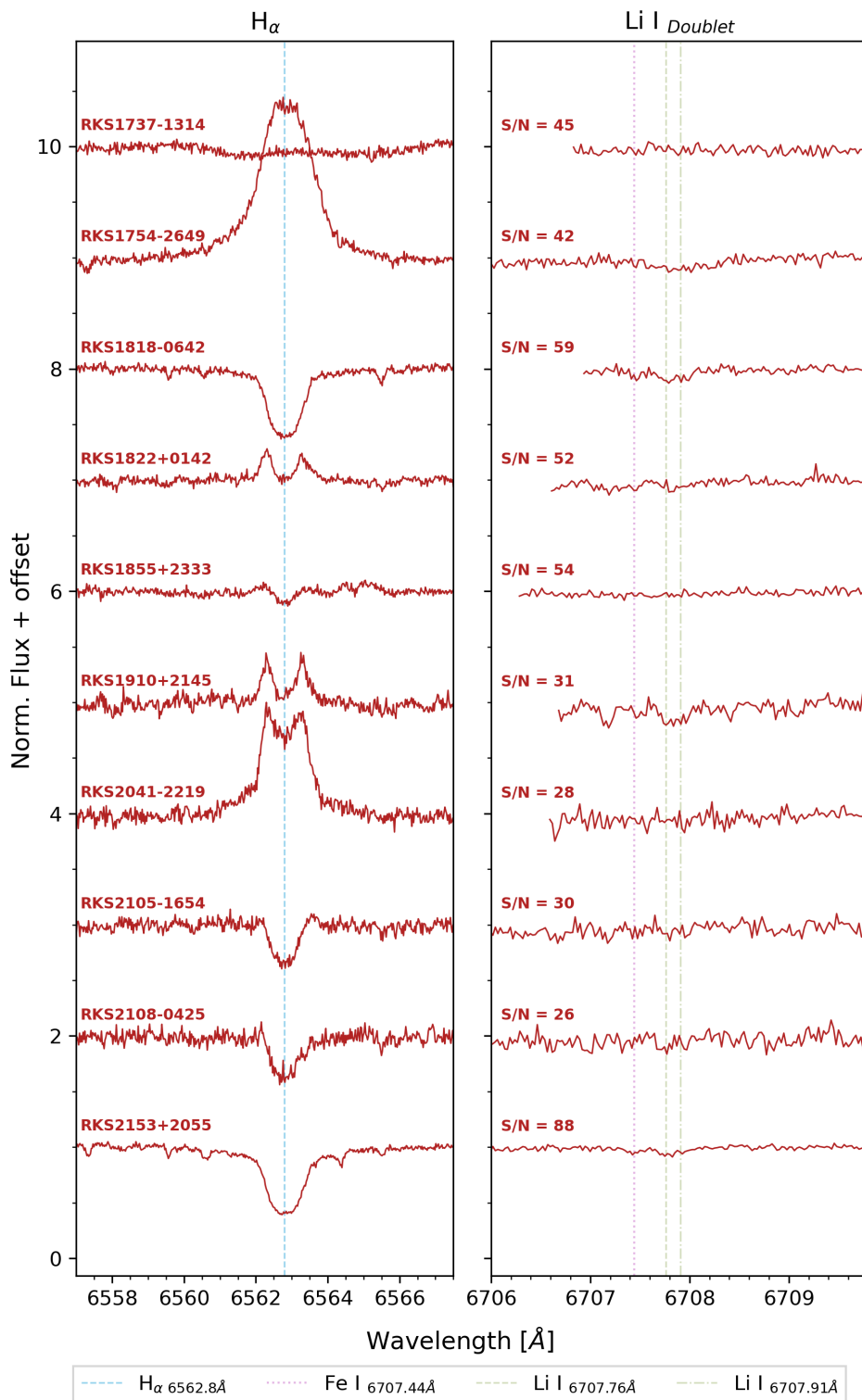


Figure 19. Group D: Spectra of young and active K dwarfs. Stars shown: RKS1737-1314 (A), RKS1754-2649 (Y+A), RKS1818-0642 (Y), RKS1822+0142 (A), RKS1855+2333 (A), RKS1910+2145 (Y+A), RKS2041-2219 (A), RKS2105-1654 (A), RKS2108-0425 (A), RKS2153+2055 (Y+A).

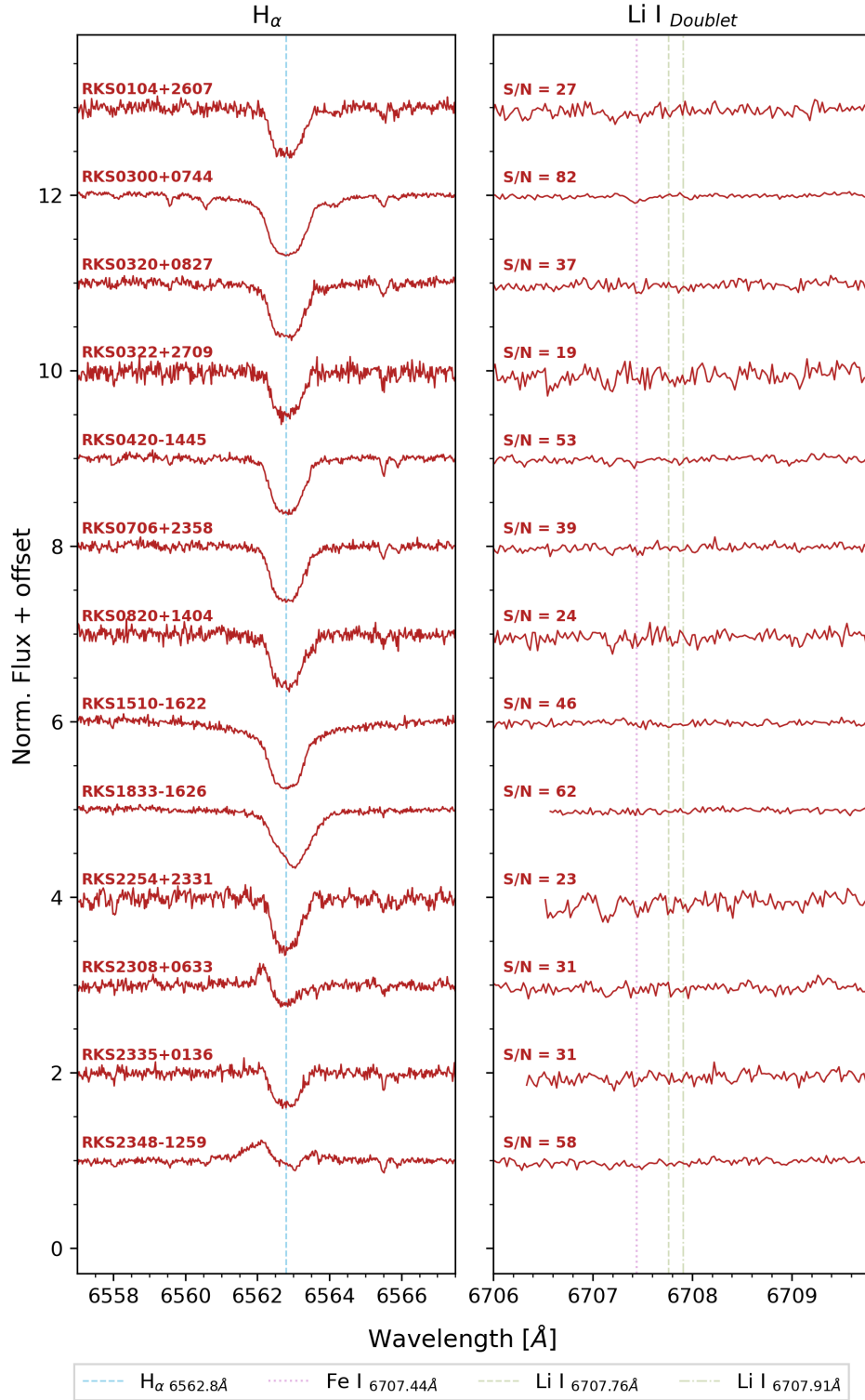


Figure 20. Group E: Spectra of young and active K dwarfs, plus moving group members and peculiar systems. Stars shown: RKS0104+2607 (MG Hyades), RKS0300+0744 (MG Hyades), RKS0320+0827 (MG Hyades), RKS0322+2709 (MG Hyades), RKS0420-1445 (MG Hyades), RKS0706+2358 (MG AB Dor), RKS0820+1404 (MG AB Dor), RKS1510-1622 (Halo), RKS1833-1626 (New SB2), RKS2254+2331 (MG Hyades), RKS2308+0633 (A), RKS2335+0136 (A), RKS2348-1259 (A).

C. ASTROMETRY AND PHOTOMETRY DATA FOR THE SURVEY SAMPLE K DWARFS

Table 8. Primary K dwarf Sample: Astrometry and Photometry Data

Star Identifiers		Coordinates				μ				Photometry			
RKS ID	Simbad Name	R.A. (hh mm ss)	Decl. (\pm dd mm ss)	$\mu_{R.A}$ (mas yr $^{-1}$)	μ_{Decl} (mas yr $^{-1}$)	π (mas)	Dist. (pc)	$B_{GaiaDR3}$ (mag)	$B_G - K_S$ (mag)	M_{B_G} (mag)			
RKS0000+1659	HD 224808	00 00 48.1	+16 59 17	-52.2	-307.39	33.26	30.07	9.02	2.68	6.63			
RKS0001-1656	BD-17 6862	00 01 25.8	-16 56 54	293.9	-253.44	31.76	31.49	11.00	3.78	8.51			
RKS0007-2349	HD 283	00 07 32.5	-23 49 07	320.87	91.24	30.49	32.79	8.91	2.23	6.33			
RKS0012+2142	G 131-35	00 12 33.5	+21 42 48	190.42	-287.33	31.94	31.31	11.97	3.93	9.49			
RKS0012+2705	BD+26 8	00 12 04.0	+27 05 56	283.17	-82.13	38.59	25.92	8.95	2.65	6.88			
RKS0016-1435	BD-15 36	00 16 11.0	-14 35 27	0.79	-6.44	30.71	32.56	9.81	3.01	7.25			
RKS0017+2057	G 131-51	00 17 59.1	+20 57 24	-252.05	-366.92	36.10	27.70	11.34	3.93	9.13			
RKS0019-0303	LP 644-95	00 19 12.3	-03 03 13	-26.88	-217.81	32.06	31.19	11.16	3.70	8.69			
RKS0019-0957	BD-10 47	00 19 05.5	-09 57 53	-36.33	-301.49	49.48	20.21	10.15	3.60	8.62			
RKS0020+1738	StKM 1-25	00 20 57.1	+17 38 15	39.0	-82.39	33.45	29.90	11.47	3.93	9.09			
RKS0021+2531	BD+24 32	00 21 16.0	+25 31 27	50.97	9.51	35.55	28.13	9.76	2.79	7.51			
RKS0022-2701	HD 1815	00 22 23.5	-27 01 57	287.8	-423.7	45.95	21.76	8.53	2.40	6.84			
RKS0024-2701	HD 2025	00 24 25.9	-27 01 36	665.76	83.96	55.82	17.91	8.15	2.59	6.88			
RKS0036+2610	BD+25 84	00 36 57.9	+26 10 54	76.16	42.0	43.61	22.93	9.28	3.10	7.48			
RKS0036-0930	BD-10 109	00 36 00.0	-09 30 56	-175.5	-568.46	32.67	30.61	11.44	3.72	9.01			
RKS0039+2115	54 Psc	00 39 21.8	+21 15 01	-461.95	-369.62	90.03	11.11	6.10	2.10	5.87			
RKS0042+2239	G 69-14	00 42 56.7	+22 39 34	400.81	22.31	31.84	31.41	11.80	3.98	9.31			
RKS0045+0147	HD 4256	00 45 04.8	+01 47 07	-49.97	-572.96	44.66	22.39	8.26	2.52	6.51			
RKS0048+0516	HD 4628	00 48 22.9	+05 16 50	755.89	-1141.72	134.50	7.44	5.96	2.28	6.60			
RKS0051+1844	HD 4913	00 51 21.7	+18 44 21	53.4	-268.55	45.02	22.21	9.47	3.23	7.74			
RKS0051-2254	HD 4967	00 51 34.0	-22 54 36	613.26	-276.45	65.09	15.36	9.19	3.45	8.26			
RKS0055-2940	HD 5425	00 55 49.2	-29 40 33	403.01	153.69	31.85	31.40	9.70	3.13	7.22			
RKS0057+0551	BD+05 127	00 57 44.5	+05 51 20	-55.52	1.4	56.15	17.81	10.50	3.86	9.25			
RKS0102+0503	HD 6101	01 02 24.5	+05 03 41	329.92	216.28	44.46	22.49	8.40	2.89	6.64			
RKS0102-1025	BD-11 192	01 02 21.1	-10 25 25	26.09	-176.92	47.38	21.10	10.25	3.72	8.63			
RKS0104+2607	BD+25 162	01 04 32.4	+26 07 12	315.46	13.62	33.57	29.79	10.26	3.30	7.89			
RKS0104-2536	HD 6378	01 04 24.1	-25 36 18	-34.46	-318.17	37.06	26.98	10.01	3.17	7.85			
RKS0105+1523	HD 6440A	01 05 29.9	+15 23 24	7.73	-199.04	36.70	27.25	9.36	2.88	7.18			
RKS0107+2257	HD 6660	01 07 37.8	+22 57 17	103.17	-490.28	48.68	20.54	8.66	2.90	7.10			
RKS0108+1714	BD+16 120	01 08 40.3	+17 14 33	-58.97	-584.11	34.95	28.62	10.79	3.51	8.51			

Table 8 continued on next page

Table 8 (continued)

RKS ID	Simbad Name	Coordinates			μ				Photometry			
		R.A. (hh mm ss)	Decl. (\pm dd mm ss)	$\mu_{R.A}$ (mas yr $^{-1}$)	μ_{Decl} (mas yr $^{-1}$)	π (mas)	Dist. (pc)	$B_{GaiaDR3}$ (mag)	$B_G - K_S$ (mag)	M_{B_G} (mag)		
RKS0112-2514	HD 7279	01 12 46.1	-25 14 08	128.34	19.84	44.19	22.63	9.79	3.37	8.02		
RKS0113+1629	BD+15 176	01 13 58.8	+16 29 40	14.06	-56.98	31.24	32.01	10.10	3.19	7.57		
RKS0116+2519	G 69-62	01 16 39.3	+25 19 53	429.2	-102.68	41.88	23.88	10.33	3.67	8.44		
RKS0117-1530	HD 7808	01 17 34.0	-15 30 11	278.04	-475.23	30.82	32.45	9.98	2.81	7.42		
RKS0118-0052	HD 7895	01 18 41.0	-00 52 03	432.56	-253.36	36.40	27.47	8.22	2.18	6.03		
RKS0121+2419	Ross 788	01 21 29.3	+24 19 50	340.5	9.07	36.89	27.11	10.95	3.84	8.78		
RKS0122-2653	HD 8326	01 22 07.6	-26 53 35	-58.32	-224.94	32.57	30.71	9.00	2.50	6.56		
RKS0123-1257	HD 8389	01 23 02.6	-12 57 57	461.9	-25.7	33.27	30.05	8.08	2.16	5.69		
RKS0124+1829	HD 8553	01 24 53.9	+18 29 59	547.14	-190.33	31.84	31.41	8.72	2.32	6.23		
RKS0125-0103	BD-01 184	01 25 09.4	-01 03 34	-193.86	-291.6	31.37	31.88	9.71	2.79	7.19		
RKS0129+2143	EO Psc	01 29 04.8	+21 43 23	458.86	-183.92	42.95	23.29	7.97	2.60	6.13		
RKS0135-2046	BD-21 262	01 35 45.6	-20 46 13	129.22	-25.6	38.13	26.22	10.33	3.38	8.24		
RKS0139+1515	BD+14 251	01 39 56.1	+15 15 33	218.03	-58.78	41.11	24.33	9.34	3.02	7.41		
RKS0142+2016	107 Psc	01 42 29.7	+20 16 06	-300.74	-673.54	130.82	7.64	5.46	2.17	6.04		
RKS0146+1224	HD 10853	01 46 38.7	+12 24 42	31.28	-74.83	41.65	24.01	9.13	2.81	7.23		
RKS0150+1817	Wolf 89	01 50 28.0	+18 17 46	240.06	-78.66	33.10	30.22	11.01	3.77	8.61		
RKS0150+2927	HD 11130	01 50 07.8	+29 27 52	-35.34	-63.38	37.10	26.96	8.26	2.15	6.11		
RKS0200+2636	SuKM 1-223	02 00 20.1	+26 36 00	177.78	64.45	31.77	31.48	11.24	3.65	8.75		
RKS0205-2804	CD-28 657	02 05 23.6	-28 04 11	334.43	421.45	38.36	26.07	11.14	3.98	9.06		
RKS0209-1620	BD-17 400	02 09 10.9	-16 20 22	516.41	79.44	35.11	28.48	11.13	3.88	8.86		
RKS0213-2111	BD-21 397	02 13 12.1	-21 11 47	375.45	55.72	42.12	23.74	10.09	3.59	8.21		
RKS0214-0338	HD 13789	02 14 13.5	-03 38 06	-12.33	-219.26	43.98	22.74	8.79	2.78	7.01		
RKS0215-1814	HD 14001A	02 15 46.1	-18 14 17	-33.2	-124.58	43.48	23.00	8.57	3.14	6.76		
RKS0221-0652	HD 14635	02 21 44.4	-06 52 46	295.34	51.4	36.06	27.73	9.31	2.84	7.10		
RKS0229-1958	HD 15468	02 29 01.7	-19 58 45	588.79	266.76	51.61	19.38	9.01	3.18	7.57		
RKS0231-1516	HD 15767	02 31 42.4	-15 16 24	-73.37	-117.84	37.19	26.89	8.90	2.50	6.75		
RKS0231-2001	BD-20 470	02 31 30.8	-20 01 41	192.29	26.47	30.28	33.02	10.44	3.27	7.85		
RKS0236+0653	HD 16160	02 36 04.9	+06 53 12	1778.59	1477.31	138.34	7.23	6.05	2.57	6.75		
RKS0236-0309	FT Cet	02 36 41.7	-03 09 22	323.28	58.33	40.95	24.42	8.35	2.41	6.41		
RKS0236-2331	HD 16270	02 36 00.7	-23 31 16	83.28	14.01	47.09	21.24	8.57	2.74	6.93		
RKS0236-2710	HD 16280	02 36 00.7	-27 10 42	76.42	-167.87	30.27	33.03	9.71	2.79	7.12		
RKS0240+0111	BD+00 444	02 40 42.8	+01 11 55	283.92	231.75	41.82	23.91	9.75	3.25	7.86		

Table 8 continued on next page

Table 8 (continued)

RKS ID	Simbad Name	Coordinates			μ			Photometry			
		R.A. (hh mm ss)	Decl. (\pm dd mm ss)	$\mu_{R,A}$ (mas yr $^{-1}$)	μ_{Decl} (mas yr $^{-1}$)	π (mas)	Dist. (pc)	$B_{GaiaDR3}$ (mag)	$B_G - K_S$ (mag)	M_{B_G} (mag)	
RKS0242+0322	BD+02 418	02 42 32.5	+03 22 26	-142.08	-148.0	40.77	24.53	10.39	3.56	8.44	
RKS0243+1925	HD 16909	02 43 20.8	+19 25 45	455.66	2.85	53.56	18.67	8.47	2.93	7.11	
RKS0246+1146	HD 17230	02 46 17.2	+11 46 30	263.88	-211.58	61.89	16.16	8.85	3.32	7.81	
RKS0246+2538	HD 17190	02 46 15.2	+25 38 59	237.59	-149.14	39.61	25.24	8.11	2.24	6.10	
RKS0246-2305	CD-23 1056	02 46 42.8	-23 05 11	294.72	140.97	42.69	23.42	10.49	3.75	8.64	
RKS0247+2842	LP 298-33	02 47 55.8	+28 42 44	-164.75	11.87	34.86	28.69	11.36	3.88	9.07	
RKS0248+2704	HD 17382	02 48 09.1	+27 04 07	278.47	-119.19	43.57	22.95	7.82	2.20	6.02	
RKS0248-1145	BD-12 525	02 48 06.5	-11 45 47	-65.33	-218.14	35.12	28.47	11.02	3.80	8.75	
RKS0250+1542	HD 17660	02 50 36.8	+15 42 35	342.38	-395.39	42.85	23.34	9.14	3.01	7.30	
RKS0251+1038	BD+10 378	02 51 42.8	+10 38 42	-116.98	-136.35	34.55	28.94	10.22	3.24	7.91	
RKS0251-0816	BD-08 535	02 51 44.4	-08 16 09	29.92	-10.56	32.42	30.85	10.06	3.09	7.61	
RKS0252-1246	HD 17925	02 52 32.1	-12 46 10	397.35	-189.28	96.52	10.36	6.28	2.11	6.20	
RKS0255+2652	HD 18143A	02 55 39.0	+26 52 23	264.6	-193.33	44.43	22.51	7.82	2.39	6.06	
RKS0255+2807	G 36-45	02 55 41.2	+28 07 47	270.82	-146.47	30.20	33.12	11.30	3.78	8.70	
RKS0257-2458	HD 18445	02 57 13.1	-24 58 30	12.81	-32.4	40.99	24.40	8.05	2.63	6.11	
RKS0258+2646	HD 18450	02 58 52.4	+26 46 26	-16.71	125.17	34.51	28.98	8.43	2.30	6.12	
RKS0300+0744	BZ Cet	03 00 02.8	+07 44 59	328.03	21.18	42.08	23.77	8.22	2.38	6.34	
RKS0303+2006	BD+19 451	03 03 49.0	+20 06 39	31.28	-64.93	46.76	21.39	8.86	2.90	7.21	
RKS0306+0157	HD 19305	03 06 26.7	+01 57 54	389.25	-925.03	67.93	14.72	9.31	3.66	8.47	
RKS0308-2410	CD-24 1458	03 08 25.6	-24 10 03	-13.73	-165.53	34.93	28.63	10.35	3.38	8.07	
RKS0310+1203	BD+11 444	03 10 15.1	+12 03 01	248.71	-157.7	34.66	28.85	9.62	3.00	7.32	
RKS0314+0858	HD 20165	03 14 47.2	+08 58 50	400.58	-404.43	43.27	23.11	8.04	2.29	6.22	
RKS0314-2626	HD 20280	03 14 44.6	-26 26 46	216.81	98.17	53.55	18.67	9.39	3.32	8.03	
RKS0320+0827	BD+07 499	03 20 29.1	+08 27 16	226.37	5.97	31.60	31.64	9.86	2.98	7.36	
RKS0322+2709	LP 355-64	03 22 28.1	+27 09 21	220.91	-64.35	31.47	31.78	11.27	3.85	8.76	
RKS0324-0521	HD 21197	03 24 59.7	-05 21 49	-230.88	-768.48	65.26	15.32	8.11	2.99	7.18	
RKS0329-1140	BD-12 662	03 29 19.7	-11 40 42	54.47	-304.36	47.55	21.03	10.24	3.79	8.63	
RKS0332-0927	eps Eri	03 32 55.8	-09 27 29	-974.76	20.88	310.58	3.22	4.00	2.22	6.46	
RKS0341+0336	BD+03 515	03 41 10.5	+03 36 40	-44.56	-238.7	38.62	25.89	9.85	3.70	7.78	
RKS0342-2427	CD-24 1826	03 42 44.6	-24 27 58	24.43	-374.0	38.39	26.05	9.42	2.98	7.34	
RKS0343+1640	BD+16 502	03 43 52.5	+16 40 19	157.86	-316.2	58.04	17.23	10.17	3.92	8.99	
RKS0343-1253	BD-13 718	03 43 06.1	-12 53 39	-236.4	30.03	35.25	28.37	11.11	3.61	8.85	

Table 8 continued on next page

Table 8 (continued)

Star Identifiers		Coordinates			μ			Photometry		
RKS ID	Simbad Name	R.A. (hh mm ss)	Decl. (\pm dd mm ss)	$\mu_{R,A}$ (mas yr $^{-1}$)	μ_{Decl} (mas yr $^{-1}$)	π (mas)	Dist. (pc)	$B_{GaiaDR3}$ (mag)	$B_G - K_S$ (mag)	M_{B_G} (mag)
RKS0343-1906	HD 23356	03 43 55.3	-19 06 39	310.1	157.19	71.75	13.94	7.32	2.48	6.60
RKS0344+1155	BD+11 514	03 44 51.1	+11 55 12	314.06	127.54	45.63	21.92	9.34	3.14	7.64
RKS0345-2751	HD 23588A	03 45 24.1	-27 51 44	303.24	111.83	48.49	20.62	8.43	2.83	6.86
RKS0348+1512	BD+14 611	03 48 32.9	+15 12 07	98.99	-86.66	30.28	33.03	9.74	2.78	7.15
RKS0348+2519	HD 23742	03 48 26.3	+25 19 23	14.78	-99.03	30.95	32.31	8.75	2.25	6.20
RKS0349-1329	StKM 1-413	03 49 15.9	-13 29 29	-66.76	-108.32	30.40	32.89	11.13	3.66	8.54
RKS0350-2349	CD-24 1905	03 50 19.5	-23 49 44	79.42	-235.12	30.74	32.54	10.07	3.16	7.51
RKS0354-0649	BD-07 699	03 54 35.4	-06 49 33	-5.53	527.35	63.81	15.67	9.26	3.63	8.28
RKS0357-0109	HD 24916	03 57 28.6	-01 09 34	-185.71	-142.91	65.43	15.28	8.30	2.96	7.38
RKS0404+2634	HG 8-5	04 04 15.2	+26 34 24	215.02	-112.14	33.43	29.92	11.46	3.83	9.08
RKS0406-2051	BD-21 784	04 06 34.8	-20 51 11	52.8	-778.89	38.65	25.88	9.92	3.22	7.86
RKS0407+1413	LP 474-123	04 07 43.9	+14 13 24	173.57	-156.67	32.13	31.12	11.03	3.85	8.56
RKS0408+1220	HD 26129	04 08 30.8	+12 20 16	154.41	-336.19	32.42	30.84	8.82	2.40	6.37
RKS0417+2033	HD 284336	04 17 26.9	+20 33 17	-40.68	-60.19	34.86	28.69	9.80	2.99	7.51
RKS0419-0408	BD-04 797	04 19 05.7	-04 08 55	101.22	-11.35	34.20	29.24	10.76	3.62	8.43
RKS0420-1445	BD-15 767	04 20 10.5	-14 45 39	177.49	114.41	34.13	29.30	10.02	3.19	7.69
RKS0421-1945	CPD-20 550	04 21 31.6	-19 45 23	-202.98	-289.81	40.55	24.66	10.68	3.57	8.72
RKS0427+2426	HD 283668	04 27 52.9	+24 26 41	395.97	53.39	33.99	29.42	9.63	2.61	7.29
RKS0429+2155	HD 28343	04 29 00.1	+21 55 21	-67.02	174.63	89.06	11.23	8.56	3.68	8.31
RKS0430+0058	MCC 446	04 30 16.7	+00 58 47	83.78	-67.43	37.53	26.64	10.77	3.77	8.64
RKS0436+2707	HD 283750	04 36 48.2	+27 07 55	232.17	-147.48	57.49	17.40	8.36	3.12	7.16
RKS0441+2054	HD 29697	04 41 18.8	+20 54 05	-234.26	-254.31	75.69	13.21	8.18	3.03	7.58
RKS0445+0938	StKM 1-508	04 45 27.2	+09 38 27	150.58	-109.35	33.05	30.25	11.43	3.93	9.03
RKS0448-1056	HD 30523	04 48 01.1	-10 56 01	82.35	-108.92	37.78	26.47	9.72	3.12	7.61
RKS0449-1447	BD-15 869	04 49 32.7	-14 47 22	-205.59	-285.2	39.86	25.09	11.12	3.92	9.12
RKS0451+2837	HD 30754	04 51 33.3	+28 37 49	93.43	-62.93	30.62	32.66	9.76	2.88	7.19
RKS0453+2214	HD 30973	04 53 04.7	+22 14 06	146.83	-133.03	37.84	26.43	9.04	2.75	6.93
RKS0454+0722	HD 31208	04 54 16.6	+07 22 22	248.0	-201.86	33.76	29.62	8.43	2.25	6.07
RKS0455-2833	HD 31560	04 55 41.9	-28 33 50	187.89	-226.51	54.92	18.21	8.36	2.82	7.06
RKS0503+0322	StKM 1-542	05 03 32.1	+03 22 56	-17.12	-57.4	31.38	31.87	11.51	3.77	8.99
RKS0506-1102	HD 32965	05 06 30.0	-11 02 34	36.66	-55.1	32.69	30.59	9.83	3.00	7.40
RKS0512+1943	HD 241596	05 12 53.4	+19 43 19	367.81	-673.76	32.45	30.81	10.06	2.99	7.62

Table 8 continued on next page

Table 8 (continued)

Star Identifiers		Coordinates				μ				Photometry			
RKS ID	Simbad Name	R.A. (hh mm ss)	Decl. (\pm dd mm ss)	$\mu_{R.A}$ (mas yr $^{-1}$)	μ_{Decl} (mas yr $^{-1}$)	π (mas)	Dist. (pc)	$B_{GaiaDR3}$ (mag)	$B_G - K_S$ (mag)	M_{B_G} (mag)			
RKS0513-2158	BD-22 1050	05 13 59.1	-21 58 24	64.8	58.46	31.68	31.57	10.66	3.48	8.16			
RKS0514+0039	HD 290054	05 14 48.1	+00 39 43	232.04	-444.72	34.66	28.86	10.23	3.24	7.93			
RKS0514+1952	HD 241814	05 14 17.0	+19 52 58	245.08	-225.9	31.43	31.81	9.71	2.94	7.20			
RKS0518-2123	HD 34751	05 18 47.1	-21 23 37	-137.04	-36.95	48.97	20.42	9.63	3.48	8.08			
RKS0519-0304	HD 34673	05 19 12.6	-03 04 25	699.91	137.82	63.64	15.71	8.04	2.99	7.06			
RKS0519-1550	HD 34865	05 19 59.5	-15 50 22	173.7	207.71	42.09	23.76	8.96	2.75	7.08			
RKS0522+0236	HD 35112	05 22 37.4	+02 36 11	65.95	-182.17	50.52	19.80	8.01	2.71	6.53			
RKS0523+1719	111 Tau B	05 23 38.3	+17 19 26	250.98	-5.71	68.77	14.54	8.17	2.94	7.36			
RKS0533-2643	CD-26 2288	05 33 04.6	-26 43 28	16.89	150.78	30.65	32.62	9.36	2.64	6.79			
RKS0534-2328	HD 37065	05 34 48.6	-23 28 08	318.5	-433.35	36.04	27.75	9.02	2.54	6.80			
RKS0535+2805	HD 244957	05 35 00.8	+28 05 54	202.0	-269.94	30.50	32.79	10.30	3.30	7.72			
RKS0536+1119	V2689 Ori	05 36 30.9	+11 19 40	-2.82	-56.35	87.53	11.42	9.12	3.85	8.83			
RKS0542+0240	HD 38014	05 42 45.8	+02 40 44	253.9	-526.52	30.85	32.41	8.77	2.34	6.22			
RKS0544-2225	AK Lep	05 44 26.5	-22 25 18	-304.91	-352.61	112.47	8.89	6.39	2.26	6.65			
RKS0549-1734	HD 39071	05 49 22.5	-17 34 44	-22.09	101.18	34.98	28.58	8.74	2.42	6.46			
RKS0552-2246	BD-22 1252	05 52 31.9	-22 46 36	260.36	318.7	30.66	32.61	10.81	3.45	8.24			
RKS0553-0559	BD-06 1339	05 53 00.2	-05 59 41	-1.17	-346.76	49.25	20.30	9.95	3.65	8.41			
RKS0554+0208	HD 39715	05 54 28.5	+02 08 32	78.67	-645.33	38.93	25.69	9.07	2.72	7.02			
RKS0554-1942	TYC 5939-2260-1	05 54 30.4	-19 42 05	96.22	-11.83	42.97	23.27	10.93	3.71	9.10			
RKS0600+2101	HD 250268	06 00 53.9	+21 01 15	-33.43	-360.56	34.39	29.07	10.24	3.24	7.92			
RKS0602+0848	P.M. J06027+0848	06 02 44.2	+08 48 30	71.26	21.36	32.84	30.45	11.24	3.76	8.82			
RKS0608+2630	HD 252023	06 08 13.2	+26 30 08	-31.81	-42.08	37.61	26.59	9.51	2.97	7.39			
RKS0609+0009	HD 291290	06 09 46.1	+00 09 32	151.56	-119.26	31.96	31.29	11.05	3.82	8.57			
RKS0609+0540	HD 42182	06 09 35.9	+05 40 08	58.79	46.44	33.12	30.20	8.68	2.41	6.28			
RKS0612+1023	TYC 734-1988-1	06 12 08.4	+10 23 39	-37.69	-32.89	32.27	30.99	9.98	3.10	7.52			
RKS0614+0510	HD 43062	06 14 24.4	+05 10 05	57.0	-283.5	33.17	30.15	8.63	2.41	6.23			
RKS0616+2512	HD 254229	06 16 39.5	+25 12 21	55.66	-403.01	32.60	30.67	9.60	2.85	7.17			
RKS0617+1759	HD 254504	06 17 25.8	+17 59 21	113.62	-96.15	32.49	30.78	10.56	3.39	8.12			
RKS0618-1352	BD-13 1434	06 18 22.1	-13 52 07	64.34	340.55	34.64	28.87	10.14	3.22	7.84			
RKS0620+0215	HD 288595	06 20 13.2	+02 15 32	-123.81	-96.75	37.20	26.88	10.06	3.36	7.91			
RKS0621-2212	HD 44573	06 21 33.1	-22 12 53	25.58	-239.22	34.81	28.72	8.70	2.42	6.41			
RKS0626+1845	HD 45088	06 26 10.2	+18 45 24	-131.62	-150.57	68.41	14.62	7.02	2.75	6.20			

Table 8 continued on next page

Table 8 (continued)

Star Identifiers		Coordinates				μ				Photometry			
RKS ID	Simbad Name	R.A. (hh mm ss)	Decl. (\pm dd mm ss)	$\mu_{R.A}$ (mas yr $^{-1}$)	μ_{Decl} (mas yr $^{-1}$)	π (mas)	Dist. (pc)	$B_{GaiaDR3}$ (mag)	$B_G - K_S$ (mag)	M_{B_G} (mag)			
RKS0629+2700	HD 257886	06 29 05.5	+27 00 31	-243.86	-418.37	34.82	28.72	8.81	2.45	6.52			
RKS0630-1148	HD 45977	06 30 07.3	-11 48 32	-153.14	78.93	37.07	26.98	9.34	2.93	7.18			
RKS0632-2701	CD-26 3096	06 32 08.8	-27 01 58	398.0	-245.48	33.26	30.06	11.66	3.87	9.27			
RKS0633+0527	HD 46375	06 33 12.6	+05 27 46	111.62	-96.95	33.88	29.52	8.15	2.15	5.80			
RKS0637+1945	HD 260564	06 37 05.2	+19 45 10	10.34	-34.27	31.64	31.60	10.39	3.23	7.89			
RKS0641+2357	HD 47752	06 41 15.7	+23 57 27	205.78	-276.6	57.95	17.26	8.32	2.77	7.13			
RKS0647-1815	BPM 72121	06 47 15.7	-18 15 31	-104.16	67.32	32.25	31.01	10.79	3.59	8.33			
RKS0652-0510	HD 50281	06 52 18.0	-05 10 25	-543.69	-3.52	114.36	8.74	6.82	2.71	7.11			
RKS0652-2306	HD 50590	06 52 59.6	-23 06 27	218.94	76.58	32.85	30.44	9.22	2.63	6.80			
RKS0658-1259	HD 51849	06 58 26.0	-12 59 30	87.76	-110.4	45.15	22.15	9.40	3.21	7.67			
RKS0700-2847	WT 1539	07 00 09.4	-28 47 02	-219.16	-90.25	46.00	21.74	11.02	3.90	9.33			
RKS0701+0655	HD 52456	07 01 35.5	+06 55 36	-30.7	27.85	35.45	28.21	8.38	2.23	6.13			
RKS0701-2556	HD 52698	07 01 13.7	-25 56 55	205.95	42.34	67.80	14.75	6.93	2.29	6.09			
RKS0702-0647	HD 52919	07 02 42.9	-06 47 57	-201.31	-313.61	52.32	19.11	8.60	2.85	7.19			
RKS0706+2358	BD+24 1529	07 06 52.1	+23 58 08	-85.22	-205.04	31.32	31.93	10.37	3.24	7.85			
RKS0707+0326	BD+03 1552	07 07 09.3	+03 26 50	12.72	-258.74	36.39	27.48	10.07	3.40	7.87			
RKS0708+2950	HD 53927	07 08 04.2	+29 50 04	-156.41	-294.06	43.51	22.99	8.55	2.49	6.74			
RKS0708-0958	HD 54359	07 08 09.3	-09 58 07	-200.74	27.58	35.27	28.36	9.09	2.58	6.83			
RKS0710-1425	BD-14 1750	07 10 49.5	-14 25 58	-472.49	304.0	42.87	23.33	10.18	3.55	8.34			
RKS0712-2453	CD-24 5005	07 12 04.8	-24 53 31	-114.39	-4.32	35.14	28.46	10.60	3.71	8.33			
RKS0713+2500	HD 55458	07 13 53.1	+25 00 40	-405.41	-88.49	36.31	27.54	8.60	2.38	6.40			
RKS0716-0339	BD-03 1821	07 16 10.6	-03 39 57	104.98	-50.55	30.07	33.25	9.25	2.58	6.64			
RKS0723+1257	HD 57901	07 23 47.0	+12 57 52	84.27	-424.95	41.62	24.03	8.42	2.53	6.52			
RKS0723+2024	BD+20 1790	07 23 43.5	+20 24 58	-65.64	-230.69	36.09	27.71	10.23	3.35	8.02			
RKS0723-2001	BD-19 1855	07 23 29.2	-20 01 24	45.2	-335.72	31.95	31.30	10.14	3.20	7.66			
RKS0724-1753	BD-17 1959	07 24 34.2	-17 53 31	-48.22	-45.57	41.11	24.33	10.56	3.72	8.63			
RKS0725-1041	LP 722-21	07 25 29.8	-10 41 59	-204.0	-197.59	30.23	33.08	11.81	3.89	9.21			
RKS0726-1546	HD 58760	07 26 26.5	-15 46 13	45.62	-97.52	38.54	25.95	9.44	3.02	7.37			
RKS0730-0340	G 112-24	07 30 17.5	-03 40 24	-154.58	44.8	40.83	24.49	10.66	3.92	8.72			
RKS0732+1719	G 88-36	07 32 02.8	+17 19 09	-218.53	-183.31	37.05	26.99	11.21	3.89	9.05			
RKS0734-0653	HD 60491	07 34 26.1	-06 53 48	-80.26	-43.04	42.63	23.46	8.38	2.36	6.53			
RKS0739-0335	HD 61606	07 39 59.3	-03 35 51	70.08	-278.12	71.03	14.08	7.40	2.52	6.66			

Table 8 continued on next page

Table 8 (continued)

RKS ID	Star Identifiers	Coordinates			μ			Photometry			
		Simbad Name	R.A. (hh mm ss)	Decl. (\pm dd mm ss)	$\mu_{R.A}$ (mas yr $^{-1}$)	μ_{Decl} (mas yr $^{-1}$)	π (mas)	Dist. (pc)	$B_{GaiaDR3}$ (mag)	$B_G - K_S$ (mag)	M_{B_G} (mag)
RKS0741-2921	TYC 6552-2083-1		07 41 17.4	-29 21 32	-155.33	73.67	33.04	30.27	10.92	3.64	8.51
RKS0745+0208	BD+02 1766		07 45 01.1	+02 08 14	64.37	-203.41	37.52	26.65	10.42	3.65	8.29
RKS0752+2555	HD 63991		07 52 47.4	+25 55 35	39.77	-144.58	45.82	21.82	8.82	2.77	7.13
RKS0754+1914	HD 64468		07 54 54.0	+19 14 10	95.08	-453.93	49.24	20.31	7.99	2.54	6.45
RKS0754-2518	CD-24 6144		07 54 10.8	-25 18 11	-300.86	201.04	56.24	17.78	9.98	3.81	8.73
RKS0757-0048	HD 65277		07 57 57.7	-00 48 51	-157.14	7.58	56.64	17.66	8.31	2.80	7.08
RKS0758-1501	BD-14 2308		07 58 25.5	-15 01 13	14.89	-235.45	33.13	30.18	9.54	3.01	7.14
RKS0758-2537	HD 65486		07 58 04.3	-25 37 35	362.41	-245.79	54.16	18.46	8.66	2.83	7.33
RKS0759+2050	HD 65430		07 59 33.9	+20 50 38	176.03	-568.33	41.69	23.99	7.89	2.25	5.99
RKS0808+2106	BD+21 1764		08 08 13.1	+21 06 18	-296.7	-355.72	56.01	17.85	9.68	3.60	8.42
RKS0813-1355	BD-13 2439A		08 13 08.4	-13 55 01	-214.03	-483.21	46.96	21.30	9.77	3.95	8.13
RKS0814+1301	HD 68834		08 14 35.9	+13 01 22	-420.8	97.36	51.98	19.24	9.03	3.14	7.61
RKS0815-2600	V430 Pup		08 15 40.0	-26 00 35	228.49	-191.45	34.93	28.63	10.35	3.47	8.07
RKS0817+1717	LSPM J0817+1717		08 17 08.0	+17 17 56	111.9	-110.61	35.26	28.36	9.71	2.98	7.45
RKS0819+0120	BD+01 2063		08 19 19.0	+01 20 19	-164.19	-53.3	44.68	22.38	8.58	2.47	6.83
RKS0820+1404	BD+14 1876		08 20 55.3	+14 04 16	-83.68	-261.77	43.98	22.74	10.00	3.42	8.22
RKS0823+2150	BD+22 1921		08 23 30.9	+21 50 57	298.44	-245.47	39.82	25.12	9.73	3.18	7.73
RKS0827+2855	BD+29 1754		08 27 11.4	+28 55 53	-234.43	230.26	32.25	31.01	9.85	2.96	7.39
RKS0832-2323	BD-22 2311		08 32 33.3	-23 23 06	-113.68	103.51	35.56	28.12	10.40	3.46	8.15
RKS0838-0415	G 114-7		08 38 19.2	-04 15 29	-39.56	-333.51	31.87	31.38	11.69	3.92	9.21
RKS0838-1315	HD 73583		08 38 45.2	-13 15 24	-63.83	38.48	31.66	31.59	9.91	2.96	7.41
RKS0839+0657	HD 73512		08 39 00.2	+06 57 19	-89.93	-294.12	37.97	26.34	8.12	2.50	6.02
RKS0839+1131	HD 73667		08 39 50.7	+11 31 21	-109.22	-500.4	54.25	18.43	7.82	2.38	6.49
RKS0840-0628	BD-05 2603		08 40 00.2	-06 28 33	118.81	-149.44	39.28	25.46	10.12	3.74	8.09
RKS0848+0628	BD+07 2031A		08 48 26.1	+06 28 06	222.05	-439.39	35.18	28.42	10.67	3.68	8.40
RKS0850+0751	BD+08 2131A		08 50 42.2	+07 51 52	-43.41	-26.99	56.01	17.85	9.31	3.71	8.05
RKS0852+2819	rho01 Cnc		08 52 35.8	+28 19 50	-485.68	-233.52	79.45	12.59	6.17	2.16	5.67
RKS0855+0132	BD+02 2098		08 55 07.6	+01 32 47	44.94	-1045.88	48.74	20.52	10.21	3.86	8.65
RKS0901+1515	HD 77175A		09 01 17.4	+15 15 56	-125.93	-321.22	54.15	18.47	9.50	3.56	8.17
RKS0904-1554	HD 77825		09 04 20.6	-15 54 51	-107.74	-30.69	36.51	27.39	8.99	2.60	6.80
RKS0905+2517	BD+25 2037		09 05 18.4	+25 17 52	-312.19	-285.04	34.76	28.77	10.76	3.46	8.47
RKS0907+2252	HD 78141		09 07 18.0	+22 52 21	-1.13	-62.64	39.53	25.30	8.23	2.45	6.21

Table 8 continued on next page

Table 8 (continued)

RKS ID	Simbad Name	Coordinates			μ			Photometry		
		R.A. (hh mm ss)	Decl. (\pm dd mm ss)	$\mu_{R.A}$ (mas yr $^{-1}$)	μ_{Decl} (mas yr $^{-1}$)	π (mas)	Dist. (pc)	$B_{GaiaDR3}$ (mag)	$B_G - K_S$ (mag)	M_{B_G} (mag)
RKS0909+0512	HD 78727	09 09 54.1	+05 12 12	-63.48	-23.81	38.28	26.12	8.61	2.54	6.53
RKS0914+0426	HD 79555	09 14 53.6	+04 26 34	-75.45	19.6	55.93	17.88	8.18	2.93	6.92
RKS0918+2718	BD+27 1739	09 18 21.5	+27 18 41	-204.47	-164.76	47.72	20.96	9.77	3.53	8.16
RKS0919+0053	HD 80367	09 19 28.3	+00 53 49	-137.44	-125.76	34.94	28.62	8.36	2.32	6.08
RKS0920-0545	HD 80632	09 20 44.3	-05 45 14	-366.02	-116.56	41.42	24.15	9.33	3.06	7.42
RKS0929+0539	HD 82106	09 29 54.8	+05 39 18	-502.66	108.54	78.20	12.79	7.44	2.65	6.91
RKS0929-0522	BD-04 2639	09 29 35.0	-05 22 21	-479.74	25.63	41.45	24.13	9.99	3.47	8.08
RKS0932+2909	StKM 1-780	09 32 11.1	+29 09 25	24.98	-62.1	31.87	31.38	11.71	3.90	9.23
RKS0932-1111	LQ Hya	09 32 25.5	-11 11 04	-248.04	34.28	54.74	18.27	8.01	2.56	6.70
RKS0937+2231	BD+23 2124	09 37 58.3	+22 31 23	-78.69	-124.21	32.37	30.89	10.14	3.29	7.69
RKS0937+2241	BD+23 2121	09 37 11.3	+22 41 38	-151.29	-177.92	44.31	22.57	9.67	3.33	7.90
RKS0938+0240	Ross 888	09 38 23.9	+02 40 36	-335.02	-789.43	33.48	29.87	12.15	3.87	9.77
RKS0947+0134	G 53-4	09 47 16.6	+01 34 36	-49.93	283.06	33.50	29.86	11.18	3.62	8.80
RKS0952+0307	MCC 559	09 52 39.1	+03 07 48	-61.56	-32.97	37.28	26.82	10.81	3.73	8.67
RKS0959-0911	BD-08 2813	09 59 11.3	-09 11 00	-56.47	-73.33	30.26	33.05	10.11	2.97	7.51
RKS1000+2433	DH Leo	10 00 01.7	+24 33 10	-236.14	-37.67	32.17	31.09	8.25	2.81	5.79
RKS1001-1525	HD 86972	10 01 37.2	-15 25 29	-251.42	29.8	39.72	25.17	8.89	2.68	6.89
RKS1004-1143	HD 87424	10 04 37.6	-11 43 46	-191.59	-24.53	42.96	23.28	8.38	2.39	6.55
RKS1005+2629	HD 87445	10 05 26.5	+26 29 16	-187.38	-88.39	32.82	30.47	9.35	2.70	6.93
RKS1006+0257	BD+03 2316	10 06 56.8	+02 57 51	-67.57	-102.84	45.23	22.11	10.20	3.81	8.48
RKS1008+1159	HD 87884	10 08 12.7	+11 59 49	-254.4	8.13	41.28	24.23	8.37	2.49	6.45
RKS1011-2425	WT 1757	10 11 45.0	-24 25 33	175.56	-21.46	33.91	29.49	11.28	3.96	8.93
RKS1020-0128	HD 89668	10 20 43.4	-01 28 11	-664.87	-170.61	31.25	32.00	9.65	2.89	7.12
RKS1024-1024	BD-09 3063	10 24 14.9	-10 24 21	281.73	-249.19	34.45	29.03	10.22	3.30	7.91
RKS1026+2638	HD 90442	10 26 59.5	+26 38 29	161.26	-85.84	33.64	29.73	8.46	2.20	6.09
RKS1026-0631	BD-05 3063	10 26 41.2	-06 31 34	0.48	-641.53	32.56	30.71	9.99	2.79	7.55
RKS1028+0644	HD 90663	10 28 10.4	+06 44 06	26.4	327.84	38.32	26.09	8.76	2.50	6.68
RKS1030-2114	BD-20 3194	10 30 21.9	-21 14 12	-449.46	-47.15	34.58	28.92	9.86	3.04	7.55
RKS1032+0830	BD+09 2366	10 32 00.6	+08 30 38	83.63	-189.17	33.89	29.51	11.05	3.82	8.70
RKS1036-1350	V418 Hya	10 36 30.7	-13 50 35	-163.75	22.73	31.49	31.76	8.93	2.36	6.42
RKS1043-2903	V419 Hya	10 43 28.2	-29 03 51	-215.48	-49.89	46.49	21.51	7.95	2.29	6.29
RKS1046-2435	HD 93380	10 46 36.9	-24 35 07	-141.57	-110.04	46.97	21.29	9.61	3.17	7.97

Table 8 continued on next page

Table 8 (continued)

RKS ID	Simbad Name	Coordinates			μ			Photometry			
		R.A. (hh mm ss)	Decl. (\pm dd mm ss)	$\mu_{R,A}$ (mas yr $^{-1}$)	μ_{Decl} (mas yr $^{-1}$)	π (mas)	Dist. (pc)	$B_{GaiaDR3}$ (mag)	$B_G - K_S$ (mag)	M_{B_G} (mag)	
RKS1053-1422	HD 94374	10 53 22.5	-14 22 28	-426.01	-314.12	30.94	32.32	9.49	2.70	6.94	
RKS1054-0432	StKM 1-896	10 54 49.1	-04 32 30	-14.8	-25.28	35.41	28.24	10.81	3.73	8.56	
RKS1056+0723	HD 94765	10 56 30.7	+07 23 18	-256.99	-77.41	57.80	17.30	7.60	2.40	6.41	
RKS1057+2856	HD 94818	10 57 11.4	+28 56 16	353.58	-176.49	36.40	27.47	9.18	2.78	6.99	
RKS1059+2526	HD 95174A	10 59 38.3	+25 26 15	-176.72	-50.75	46.97	21.29	8.70	2.86	7.06	
RKS1102-0919	AB Cr1	11 02 50.1	-09 19 49	-193.33	-62.98	32.10	31.15	9.24	2.60	6.77	
RKS1108+1546	HD 96692	11 08 31.7	+15 46 03	154.61	-375.86	35.50	28.17	9.96	3.14	7.71	
RKS1108-2816	CD-27 7881	11 08 06.3	-28 16 04	-513.13	-62.69	36.77	27.19	9.56	3.43	7.39	
RKS1111-1057	HD 97214	11 11 10.7	-10 57 03	-942.34	592.92	50.30	19.88	9.45	3.12	7.96	
RKS1111-1459	HD 97233	11 11 33.1	-14 59 28	693.07	-599.18	51.88	19.28	9.27	3.40	7.84	
RKS1113+0428	HD 97503	11 13 13.2	+04 28 56	-315.52	-33.14	54.51	18.35	8.95	3.10	7.63	
RKS1114+2542	HD 97658	11 14 33.1	+25 42 37	-107.48	48.77	46.38	21.56	7.97	2.24	6.30	
RKS1114-2306	HD 97782A	11 14 48.1	-23 06 17	-296.25	-367.69	43.32	23.08	9.27	3.24	7.45	
RKS1115-1808	BD-17 3337	11 15 20.7	-18 08 37	144.01	-734.1	43.66	22.91	10.19	3.59	8.39	
RKS1116-1441	BD-13 3333	11 16 22.1	-14 41 36	-174.27	-120.51	54.79	18.25	10.23	3.77	8.92	
RKS1117-0158	BD-01 2505	11 17 13.6	-01 58 54	-568.3	-14.31	30.14	33.18	10.00	3.04	7.40	
RKS1117-2748	CD-27 7978	11 17 07.5	-27 48 48	204.84	-76.12	56.69	17.64	10.01	3.81	8.78	
RKS1121+1811	HD 98736	11 21 49.3	+18 11 24	-151.95	-92.39	30.95	32.31	8.20	2.17	5.65	
RKS1121-2027	HD 98712A	11 21 26.6	-20 27 13	174.02	-79.43	72.86	13.72	8.93	3.63	8.24	
RKS1125+2000	HD 99303	11 25 39.9	+20 00 07	-202.89	-91.7	31.72	31.53	8.55	2.20	6.06	
RKS1126+1517	BD+16 2260	11 26 49.9	+15 17 38	140.89	-30.94	38.00	26.31	10.68	3.71	8.58	
RKS1127+0358	BD+04 2470	11 27 38.5	+03 58 35	-97.46	14.09	34.81	28.73	10.90	3.91	8.61	
RKS1128+0731	Wolf 397	11 28 27.7	+07 31 02	-272.26	-1220.42	35.33	28.30	10.42	3.36	8.16	
RKS1134-1314	BD-12 3458	11 34 50.4	-13 14 31	-285.44	-68.71	33.06	30.25	10.58	3.25	8.18	
RKS1135+1658	BD+17 2376	11 35 59.1	+16 58 05	36.12	-36.19	31.33	31.92	9.81	2.97	7.29	
RKS1139-2741	CD-26 8683	11 39 08.1	-27 41 46	358.57	-275.99	33.37	29.97	10.21	3.30	7.83	
RKS1141+0508	BD+05 2529	11 41 49.5	+05 08 26	230.64	-469.13	31.76	31.48	9.82	3.40	7.33	
RKS1147-1149	HD 102392A	11 47 03.8	-11 49 26	-204.68	-77.18	38.55	25.94	9.28	3.09	7.21	
RKS1152+1845	HD 103072	11 52 08.3	+18 45 18	29.34	-302.86	37.32	26.80	8.62	2.35	6.48	
RKS1154+2844	BD+29 2228	11 54 57.4	+28 44 15	191.38	-299.88	36.63	27.30	10.74	3.74	8.56	
RKS1157+1959	GR Leo	11 57 28.9	+19 59 02	-387.04	53.88	36.02	27.76	8.28	2.19	6.06	
RKS1157-2608	HD 103836	11 57 16.2	-26 08 29	-351.02	145.34	38.92	25.70	9.17	2.76	7.12	

Table 8 continued on next page

Table 8 (continued)

Star Identifiers		Coordinates				μ				Photometry			
RKS ID	Simbad Name	R.A. (hh mm ss)	Decl. (\pm dd mm ss)	$\mu_{R,A}$ (mas yr $^{-1}$)	μ_{Decl} (mas yr $^{-1}$)	π (mas)	Dist. (pc)	$B_{GaiaDR3}$ (mag)	$B_G - K_S$ (mag)	M_{B_G} (mag)			
RKS1157-2742	HD 103932	11 57 56.2	-27 42 25	-1080.9	-620.93	98.30	10.17	7.20	2.67	7.16			
RKS1158-2355	HD 103949	11 58 11.7	-23 55 25	-172.75	-54.31	37.74	26.50	8.94	2.63	6.82			
RKS1159-2021	HD 104067	11 59 10.0	-20 21 13	141.71	-423.78	49.15	20.35	8.15	2.54	6.61			
RKS1204+0911	HD 104828	12 04 17.4	+09 11 35	-253.99	39.23	30.63	32.65	10.09	3.03	7.52			
RKS1204-0013	BD+00 2888	12 04 47.8	-00 13 36	-156.82	-53.73	34.63	28.88	11.05	2.87	8.75			
RKS1205-1852	HD 105065	12 05 50.6	-18 52 30	-15.02	-317.78	43.37	23.06	10.23	3.61	8.42			
RKS1206-2336	HD 105110	12 06 09.0	-23 36 08	62.7	-97.27	31.41	31.83	8.82	2.29	6.31			
RKS1208-0028	Wolf 406	12 08 22.2	-00 28 57	-962.73	-93.99	34.33	29.13	11.49	3.90	9.17			
RKS1209-2646	PM J12093-2646	12 09 23.4	-26 46 46	-70.7	-165.76	32.25	31.01	11.25	3.85	8.79			
RKS1210-1126	LP 734-35	12 10 33.6	-11 26 59	-212.01	-75.4	32.27	30.99	11.39	3.74	8.93			
RKS1220-1953	HD 107388	12 20 46.8	-19 53 45	-360.42	-61.2	34.02	29.40	9.24	2.65	6.90			
RKS1222+2736	BD+28 2110	12 22 34.0	+27 36 16	-145.61	-29.34	33.69	29.69	11.11	3.89	8.75			
RKS1223+2754	Wolf 411	12 23 34.7	+27 54 47	-137.5	120.76	33.87	29.52	11.55	3.88	9.20			
RKS1228-1654	HD 108564	12 28 19.1	-16 54 39	-558.28	45.11	36.68	27.27	9.67	2.77	7.49			
RKS1231+2013	HD 108984	12 31 18.2	+20 13 04	-22.02	-169.39	37.96	26.34	8.13	2.23	6.03			
RKS1233-1438	HD 109333	12 33 59.7	-14 38 19	-504.45	-27.03	38.05	26.28	9.35	2.91	7.25			
RKS1241+1951	HD 110376	12 41 37.0	+19 51 05	22.36	-23.46	31.35	31.90	9.32	2.58	6.80			
RKS1248-1543	HD 111312	12 48 32.2	-15 43 09	97.94	27.23	39.21	25.50	8.11	2.53	6.08			
RKS1248-2448	HD 111261	12 48 10.7	-24 48 23	-315.44	169.49	53.33	18.75	9.13	3.10	7.76			
RKS1250-0046	HD 111631	12 50 43.5	-00 46 05	-29.87	-397.0	93.86	10.65	8.72	3.84	8.58			
RKS1253+0645	HD 112099	12 53 54.4	+06 45 46	-231.85	93.54	36.59	27.33	8.46	2.31	6.28			
RKS1256-2455	CD-24 10619	12 56 30.0	-24 55 31	75.03	-218.45	32.24	31.02	10.28	3.27	7.82			
RKS1257-1427	HD 112575	12 57 43.9	-14 27 48	-361.65	6.05	39.50	25.32	9.40	2.97	7.38			
RKS1259-0950	HD 112758	12 59 01.5	-09 50 02	-824.46	195.01	49.83	20.07	7.76	2.23	6.25			
RKS1300-0242	HD 112943	13 00 16.9	-02 42 17	-806.69	7.37	36.63	27.30	10.01	3.24	7.83			
RKS1302-2647	HD 113194	13 02 20.6	-26 47 13	-157.13	-199.67	56.94	17.56	8.59	3.33	7.37			
RKS1303-0509	PX Vir	13 03 49.7	-05 09 42	-189.81	-222.36	48.88	20.46	7.89	2.38	6.34			
RKS1306+2043	BD+21 2486A	13 06 15.3	+20 43 45	-56.04	94.55	50.81	19.68	9.73	3.69	8.26			
RKS1310+0932	BD+10 2518	13 10 16.9	+09 32 09	182.85	-153.04	36.08	27.71	9.54	2.85	7.33			
RKS1312-0215	HD 114783	13 12 43.7	-02 15 54	-138.36	10.28	47.55	21.03	7.80	2.33	6.19			
RKS1316+1701	HD 115404	13 16 51.0	+17 01 01	636.29	-264.68	91.02	10.99	6.78	2.40	6.58			
RKS1318-1446	BD-14 3687	13 18 05.8	-14 46 48	-332.78	-235.79	34.37	29.10	11.11	3.61	8.79			

Table 8 continued on next page

Table 8 (continued)

RKS ID	Simbad Name	Coordinates			μ			Photometry			
		R.A. (hh mm ss)	Decl. (\pm dd mm ss)	$\mu_{R.A}$ (mas yr $^{-1}$)	μ_{Decl} (mas yr $^{-1}$)	π (mas)	Dist. (pc)	$B_{GaiaDR3}$ (mag)	$B_G - K_S$ (mag)	M_{B_G} (mag)	
RKSI320+0407	HD 116012	13 20 43.7	+04 07 58	-506.79	201.4	33.01	30.30	8.83	2.44	6.42	
RKSI323+0243	HD 116442	13 23 39.1	+02 43 23	12.47	199.29	60.28	16.59	7.27	2.17	6.17	
RKSI327-2417	HD 116920	13 27 02.9	-24 17 25	-339.25	-67.01	33.48	29.87	8.95	2.50	6.57	
RKSI331-0219	HD 117635	13 31 39.9	-02 19 02	-828.84	293.79	37.76	26.48	7.54	2.23	5.43	
RKSI333+0835	HD 117936	13 33 32.4	+08 35 12	-506.37	93.77	55.12	18.14	8.20	2.71	6.91	
RKSI334+0440	BD+05 2767	13 34 21.5	+04 40 02	153.86	-123.41	48.97	20.42	10.18	3.84	8.63	
RKSI334-0018	HD 118036A	13 34 16.2	-00 18 49	-197.84	20.18	37.20	26.88	7.87	2.62	5.72	
RKSI334-0820	HD 118100	13 34 43.2	-08 20 31	-286.59	-91.68	48.82	20.48	9.42	3.30	7.86	
RKSI335+0650	HD 118206	13 35 06.3	+06 50 27	-94.86	-69.93	32.21	31.04	9.14	2.65	6.68	
RKSI335-0023	BD+00 3077	13 35 24.7	-00 23 20	35.12	183.32	51.93	19.26	10.51	3.85	9.09	
RKSI336+0746	BD+08 2735	13 36 56.6	+07 46 01	-775.55	-361.21	31.84	31.41	10.21	3.02	7.72	
RKSI340-0411	HD 118926	13 40 07.1	-04 11 09	-385.22	481.31	66.20	15.11	9.84	3.80	8.94	
RKSI341-0007	HD 119217	13 41 55.6	-00 07 44	-162.21	-429.08	40.49	24.70	9.98	3.49	8.02	
RKSI342-0141	HD 119291	13 42 26.0	-01 41 10	-289.03	-154.63	40.61	24.62	9.46	3.13	7.50	
RKSI345+0850	HD 119802	13 45 14.7	+08 50 09	-66.36	-96.29	45.43	22.01	8.72	2.75	7.01	
RKSI345+1747	BD+18 2776	13 45 05.0	+17 47 07	450.97	-1833.25	77.44	12.91	10.02	3.80	9.47	
RKSI345-0437	BD-03 3527	13 45 05.3	-04 37 13	-163.83	-96.22	33.97	29.44	10.77	3.57	8.43	
RKSI347+0618	BD+07 2692	13 47 28.7	+06 18 56	-509.3	-111.0	31.84	31.41	10.24	3.23	7.75	
RKSI349-2206	HD 120467	13 49 44.8	-22 06 39	-1749.86	-494.21	71.08	14.07	8.41	3.25	7.67	
RKSI353+1256	BD+13 2721	13 53 27.5	+12 56 32	-171.76	-604.27	45.62	21.92	10.02	3.87	8.32	
RKSI353+2748	HD 121131	13 53 05.2	+27 48 24	226.57	-375.79	33.90	29.50	8.58	2.23	6.23	
RKSI359+2252	HD 122120	13 59 19.4	+22 52 11	-160.86	12.97	41.94	23.84	9.29	3.05	7.40	
RKSI411-1236	HD 124106	14 11 46.1	-12 36 42	-254.02	-179.73	43.39	23.05	8.15	2.29	6.34	
RKSI412+2348	GY Boo	14 12 41.5	+23 48 51	-26.86	-6.26	31.86	31.39	9.13	2.69	6.65	
RKSI413-0657	BD-06 3950	14 13 31.1	-06 57 32	110.45	136.72	54.59	18.32	10.40	3.83	9.09	
RKSI414-1521	HD 124498A	14 14 21.3	-15 21 22	-124.5	-168.12	34.50	28.99	10.50	3.90	8.19	
RKSI418-0636	HD 125354	14 18 58.2	-06 36 12	2.71	-432.22	44.38	22.53	9.35	3.50	7.59	
RKSI419-0509	HD 125455	14 19 34.8	-05 09 04	-632.95	-120.71	48.90	20.45	7.80	2.26	6.25	
RKSI421+2937	BD+30 2512	14 21 57.2	+29 37 46	-631.66	-308.47	68.85	14.52	8.77	3.35	7.96	
RKSI430-0838	HD 127339	14 30 47.7	-08 38 46	-1270.99	-238.52	63.36	15.78	9.63	3.86	8.64	
RKSI432+1121	BD+11 2687	14 32 13.1	+11 21 11	57.22	171.89	33.06	30.25	9.91	3.40	7.51	
RKSI433+0920	HD 127871	14 33 34.9	+09 20 03	158.36	-513.11	31.03	32.23	9.05	2.46	6.51	

Table 8 continued on next page

Table 8 (continued)

RKS ID	Simbad Name	Coordinates			μ			Photometry			
		R.A. (hh mm ss)	Decl. (\pm dd mm ss)	$\mu_{R,A}$ (mas yr $^{-1}$)	μ_{Decl} (mas yr $^{-1}$)	π (mas)	Dist. (pc)	$B_{GaiaDR3}$ (mag)	$B_G - K_S$ (mag)	M_{B_G} (mag)	
RKSI436+0944	HD 128311	14 36 00.5	+09 44 47	204.81	-250.46	61.28	16.32	7.70	2.56	6.64	
RKSI437-2548	HD 128356	14 37 04.8	-25 48 09	-18.43	-139.58	38.38	26.05	8.51	2.51	6.43	
RKSI442+1930	BD+20 3009	14 42 26.2	+19 30 12	-261.11	-178.35	42.32	23.63	10.26	3.60	8.39	
RKSI444+2211	BD+22 2742	14 44 11.9	+22 11 07	2.06	118.44	36.58	27.34	10.12	3.22	7.94	
RKSI444-2215	HD 129715	14 44 35.5	-22 15 11	-106.33	-338.88	33.01	30.30	9.54	2.97	7.13	
RKSI445+1350	HD 130004	14 45 24.1	+13 50 46	-231.64	-225.65	53.16	18.81	8.09	2.48	6.72	
RKSI446+1629	BD+17 2785	14 46 23.2	+16 29 48	-108.62	-921.88	56.37	17.74	9.48	3.42	8.24	
RKSI446+2730	HO Boo	14 46 03.0	+27 30 44	17.31	-40.99	37.76	26.48	8.19	2.21	6.08	
RKSI447+0242	HD 130307	14 47 16.1	+02 42 11	-287.14	-78.61	51.76	19.32	8.00	2.38	6.57	
RKSI450+0648	HD 130871	14 50 20.9	+06 48 53	-617.42	-66.23	32.20	31.06	9.31	2.59	6.85	
RKSI451-2418	HD 130992	14 51 40.4	-24 18 14	-944.62	-431.62	59.64	16.77	8.05	2.67	6.93	
RKSI453+2320	HD 131582	14 53 41.5	+23 20 42	-829.1	0.75	42.42	23.57	8.88	2.70	7.02	
RKSI455-2707	HD 131719	14 55 55.0	-27 07 38	-103.88	-22.75	36.68	27.26	9.23	2.75	7.05	
RKSI457-2124	HD 131977	14 57 28.0	-21 24 55	1031.47	-1723.62	169.88	5.89	5.98	2.93	7.13	
RKSI500-1108	HD 132683	15 00 43.4	-11 08 06	-15.48	-481.1	56.07	17.84	9.72	3.73	8.46	
RKSI500-2427	CD-23 12010	15 00 19.3	-24 27 14	-199.48	-28.0	36.35	27.51	10.15	3.35	7.95	
RKSI500-2905	TYC 6760-1510-1	15 00 09.5	-29 05 27	-3.24	-0.55	31.43	31.81	11.53	3.90	9.02	
RKSI501+1341	StKM 1-1198	15 01 06.5	+13 41 39	-143.44	7.44	30.71	32.56	11.24	3.71	8.68	
RKSI501+1552	HD 132950	15 01 29.9	+15 52 07	102.91	-237.45	34.37	29.10	9.34	2.76	7.02	
RKSI504+0538	BD+06 2986	15 04 53.5	+05 38 17	-607.63	-506.51	52.51	19.05	10.06	3.59	8.66	
RKSI504-1835	HD 133412	15 04 53.9	-18 35 27	-126.23	-123.42	30.30	33.00	9.74	3.30	7.15	
RKSI507+2456	BD+25 2874	15 07 23.5	+24 56 07	-845.74	494.22	52.54	19.03	10.29	3.82	8.89	
RKSI509+2400	BD+24 2824	15 09 04.2	+24 00 57	-471.67	161.12	30.73	32.54	9.56	2.82	7.00	
RKSI510-1622	HD 134439	15 10 13.0	-16 22 45	-998.06	-3542.27	34.02	29.40	9.26	2.28	6.92	
RKSI515+0047	HD 135599	15 15 59.1	+00 47 46	178.1	-137.16	63.21	15.82	7.14	2.18	6.14	
RKSI515+0735	BD+08 3000	15 15 45.4	+07 35 52	-28.37	-187.35	31.57	31.67	10.94	3.52	8.44	
RKSI519+1155	BD+12 2823	15 19 35.3	+11 55 19	-55.35	17.14	31.26	31.99	10.24	3.17	7.71	
RKSI519+2912	BD+29 2654	15 19 21.1	+29 12 22	-141.02	395.5	35.67	28.04	10.47	3.37	8.23	
RKSI520+1522	BD+15 2847	15 20 38.9	+15 22 48	-421.05	-162.4	32.59	30.69	9.03	2.79	6.60	
RKSI522+0125	HD 136834	15 22 42.5	+01 25 07	-364.21	-364.11	38.50	25.97	8.52	2.48	6.45	
RKSI522-0446	BD-04 3873	15 22 04.1	-04 46 38	-296.98	-12.5	52.21	19.15	9.70	3.52	8.29	
RKSI522-1039	HD 136713	15 22 36.6	-10 39 40	-57.39	-203.77	45.28	22.08	8.20	2.48	6.48	

Table 8 continued on next page

Table 8 (continued)

Star Identifiers		Coordinates				μ				Photometry			
RKS ID	Simbad Name	R.A. (hh mm ss)	Decl. (\pm dd mm ss)	$\mu_{R,A}$ (mas yr $^{-1}$)	μ_{Decl} (mas yr $^{-1}$)	π (mas)	Dist. (pc)	$B_{GaiaDR3}$ (mag)	$B_G - K_S$ (mag)	M_{B_G} (mag)			
RKS1525-2642	HD 137303	15 25 58.5	-26 42 20	-818.91	-9.97	45.10	22.17	9.04	2.88	7.31			
RKS1527+0235	BD+03 3032	15 27 42.6	+02 35 51	-51.83	-18.41	35.36	28.28	10.45	3.55	8.19			
RKS1527+1035	BD+11 2811	15 27 38.0	+10 35 39	-424.07	-262.34	36.55	27.36	10.07	3.42	7.88			
RKS1528-0920	HD 137763	15 28 09.6	-09 20 52	73.58	-375.35	51.14	19.55	7.10	2.21	5.64			
RKS1540-1802	HD 139763	15 40 34.5	-18 02 56	161.15	89.73	64.18	15.58	9.15	3.46	8.19			
RKS1552+1052	BD+11 2874	15 52 08.2	+10 52 28	-265.28	-240.14	47.43	21.08	9.61	3.79	7.99			
RKS1554-2600	HD 142288	15 54 38.4	-26 00 15	-230.61	101.05	42.14	23.73	9.43	3.19	7.55			
RKS1555+1602	V383 Ser	15 55 19.0	+16 02 39	-222.35	-216.2	30.98	32.28	8.92	2.75	6.38			
RKS1600-0147	BD-01 3125	16 00 16.4	-01 47 55	124.5	-135.31	32.66	30.62	10.50	3.35	8.07			
RKS1601-2625	PM J16016-2625	16 01 39.7	-26 25 15	137.86	-43.55	40.90	24.45	11.05	3.87	9.11			
RKS1604-1126	HD 144088	16 04 26.7	-11 26 59	-56.33	-20.36	35.87	27.88	8.23	2.12	6.00			
RKS1607-0542	G 153-25	16 07 34.3	-05 42 25	150.2	-178.45	30.41	32.88	10.63	3.53	8.05			
RKS1608+1713	BD+17 2966	16 08 05.3	+17 13 44	-58.38	37.01	31.24	32.01	9.37	2.62	6.84			
RKS1608-1308	HD 144840	16 08 24.4	-13 08 07	-61.59	-285.26	35.38	28.26	8.92	2.54	6.66			
RKS1613+1331	49 Ser A	16 13 18.4	+13 31 36	178.93	-419.94	41.13	24.31	7.57	2.40	5.64			
RKS1615+0721	HD 146413A	16 15 57.0	+07 21 25	177.31	-476.11	37.06	26.99	9.51	3.45	7.35			
RKS1621+1713	G 138-22	16 21 38.0	+17 13 33	-46.48	-271.74	30.92	32.34	10.85	3.48	8.30			
RKS1624-1338	V2578 Oph	16 24 19.8	-13 38 29	-218.79	-206.55	46.87	21.34	8.61	2.61	6.96			
RKS1625-2156	BD-21 4352	16 25 13.0	-21 56 14	-571.03	-337.8	53.74	18.61	10.62	3.90	9.27			
RKS1626+1539	G 138-28	16 26 33.4	+15 39 53	9.33	265.26	36.49	27.40	10.78	3.58	8.59			
RKS1627+0055	BD+01 3236	16 27 20.3	+00 55 29	-23.48	24.59	35.08	28.51	10.21	3.42	7.94			
RKS1627+0718	HD 148467	16 27 56.9	+07 18 19	-248.8	-264.66	57.09	17.52	9.06	3.26	7.84			
RKS1629+2346	BD+24 3014	16 29 14.3	+23 46 34	-63.01	-315.13	30.51	32.78	10.30	3.25	7.72			
RKS1630-0359	BD-03 3952	16 30 43.0	-03 59 21	-154.53	-20.89	36.73	27.22	9.80	3.21	7.63			
RKS1632-1235	BD-12 4542	16 32 57.8	-12 35 30	-312.0	-223.85	31.54	31.71	10.83	3.58	8.32			
RKS1633-0933	LP 745-70	16 33 41.6	-09 33 11	-64.89	-177.91	32.17	31.09	11.46	3.91	9.00			
RKS1647-0111	BD-00 3182	16 47 17.5	-01 11 20	-16.39	-244.18	32.99	30.31	10.96	3.54	8.55			
RKS1649-2426	HD 151692	16 49 53.1	-24 26 48	-276.59	-109.08	30.13	33.19	9.81	2.92	7.20			
RKS1650+1854	HD 151995	16 50 05.2	+18 54 01	-46.93	-71.98	36.47	27.42	9.09	2.72	6.90			
RKS1654+1154	Ross 644	16 54 12.0	+11 54 52	-543.69	316.21	49.80	20.08	10.99	3.88	9.48			
RKS1659-2616	CD-26 11751	16 59 33.2	-26 16 04	129.06	-286.62	35.98	27.79	10.61	3.69	8.39			
RKS1701+2256	BD+23 3035	17 01 59.8	+22 56 09	-131.43	84.67	36.21	27.62	9.05	2.66	6.84			

Table 8 continued on next page

Table 8 (continued)

RKS ID	Star Identifiers	Coordinates			μ			Photometry		
		R.A. (hh mm ss)	Decl. (\pm dd mm ss)	$\mu_{R.A}$ (mas yr $^{-1}$)	μ_{Decl} (mas yr $^{-1}$)	π (mas)	Dist. (pc)	$B_{GaiaDR3}$ (mag)	$B_G - K_S$ (mag)	M_{B_G} (mag)
RKSI705-0147	HD 154361	17 05 08.5	-01 47 09	75.39	-43.47	32.19	31.07	9.58	2.78	7.12
RKSI705-0503	HD 154363	17 05 03.3	-05 03 59	-916.34	-1138.76	95.57	10.46	7.95	3.22	7.85
RKSI706-0610	HD 154518	17 06 08.2	-06 10 02	-92.24	-63.47	33.09	30.22	9.03	2.58	6.63
RKSI712+1821	HD 155712	17 12 37.6	+18 21 04	101.8	-116.87	48.05	20.81	8.18	2.51	6.59
RKSI714-0824	HD 155802A	17 14 08.0	-08 24 13	-99.84	71.94	33.66	29.71	8.73	2.56	6.37
RKSI716-1210	BD-12 4699	17 16 20.2	-12 10 41	143.44	-22.82	38.20	26.18	10.56	3.65	8.47
RKSI717+2913	HD 156668	17 17 40.4	+29 13 38	-72.48	216.85	41.11	24.32	8.66	2.66	6.73
RKSI725+0206	HD 157881	17 25 45.2	+02 06 41	-580.33	-1184.74	129.65	7.71	7.77	3.40	8.33
RKSI729-2350	HD 158233	17 29 06.5	-23 50 10	-288.67	-72.79	54.37	18.39	9.85	3.46	8.53
RKSI733+0914	RX J1733.1+0914	17 33 07.2	+09 14 37	31.16	-19.98	31.89	31.35	9.85	3.10	7.37
RKSI737+2257	BD+23 3151A	17 37 48.7	+22 57 20	-151.59	-146.03	43.86	22.80	10.18	3.89	8.39
RKSI737-1314	HD 159911	17 37 46.4	-13 14 46	-17.39	-126.18	30.11	33.21	10.30	3.47	7.69
RKSI739+0333	HD 160346	17 39 16.9	+03 33 18	-194.61	-100.64	99.14	10.09	6.75	2.65	6.73
RKSI750-0603	HD 162283	17 50 34.0	-06 03 01	-27.71	-132.78	45.02	22.21	10.40	3.86	8.67
RKSI752-0733	HD 162598	17 52 16.6	-07 33 37	-229.39	352.9	32.63	30.65	10.17	3.20	7.74
RKSI753+2119	BD+21 3245	17 53 29.9	+21 19 31	-73.09	57.71	40.78	24.52	8.72	2.52	6.77
RKSI754-2649	HD 314741	17 54 54.1	-26 49 41	42.51	-104.29	31.80	31.45	10.63	3.72	8.14
RKSI755+0345	BD+03 3531a	17 55 24.7	+03 45 16	-79.62	24.27	39.74	25.16	10.37	3.55	8.37
RKSI755+1830	BD+18 3497	17 55 44.8	+18 30 01	-46.4	-47.43	44.43	22.51	9.43	3.13	7.67
RKSI757-2143	HD 163573	17 57 40.9	-21 43 10	39.99	-154.3	30.64	32.64	10.23	3.55	7.66
RKSI803+2545	Ross 820	18 03 47.7	+25 45 20	-46.84	-230.02	35.97	27.80	11.10	3.90	8.88
RKSI804+0149	HD 165045	18 04 01.8	+01 49 56	96.0	-28.12	32.69	30.59	8.33	2.22	5.90
RKSI809-0019	HD 166184	18 09 32.2	-00 19 37	79.08	-13.05	34.45	29.03	9.17	2.63	6.86
RKSI809-1202	BD-12 4935	18 09 33.2	-12 02 19	67.01	-206.82	36.67	27.27	10.73	3.74	8.55
RKSI815+1829	HD 348282	18 15 18.2	+18 29 59	50.14	59.56	34.26	29.19	10.29	3.47	7.96
RKSI816+1354	BD+13 3578	18 16 02.2	+13 54 48	98.79	-501.1	54.73	18.27	10.41	3.85	9.10
RKSI817+2640	HD 335828	18 17 49.8	+26 40 16	328.37	107.52	32.56	30.71	9.79	2.84	7.35
RKSI818-0642	HD 168159	18 18 40.6	-06 42 03	-67.15	-10.48	33.43	29.91	9.51	2.79	7.13
RKSI819-0156	HD 168442	18 19 50.8	-01 56 19	-0.41	-0.11	52.40	19.09	9.90	3.62	8.50
RKSI822+0142	BD+01 3657	18 22 17.2	+01 42 25	84.2	-19.69	37.86	26.41	10.37	3.51	8.26
RKSI829+0903	HD 170510	18 29 31.9	+09 03 43	188.79	72.82	36.26	27.58	8.88	2.55	6.68
RKSI829-0149	HD 170493	18 29 52.4	-01 49 05	172.06	-193.42	53.16	18.81	8.28	2.80	6.91

Table 8 continued on next page

Table 8 (continued)

RKS ID	Star Identifiers	Coordinates			μ			Photometry			
		R.A. (hh mm ss)	Decl. (\pm dd mm ss)	$\mu_{R.A}$ (mas yr $^{-1}$)	μ_{Decl} (mas yr $^{-1}$)	π (mas)	Dist. (pc)	$B_{GaiaDR3}$ (mag)	$B_G - K_S$ (mag)	M_{B_G} (mag)	
RKS1829-2758	HD 170209	18 29 22.3	-27 58 19	-67.38	-448.34	36.73	27.23	9.62	3.13	7.44	
RKS1831-1854	HD 170657	18 31 18.9	-18 54 31	-138.22	-195.47	75.85	13.18	7.04	2.34	6.44	
RKS1833+2218	HD 171314	18 33 17.7	+22 18 51	-176.25	-472.62	42.73	23.41	9.14	2.98	7.29	
RKS1833-1138	BD-11 4672	18 33 28.8	-11 38 09	-288.44	-235.62	36.75	27.21	10.25	3.38	8.08	
RKS1833-1626	HD 171075	18 33 24.8	-16 26 39	-0.06	-40.45	31.69	31.56	9.32	2.88	6.82	
RKS1847-0338	HD 173818	18 47 27.2	-03 38 23	-132.28	-274.87	70.13	14.26	9.05	3.47	8.28	
RKS1848+1044	HD 174080	18 48 29.2	+10 44 43	128.09	-436.54	59.24	16.88	8.20	2.81	7.06	
RKS1848+1726	HD 229590	18 48 51.8	+17 26 20	-408.8	-422.82	59.78	16.73	9.42	3.50	8.30	
RKS1848-1008	HD 173872	18 48 01.4	-10 08 46	111.07	-175.44	35.09	28.50	8.68	2.59	6.41	
RKS1850-2655	CD-27 13268	18 50 21.1	-26 55 25	-140.52	-23.19	56.66	17.65	9.94	3.76	8.71	
RKS1854+0051	BD+00 4050	18 54 53.2	+00 51 46	-70.4	-126.77	40.12	24.93	10.85	3.88	8.87	
RKS1854+1058	HD 230017A	18 54 53.6	+10 58 40	29.43	129.98	53.42	18.72	9.66	3.77	8.30	
RKS1854+2844	PM J18547+2844	18 54 43.7	+28 44 55	-6.6	116.53	31.30	31.95	11.52	3.83	9.00	
RKS1855+2333	HD 175742	18 55 53.2	+23 33 23	130.96	-283.56	46.88	21.33	8.35	2.71	6.71	
RKS1858-0030	HD 176157	18 58 56.4	-00 30 14	-110.33	-117.94	31.86	31.38	8.60	2.22	6.12	
RKS1858-1014	BD-10 4886	18 58 03.3	-10 14 37	102.46	-35.29	30.66	32.62	10.10	3.06	7.53	
RKS1859+0759	BD+07 3922	18 59 38.6	+07 59 14	366.17	-181.28	35.33	28.30	11.07	3.92	8.81	
RKS1859+1107	HD 230325	18 59 39.2	+11 07 04	10.51	64.03	32.92	30.37	9.44	2.80	7.03	
RKS1901+0328	TYC 466-2991-1	19 01 51.0	+03 28 14	114.73	5.83	32.19	31.07	10.00	3.06	7.54	
RKS1903-1102	HD 176986	19 03 05.8	-11 02 38	-126.95	-235.94	35.86	27.89	8.65	2.43	6.42	
RKS1907+0736	HD 178126	19 07 02.0	+07 36 57	-324.45	-759.86	40.95	24.42	9.45	2.98	7.51	
RKS1908+1627	HD 230742	19 08 02.6	+16 27 37	-144.98	-145.24	31.28	31.97	10.48	3.33	7.96	
RKS1908-1640	PM J19081-1640	19 08 10.7	-16 40 41	-89.43	-59.28	37.86	26.41	10.64	3.59	8.53	
RKS1910+2145	TYC 1598-1505-1	19 10 32.1	+21 45 46	-12.23	-18.38	30.08	33.25	11.54	3.84	8.93	
RKS1915+1133	V1688 Aql	19 15 35.0	+11 33 16	183.5	-173.0	37.87	26.41	8.28	2.34	6.17	
RKS1915+2453	HD 338030	19 15 18.8	+24 53 49	240.47	219.05	34.57	28.93	9.94	3.57	7.63	
RKS1923-0635	HD 182085	19 23 16.4	-06 35 07	-171.92	-198.48	32.04	31.21	9.92	3.11	7.45	
RKS1924+2525	PM J19244+2525	19 24 26.5	+25 25 50	-30.57	-75.07	31.44	31.81	11.18	3.75	8.67	
RKS1924-2203	CD-22 13916	19 24 34.2	-22 03 43	-230.9	-451.83	36.15	27.66	11.16	3.73	8.95	
RKS1928+1232	HD 231512A	19 28 15.3	+12 32 09	-52.79	-39.96	34.46	29.02	9.41	3.06	7.10	
RKS1928+2854	PM J19284+2854	19 28 25.5	+28 54 10	-9.41	-40.8	38.60	25.91	11.09	3.85	9.02	
RKS1929+0709	BD+06 4156	19 29 05.1	+07 09 35	246.24	240.5	37.83	26.44	10.90	3.71	8.79	

Table 8 continued on next page

Table 8 (continued)

Star Identifiers		Coordinates				μ			Photometry			
RKS ID	Simbad Name	R.A. (hh mm ss)	Decl. (\pm dd mm ss)	$\mu_{R,A}$ (mas yr $^{-1}$)	μ_{Decl} (mas yr $^{-1}$)	π (mas)	Dist. (pc)	$B_{GaiaDR3}$ (mag)	$B_G - K_S$ (mag)	M_{B_G} (mag)		
RKS1930+2140	HD 344502	19 30 05.4	+21 40 34	-215.93	-200.29	34.46	29.02	10.18	3.11	7.87		
RKS1932+0034	BD+00 4241	19 32 37.9	+00 34 39	218.12	25.03	45.14	22.15	10.67	3.86	8.94		
RKS1932-1116	HD 183870	19 32 06.7	-11 16 29	234.59	18.16	56.57	17.68	7.75	2.42	6.51		
RKS1934+0434	HD 184489	19 34 39.8	+04 34 57	524.41	311.08	69.26	14.44	9.57	3.65	8.77		
RKS1936-1026	HD 184860A	19 36 45.6	-10 26 36	-290.8	-270.84	33.38	29.96	8.87	2.55	6.49		
RKS1943+1005	HD 355784	19 43 25.3	+10 05 22	186.19	101.98	38.36	26.07	10.21	3.37	8.13		
RKS1952-2356	HD 187760	19 52 29.9	-23 56 57	19.74	-41.35	38.83	25.75	9.69	3.08	7.64		
RKS1954+2013	PM J19546+2013	19 54 37.5	+20 13 06	-38.04	-62.89	36.39	27.48	11.06	3.83	8.86		
RKS1954-2356	HD 188088	19 54 17.7	-23 56 27	-124.17	-410.68	70.70	14.14	6.44	2.40	5.69		
RKS1957+1313	HD 356314	19 57 25.4	+13 13 24	-8.4	-42.73	38.17	26.20	10.39	3.53	8.30		
RKS2000+2242	HD 189733	20 00 43.7	+22 42 39	-3.21	-250.32	50.57	19.78	7.91	2.37	6.43		
RKS2002+0319	HD 190007	20 02 47.0	+03 19 34	-90.38	119.43	78.65	12.72	7.70	2.90	7.18		
RKS2003+2005	HD 351151	20 03 00.9	+20 05 49	180.61	-12.57	33.30	30.03	10.84	3.57	8.45		
RKS2003+2320	HD 190404	20 03 52.1	+23 20 26	-1003.99	-912.72	64.01	15.62	7.49	2.38	6.52		
RKS2004+2547	HD 190470	20 04 10.0	+25 47 24	-75.4	-39.36	45.22	22.11	8.04	2.40	6.32		
RKS2008+0640	BD+06 4450	20 08 24.3	+06 40 43	170.71	169.48	34.68	28.83	10.05	3.12	7.75		
RKS2009+1648	HD 191499A	20 09 34.3	+16 48 20	2.9	175.71	40.33	24.80	7.89	2.26	5.92		
RKS2009-0307	BD-03 4797	20 09 41.0	-03 07 44	-196.99	-42.23	32.35	30.91	9.81	3.07	7.36		
RKS2009-1417	HD 191285	20 09 36.4	-14 17 12	78.89	-91.88	31.79	31.45	10.00	3.03	7.51		
RKS2010-2029	HD 191391	20 10 19.5	-20 29 36	-427.58	-367.38	63.21	15.82	9.15	3.45	8.15		
RKS2011+1611	HD 191785	20 11 06.0	+16 11 16	-415.06	398.49	48.93	20.44	7.55	2.20	6.00		
RKS2012-1253	LP 754-50	20 12 09.4	-12 53 35	192.66	-194.04	35.43	28.22	11.54	3.92	9.29		
RKS2013-0052	HD 192263	20 13 59.8	-00 52 00	-62.73	260.82	50.94	19.63	8.01	2.47	6.55		
RKS2014-0716	BD-07 5223	20 14 28.1	-07 16 55	10.77	-271.1	46.14	21.67	10.42	3.69	8.74		
RKS2015-2701	HD 192310	20 15 17.3	-27 01 58	1242.76	-181.18	113.49	8.81	5.95	2.45	6.23		
RKS2016-0204	G 24-12	20 16 22.0	-02 04 08	289.95	-31.96	37.62	26.59	11.40	3.85	9.28		
RKS2030+2650	HD 340345	20 30 10.6	+26 50 34	-156.7	-132.11	49.03	20.40	9.94	3.59	8.39		
RKS2035+0607	HD 196124	20 35 12.7	+06 07 37	389.05	-227.71	33.11	30.21	9.14	2.61	6.74		
RKS2038+2346	HD 347103	20 38 26.2	+23 46 41	57.14	-55.19	30.11	33.21	8.96	2.33	6.35		
RKS2039+1004	HD 196794	20 39 22.0	+10 04 32	318.02	21.31	33.44	29.90	8.75	2.34	6.37		
RKS2041-0529	BD-06 5559	20 41 40.6	-05 29 34	77.43	65.22	32.63	30.65	10.77	3.54	8.34		
RKS2041-2219	HD 196998	20 41 42.2	-22 19 20	656.07	-538.71	41.33	24.20	10.11	3.50	8.19		

Table 8 continued on next page

Table 8 (continued)

RKS ID	Star Identifiers	Coordinates			μ			Photometry			
		R.A. (hh mm ss)	Decl. (\pm dd mm ss)	$\mu_{R.A}$ (mas yr $^{-1}$)	μ_{Decl} (mas yr $^{-1}$)	π (mas)	Dist. (pc)	$B_{GaiaDR3}$ (mag)	$B_G - K_S$ (mag)	M_{B_G} (mag)	
RKS2042+2050	HD 197396	20 42 49.3	+20 50 40	-80.98	-353.25	40.42	24.74	8.49	2.48	6.52	
RKS2042-2116	HD 197092	20 42 05.8	-21 16 37	-43.4	-47.03	50.53	19.79	9.49	2.31	8.01	
RKS2044-2121	BD-21 5811	20 44 00.6	-21 21 20	57.41	-276.41	38.43	26.02	10.10	3.35	8.02	
RKS2047+1051	BD+10 4379	20 47 16.8	+10 51 36	89.6	-591.62	31.50	31.75	9.96	2.96	7.45	
RKS2050+2923	HD 198550	20 50 10.5	+29 23 02	-3.08	-36.29	49.59	20.16	8.57	2.96	7.05	
RKS2053-0245	BD-03 5059	20 53 56.9	-02 45 57	-610.88	-369.03	30.95	32.31	11.30	3.63	8.75	
RKS2055+1310	BD+12 4499	20 55 06.8	+13 10 36	557.52	369.83	42.37	23.60	9.04	2.86	7.18	
RKS2059+0333	Wolf 901	20 59 08.5	+03 33 09	324.82	-725.88	30.57	32.71	12.22	3.81	9.65	
RKS2059-1042	HD 199704	20 59 14.4	-10 42 49	47.13	-21.56	30.90	32.36	8.74	2.48	6.19	
RKS2105+0704	HD 200779	21 05 19.7	+07 04 09	78.56	-563.91	66.46	15.05	8.53	3.22	7.64	
RKS2105-1654	HD 358850	21 05 43.4	-16 54 49	-14.5	-58.4	45.73	21.87	10.55	3.86	8.85	
RKS2107-1355	HD 200968A	21 07 10.3	-13 55 22	382.97	-50.69	57.52	17.38	7.40	2.38	6.20	
RKS2108-0425	BD-05 5480	21 08 45.4	-04 25 36	-80.36	-29.12	34.85	28.69	9.66	3.23	7.37	
RKS2116+0923	HD 202575	21 16 32.4	+09 23 37	145.63	-118.6	61.84	16.17	8.15	2.76	7.11	
RKS2118+0009	HD 202751	21 18 02.9	+00 09 41	467.41	-188.34	49.48	20.21	8.41	2.67	6.88	
RKS2119-2621	HD 202940	21 19 45.6	-26 21 10	-589.25	-351.16	54.03	18.51	6.76	2.19	5.42	
RKS2120-1951	HD 203040	21 20 13.8	-19 51 08	-173.09	-721.09	63.39	15.78	9.34	3.62	8.35	
RKS2122+1052	BD+10 4534	21 22 26.6	+10 52 25	-56.8	32.88	47.14	21.21	10.16	3.72	8.53	
RKS2125+2712	HD 204079	21 25 29.0	+27 12 38	-180.43	-155.05	39.70	25.19	8.50	2.30	6.49	
RKS2126+0344	MCC 70	21 26 42.4	+03 44 13	-39.99	-53.59	36.07	27.73	10.72	3.72	8.51	
RKS2130-1230	HD 204587	21 30 02.7	-12 30 36	1019.8	-259.6	56.43	17.72	9.32	3.44	8.08	
RKS2132-2057	HD 204941	21 32 23.5	-20 57 26	-278.87	-124.32	34.88	28.67	8.67	2.31	6.38	
RKS2141+1115	HD 206315	21 41 01.3	+11 15 46	-75.12	-109.89	31.43	31.82	9.41	2.77	6.90	
RKS2149+0543	HD 207491	21 49 12.2	+05 43 22	541.96	-27.03	44.31	22.57	8.90	2.74	7.13	
RKS2149-1140	BD-12 6102	21 49 45.9	-11 40 57	-301.92	-309.56	32.60	30.67	11.10	3.75	8.67	
RKS2152+0154	HD 207874	21 52 06.5	+01 54 23	-75.16	-188.52	32.56	30.71	8.42	2.24	5.98	
RKS2153+2055	HD 208038	21 53 05.3	+20 55 49	-5.26	-100.69	43.03	23.24	8.41	2.46	6.58	
RKS2153+2850	StKM 1-1953	21 53 07.2	+28 50 15	-60.22	-60.39	37.02	27.01	11.71	3.92	9.55	
RKS2153-1249	LP 758-74	21 53 07.5	-12 49 40	-145.79	-135.86	41.53	24.08	11.24	3.88	9.33	
RKS2155-2942	HD 208272	21 55 41.9	-29 42 22	57.24	-180.08	30.63	32.65	8.68	2.19	6.11	
RKS2210+2247	BD+22 4567	22 10 31.4	+22 47 49	-570.45	-50.95	30.10	33.22	9.43	2.62	6.82	
RKS2214+2751	G 188-49	22 14 31.4	+27 51 18	-211.58	532.4	50.82	19.68	10.57	3.84	9.10	

Table 8 continued on next page

Table 8 (continued)

RKS ID	Simbad Name	Coordinates			μ			Photometry			
		R.A. (hh mm ss)	Decl. (\pm dd mm ss)	$\mu_{R.A}$ (mas yr $^{-1}$)	μ_{Decl} (mas yr $^{-1}$)	π (mas)	Dist. (pc)	$B_{GaiaDR3}$ (mag)	$B_G - K_S$ (mag)	M_{B_G} (mag)	
RKS2224+2233	BD+21 4747A	22 24 45.5	+22 33 04	-183.49	-76.66	47.92	20.87	9.16	3.40	7.56	
RKS2226-1911	HD 212658	22 26 13.5	-19 11 18	235.02	-24.89	39.16	25.53	9.49	3.01	7.45	
RKS2239+0406	HD 214683	22 39 50.7	+04 06 58	178.16	108.81	44.30	22.57	8.71	2.57	6.94	
RKS2240-2940	HD 214749	22 40 43.3	-29 40 28	380.49	-16.94	75.33	13.28	8.07	3.03	7.45	
RKS2241+1849	BD+18 5029	22 41 35.0	+18 49 27	253.15	89.57	32.36	30.91	10.96	3.90	8.51	
RKS2243-0624	HD 215152	22 43 21.3	-06 24 02	-154.1	-289.92	46.33	21.58	8.34	2.56	6.67	
RKS2247+1823	BD+17 4808	22 47 13.6	+18 23 04	251.85	88.6	37.47	26.69	9.25	2.82	7.12	
RKS2248+2443	MCC 209	22 48 35.5	+24 43 26	176.9	9.34	33.27	30.06	11.18	3.74	8.79	
RKS2251+1358	HD 216259	22 51 26.3	+13 58 11	406.24	202.5	44.31	22.57	8.51	2.43	6.74	
RKS2252+2324	BD+22 4725	22 52 02.5	+23 24 47	131.46	-153.78	35.78	27.95	10.03	3.21	7.80	
RKS2254+2331	G 67-33	22 54 30.8	+23 31 06	257.6	73.77	30.05	33.28	11.35	3.84	8.74	
RKS2258-1338	HD 217065	22 58 06.2	-13 38 33	37.47	-327.78	35.83	27.91	10.36	3.34	8.13	
RKS2259-1122	BD-12 6393	22 59 53.6	-11 22 54	220.31	-69.59	38.47	26.00	10.82	3.72	8.75	
RKS2301-0350	HD 217580	23 01 51.5	-03 50 55	402.75	-213.67	61.83	16.17	7.71	2.48	6.67	
RKS2307-2309	HD 218294	23 07 07.0	-23 09 34	156.28	-255.09	45.24	22.11	9.84	3.42	8.12	
RKS2308+0633	R78b 355	23 08 52.4	+06 33 39	103.61	8.28	30.22	33.09	11.13	3.88	8.53	
RKS2309+1425	AG+14 2584	23 09 54.9	+14 25 35	-120.44	-96.62	39.76	25.15	10.48	3.64	8.48	
RKS2309-0215	HD 218566	23 09 10.7	-02 15 38	631.54	-97.4	34.70	28.82	8.83	2.61	6.53	
RKS2310-2955	HD 218760	23 10 48.8	-29 55 03	450.86	-26.06	36.33	27.52	8.88	2.56	6.68	
RKS2316+0541	BD+04 4988	23 16 51.8	+05 41 45	22.92	-27.15	38.04	26.29	10.76	3.73	8.66	
RKS2317-2323	CD-24 17578	23 17 00.2	-23 23 46	306.99	-243.22	43.03	23.24	11.11	3.86	9.28	
RKS2323-1045	HD 220339	23 23 04.8	-10 45 51	452.19	260.31	52.16	19.17	8.02	2.43	6.61	
RKS2326+0853	G 29-33	23 26 12.3	+08 53 37	518.99	213.4	44.36	22.54	10.81	3.89	9.05	
RKS2327-0117	BD-02 5958	23 27 04.8	-01 17 10	375.98	215.87	33.73	29.65	10.60	3.41	8.24	
RKS2328+1604	BD+15 4829	23 28 26.1	+16 04 00	49.09	-96.95	32.31	30.95	10.05	3.04	7.60	
RKS2332-1650	HD 221503	23 32 49.3	-16 50 44	341.15	-219.11	68.74	14.55	8.85	3.38	8.04	
RKS2335+0136	BD+00 5017	23 35 00.2	+01 36 19	340.03	28.46	47.96	20.85	9.82	3.78	8.22	
RKS2340+2021	HD 222474A	23 40 51.4	+20 21 57	221.77	53.26	39.41	25.38	8.53	2.98	6.51	
RKS2342-0234	BD-03 5691	23 42 10.6	-02 34 36	-236.11	-345.18	40.30	24.82	10.57	3.71	8.60	
RKS2345+2933	HD 222935	23 45 09.9	+29 33 42	947.12	-3.91	33.61	29.75	8.61	2.37	6.24	
RKS2348-1259	BD-13 6464	23 48 25.6	-12 59 14	235.08	15.17	35.00	28.57	9.87	3.58	7.59	
RKS2349+0310	HD 223374	23 49 01.1	+03 10 52	67.7	-0.42	39.89	25.07	8.63	2.46	6.63	

Table 8 continued on next page

Table 8 (continued)

RKS ID	Simbad Name	Coordinates			μ			Photometry			
		R.A. (hh mm ss)	Decl. (\pm dd mm ss)	$\mu_{R.A}$ (mas yr $^{-1}$)	μ_{Decl} (mas yr $^{-1}$)	π (mas)	Dist. (pc)	$B_{GaiaDR3}$ (mag)	$B_G - K_S$ (mag)	M_{B_G} (mag)	
RKS2350-2924	HD 223515	23 50 14.9	-29 24 06	186.98	18.88	38.76	25.80	8.10	2.23	6.04	
RKS2353+2901	BD+28 4660	23 53 08.5	+29 01 05	-78.55	19.39	50.23	19.91	9.98	3.59	8.48	
RKS2355+2211	HD 224129	23 55 26.5	+22 11 35	202.05	-147.05	39.26	25.47	8.99	2.79	6.96	
RKS2358+0949	HD 224476	23 58 19.8	+09 49 50	69.09	-1.77	33.44	29.90	8.56	2.31	6.18	
RKS2359+0639	HD 224660A	23 59 47.7	+06 39 50	-58.7	-166.83	43.44	23.02	9.15	3.14	7.34	
RKS2359-2602	HD 224607	23 59 13.6	-26 02 55	-229.47	12.38	43.87	22.79	8.93	2.82	7.14	

NOTE—This table presents the complete sample of 589 primary K dwarf stars in the equatorial 33.3 pc volume-limited sample. Column descriptions: RKS ID is the RECONS K Star identifier; R.A. and Decl. are J2000.0 coordinates; $\mu_{R.A.}$ and $\mu_{Decl.}$ are proper motions from Gaia DR3 with uncertainties; π is parallax with uncertainty; Dist. is distance calculated from parallax; B_{Gaia} is the Gaia G-band magnitude; $B_G - K_S$ is the color index using 2MASS K_S photometry; M_{B_G} is the absolute G-band magnitude. This represents the final sample used for all analyses presented in this work.

D. KINEMATIC PROPERTIES OF SURVEY SAMPLE K DWARFS

Table 9. Primary K dwarf Sample: Kinematic Properties

RKS ID	$\gamma_{\text{Gaia DR3}}$ (km s ⁻¹)	γ_{REC} (km s ⁻¹)	$\sigma_{\gamma_{\text{REC}}}$ (km s ⁻¹)	U (km s ⁻¹)	V (km s ⁻¹)	W (km s ⁻¹)	Group	Disk
RKS0000+1659	-17.92	-17.65	0.04	29.50	-33.84	-16.46	Field	Thin disk
RKS0001-1656	0.47	0.58	0.04	-20.08	-51.95	-15.93	Field	Thin disk
RKS0007-2349	-43.17	-43.08	0.04	-55.34	-16.44	34.82	Field	Thin disk
RKS0012+2142	-5.02	-5.01	0.05	-5.64	-39.08	-32.91	Field	Thin disk
RKS0012+2705	12.50	12.57	0.04	-30.26	-11.37	-20.62	Field	Thin disk
RKS0016-1435	-13.51	-13.62	0.04	0.26	-4.41	12.92	Field	Thin disk
RKS0017+2057	-49.24	-49.51	0.05	62.59	-44.15	1.22	Field	Thick disk
RKS0019-0303	-20.92	-20.97	0.05	21.36	-31.58	6.30	Field	Thin disk
RKS0019-0957	-10.72	-11.02	0.04	17.88	-25.36	2.30	Field	Thin disk
RKS0020+1738	-2.49	-2.14	0.05	0.72	-10.82	-7.35	Field	Thin disk
RKS0021+2531	-22.21	-22.20	0.04	0.99	-18.89	13.52	Field	Thin disk
RKS0022-2701	-2.53	-0.54	0.04	-4.09	-52.60	-3.02	Field	Thin disk
RKS0024-2701	3.05	3.23	0.04	-52.03	-21.61	-9.09	Field	Thin disk
RKS0036-0930	29.72	29.80	0.05	60.50	-44.71	-51.80	Field	Thick disk
RKS0036+2610	-15.46	-15.32	0.04	-2.71	-12.84	12.32	Field	Thin disk
RKS0039+2115	-33.07	-32.95	0.03	40.07	-19.47	8.44	Field	Thin disk
RKS0042+2239	3.98	4.23	0.05	-53.43	-27.01	-2.16	Field	Thin disk
RKS0045+0147	9.38	9.45	0.03	31.21	-37.85	-37.54	Field	Thin disk
RKS0048+0516	-10.37	-10.22	0.04	-1.07	-47.50	-13.26	Field	Thin disk
RKS0051-2254	14.52	14.62	0.04	-27.15	-40.24	-16.03	Field	Thin disk
RKS0051+1844	6.51	6.63	0.04	3.40	-15.59	-24.91	Field	Thin disk
RKS0055-2940	7.43	7.69	0.03	-62.58	-14.34	-7.68	Field	Thin disk
RKS0057+0551	-15.97	-16.08	0.05	8.97	-4.42	13.43	Field	Thin disk
RKS0102-1025	8.84	9.03	0.04	5.42	-13.67	-13.62	Field	Thin disk
RKS0102+0503	...	20.35	0.04	-46.30	5.25	-3.42	Field	Thin disk
RKS0104-2536	5.70	5.58	0.04	26.26	-31.14	-6.90	Field	Thin disk
RKS0104+2607	8.39	8.36	0.04	-41.29	-18.78	-1.19	Hyades	Thin disk
RKS0105+1523	-5.98	-5.79	0.04	11.54	-19.80	-13.05	Field	Thin disk
RKS0107+2257	6.59	6.63	0.03	4.20	-28.13	-40.19	Field	Thin disk
RKS0108+1714	-56.38	-56.88	0.05	60.89	-75.07	-15.37	Field	Thick disk
RKS0112-2514	-4.67	-4.73	0.04	-12.00	-6.11	5.93	Field	Thin disk
RKS0113+1629	26.07	26.19	0.04	-10.39	7.15	-24.62	Field	Thin disk
RKS0116+2519	-23.10	-23.39	0.04	-23.81	-48.81	9.70	Field	Thin disk
RKS0117-1530	-7.04	-7.08	0.03	7.72	-84.56	-3.62	Field	Thick disk
RKS0118-0052	16.81	17.15	0.04	-34.96	-52.55	-23.93	Field	Thin disk
RKS0121+2419	10.74	10.93	0.04	-41.06	-18.69	-0.74	Hyades	Thin disk
RKS0122-2653	21.02	21.05	0.03	24.10	-22.70	-22.16	Field	Thin disk
RKS0123-1257	34.60	34.69	0.04	-58.88	-37.34	-26.20	Field	Thick disk
RKS0124+1829	6.99	7.05	0.04	-58.55	-62.06	-14.49	Field	Thick disk
RKS0125-0103	-5.35	-5.28	0.04	46.78	-17.26	-18.50	Field	Thin disk
RKS0129+2143	21.35	20.79	0.04	-44.73	-30.93	-21.28	Field	Thin disk
RKS0135-2046	18.97	18.82	0.05	-14.46	-12.49	-16.04	Field	Thin disk
RKS0139+1515	-21.54	-21.44	0.04	-5.52	-29.40	15.59	Field	Thin disk

Continued on next page

Table 9 continued from previous page

RKS ID	$\gamma_{\text{Gaia DR3}}$ (km s ⁻¹)	γ_{REC} (km s ⁻¹)	$\sigma_{\gamma_{\text{REC}}}$ (km s ⁻¹)	U (km s ⁻¹)	V (km s ⁻¹)	W (km s ⁻¹)	Group	Disk
RKS0142+2016	-33.70	-33.63	0.04	34.90	-24.95	2.15	Field	Thin disk
RKS0146+1224	21.59	21.68	0.04	-11.07	0.63	-20.80	Field	Thin disk
RKS0150+1817	22.38	22.19	0.04	-35.09	-18.52	-15.08	Field	Thin disk
RKS0150+2927	-39.60	-39.53	0.04	29.97	-24.06	13.10	Field	Thin disk
RKS0200+2636	-17.91	-18.47	0.05	-9.37	-20.80	24.84	Field	Thin disk
RKS0205-2804	3.30	3.45	0.05	-64.92	12.04	8.63	Field	Thin disk
RKS0209-1620	13.07	13.01	0.04	-60.59	-36.88	10.66	Field	Thick disk
RKS0213-2111	2.92	3.05	0.04	-34.55	-22.77	11.04	Field	Thin disk
RKS0214-0338	-8.80	-8.67	0.04	17.44	-18.04	-2.47	Field	Thin disk
RKS0215-1814	...	3.10	0.04	9.92	-8.24	-6.39	Field	Thin disk
RKS0221-0652	26.12	26.27	0.04	-42.93	-18.64	-7.21	Field	Thin disk
RKS0229-1958	27.46	27.66	0.04	-62.05	-20.92	-1.78	Field	Thin disk
RKS0231-1516	-28.44	-28.39	0.04	27.71	-2.76	18.55	Field	Thin disk
RKS0231-2001	22.24	22.20	0.04	-30.85	-19.87	-8.33	Field	Thin disk
RKS0236-0309	20.53	35.58	0.04	-47.69	-17.35	-11.69	Field	Thin disk
RKS0236-2331	16.25	16.49	0.04	-12.13	-7.82	-11.66	Field	Thin disk
RKS0236-2710	11.64	11.73	0.04	7.13	-29.49	-7.16	Field	Thin disk
RKS0236+0653	25.21	24.39	0.03	-75.74	1.59	33.67	Field	Thick disk
RKS0240+0111	72.93	72.91	0.04	-77.58	6.11	-31.39	Field	Thick disk
RKS0242+0322	-6.80	-6.98	0.05	22.51	-2.75	-10.18	Field	Thin disk
RKS0243+1925	32.98	33.69	0.04	-50.16	-15.43	-2.85	Field	Thin disk
RKS0246-2305	32.49	32.43	0.04	-43.33	-17.73	-13.24	Field	Thin disk
RKS0246+1146	10.82	11.00	0.04	-14.61	-22.48	-8.55	Field	Thin disk
RKS0246+2538	14.06	14.13	0.04	-25.42	-24.71	-8.37	Field	Thin disk
RKS0247+2842	1.61	1.53	0.04	12.33	16.46	-9.16	Field	Thin disk
RKS0248-1145	30.44	30.31	0.04	7.52	-18.68	-38.19	Field	Thin disk
RKS0248+2704	10.13	11.19	0.05	-25.34	-23.76	-2.12	Field	Thin disk
RKS0250+1542	-29.19	-28.93	0.04	11.36	-63.38	6.34	Field	Thin disk
RKS0251-0816	18.17	18.14	0.04	-11.89	-4.95	-13.59	Field	Thin disk
RKS0251+1038	0.20	0.27	0.05	16.17	-2.85	-18.39	Field	Thin disk
RKS0252-1246	17.80	18.12	0.06	-15.33	-21.81	-9.21	Field	Thin disk
RKS0255+2652	31.92	32.09	0.04	-39.29	-19.83	-17.75	Field	Thin disk
RKS0255+2807	50.52	50.74	0.04	-62.77	-22.84	-21.19	Field	Thick disk
RKS0257-2458	...	49.20	0.09	-17.11	-17.19	-43.00	Field	Thin disk
RKS0258+2646	42.58	31.48	0.04	-26.26	24.36	-3.00	Field	Thin disk
RKS0300+0744	28.62	28.83	0.04	-42.96	-18.88	-0.93	Hyades	Thin disk
RKS0303+2006	44.89	44.98	0.04	-35.93	5.89	-27.40	Field	Thin disk
RKS0306+0157	-31.35	-31.18	0.04	35.98	-67.51	4.95	Field	Thick disk
RKS0308-2410	16.43	16.42	0.04	10.29	-19.03	-17.60	Field	Thin disk
RKS0310+1203	38.91	38.89	0.04	-41.38	-32.09	-19.80	Field	Thin disk
RKS0314-2626	15.14	15.32	0.04	-22.91	-12.18	-2.25	Field	Thin disk
RKS0314+0858	-16.73	-16.65	0.04	5.54	-63.74	8.60	Field	Thin disk
RKS0320+0827	30.81	30.94	0.05	-41.71	-19.25	-0.81	Hyades	Thin disk
RKS0322+2709	30.13	29.95	0.05	-41.53	-19.27	-1.43	Hyades	Thin disk
RKS0324-0521	-13.36	-13.10	0.04	47.81	-28.78	-21.32	Field	Thin disk
RKS0329-1140	13.49	13.52	0.04	7.89	-28.20	-16.60	Field	Thin disk

Continued on next page

Table 9 continued from previous page

RKS ID	$\gamma_{\text{Gaia DR3}}$ (km s ⁻¹)	γ_{REC} (km s ⁻¹)	$\sigma_{\gamma_{\text{REC}}}$ (km s ⁻¹)	U (km s ⁻¹)	V (km s ⁻¹)	W (km s ⁻¹)	Group	Disk
RKS0332-0927	...	16.29	0.04	-3.54	7.11	-20.59	Field	Thin disk
RKS0341+0336	0.40	1.65	0.12	13.96	-18.45	-18.86	Field	Thin disk
RKS0342-2427	15.99	16.06	0.04	25.60	-37.96	-17.43	Field	Thin disk
RKS0343-1253	-53.21	-52.97	0.05	44.76	37.27	20.99	Field	Thin disk
RKS0343-1906	25.17	25.30	0.04	-30.42	-14.86	-4.57	Field	Thin disk
RKS0343+1640	34.10	34.41	0.05	-28.99	-23.32	-25.17	Field	Thin disk
RKS0344+1155	83.68	83.88	0.04	-89.03	-6.38	-17.59	Field	Thick disk
RKS0345-2751	32.36	32.57	0.04	-35.98	-26.92	-6.26	Field	Thin disk
RKS0348+1512	-43.22	-43.01	0.04	34.13	-24.37	22.70	Field	Thin disk
RKS0348+2519	-69.17	-69.00	0.04	62.60	-27.89	17.32	Field	Thick disk
RKS0349-1329	-5.26	-5.32	0.05	18.75	-3.53	-7.62	Field	Thin disk
RKS0350-2349	-0.33	-0.31	0.04	22.27	-31.06	2.04	Field	Thin disk
RKS0354-0649	62.14	62.23	0.04	-66.53	15.64	-27.13	Field	Thick disk
RKS0357-0109	3.41	3.51	0.04	7.82	0.55	-15.46	Field	Thin disk
RKS0404+2634	62.23	62.47	0.05	-67.88	-18.96	-10.87	Field	Thick disk
RKS0406-2051	25.17	25.18	0.04	53.49	-75.93	-34.32	Field	Thick disk
RKS0407+1413	-18.23	-18.07	0.04	13.13	-34.69	11.88	Field	Thin disk
RKS0408+1220	4.96	5.11	0.04	2.22	-52.12	-15.17	Field	Thin disk
RKS0417+2033	14.24	14.29	0.04	-10.09	-1.49	-14.07	Field	Thin disk
RKS0419-0408	36.87	36.91	0.04	-32.33	-19.14	-12.25	Field	Thin disk
RKS0420-1445	36.62	36.49	0.04	-42.85	-18.80	-1.36	Hyades	Thin disk
RKS0421-1945	21.57	21.33	0.05	19.32	-15.86	-39.25	Field	Thin disk
RKS0427+2426	67.57	68.14	0.04	-81.66	-21.34	25.01	Field	Thick disk
RKS0429+2155	-35.74	-35.48	0.04	33.34	6.76	14.17	Field	Thin disk
RKS0430+0058	28.35	28.32	0.06	-22.68	-18.96	-10.61	Field	Thin disk
RKS0436+2707	40.18	43.68	0.09	-46.50	-15.75	-3.58	Field	Thin disk
RKS0441+2054	0.55	1.19	0.16	4.83	-3.49	-20.85	Field	Thin disk
RKS0445+0938	94.67	94.79	0.05	-86.31	-38.20	-28.10	Field	Thick disk
RKS0448-1056	27.16	27.32	0.05	-13.79	-26.73	-11.65	Field	Thin disk
RKS0449-1447	27.86	28.00	0.05	8.87	-20.09	-45.28	Field	Thin disk
RKS0451+2837	6.48	6.41	0.04	-9.07	-15.70	4.08	Field	Thin disk
RKS0453+2214	26.24	26.31	0.04	-27.15	-23.85	-1.73	Field	Thin disk
RKS0454+0722	46.46	46.78	0.04	-38.77	-51.75	-4.84	Field	Thin disk
RKS0455-2833	5.97	6.20	0.04	10.01	-23.60	5.13	Field	Thin disk
RKS0503+0322	-3.79	-3.80	0.05	7.53	-4.09	-4.78	Field	Thin disk
RKS0506-1102	30.17	30.42	0.05	-18.61	-22.33	-13.13	Field	Thin disk
RKS0512+1943	-0.50	-0.41	0.04	9.76	-111.16	-11.02	Field	Thick disk
RKS0513-2158	52.67	53.51	0.04	-41.26	-32.29	-16.99	Field	Thin disk
RKS0514+0039	13.41	13.18	0.04	13.59	-68.18	-6.95	Field	Thin disk
RKS0514+1952	43.92	44.04	0.04	-42.11	-51.82	2.80	Field	Thin disk
RKS0518-2123	26.89	27.12	0.04	-13.06	-10.74	-25.27	Field	Thin disk
RKS0519-0304	88.48	88.79	0.04	-85.46	-56.61	14.10	Field	Thick disk
RKS0519-1550	-14.15	-14.05	0.05	-8.45	11.16	30.52	Field	Thin disk
RKS0522+0236	36.98	37.60	0.04	-26.49	-28.70	-14.80	Field	Thin disk
RKS0523+1719	38.03	38.30	0.04	-38.74	-14.67	7.11	Field	Thin disk
RKS0533-2643	48.66	48.72	0.04	-46.79	-22.95	-14.42	Field	Thin disk

Continued on next page

Table 9 continued from previous page

RKS ID	$\gamma_{\text{Gaia DR3}}$ (km s ⁻¹)	γ_{REC} (km s ⁻¹)	$\sigma_{\gamma_{\text{REC}}}$ (km s ⁻¹)	U (km s ⁻¹)	V (km s ⁻¹)	W (km s ⁻¹)	Group	Disk
RKS0534-2328	-28.47	-28.53	0.04	60.79	-34.23	30.83	Field	Thick disk
RKS0535+2805	30.44	30.55	0.04	-31.16	-51.99	2.48	Field	Thin disk
RKS0536+1119	21.36	21.66	0.05	-19.70	-7.53	-5.79	Field	Thin disk
RKS0542+0240	52.89	53.00	0.03	-12.17	-102.09	-17.45	Field	Thick disk
RKS0544-2225	-9.80	-9.57	0.04	17.64	5.15	-11.83	Field	Thin disk
RKS0549-1734	4.18	4.32	0.04	-12.96	6.85	0.83	Field	Thin disk
RKS0552-2246	78.18	78.09	0.04	-85.96	-48.13	20.97	Field	Thick disk
RKS0553-0559	22.97	23.04	0.04	0.23	-34.88	-20.69	Field	Thin disk
RKS0554-1942	44.02	43.90	0.05	-27.64	-35.03	-7.10	Field	Thin disk
RKS0554+0208	-33.90	-33.81	0.04	65.91	-51.09	-21.37	Field	Thick disk
RKS0600+2101	-2.13	-2.09	0.04	8.68	-40.03	-28.59	Field	Thin disk
RKS0602+0848	-39.13	-39.25	0.05	36.37	10.45	14.97	Field	Thin disk
RKS0608+2630	25.57	28.47	0.04	-28.44	-5.01	-4.52	Field	Thin disk
RKS0609+0009	36.95	36.88	0.04	-21.56	-41.00	5.71	Field	Thin disk
RKS0609+0540	60.77	60.75	0.03	-57.38	-22.39	3.46	Field	Thin disk
RKS0612+1023	40.65	40.69	0.04	-37.36	-14.70	-9.89	Field	Thin disk
RKS0614+0510	71.23	71.24	0.04	-47.46	-64.58	-19.00	Field	Thick disk
RKS0616+2512	42.19	47.26	0.04	-41.85	-60.77	-16.99	Field	Thick disk
RKS0617+1759	4.08	3.90	0.04	0.91	-20.54	8.00	Field	Thin disk
RKS0618-1352	101.05	101.15	0.04	-103.80	-41.16	3.33	Field	Thick disk
RKS0620+0215	31.49	31.71	0.04	-24.55	-16.78	-22.84	Field	Thin disk
RKS0621-2212	-31.45	-31.22	0.04	44.98	4.89	-0.53	Field	Thin disk
RKS0626+1845	...	-59.51	0.09	58.29	8.74	-16.11	Field	Thin disk
RKS0629+2700	-47.73	-47.67	0.03	43.82	-31.30	-60.97	Field	Thick disk
RKS0630-1148	43.24	43.33	0.04	-41.99	-13.29	-20.57	Field	Thin disk
RKS0632-2701	73.46	73.47	0.05	-1.23	-97.69	17.16	Field	Thick disk
RKS0633+0527	-1.09	-1.03	0.04	9.17	-16.93	7.64	Field	Thin disk
RKS0637+1945	82.49	82.72	0.04	-78.79	-24.65	7.49	Field	Thick disk
RKS0641+2357	-44.59	-44.27	0.04	48.81	-19.27	-1.42	Field	Thin disk
RKS0647-1815	99.62	99.65	0.04	-75.46	-62.73	-25.16	Field	Thick disk
RKS0652-0510	-7.34	-7.07	0.04	0.02	12.79	-19.86	Field	Thin disk
RKS0652-2306	61.20	61.27	0.04	-36.11	-55.50	22.15	Field	Thin disk
RKS0658-1259	-4.65	-5.03	0.05	13.68	-6.80	3.36	Field	Thin disk
RKS0700-2847	47.92	47.91	0.05	-22.32	-36.07	-33.05	Field	Thin disk
RKS0701-2556	12.44	9.81	0.04	-3.50	-12.05	12.44	Field	Thin disk
RKS0701+0655	-12.09	-11.89	0.04	7.88	10.02	-3.10	Field	Thin disk
RKS0702-0647	-30.60	-30.48	0.04	34.41	6.99	-28.91	Field	Thin disk
RKS0706+2358	6.99	6.99	0.04	-7.17	-25.40	-21.95	AB Dor	Thin disk
RKS0707+0326	-17.45	-19.70	0.04	31.83	-16.56	-15.49	Field	Thin disk
RKS0708-0958	26.41	26.58	0.03	-29.83	-6.77	-22.64	Field	Thin disk
RKS0708+2950	19.63	19.68	0.04	-23.58	-26.43	-21.21	Field	Thin disk
RKS0710-1425	71.21	71.04	0.04	-86.73	-15.69	-33.76	Field	Thick disk
RKS0712-2453	41.60	41.69	0.04	-26.80	-30.01	-18.91	Field	Thin disk
RKS0713+2500	-54.43	-54.54	0.04	34.95	18.07	-66.04	Field	Thick disk
RKS0716-0339	10.96	11.12	0.03	1.22	-17.96	11.71	Field	Thin disk
RKS0723-2001	12.61	12.53	0.03	31.36	-37.07	-18.04	Field	Thin disk

Continued on next page

Table 9 continued from previous page

RKS ID	$\gamma_{\text{Gaia DR3}}$ (km s ⁻¹)	γ_{REC} (km s ⁻¹)	$\sigma_{\gamma_{\text{REC}}}$ (km s ⁻¹)	U (km s ⁻¹)	V (km s ⁻¹)	W (km s ⁻¹)	Group	Disk
RKS0723+1257	37.79	37.88	0.03	-15.83	-60.08	-3.20	Field	Thin disk
RKS0723+2024	7.56	7.88	0.18	-5.02	-27.18	-17.05	AB Dor	Thin disk
RKS0724-1753	-8.79	-8.48	0.05	6.82	5.63	-7.23	Field	Thin disk
RKS0725-1041	27.89	27.62	0.05	-11.57	-29.75	-41.56	Field	Thin disk
RKS0726-1546	-1.08	-1.07	0.04	10.93	-7.51	-0.78	Field	Thin disk
RKS0730-0340	45.78	45.79	0.04	-44.17	-20.83	-7.80	Field	Thin disk
RKS0732+1719	22.72	27.67	0.05	-30.24	-22.84	-25.71	Field	Thin disk
RKS0734-0653	-9.96	-9.67	0.06	6.09	5.93	-11.13	Field	Thin disk
RKS0739-0335	-18.40	-18.19	0.04	25.22	-2.38	-7.47	Field	Thin disk
RKS0741-2921	31.51	31.63	0.04	-31.48	-19.08	-15.95	Field	Thin disk
RKS0745+0208	-34.77	-34.66	0.04	42.16	-1.36	-12.20	Field	Thin disk
RKS0752+2555	-43.51	-43.38	0.04	41.74	-4.83	-18.90	Field	Thin disk
RKS0754-2518	63.08	63.35	0.04	-53.93	-43.60	-11.57	Field	Thick disk
RKS0754+1914	-18.56	-18.63	0.03	29.57	-35.41	-14.55	Field	Thin disk
RKS0757-0048	-4.62	-4.44	0.03	-3.37	6.09	-12.03	Field	Thin disk
RKS0758-1501	52.12	47.88	0.03	-4.70	-57.69	-9.06	Field	Thin disk
RKS0758-2537	-8.19	-8.00	0.04	34.99	-8.17	15.57	Field	Thin disk
RKS0759+2050	-28.16	-28.37	0.04	46.34	-54.57	-16.03	Field	Thick disk
RKS0808+2106	79.32	79.17	0.04	-73.24	-49.24	3.87	Field	Thick disk
RKS0813-1355	8.00
RKS0814+1301	21.10	21.39	0.04	-39.97	4.25	-19.84	Field	Thin disk
RKS0815-2600	12.78	12.70	0.04	30.51	-26.63	12.57	Field	Thin disk
RKS0817+1717	-22.70	-22.47	0.04	29.95	-6.97	-2.59	Field	Thin disk
RKS0819+0120	...	27.59	0.06	-26.05	-19.04	-7.43	Field	Thin disk
RKS0820+1404	7.22	7.17	0.05	-1.97	-26.77	-14.43	AB Dor	Thin disk
RKS0823+2150	-27.30	-26.93	0.04	47.28	-23.53	7.25	Field	Thin disk
RKS0827+2855	54.85	55.06	0.04	-67.97	25.73	9.11	Field	Thick disk
RKS0832-2323	25.02	25.15	0.04	-28.78	-14.98	-0.12	Field	Thin disk
RKS0838-0415	52.96	52.95	0.05	-9.03	-71.63	-9.37	Field	Thick disk
RKS0838-1315	20.46	20.64	0.05	-19.80	-12.52	1.41	Field	Thin disk
RKS0839+0657
RKS0839+1131	-12.02	-12.04	0.04	18.08	-30.90	-29.43	Field	Thin disk
RKS0840-0628	-12.32	-11.28	0.11	25.10	-5.04	-1.61	Field	Thin disk
RKS0848+0628	...	-23.26	0.04	58.52	-37.07	-11.94	Field	Thick disk
RKS0850+0751	...	-12.73	0.06	7.06	5.38	-10.11	Field	Thin disk
RKS0852+2819	27.19	27.27	0.04	-37.16	-18.14	-8.22	Field	Thin disk
RKS0855+0132	-4.27	-4.10	0.04	52.87	-75.35	-43.70	Field	Thick disk
RKS0901+1515	-12.34	-12.19	0.04	9.91	-19.43	-24.19	Field	Thin disk
RKS0904-1554	4.57	4.59	0.05	-8.75	-5.70	-11.11	Field	Thin disk
RKS0905+2517	-24.96	-24.80	0.05	-3.10	-29.48	-55.33	Field	Thin disk
RKS0907+2252	-12.41	-23.16	0.08	17.88	0.35	-16.52	Field	Thin disk
RKS0909+0512	-8.95	-8.71	0.03	1.07	2.85	-11.71	Field	Thin disk
RKS0914+0426	12.19	13.32	0.04	-12.77	-6.79	3.47	Field	Thin disk
RKS0918+2718	6.62	6.72	0.04	-15.76	-17.89	-12.54	Field	Thin disk
RKS0919+0053	51.06	51.03	0.04	-31.97	-46.63	6.81	Field	Thin disk
RKS0920-0545	37.00	36.96	0.04	-39.69	-37.28	-18.27	Field	Thin disk

Continued on next page

Table 9 continued from previous page

RKS ID	$\gamma_{\text{Gaia DR3}}$ (km s ⁻¹)	γ_{REC} (km s ⁻¹)	$\sigma_{\gamma_{\text{REC}}}$ (km s ⁻¹)	U (km s ⁻¹)	V (km s ⁻¹)	W (km s ⁻¹)	Group	Disk
RKS0929-0522	27.63	27.72	0.04	-53.60	-21.03	-21.72	Field	Thin disk
RKS0929+0539	29.75	29.86	0.04	-40.92	-13.76	-0.07	Field	Thin disk
RKS0932-1111	6.99	7.50	1.37	-20.23	-5.44	-9.37	Field	Thin disk
RKS0932+2909	-29.78	-29.73	0.06	23.95	-2.42	-20.08	Field	Thin disk
RKS0937+2231	...	-4.02	0.04	-1.19	-16.72	-14.11	Field	Thin disk
RKS0937+2241	-36.38	-36.27	0.04	15.42	-7.49	-40.57	Field	Thin disk
RKS0938+0240	116.98	116.99	0.06	-40.21	-163.57	-7.58	Field	Thick disk
RKS0947+0134	31.11	31.05	0.05	-38.10	10.16	32.62	Field	Thin disk
RKS0952+0307	13.36	13.43	0.04	-10.01	-12.42	2.15	Field	Thin disk
RKS0959-0911	30.89	32.78	0.04	-10.87	-33.44	6.92	Field	Thin disk
RKS1000+2433	-0.72
RKS1001-1525	19.06	19.33	0.05	-30.28	-18.28	-5.95	Field	Thin disk
RKS1004-1143	-12.34	-12.10	0.05	-12.02	4.69	-20.84	Field	Thin disk
RKS1005+2629	0.37	0.33	0.04	-18.22	-16.46	-17.11	Field	Thin disk
RKS1006+0257	-15.92	-15.46	0.04	5.40	-0.14	-19.39	Field	Thin disk
RKS1008+1159	6.59	6.83	0.05	-26.77	-7.16	-11.56	Field	Thin disk
RKS1011-2425	10.41	10.31	0.05	20.25	-6.26	16.39	Field	Thin disk
RKS1020-0128	23.07	23.12	0.03	-76.59	-53.83	-51.12	Field	Thick disk
RKS1024-1024	-3.49	-3.58	0.04	50.77	-10.58	-1.34	Field	Thin disk
RKS1026-0631	30.64	32.24	0.05	40.39	-85.52	-28.56	Field	Thick disk
RKS1026+2638	-13.72	-14.44	0.04	29.30	-3.35	-1.34	Field	Thin disk
RKS1028+0644	24.78	25.00	0.03	-24.03	20.37	35.89	Field	Thin disk
RKS1030-2114	31.55	31.56	0.04	-50.24	-43.73	-19.95	Field	Thin disk
RKS1032+0830	...	-39.24	0.05	34.83	0.57	-34.12	Field	Thin disk
RKS1036-1350	18.90	19.06	0.04	-25.03	-18.81	1.55	Field	Thin disk
RKS1043-2903	22.57	22.89	0.07	-15.10	-28.04	-4.22	Field	Thin disk
RKS1046-2435	-11.93	-11.97	0.04	-6.16	1.81	-20.73	Field	Thin disk
RKS1053-1422	74.79	74.89	0.04	-36.07	-103.70	-11.41	Field	Thick disk
RKS1054-0432	17.06	16.94	0.05	-2.61	-14.05	9.90	Field	Thin disk
RKS1056+0723	5.32	5.44	0.04	-16.47	-14.06	-6.72	Field	Thin disk
RKS1057+2856	-30.54	-32.93	0.04	60.09	-2.82	-10.67	Field	Thin disk
RKS1059+2526	-2.99	-2.81	0.04	-12.42	-9.52	-10.37	Field	Thin disk
RKS1102-0919	-6.33	-6.48	0.05	-19.33	-10.24	-21.56	Field	Thin disk
RKS1108-2816	...	20.69	0.04	-50.98	-42.34	-21.84	Field	Thin disk
RKS1108+1546	104.19	104.13	0.04	11.45	-74.38	90.14	Field	Thick disk
RKS1111-1057	37.40	37.08	0.04	-106.14	-20.75	26.23	Field	Thick disk
RKS1111-1459	-14.13	-13.82	0.04	82.24	0.00	-20.89	Field	Thick disk
RKS1113+0428	16.40	16.51	0.04	-25.07	-19.97	2.64	Field	Thin disk
RKS1114-2306	32.26	32.11	0.04	-5.72	-55.92	-23.27	Field	Thin disk
RKS1114+2542	-1.82	-1.59	0.04	-10.94	1.18	-5.20	Field	Thin disk
RKS1115-1808	8.07	7.96	0.04	53.40	-43.25	-44.03	Field	Thick disk
RKS1116-1441	16.11	16.33	0.04	-7.67	-23.29	-1.19	Field	Thin disk
RKS1117-0158	4.56	4.65	0.04	-76.96	-35.27	-29.16	Field	Thick disk
RKS1117-2748	-20.70	-20.39	0.04	15.28	20.75	-9.27	Field	Thin disk
RKS1121-2027	-0.15	-2.79	0.05	12.13	3.62	-1.54	Field	Thin disk
RKS1121+1811	-3.42	-3.32	0.04	-13.37	-19.83	-13.46	Field	Thin disk

Continued on next page

Table 9 continued from previous page

RKS ID	$\gamma_{\text{Gaia DR3}}$ (km s ⁻¹)	γ_{REC} (km s ⁻¹)	$\sigma_{\gamma_{\text{REC}}}$ (km s ⁻¹)	U (km s ⁻¹)	V (km s ⁻¹)	W (km s ⁻¹)	Group	Disk
RKS1125+2000	4.22	4.47	0.04	-21.62	-24.51	-7.68	Field	Thin disk
RKS1126+1517	-4.34	-4.32	0.04	17.91	4.59	0.81	Field	Thin disk
RKS1127+0358	-2.89	-2.30	0.04	-12.26	-2.27	-5.44	Field	Thin disk
RKS1128+0731	39.51	39.56	0.04	40.19	-164.40	-32.70	Field	Thick disk
RKS1134-1314	82.68	82.41	0.04	-25.21	-79.24	40.62	Field	Thick disk
RKS1135+1658	0.03	-0.02	0.04	7.26	-2.63	0.51	Field	Thin disk
RKS1139-2741	38.15	38.07	0.04	69.54	-27.12	3.27	Field	Thick disk
RKS1141+0508	18.95	18.96	0.04	62.68	-50.18	-0.49	Field	Thick disk
RKS1147-1149	18.64	18.81	0.03	-15.58	-28.83	1.88	Field	Thin disk
RKS1152+1845	1.74	1.73	0.04	20.97	-32.34	-3.45	Field	Thin disk
RKS1154+2844	-14.71	-17.55	0.04	42.32	-22.62	-11.17	Field	Thin disk
RKS1157-2608	-10.61	-10.59	0.04	-47.40	-2.56	-1.01	Field	Thin disk
RKS1157-2742	48.29	48.51	0.04	-20.45	-74.07	-7.97	Field	Thick disk
RKS1157+1959	4.91	5.06	0.05	-48.47	-17.27	-4.73	Field	Thin disk
RKS1158-2355	-10.30	-10.21	0.03	-18.53	-5.11	-15.88	Field	Thin disk
RKS1159-2021	14.89	15.04	0.04	33.01	-26.42	-17.21	Field	Thin disk
RKS1204-0013	...	-18.50	0.07	-16.55	-6.23	-23.33	Field	Thin disk
RKS1204+0911	-6.64	-7.16	0.04	-37.20	-10.32	-11.94	Field	Thin disk
RKS1205-1852	-3.16	-8.27	0.05	11.71	-14.11	-30.69	Field	Thin disk
RKS1206-2336	40.29	40.43	0.04	25.03	-32.83	15.34	Field	Thin disk
RKS1208-0028	3.99	4.24	0.05	-109.12	-73.19	-24.43	Field	Thick disk
RKS1209-2646	10.35	10.45	0.05	3.61	-23.81	-15.20	Field	Thin disk
RKS1210-1126	21.75	23.73	0.05	-17.56	-36.14	6.43	Field	Thin disk
RKS1220-1953	-11.82	-11.64	0.04	-43.33	-21.28	-20.02	Field	Thin disk
RKS1222+2736	-22.24	-22.27	0.04	-13.44	-12.52	-24.40	Field	Thin disk
RKS1223+2754	-31.27	-31.40	0.05	-21.87	6.58	-33.47	Field	Thin disk
RKS1228-1654	111.33	111.20	0.05	-31.58	-103.32	77.04	Field	Thick disk
RKS1231+2013	-9.04	-8.23	0.04	8.55	-18.17	-10.93	Field	Thin disk
RKS1233-1438	5.93	6.12	0.04	-50.52	-37.97	-1.94	Field	Thin disk
RKS1241+1951	-9.74	-8.03	0.04	4.46	-0.17	-8.29	Field	Thin disk
RKS1248-1543	...	-0.12	0.06	8.61	8.47	2.29	Field	Thin disk
RKS1248-2448	-13.27	-13.13	0.04	-34.23	1.43	3.41	Field	Thin disk
RKS1250-0046	4.39	4.63	0.04	9.53	-17.52	-5.29	Field	Thin disk
RKS1253+0645	-21.41	-27.63	0.04	-36.79	0.98	-21.40	Field	Thin disk
RKS1256-2455	17.12	16.97	0.04	27.24	-21.70	-15.11	Field	Thin disk
RKS1257-1427	-6.46	-6.65	0.04	-38.96	-19.98	-3.43	Field	Thin disk
RKS1259-0950	4.98	5.87	0.04	-71.05	-33.97	18.16	Field	Thick disk
RKS1300-0242	-16.06	-16.04	0.04	-91.86	-51.20	-9.85	Field	Thick disk
RKS1302-2647	-17.56	-41.98	0.04	-25.72	11.74	-37.56	Field	Thin disk
RKS1303-0509	-7.55	9.15	0.07	-2.29	-29.56	-2.91	Field	Thin disk
RKS1306+2043	-2.80	-2.69	0.05	-9.53	4.44	-1.38	Field	Thin disk
RKS1310+0932	18.70	18.88	0.04	34.62	-6.10	10.10	Field	Thin disk
RKS1312-0215	-12.07	-12.02	0.03	-15.82	-2.88	-8.78	Field	Thin disk
RKS1316+1701	7.62	7.79	0.04	35.91	7.49	1.92	Field	Thin disk
RKS1318-1446	11.99	11.98	0.05	-19.12	-53.64	-8.08	Field	Thin disk
RKS1320+0407	-21.38	-21.24	0.03	-79.72	-15.17	0.17	Field	Thick disk

Continued on next page

Table 9 continued from previous page

RKS ID	$\gamma_{\text{Gaia DR3}}$ (km s ⁻¹)	γ_{REC} (km s ⁻¹)	$\sigma_{\gamma_{\text{REC}}}$ (km s ⁻¹)	U (km s ⁻¹)	V (km s ⁻¹)	W (km s ⁻¹)	Group	Disk
RKS1323+0243	28.30	28.47	0.04	2.61	4.90	32.04	Field	Thin disk
RKS1327-2417	-13.49	-13.62	0.04	-42.63	-26.12	-9.12	Field	Thin disk
RKS1331-0219	-53.51	-51.83	0.05	-119.98	-19.38	-10.14	Field	Thick disk
RKS1333+0835	-6.35	-6.08	0.04	-40.25	-19.04	3.99	Field	Thin disk
RKS1334-0018	...	-6.11	0.04	-23.33	-11.64	0.03	Field	Thin disk
RKS1334-0820	-22.80	-22.20	0.17	-28.27	-14.66	-18.23	Field	Thin disk
RKS1334+0440	14.40	14.59	0.04	22.98	-3.25	6.21	Field	Thin disk
RKS1335-0023	4.87	5.05	0.04	-3.51	13.01	11.59	Field	Thin disk
RKS1335+0650	7.99	8.08	0.03	-2.65	-17.90	6.22	Field	Thin disk
RKS1336+0746	-88.51	-88.60	0.04	-90.69	-97.43	-79.74	Field	Thick disk
RKS1340-0411	27.68	27.75	0.04	-24.18	-0.56	46.19	Field	Thin disk
RKS1341-0007	46.28	46.22	0.04	29.44	-61.01	20.78	Field	Thick disk
RKS1342-0141	-42.89	-42.81	0.04	-36.15	-22.30	-38.63	Field	Thin disk
RKS1345-0437	5.03	5.00	0.04	-8.98	-25.38	1.81	Field	Thin disk
RKS1345+0850	-13.38	-13.22	0.04	-4.49	-10.38	-13.99	Field	Thin disk
RKS1345+1747	20.75	20.40	0.05	93.04	-71.34	-5.09	Field	Thick disk
RKS1347+0618	-30.46	-30.44	0.04	-60.25	-54.97	-17.24	Field	Thick disk
RKS1349-2206	-37.95	-37.81	0.04	-101.03	-73.74	-22.15	Field	Thick disk
RKS1353+1256	-12.59	-16.49	0.04	17.22	-59.20	-27.06	Field	Thin disk
RKS1353+2748	49.28	49.30	0.04	66.39	-13.01	40.24	Field	Thick disk
RKS1359+2252	-57.48	-57.42	0.04	-28.92	-16.06	-50.36	Field	Thin disk
RKS1411-1236	3.14	3.32	0.04	-10.44	-32.49	-1.46	Field	Thin disk
RKS1412+2348	-12.10	-11.85	0.04	-5.56	-5.00	-10.07	Field	Thin disk
RKS1413-0657	-1.63	-1.80	0.05	0.72	15.19	2.19	Field	Thin disk
RKS1414-1521	1.65
RKS1418-0636	...	16.33	0.05	29.22	-37.14	-12.86	Field	Thin disk
RKS1419-0509	-9.97	-9.80	0.04	-42.70	-46.15	6.66	Field	Thin disk
RKS1421+2937	-37.19	-37.05	0.04	-23.72	-52.57	-19.70	Field	Thin disk
RKS1430-0838	-22.49	-22.38	0.04	-69.94	-69.91	9.01	Field	Thick disk
RKS1432+1121	-44.17	-42.98	0.04	-29.57	22.50	-33.79	Field	Thin disk
RKS1433+0920	30.52	30.59	0.04	75.88	-42.98	-7.84	Field	Thick disk
RKS1436+0944	-9.72	-9.59	0.05	16.58	-4.43	-20.59	Field	Thin disk
RKS1437-2548	39.76	39.93	0.03	31.39	-28.95	8.57	Field	Thin disk
RKS1442+1930	-27.95	-27.91	0.04	-16.71	-38.63	-16.18	Field	Thin disk
RKS1444-2215	8.64	9.03	0.03	7.75	-45.48	-23.55	Field	Thin disk
RKS1444+2211	-30.19	-30.34	0.04	-22.01	4.96	-25.44	Field	Thin disk
RKS1445+1350	-9.82	-9.67	0.04	-5.05	-29.61	-4.77	Field	Thin disk
RKS1446+1629	42.88	42.76	0.04	63.59	-57.17	24.72	Field	Thick disk
RKS1446+2730	-20.66	-20.49	0.04	-1.66	-7.86	-19.66	Field	Thin disk
RKS1447+0242	12.55	12.89	0.04	-4.73	-23.24	18.62	Field	Thin disk
RKS1450+0648	-32.29	-32.15	0.04	-67.98	-68.32	10.18	Field	Thick disk
RKS1451-2418	-57.23	-57.17	0.03	-83.52	-51.60	-21.07	Field	Thick disk
RKS1453+2320	-32.92	-36.53	0.04	-69.81	-70.37	9.63	Field	Thick disk
RKS1455-2707	16.25	16.44	0.04	5.55	-17.08	11.69	Field	Thin disk
RKS1457-2124	26.75
RKS1500-1108	14.71	14.76	0.04	24.30	-33.03	-13.89	Field	Thin disk

Continued on next page

Table 9 continued from previous page

RKS ID	$\gamma_{\text{Gaia DR3}}$ (km s ⁻¹)	γ_{REC} (km s ⁻¹)	$\sigma_{\gamma_{\text{REC}}}$ (km s ⁻¹)	U (km s ⁻¹)	V (km s ⁻¹)	W (km s ⁻¹)	Group	Disk
RKS1500-2427	-26.56	-26.38	0.04	-35.48	-10.73	-3.41	Field	Thin disk
RKS1500-2905	18.03	18.10	0.06	14.37	-7.49	8.07	Field	Thin disk
RKS1501+1341	-22.96	-22.85	0.05	-25.48	-17.20	-8.27	Field	Thin disk
RKS1501+1552	-1.55	-1.55	0.04	28.53	-14.65	-15.75	Field	Thin disk
RKS1504-1835	...	-21.38	0.04	-23.26	-21.15	-15.21	Field	Thin disk
RKS1504+0538	-83.91	-84.15	0.04	-57.95	-74.99	-56.58	Field	Thick disk
RKS1507+2456	-69.17	-74.90	0.18	-105.32	-42.94	-21.99	Field	Thick disk
RKS1509+2400	-55.90	-55.77	0.04	-81.64	-47.85	-8.24	Field	Thick disk
RKS1510-1622	310.27	310.05	0.07	302.96	-512.37	-69.55	Kapteyn	Halo
RKS1515+0047	-3.36	-3.16	0.05	10.00	1.13	-13.89	Field	Thin disk
RKS1515+0735	39.55	39.75	0.04	38.64	-19.26	22.93	Field	Thin disk
RKS1519+1155	12.45	12.31	0.04	1.27	-1.53	14.99	Field	Thin disk
RKS1519+2912	-25.57	-25.63	0.05	-59.67	11.46	-8.89	Field	Thin disk
RKS1520+1522	...	-67.57	0.04	-53.56	-72.57	-27.21	Field	Thick disk
RKS1522-0446	-19.09	-19.01	0.04	-27.55	-18.13	1.46	Field	Thin disk
RKS1522-1039	-6.15	-5.99	0.03	-0.45	-19.12	-12.70	Field	Thin disk
RKS1522+0125	-26.46	-26.39	0.03	-18.87	-64.53	-14.03	Field	Thin disk
RKS1525-2642	-133.45	-133.17	0.04	-157.33	-17.95	-8.34	Field	Thick disk
RKS1527+0235	-42.54	-42.57	0.04	-31.92	-9.82	-27.41	Field	Thin disk
RKS1527+1035	-21.88	-21.74	0.03	-20.05	-65.14	3.32	Field	Thin disk
RKS1528-0920	9.01	26.60	0.04
RKS1540-1802	4.47	4.80	0.04	8.03	11.99	-0.58	Field	Thin disk
RKS1552+1052	-1.15	-0.73	0.04	3.38	-34.63	8.32	Field	Thin disk
RKS1554-2600	5.20	5.32	0.04	-6.82	-9.86	26.21	Field	Thin disk
RKS1555+1602	...	-110.98	0.04	-59.21	-81.06	-67.04	Field	Thick disk
RKS1600-0147	24.09	24.10	0.04	35.29	-0.22	-6.91	Field	Thin disk
RKS1601-2625	-20.88	-20.52	0.05	-12.32	10.87	-20.78	Field	Thin disk
RKS1604-1126	-32.28	-32.09	0.04	-29.90	-6.85	-12.31	Field	Thin disk
RKS1607-0542	21.82	22.01	0.04	38.19	-4.14	-18.19	Field	Thin disk
RKS1608-1308	-37.83	-37.65	0.03	-25.28	-34.08	-33.86	Field	Thin disk
RKS1608+1713	-21.55	-21.59	0.04	-20.47	-10.07	-7.48	Field	Thin disk
RKS1613+1331	18.16	18.30	0.04	51.21	-13.62	-17.17	Field	Thin disk
RKS1615+0721	3.80	5.15	0.04	46.92	-27.77	-35.75	Field	Thin disk
RKS1621+1713	18.34	18.33	0.05	38.78	-24.26	5.52	Field	Thin disk
RKS1624-1338	7.14	7.30	0.04	5.71	-29.99	6.89	Field	Thin disk
RKS1625-2156	...	-63.04	0.05	-70.38	-49.38	-2.75	Field	Thick disk
RKS1626+1539	-52.98	-52.96	0.05	-58.44	2.06	-23.97	Field	Thin disk
RKS1627+0055	-14.58	-14.64	0.04	-14.53	-2.84	-4.00	Field	Thin disk
RKS1627+0718	-36.42	-36.18	0.04	-20.55	-39.86	-14.39	Field	Thin disk
RKS1629+2346	-29.78	-32.44	0.04	16.98	-51.57	-24.45	Field	Thin disk
RKS1630-0359	-17.25	-17.19	0.03	-19.25	-17.48	4.94	Field	Thin disk
RKS1632-1235	-77.90	-77.64	0.04	-74.20	-60.25	-14.93	Field	Thick disk
RKS1633-0933	-14.79	-13.90	0.07	-6.22	-27.74	-12.81	AB Dor	Thin disk
RKS1647-0111	19.12	19.02	0.05	32.14	-23.02	-5.99	Field	Thin disk
RKS1649-2426	-29.76	-29.87	0.03	-36.72	-38.21	16.48	Field	Thin disk
RKS1650+1854	-5.69	-5.60	0.03	1.96	-12.28	-1.19	Field	Thin disk

Continued on next page

Table 9 continued from previous page

RKS ID	$\gamma_{\text{Gaia DR3}}$ (km s ⁻¹)	γ_{REC} (km s ⁻¹)	$\sigma_{\gamma_{\text{REC}}}$ (km s ⁻¹)	U (km s ⁻¹)	V (km s ⁻¹)	W (km s ⁻¹)	Group	Disk
RKS1654+1154	-66.35	-66.69	0.05	-78.64	-39.82	16.18	Field	Thick disk
RKS1659-2616	14.93	15.06	0.04	19.83	-21.15	-33.18	Field	Thin disk
RKS1701+2256	-25.06	-24.92	0.04	-26.52	-18.15	2.67	Field	Thin disk
RKS1705-0147	-14.01	-13.48	0.13	-7.18	-2.27	-17.01	Field	Thin disk
RKS1705-0503	34.12	34.12	0.04	46.65	-61.77	20.69	Field	Thick disk
RKS1706-0610	-16.27	-16.22	0.03	-13.20	-18.60	0.46	Field	Thin disk
RKS1712+1821	19.68	19.81	0.03	22.97	9.75	-1.92	Field	Thin disk
RKS1714-0824	-33.79	-33.36	0.05	-36.22	-7.57	6.64	Field	Thin disk
RKS1716-1210	5.34	5.50	0.05	8.03	8.84	-14.57	Field	Thin disk
RKS1717+2913	-44.68	-44.51	0.03	-45.28	-22.37	-11.21	Field	Thin disk
RKS1725+0206	-23.87	-23.58	0.04	0.61	-52.80	-9.69	Field	Thin disk
RKS1729-2350	-32.27	-32.28	0.04	-33.10	-20.44	14.23	Field	Thin disk
RKS1733+0914	-24.27	-23.78	0.04	-16.61	-11.36	-13.82	Field	Thin disk
RKS1737-1314	-17.11	-56.61	0.00	-49.17	-29.78	-17.36	Field	Thin disk
RKS1737+2257	2.80	3.03	0.04	13.79	-15.20	10.26	Field	Thin disk
RKS1739+0333	22.08	22.67	0.03	21.48	1.64	12.64	Field	Thin disk
RKS1750-0603	-26.03	-26.08	0.04	-18.52	-21.45	-8.98	Field	Thin disk
RKS1752-0733	-24.41	-24.58	0.04	-40.72	15.89	49.33	Field	Thin disk
RKS1753+2119	-13.29	-13.13	0.05	-13.29	-9.52	4.73	Field	Thin disk
RKS1754-2649	-32.04	-31.28	0.46	-30.89	-11.78	-12.95	Field	Thin disk
RKS1755+0345	-8.67	-8.46	0.04	-8.32	-6.79	7.41	Field	Thin disk
RKS1755+1830	-29.80	-29.68	0.04	-16.14	-24.67	-7.89	Field	Thin disk
RKS1757-2143	...	-2.61	0.04	0.14	-17.71	-17.36	Field	Thin disk
RKS1803+2545	5.51	5.67	0.05	28.39	-13.28	-2.59	Field	Thin disk
RKS1804+0149	-11.54	-7.91	0.06	-5.66	0.01	-15.52	Field	Thin disk
RKS1809-0019	-39.41	-39.06	0.04	-34.23	-14.17	-16.56	Field	Thin disk
RKS1809-1202	-1.31	-1.18	0.04	5.89	-18.36	-20.48	Field	Thin disk
RKS1815+1829	1.77	1.59	0.04	-5.77	8.90	-2.46	Field	Thin disk
RKS1816+1354	6.31	6.40	0.05	33.09	-18.40	-23.75	Field	Thin disk
RKS1817+2640	-49.24	-49.44	0.04	-46.26	-8.90	-52.49	Field	Thick disk
RKS1818-0642	-28.54	-28.51	0.04	-24.37	-16.74	5.62	Field	Thin disk
RKS1819-0156	-14.42	-14.39	0.04	-12.67	-6.65	-1.51	Field	Thin disk
RKS1822+0142	-17.25	-16.89	0.09	-14.56	-5.74	-12.56	Field	Thin disk
RKS1829-0149	-54.90	-54.75	0.03	-42.55	-32.88	-25.29	Field	Thin disk
RKS1829-2758	-31.20	-30.99	0.04	-27.70	-58.58	-13.64	Field	Thin disk
RKS1829+0903	-42.36	-42.15	0.04	-42.49	-9.01	-24.27	Field	Thin disk
RKS1831-1854	-43.38	-43.15	0.04	-38.09	-24.64	5.27	Field	Thin disk
RKS1833-1138	-87.20	-87.44	0.04	-65.96	-71.83	21.08	Field	Thick disk
RKS1833-1626	-30.67	-41.50	0.06
RKS1833+2218	38.33	38.38	0.04	67.41	-5.30	5.77	Field	Thin disk
RKS1847-0338	15.38	15.54	0.04	23.62	-10.40	-0.73	Field	Thin disk
RKS1848-1008	53.31	49.18	0.04	49.24	5.76	-27.35	Field	Thin disk
RKS1848+1044	-7.30	-7.10	0.04	14.43	-22.88	-25.38	Field	Thin disk
RKS1848+1726	-22.09	-22.06	0.04	17.14	-47.37	11.14	Field	Thin disk
RKS1850-2655	22.06	22.00	0.04	24.28	-3.11	5.21	Field	Thin disk
RKS1854+0051	24.49	24.70	0.05	30.06	-0.33	0.41	Field	Thin disk

Continued on next page

Table 9 continued from previous page

RKS ID	$\gamma_{\text{Gaia DR3}}$ (km s ⁻¹)	γ_{REC} (km s ⁻¹)	$\sigma_{\gamma_{\text{REC}}}$ (km s ⁻¹)	U (km s ⁻¹)	V (km s ⁻¹)	W (km s ⁻¹)	Group	Disk
RKS1854+1058	-26.56	-26.20	0.04	-27.07	-9.63	0.94	Field	Thin disk
RKS1854+2844	-34.22	-34.30	0.05	-31.47	-22.31	0.92	Field	Thin disk
RKS1855+2333	3.69	-21.60	0.40	6.44	-25.75	-27.56	Field	Thin disk
RKS1858-0030	29.92	29.95	0.04	37.88	-2.73	5.61	Field	Thin disk
RKS1858-1014	-44.75	-44.87	0.04	-43.11	-17.26	-11.74	Field	Thin disk
RKS1859+0759	-83.57	-83.39	0.04	-62.12	-52.93	-57.44	Field	Thick disk
RKS1859+1107	-28.59	-28.44	0.04	-26.78	-13.32	1.22	Field	Thin disk
RKS1901+0328	-35.19	-35.17	0.04	-33.29	-14.61	-14.18	Field	Thin disk
RKS1903-1102	37.42	37.62	0.03	48.72	-16.80	-3.73	Field	Thin disk
RKS1907+0736	9.10	8.90	0.04	69.85	-65.57	-7.11	Field	Thick disk
RKS1908-1640	-35.91	-35.98	0.04	-28.07	-22.29	13.78	Field	Thin disk
RKS1908+1627	-63.57	-63.59	0.04	-19.15	-67.95	5.19	Field	Thick disk
RKS1910+2145	-31.84	-31.80	0.06	-15.60	-27.79	-2.79	Field	Thin disk
RKS1915+1133	-58.17	-57.99	0.04	-34.24	-47.58	-30.39	Field	Thin disk
RKS1915+2453	-74.99	-69.67	0.14	-71.36	-34.90	-23.12	Field	Thick disk
RKS1923-0635	...	24.62	0.04	41.49	-19.15	5.23	Field	Thin disk
RKS1924-2203	52.39	52.58	0.05	68.25	-49.16	-10.77	Field	Thick disk
RKS1924+2525	-11.26	-10.88	0.05	4.95	-15.46	-2.10	Field	Thin disk
RKS1928+1232	-18.47	-18.44	0.04	-5.98	-19.16	4.50	Field	Thin disk
RKS1928+2854	-14.74	-14.70	0.05	-2.24	-15.17	-2.73	Field	Thin disk
RKS1929+0709	14.94	14.92	0.04	-18.45	39.25	-14.22	Field	Thin disk
RKS1930+2140	11.53	11.34	0.04	38.09	-12.06	13.20	Field	Thin disk
RKS1932-1116	-49.03	-48.87	0.04	-50.32	-14.93	-4.70	Field	Thin disk
RKS1932+0034	-48.17	-48.06	0.05	-47.63	-21.01	-11.43	Field	Thin disk
RKS1934+0434	-58.93	-58.70	0.04	-69.24	-14.29	-13.79	Field	Thick disk
RKS1936-1026	62.78	63.83	0.03	83.95	-14.05	3.76	Field	Thick disk
RKS1943+1005	-12.12	-12.39	0.04	-25.83	4.54	-12.40	Field	Thin disk
RKS1952-2356	-22.56	-22.49	0.04	-20.12	-10.21	5.29	Field	Thin disk
RKS1954-2356
RKS1954+2013	...	-48.60	0.05	-17.50	-46.22	3.44	Field	Thin disk
RKS1957+1313	5.91	5.90	0.04	7.45	1.31	-2.61	Field	Thin disk
RKS2000+2242	-2.53	-2.15	0.05	16.17	-12.37	-11.87	Field	Thin disk
RKS2002+0319	-30.49	-30.31	0.03	-22.12	-16.49	15.45	Field	Thin disk
RKS2003+2005	...	-62.56	0.05	-43.49	-49.16	-16.45	Field	Thin disk
RKS2003+2320	-2.50	-2.54	0.04	85.05	-46.05	27.37	Field	Thick disk
RKS2004+2547	-7.39	-7.19	0.04	3.87	-9.62	4.86	Field	Thin disk
RKS2008+0640	-34.14	-34.02	0.04	-47.06	-4.85	-0.22	Field	Thin disk
RKS2009-0307	-7.99	-7.90	0.03	11.82	-14.71	24.04	Field	Thin disk
RKS2009-1417	-18.12	-18.03	0.04	-16.54	-17.84	-7.68	Field	Thin disk
RKS2009+1648	-30.98	-30.78	0.04	-30.53	-14.50	15.22	Field	Thin disk
RKS2010-2029	21.45	21.27	0.04	39.92	-23.92	8.61	Field	Thin disk
RKS2011+1611	-49.37	-49.26	0.04	-31.35	-26.84	61.90	Field	Thick disk
RKS2012-1253	27.46	27.57	0.05	16.57	-5.53	-42.35	Field	Thin disk
RKS2013-0052	-10.95	-10.83	0.04	-16.04	10.55	19.28	Field	Thin disk
RKS2014-0716	7.03	7.16	0.05	15.71	-18.83	-15.06	Field	Thin disk
RKS2015-2701	-54.41	-54.34	0.03	-72.33	-11.55	-18.45	Field	Thick disk

Continued on next page

Table 9 continued from previous page

RKS ID	$\gamma_{\text{Gaia DR3}}$ (km s^{-1})	γ_{REC} (km s^{-1})	$\sigma_{\gamma_{\text{REC}}}$ (km s^{-1})	U (km s^{-1})	V (km s^{-1})	W (km s^{-1})	Group	Disk
RKS2016-0204	-16.53	-16.52	0.05	-29.43	-7.47	-26.51	Field	Thin disk
RKS2030+2650	...	16.34	0.05	24.08	8.47	2.86	Field	Thin disk
RKS2035+0607	-42.41	-42.36	0.03	-39.97	-47.03	-46.39	Field	Thick disk
RKS2038+2346	-22.17	-21.99	0.04	-7.86	-22.62	-8.16	Field	Thin disk
RKS2039+1004	-53.51	-53.43	0.04	-57.81	-35.47	-17.20	Field	Thin disk
RKS2041-0529	-12.48	-12.63	0.04	-19.33	1.25	0.78	Field	Thin disk
RKS2041-2219	-61.72	-41.36	0.10	-64.56	-65.05	-52.85	Field	Thick disk
RKS2042-2116	...	19.89	0.05	18.60	2.35	-8.95	Field	Thin disk
RKS2042+2050	-36.74	-36.66	0.04	18.62	-52.34	-8.02	Field	Thin disk
RKS2044-2121	...	-73.70	0.04	-52.48	-56.59	26.23	Field	Thick disk
RKS2047+1051	58.57	58.35	0.04	74.09	-7.17	-77.28	Field	Thick disk
RKS2050+2923	-8.69	-8.71	0.04	0.15	-9.36	-0.51	Field	Thin disk
RKS2053-0245	14.34	14.55	0.05	94.66	-39.77	40.24	Field	Thick disk
RKS2055+1310	-40.88	-41.66	0.03	-84.70	-7.09	-10.72	Field	Thick disk
RKS2059-1042	-30.22	-28.96	0.03	-22.65	-17.43	9.20	Field	Thin disk
RKS2059+0333	5.72	5.70	0.06	28.59	-73.36	-95.07	Field	Thick disk
RKS2105-1654	...	-20.88	0.05	-11.35	-14.26	11.94	Field	Thin disk
RKS2105+0704	-66.81	-66.64	0.04	-14.94	-76.49	3.93	Field	Thick disk
RKS2107-1355	-33.16	-32.87	0.04	-41.51	-18.55	-5.20	Field	Thin disk
RKS2108-0425	-2.02	3.78	0.05	11.38	-0.97	4.36	Field	Thin disk
RKS2116+0923	-18.35	-18.08	0.04	-10.67	-19.92	-4.83	Field	Thin disk
RKS2118+0009	-27.48	-27.42	0.03	-36.95	-32.51	-25.70	Field	Thin disk
RKS2119-2621	-22.40	12.90	0.05	51.42	-25.15	22.64	Field	Thin disk
RKS2120-1951	17.80	17.87	0.04	35.82	-43.11	-15.91	Field	Thin disk
RKS2122+1052	8.53	8.40	0.04	5.62	8.85	2.07	Field	Thin disk
RKS2125+2712	-29.96	-31.05	0.04	20.65	-34.77	11.63	Field	Thin disk
RKS2126+0344	-4.95	-4.91	0.04	5.12	-8.21	2.77	Field	Thin disk
RKS2130-1230	-84.69	-84.66	0.04	-103.45	-64.59	-10.43	Field	Thick disk
RKS2132-2057	32.48	32.50	0.03	52.66	-2.13	-0.72	Field	Thin disk
RKS2141+1115	-49.49	-51.35	0.04	-0.13	-49.77	23.74	Field	Thin disk
RKS2149-1140	20.93	21.11	0.04	61.91	-23.75	-1.44	Field	Thin disk
RKS2149+0543	-11.03	-10.94	0.04	-46.93	-16.15	-32.05	Field	Thin disk
RKS2152+0154	-26.61	-26.68	0.04	11.42	-36.75	10.21	Field	Thin disk
RKS2153-1249	6.38	6.13	0.05	21.87	-8.68	1.27	Field	Thin disk
RKS2153+2055	13.43	13.69	0.05	10.00	6.94	-12.75	Field	Thin disk
RKS2153+2850	19.77	19.56	0.05	13.27	16.55	-7.20	Field	Thin disk
RKS2155-2942	-12.22	-12.00	0.04	-7.83	-30.58	1.73	Field	Thin disk
RKS2210+2247	-24.46	-24.30	0.04	73.29	-9.89	57.09	Field	Thick disk
RKS2214+2751	20.06	20.04	0.05	-11.71	39.82	39.18	Field	Thin disk
RKS2224+2233	-7.09	-7.07	0.04	18.51	-5.78	7.80	Field	Thin disk
RKS2226-1911	-21.10	-20.82	0.04	-31.49	-16.05	1.65	Field	Thin disk
RKS2239+0406	23.71	24.05	0.04	-16.72	19.50	-20.44	Field	Thin disk
RKS2240-2940	-0.31	-0.02	0.05	-19.81	-7.03	-11.51	Field	Thin disk
RKS2241+1849	-15.48	-14.90	0.04	-39.31	-14.98	-0.48	Field	Thin disk
RKS2243-0624	-13.88	-13.78	0.03	22.82	-27.22	7.53	Field	Thin disk
RKS2247+1823	-24.07	-23.81	0.04	-34.26	-22.10	6.72	Field	Thin disk

Continued on next page

Table 9 continued from previous page

RKS ID	$\gamma_{\text{Gaia DR3}}$ (km s ⁻¹)	γ_{REC} (km s ⁻¹)	$\sigma_{\gamma_{\text{REC}}}$ (km s ⁻¹)	U (km s ⁻¹)	V (km s ⁻¹)	W (km s ⁻¹)	Group	Disk
RKS2248+2443	16.02	16.26	0.04	-22.19	7.75	-18.68	Field	Thin disk
RKS2251+1358	1.28	1.30	0.04	-48.11	1.40	-6.55	Field	Thin disk
RKS2252+2324	-8.28	-7.92	0.04	-4.09	-20.71	-18.32	Field	Thin disk
RKS2254+2331	-14.21	-14.11	0.05	-40.53	-18.46	-1.71	Hyades	Thin disk
RKS2258-1338	9.70	9.90	0.04	17.17	-35.06	-21.90	Field	Thin disk
RKS2259-1122	-36.16	-35.96	0.05	-29.06	-31.06	17.17	Field	Thin disk
RKS2301-0350	-44.17	-45.49	0.03	-27.82	-46.82	18.03	Field	Thin disk
RKS2307-2309	15.23	15.26	0.04	1.18	-26.03	-23.16	Field	Thin disk
RKS2308+0633	-13.35	-5.74	0.06	-15.17	-8.20	-1.28	Field	Thin disk
RKS2309-0215	-37.99	-37.81	0.03	-74.16	-59.10	-7.77	Field	Thick disk
RKS2309+1425	-2.16	-2.39	0.04	18.18	-3.76	-0.32	Field	Thin disk
RKS2310-2955	-13.14	-12.91	0.04	-54.28	-24.21	-10.29	Field	Thin disk
RKS2316+0541	-9.05	-9.21	0.04	-1.38	-9.20	4.23	Field	Thin disk
RKS2317-2323	51.66	51.45	0.05	-3.60	-24.51	-62.41	Field	Thin disk
RKS2323-1045	33.83	33.98	0.04	-40.71	18.97	-37.23	Field	Thin disk
RKS2326+0853	-44.71	-44.66	0.05	-59.46	-35.11	28.70	Field	Thick disk
RKS2327-0117	32.01	31.82	0.04	-58.13	20.56	-30.40	Field	Thin disk
RKS2328+1604	-53.66	-53.72	0.04	4.39	-50.25	24.40	Field	Thin disk
RKS2332-1650	-1.14	-0.77	0.05	-13.92	-22.43	-9.25	Field	Thin disk
RKS2335+0136	-10.44	-10.46	0.05	-31.02	-16.85	0.21	Field	Thin disk
RKS2340+2021	-18.04	-17.54	0.04	-23.63	-20.69	8.60	Field	Thin disk
RKS2342-0234	22.60	23.75	0.05	44.74	-8.30	-30.24	Field	Thin disk
RKS2345+2933	59.83	46.82	0.04	-127.78	-16.74	-58.56	Field	Thick disk
RKS2348-1259	-9.04	-7.92	0.05	-29.61	-14.27	0.24	Field	Thin disk
RKS2349+0310	-18.74	-18.69	0.04	-6.27	-13.80	13.57	Field	Thin disk
RKS2350-2924	10.91	11.02	0.04	-18.56	-6.72	-16.13	Field	Thin disk
RKS2353+2901	1.78	1.83	0.05	5.26	5.41	2.18	Field	Thin disk
RKS2355+2211	-11.66	-11.45	0.04	-11.14	-28.08	-11.36	Field	Thin disk
RKS2358+0949	-0.31	-0.22	0.04	-8.41	-4.62	-1.98	Field	Thin disk
RKS2359-2602	1.67	1.69	0.04	21.33	12.37	3.36	Field	Thin disk
RKS2359+0639	6.30	6.44	0.04	13.52	-5.89	-14.01	Field	Thin disk

E. TABLE OF STELLAR PROPERTIES FOR SURVEY SAMPLE K DWARFS

Table Key:EW[H α]: Equivalent width of the H α line at 6563 Å

EW[Li I]: Equivalent width of the Li I line at 6707.8 Å

NM: Not Measured

In the Status column:

M represents Mature K dwarfs identified by this work.

Y represents Youth,

A represents Active,

Y+A represents both Youth and Active,

Table 10. Primary K dwarf Sample: Stellar Properties

RKS ID	T_{eff} (K)	$\sigma_{T_{\text{eff}}}$ (K)	[Fe/H] (dex)	$\sigma_{[\text{Fe}/\text{H}]}$ (dex)	$\log g$ (dex)	$\sigma_{\log g}$ (dex)	$v \sin i$ (km s $^{-1}$)	EW(H α) (Å)	S/N(H α)	EW(Li I) (Å)	S/N(Li I)	Status
RKS0000+1659	4896	101	-0.12	0.10	4.52	0.68	<5	0.98	88	0.00	88	M
RKS0001-1656	4017	393	0.05	0.23	4.67	0.70	<5	0.51	32	0.00	30	M
RKS0007-2349	5212	109	-0.50	0.10	4.54	0.68	<5	1.14	71	0.00	71	M
RKS0012+2142	3764	111	-0.18	0.09	4.75	0.71	<5	0.43	23	0.00	21	M
RKS0012+2705	4805	100	-0.02	0.09	4.50	0.68	<5	0.88	64	0.00	62	M
RKS0016-1435	4580	100	0.06	0.09	4.57	0.69	<5	0.79	55	0.00	54	M
RKS0017+2057	3806	106	-0.01	0.14	4.70	0.71	<5	0.45	36	0.00	34	M
RKS0019-0303	3949	100	-0.23	0.11	4.71	0.71	<5	0.51	27	0.00	25	M
RKS0019-0957	3918	135	-0.15	0.13	4.69	0.70	<5	0.53	38	0.00	37	M
RKS0020+1738	3832	101	0.00	0.11	4.69	0.70	<5	0.42	45	0.00	43	M
RKS0021+2531	4628	101	0.07	0.09	4.56	0.68	<5	0.83	70	0.00	69	M
RKS0022-2701	5003	101	-0.17	0.09	4.56	0.68	<5	0.97	41	0.00	40	M
RKS0024-2701	4825	102	-0.34	0.10	4.53	0.68	<5	0.95	113	0.00	111	M
RKS0036+2610	4381	100	0.14	0.09	4.63	0.69	<5	0.72	36	0.00	35	M
RKS0036-0930	3833	159	-0.24	0.34	4.74	0.71	<5	0.48	35	0.00	34	M
RKS0039+2115	5204	104	0.19	0.09	4.44	0.67	<5	1.09	232	0.00	225	M
RKS0042+2239	3817	101	-0.23	0.09	4.78	0.72	<5	0.44	34	0.00	32	M
RKS0045+0147	4905	112	0.21	0.09	4.51	0.68	<5	0.88	38	0.00	37	M
RKS0048+0516	4956	101	-0.30	0.09	4.57	0.69	<5	1.02	255	0.00	250	M
RKS0051+1844	4278	106	-0.13	0.11	4.66	0.70	<5	0.67	32	0.00	31	M
RKS0051-2254	4134	109	-0.24	0.09	4.69	0.70	<5	0.60	84	0.00	82	M
RKS0055-2940	4409	101	0.11	0.10	4.63	0.69	<5	0.78	60	0.00	59	M
RKS0057+0551	3785	105	-0.10	0.13	4.72	0.71	<5	0.44	40	0.00	38	M
RKS0102+0503	4766	104	-0.08	0.09	4.50	0.68	<5	0.86	102	0.00	100	M
RKS0102-1025	3937	100	-0.17	0.09	4.71	0.71	<5	0.54	36	0.00	35	M
RKS0104+2607	4161	104	-0.07	0.11	4.67	0.70	<5	0.57	28	0.00	27	M
RKS0104-2536	4266	102	-0.26	0.11	4.66	0.70	<5	0.66	56	0.00	55	M
RKS0105+1523	4670	100	-0.02	0.09	4.56	0.68	<5	0.84	51	0.00	50	M
RKS0107+2257	4569	101	0.20	0.09	4.54	0.68	<5	0.83	52	0.00	51	M
RKS0108+1714	3928	104	-0.25	0.09	4.70	0.71	<5	0.64	22	0.00	22	M
RKS0112-2514	4177	102	-0.09	0.14	4.67	0.70	<5	0.59	44	0.00	43	M
RKS0113+1629	4333	101	0.13	0.09	4.64	0.70	<5	0.73	70	0.00	70	M
RKS0116+2519	3946	101	-0.16	0.10	4.70	0.71	<5	0.56	25	0.00	24	M

Continued on next page

Table 10 continued from previous page

RKS ID	T_{eff} (K)	$\sigma_{T_{\text{eff}}}$ (K)	[Fe/H] (dex)	$\sigma_{[\text{Fe}/\text{H}]}$ (dex)	$\log g$ (dex)	$\sigma_{\log g}$ (dex)	$v \sin i$ (km s ⁻¹)	EW(H α) (Å)	S/N(H α)	EW(Li I) (Å)	S/N(Li I)	Status
RKS0117-1530	5302	108	-0.48	0.09	4.17	0.63	<5	0.63	44	0.00	44	A
RKS0118-0052	5333	101	-0.08	0.10	4.55	0.68	<5	1.12	135	0.00	135	M
RKS0121+2419	3942	122	0.06	0.13	4.68	0.71	...	0.26	33	0.00	32	A
RKS0122-2653	4943	100	0.18	0.09	4.51	0.68	<5	0.96	70	0.00	69	M
RKS0123-1257	5467	110	0.55	0.09	4.51	0.68	<5	1.06	115	0.00	113	M
RKS0124+1829	5125	109	-0.06	0.09	4.54	0.68	<5	1.01	69	0.00	68	M
RKS0125-0103	4633	106	-0.11	0.12	4.58	0.69	<5	0.84	46	0.00	46	M
RKS0129+2143	4962	115	0.00	0.09	4.51	0.68	<5	0.93	53	0.00	52	M
RKS0135-2046	4087	101	-0.28	0.09	4.70	0.71	<5	0.57	42	0.00	41	M
RKS0139+1515	4426	100	0.05	0.09	4.64	0.70	<5	0.74	32	0.00	32	M
RKS0142+2016	5307	103	0.02	0.09	4.54	0.68	<5	1.10	247	0.00	241	M
RKS0146+1224	4680	105	-0.04	0.09	4.54	0.68	<5	0.79	34	0.00	34	M
RKS0150+1817	3943	103	0.02	0.10	4.68	0.70	<5	0.57	37	0.00	35	M
RKS0150+2927	5297	101	-0.53	0.12	4.51	0.68	<5	1.13	70	0.00	68	M
RKS0200+2636	3913	103	-0.27	0.10	4.71	0.71	<5	0.48	29	0.00	28	M
RKS0205-2804	3768	110	-0.02	0.23	4.74	0.71	<5	0.53	33	0.00	30	M
RKS0209-1620	3936	102	0.23	0.09	4.67	0.70	<5	0.55	32	0.00	29	M
RKS0213-2111	4050	100	0.26	0.09	4.66	0.70	<5	0.54	38	0.00	36	M
RKS0214-0338	4698	109	0.06	0.10	4.55	0.68	<5	0.82	66	0.00	65	M
RKS0215-1814	4687	100	-0.06	0.09	4.55	0.68	<5	0.79	38	0.00	38	M
RKS0221-0652	4639	105	0.07	0.09	4.56	0.68	<5	0.81	40	0.00	40	M
RKS0229-1958	4376	108	-0.28	0.10	4.66	0.70	<5	0.67	90	0.00	88	M
RKS0231-1516	4920	106	-0.11	0.10	4.54	0.68	<5	0.94	82	0.00	80	M
RKS0231-2001	4257	100	-0.02	0.09	4.66	0.70	<5	0.68	31	0.00	30	M
RKS0236+0653	4732	103	-0.11	0.09	4.52	0.68	<5	0.84	217	0.00	214	M
RKS0236-0309	5046	100	0.21	0.09	4.51	0.68	<5	1.00	43	0.00	43	M
RKS0236-2331	4722	106	0.15	0.09	4.51	0.68	<5	0.78	66	0.00	65	M
RKS0236-2710	4611	101	-0.02	0.09	4.61	0.69	<5	0.88	38	0.00	38	M
RKS0240+0111	4267	106	-0.36	0.09	4.68	0.70	<5	0.72	40	0.00	39	M
RKS0242+0322	4010	120	-0.06	0.09	4.69	0.70	<5	0.41	25	0.00	24	M
RKS0243+1925	4637	100	0.05	0.09	4.57	0.69	<5	0.77	83	0.00	80	M
RKS0246+1146	4253	104	0.03	0.09	4.66	0.70	<5	0.71	62	0.00	61	M
RKS0246+2538	5268	100	-0.03	0.09	4.55	0.68	<5	1.20	57	0.00	56	M
RKS0246-2305	3940	100	0.01	0.14	4.68	0.70	<5	0.49	32	0.00	30	M
RKS0247+2842	3843	120	-0.13	0.16	4.70	0.71	<5	0.47	26	0.00	24	M
RKS0248+2704	5335	100	0.09	0.09	4.53	0.68	<5	1.14	78	0.00	76	M
RKS0248-1145	3927	100	0.05	0.13	4.67	0.70	<5	0.53	34	0.00	32	M
RKS0250+1542	4438	130	0.18	0.11	4.60	0.69	<5	0.70	39	0.00	38	M
RKS0251+1038	4226	117	-0.19	0.11	4.67	0.70	<5	0.58	29	0.00	28	M
RKS0251-0816	4416	101	0.05	0.09	4.64	0.70	<5	0.63	33	0.00	33	M
RKS0252-1246	5165	103	0.11	0.09	4.51	0.68	<5	0.92	191	0.21	189	Y+A
RKS0255+2652	5130	100	0.31	0.09	4.46	0.67	<5	1.02	82	0.00	80	M
RKS0255+2807	3937	100	-0.09	0.13	4.69	0.70	<5	0.41	24	0.00	22	M
RKS0257-2458	4868	102	-0.15	0.13	4.50	0.68	<5	0.91	119	0.00	118	M
RKS0258+2646	5191	100	-0.05	0.09	4.53	0.68	<5	1.09	28	0.00	28	M
RKS0300+0744	5058	100	0.28	0.09	4.49	0.67	<5	0.99	84	0.00	82	M

Continued on next page

Table 10 continued from previous page

RKS ID	T_{eff} (K)	$\sigma_{T_{\text{eff}}}$ (K)	[Fe/H] (dex)	$\sigma_{[\text{Fe}/\text{H}]}$ (dex)	$\log g$ (dex)	$\sigma_{\log g}$ (dex)	$v \sin i$ (km s ⁻¹)	EW(H α) (\AA)	S/N(H α)	EW(Li I) (\AA)	S/N(Li I)	Status
RKS0303+2006	4551	100	0.05	0.09	4.59	0.69	<5	0.79	52	0.00	51	M
RKS0306+0157	4000	100	-0.18	0.11	4.68	0.70	<5	0.56	82	0.00	79	M
RKS0308-2410	4181	107	-0.17	0.10	4.67	0.70	<5	0.62	47	0.00	46	M
RKS0310+1203	4531	100	0.10	0.09	4.57	0.69	<5	0.75	56	0.00	55	M
RKS0314+0858	5157	101	0.00	0.09	4.52	0.68	<5	1.06	64	0.00	63	M
RKS0314-2626	4232	104	-0.26	0.10	4.67	0.70	<5	0.63	69	0.00	67	M
RKS0320+0827	4520	101	0.08	0.09	4.60	0.69	<5	0.74	38	0.00	37	M
RKS0322+2709	3947	102	0.13	0.15	4.68	0.70	<5	0.42	21	0.00	19	M
RKS0324-0521	4469	115	0.20	0.10	4.59	0.69	<5	0.80	89	0.00	87	M
RKS0329-1140	3966	103	0.13	0.15	4.67	0.70	<5	0.52	49	0.00	46	M
RKS0332-0927	5044	102	-0.09	0.09	4.55	0.68	<5	1.01	346	0.00	340	M
RKS0341+0336	3971	104	-0.15	0.09	4.70	0.71	5.3	0.56	83	0.00	80	M
RKS0342-2427	4448	100	0.05	0.09	4.63	0.69	<5	0.78	51	0.00	50	M
RKS0343+1640	3899	100	0.07	0.13	4.66	0.70	<5	0.50	47	0.00	44	M
RKS0343-1253	3890	162	-0.12	0.28	4.69	0.70	<5	0.50	21	0.00	20	M
RKS0343-1906	4925	104	-0.07	0.10	4.51	0.68	<5	0.97	112	0.00	111	M
RKS0344+1155	4358	100	-0.03	0.09	4.65	0.70	<5	0.75	42	0.00	41	M
RKS0345-2751	4821	100	-0.23	0.09	4.50	0.68	<5	0.83	60	0.00	59	M
RKS0348+1512	4641	101	0.00	0.09	4.58	0.69	<5	0.79	26	0.00	25	M
RKS0348+2519	5158	149	-0.37	0.13	4.55	0.69	...	1.07	72	0.00	71	M
RKS0349-1329	3962	100	-0.08	0.10	4.70	0.71	<5	0.53	51	0.00	50	M
RKS0350-2349	4351	100	0.23	0.09	4.63	0.69	<5	0.73	37	0.00	36	M
RKS0354-0649	4087	100	0.18	0.09	4.65	0.70	<5	0.59	59	0.00	57	M
RKS0357-0109	4503	102	0.00	0.09	4.62	0.69	<5	0.74	61	0.00	61	M
RKS0404+2634	3823	102	-0.06	0.09	4.70	0.71	<5	0.48	39	0.00	38	M
RKS0406-2051	4235	100	-0.22	0.09	4.68	0.70	<5	0.69	36	0.00	36	M
RKS0407+1413	3967	108	0.15	0.10	4.66	0.70	<5	0.58	48	0.00	46	M
RKS0408+1220	5011	107	0.01	0.10	4.50	0.68	<5	1.04	44	0.00	44	M
RKS0417+2033	4446	106	-0.06	0.12	4.64	0.70	<5	0.72	72	0.13	72	Y
RKS0419-0408	4082	118	0.04	0.22	4.67	0.70	<5	0.45	23	0.00	22	M
RKS0420-1445	4368	100	0.07	0.10	4.64	0.70	<5	0.64	54	0.00	53	M
RKS0421-1945	3971	100	-0.33	0.09	4.70	0.71	<5	0.57	22	0.00	21	M
RKS0427+2426	4952	100	-0.60	0.09	4.54	0.68	<5	0.91	41	0.00	39	M
RKS0429+2155	4089	101	0.32	0.12	4.65	0.70	<5	0.59	67	0.00	64	M
RKS0430+0058	4011	102	0.03	0.10	4.68	0.70	<5	-0.14	33	0.00	31	A
RKS0436+2707	4671	161	0.15	0.10	4.55	0.68	<5	-0.39	102	0.00	100	A
RKS0441+2054	4572	104	-0.22	0.11	4.58	0.69	8.0	-0.18	97	0.06	95	Y+A
RKS0445+0938	3835	116	0.02	0.15	4.69	0.70	<5	0.48	44	0.00	42	M
RKS0448-1056	4392	114	0.02	0.10	4.64	0.70	<5	0.66	42	0.00	42	M
RKS0449-1447	3817	100	-0.02	0.11	4.71	0.71	<5	0.47	29	0.00	27	M
RKS0451+2837	4597	100	0.13	0.09	4.54	0.68	<5	0.82	60	0.00	60	M
RKS0453+2214	4758	100	0.07	0.09	4.55	0.68	<5	0.85	60	0.00	58	M
RKS0454+0722	5284	100	0.12	0.09	4.53	0.68	<5	1.05	129	0.00	129	M
RKS0455-2833	4613	109	0.07	0.09	4.58	0.69	<5	0.89	76	0.00	76	M
RKS0503+0322	3812	101	-0.03	0.10	4.69	0.70	<5	0.41	39	0.00	38	M
RKS0506-1102	4504	100	0.08	0.09	4.60	0.69	<5	0.71	77	0.00	77	M

Continued on next page

Table 10 continued from previous page

RKS ID	T_{eff} (K)	$\sigma_{T_{\text{eff}}}$ (K)	[Fe/H] (dex)	$\sigma_{[\text{Fe}/\text{H}]}$ (dex)	$\log g$ (dex)	$\sigma_{\log g}$ (dex)	$v \sin i$ (km s ⁻¹)	EW(H α) (Å)	S/N(H α)	EW(Li I) (Å)	S/N(Li I)	Status
RKS0512+1943	4413	129	-0.54	0.13	4.64	0.70	<5	0.78	30	0.00	30	M
RKS0513-2158	4120	103	-0.06	0.10	4.67	0.70	<5	0.61	31	0.00	30	M
RKS0514+0039	4271	114	-0.34	0.12	4.67	0.70	<5	0.67	40	0.00	39	M
RKS0514+1952	4523	100	0.21	0.09	4.56	0.68	<5	0.80	67	0.00	67	M
RKS0518-2123	4159	102	-0.04	0.13	4.67	0.70	<5	0.69	39	0.00	38	M
RKS0519-0304	4725	105	-0.08	0.10	4.53	0.68	<5	0.87	104	0.00	103	M
RKS0519-1550	4752	100	-0.23	0.13	4.51	0.68	<5	0.76	49	0.00	49	M
RKS0522+0236	4895	107	-0.15	0.11	4.52	0.68	<5	0.92	118	0.00	116	M
RKS0523+1719	4521	101	0.00	0.10	4.62	0.69	<5	0.68	67	0.00	66	M
RKS0533-2643	4787	100	0.15	0.09	4.51	0.68	<5	0.89	47	0.00	46	M
RKS0534-2328	4912	100	-0.32	0.09	4.57	0.69	<5	0.95	75	0.00	73	M
RKS0535+2805	4261	106	0.18	0.10	4.65	0.70	<5	0.68	31	0.00	30	M
RKS0536+1119	3936	100	-0.09	0.11	4.70	0.71	<5	0.06	59	0.00	56	A
RKS0542+0240	5056	100	0.03	0.09	4.48	0.67	<5	1.00	69	0.00	68	M
RKS0544-2225	4903	104	0.03	0.09	4.52	0.68	<5	0.92	181	0.00	179	M
RKS0549-1734	5013	100	0.03	0.11	4.52	0.68	<5	1.01	105	0.00	105	M
RKS0552-2246	3992	100	-0.36	0.09	4.70	0.71	<5	0.61	52	0.00	51	M
RKS0553-0559	3965	103	-0.20	0.11	4.69	0.70	<5	0.62	40	0.00	39	M
RKS0554+0208	4718	117	-0.06	0.09	4.53	0.68	<5	0.91	50	0.00	49	M
RKS0554-1942	3871	114	-0.19	0.14	4.70	0.71	<5	0.50	23	0.00	22	M
RKS0600+2101	4213	100	-0.20	0.09	4.68	0.70	<5	0.63	38	0.00	36	M
RKS0602+0848	3915	126	-0.11	0.11	4.69	0.70	<5	0.55	24	0.00	23	M
RKS0608+2630	4540	100	-0.19	0.09	4.60	0.69	<5	0.76	40	0.00	40	M
RKS0609+0009	3932	102	0.24	0.09	4.67	0.70	<5	0.55	27	0.00	25	M
RKS0609+0540	5046	100	0.06	0.09	4.47	0.67	<5	1.03	72	0.00	70	M
RKS0612+1023	4407	100	0.04	0.09	4.64	0.70	<5	0.72	40	0.00	39	M
RKS0614+0510	5088	100	-0.07	0.09	4.51	0.68	<5	1.01	86	0.00	85	M
RKS0616+2512	4605	103	0.12	0.09	4.55	0.68	<5	0.82	62	0.00	61	M
RKS0617+1759	4114	100	-0.21	0.12	4.68	0.70	<5	0.71	35	0.00	34	M
RKS0618-1352	4267	132	-0.21	0.11	4.67	0.70	<5	0.68	34	0.00	33	M
RKS0620+0215	4220	101	0.04	0.10	4.66	0.70	<5	0.65	37	0.00	36	M
RKS0621-2212	5039	100	0.00	0.09	4.54	0.68	<5	1.03	61	0.00	61	M
RKS0626+1845	5269	166	-0.41	0.15	4.41	0.71	<5	0.54	149	0.00	147	A
RKS0629+2700	4979	100	-0.25	0.09	4.57	0.69	<5	0.96	63	0.00	61	M
RKS0630-1148	4565	100	0.10	0.09	4.56	0.68	<5	0.78	47	0.00	47	M
RKS0632-2701	3674	110	-0.40	0.09	4.82	0.72	<5	0.47	36	0.00	34	M
RKS0633+0527	5206	100	0.30	0.09	4.42	0.66	<5	1.10	76	0.00	75	M
RKS0637+1945	4260	105	-0.30	0.09	4.68	0.70	<5	0.69	27	0.00	26	M
RKS0641+2357	4695	106	-0.06	0.09	4.54	0.68	<5	0.85	62	0.00	61	M
RKS0647-1815	3981	100	-0.02	0.12	4.69	0.70	<5	0.57	33	0.00	31	M
RKS0652-0510	4675	102	0.04	0.09	4.56	0.68	<5	0.86	151	0.00	149	M
RKS0652-2306	4760	100	-0.17	0.09	4.51	0.68	<5	0.93	46	0.00	46	M
RKS0658-1259	4357	138	-0.30	0.10	4.66	0.70	<5	0.37	38	0.07	37	Y+A
RKS0700-2847	3751	103	-0.12	0.15	4.75	0.71	<5	0.40	24	0.00	22	M
RKS0701+0655	5272	101	0.07	0.09	4.54	0.68	<5	1.16	58	0.00	57	M
RKS0701-2556	5137	106	0.20	0.09	4.48	0.67	<5	1.12	179	0.00	178	M

Continued on next page

Table 10 continued from previous page

RKS ID	T_{eff} (K)	$\sigma_{T_{\text{eff}}}$ (K)	[Fe/H] (dex)	$\sigma_{[\text{Fe}/\text{H}]}$ (dex)	$\log g$ (dex)	$\sigma_{\log g}$ (dex)	$v \sin i$ (km s ⁻¹)	EW(H α) (Å)	S/N(H α)	EW(Li I) (Å)	S/N(Li I)	Status
RKS0702-0647	4593	102	0.01	0.09	4.59	0.69	<5	0.84	74	0.00	73	M
RKS0706+2358	4281	102	-0.08	0.12	4.66	0.70	<5	0.67	40	0.00	39	M
RKS0707+0326	4203	100	0.07	0.09	4.66	0.70	<5	0.66	54	0.00	53	M
RKS0708+2950	4931	100	-0.33	0.09	4.57	0.69	<5	1.02	59	0.00	57	M
RKS0708-0958	4854	101	-0.17	0.09	4.51	0.68	<5	0.91	63	0.00	62	M
RKS0710-1425	4003	102	-0.18	0.10	4.69	0.70	<5	0.57	42	0.00	40	M
RKS0712-2453	3990	110	0.25	0.18	4.67	0.70	<5	0.57	30	0.00	28	M
RKS0713+2500	5046	100	-0.54	0.09	4.54	0.68	<5	1.03	60	0.00	58	M
RKS0716-0339	4921	100	0.19	0.09	4.51	0.68	<5	0.93	46	0.00	46	M
RKS0723+1257	4898	113	0.14	0.11	4.51	0.68	<5	0.96	59	0.00	58	M
RKS0723+2024	4285	344	-0.20	0.26	4.65	0.70	8.0	-0.55	28	0.16	27	Y+A
RKS0723-2001	4310	100	0.11	0.09	4.65	0.70	<5	0.76	42	0.00	41	M
RKS0724-1753	3954	100	-0.06	0.09	4.70	0.71	<5	0.39	26	0.00	25	M
RKS0725-1041	4418	161	0.02	0.09	4.62	0.69	<5	0.37	38	0.00	36	M
RKS0726-1546	4541	100	-0.13	0.13	4.60	0.69	<5	0.74	80	0.00	79	M
RKS0730-0340	3951	100	0.04	0.09	4.69	0.70	<5	0.47	28	0.00	26	M
RKS0732+1719	3909	100	-0.01	0.10	4.67	0.70	<5	0.41	39	0.00	37	M
RKS0734-0653	5056	108	-0.19	0.11	4.57	0.69	<5	0.97	68	0.05	67	Y
RKS0739-0335	4907	101	0.04	0.09	4.53	0.68	<5	0.52	85	0.00	82	A
RKS0741-2921	4003	100	-0.11	0.12	4.68	0.70	<5	0.55	26	0.00	25	M
RKS0745+0208	4075	100	0.27	0.10	4.66	0.70	<5	0.62	25	0.00	24	M
RKS0752+2555	4646	102	-0.06	0.09	4.59	0.69	<5	0.82	48	0.00	47	M
RKS0754+1914	4916	120	0.18	0.10	4.51	0.68	<5	0.98	67	0.00	67	M
RKS0754-2518	3916	100	-0.18	0.12	4.69	0.70	<5	0.47	41	0.00	39	M
RKS0757-0048	4703	104	-0.15	0.12	4.55	0.68	<5	0.92	79	0.00	78	M
RKS0758-1501	4574	103	0.20	0.09	4.54	0.68	<5	0.82	54	0.00	53	M
RKS0758-2537	4656	131	-0.33	0.12	4.56	0.69	<5	0.82	69	0.00	68	M
RKS0759+2050	5285	100	-0.12	0.09	4.53	0.68	<5	1.09	85	0.00	84	M
RKS0808+2106	4043	104	-0.14	0.10	4.69	0.70	<5	0.53	57	0.00	55	M
RKS0813-1355	3823	122	-0.04	0.13	4.69	0.71	...	0.56	46	0.00	43	M
RKS0814+1301	4384	103	0.02	0.10	4.64	0.70	<5	0.71	55	0.00	55	M
RKS0815-2600	4120	101	0.11	0.11	4.67	0.70	<5	0.66	32	0.00	31	M
RKS0817+1717	4481	104	-0.03	0.10	4.64	0.70	<5	0.73	41	0.00	40	M
RKS0819+0120	4965	102	-0.28	0.10	4.56	0.68	<5	0.85	56	0.12	55	Y+A
RKS0820+1404	4146	104	-0.09	0.09	4.67	0.70	<5	0.60	24	0.00	24	M
RKS0823+2150	4343	106	-0.19	0.09	4.66	0.70	<5	0.75	33	0.00	33	M
RKS0827+2855	4515	113	-0.03	0.11	4.61	0.69	<5	0.77	30	0.00	29	M
RKS0832-2323	4132	105	-0.03	0.10	4.67	0.70	<5	0.56	34	0.00	33	M
RKS0838-0415	3714	110	-0.32	0.11	4.78	0.72	<5	0.49	37	0.00	34	M
RKS0838-1315	4529	104	-0.06	0.12	4.62	0.69	<5	0.71	37	0.00	36	M
RKS0839+0657	1.08	81	0.00	80	M
RKS0839+1131	5056	104	-0.55	0.09	4.54	0.68	<5	1.03	127	0.00	126	M
RKS0840-0628	3931	100	-0.08	0.10	4.70	0.71	<5	0.49	64	0.00	62	M
RKS0848+0628	3987	100	-0.33	0.09	4.71	0.71	<5	0.53	27	0.00	26	M
RKS0850+0751	3943	104	-0.25	0.13	4.70	0.71	<5	0.31	75	0.00	72	A
RKS0852+2819	5262	116	0.42	0.09	4.40	0.66	<5	1.23	229	0.00	226	M

Continued on next page

Table 10 continued from previous page

RKS ID	T_{eff} (K)	$\sigma_{T_{\text{eff}}}$ (K)	[Fe/H] (dex)	$\sigma_{[\text{Fe}/\text{H}]}$ (dex)	$\log g$ (dex)	$\sigma_{\log g}$ (dex)	$v \sin i$ (km s ⁻¹)	EW(H α) (Å)	S/N(H α)	EW(Li I) (Å)	S/N(Li I)	Status
RKS0855+0132	3933	108	0.12	0.12	4.67	0.70	<5	0.59	53	0.00	50	M
RKS0901+1515	4229	105	-0.27	0.10	4.67	0.70	<5	0.60	69	0.00	68	M
RKS0904-1554	4895	100	0.08	0.09	4.50	0.68	<5	0.81	81	0.05	80	Y
RKS0905+2517	3968	110	-0.34	0.10	4.70	0.71	<5	0.59	35	0.00	34	M
RKS0907+2252	5257	101	0.13	0.09	4.49	0.67	<5	0.83	106	0.12	104	Y+A
RKS0909+0512	4827	147	0.17	0.11	4.52	0.68	<5	0.92	97	0.00	96	M
RKS0914+0426	4787	102	-0.01	0.09	4.52	0.68	<5	0.72	113	0.00	111	M
RKS0918+2718	4079	103	0.18	0.15	4.66	0.70	<5	0.60	37	0.00	36	M
RKS0919+0053	5154	100	0.02	0.09	4.50	0.68	<5	1.04	80	0.00	79	M
RKS0920-0545	4429	101	0.05	0.09	4.64	0.70	<5	0.81	69	0.00	69	M
RKS0929+0539	4842	103	0.03	0.11	4.51	0.68	<5	0.88	36	0.00	35	M
RKS0929-0522	4133	100	0.00	0.10	4.67	0.70	<5	0.60	41	0.00	40	M
RKS0932+2909	3773	106	-0.02	0.09	4.71	0.71	<5	0.41	19	0.00	18	M
RKS0932-1111	6177	184	0.01	0.12	4.31	0.65	27.4	-0.06	89	0.19	88	Y+A
RKS0937+2231	4303	101	0.01	0.09	4.65	0.70	<5	0.70	44	0.00	43	M
RKS0937+2241	4200	101	0.00	0.09	4.66	0.70	<5	0.67	39	0.00	38	M
RKS0938+0240	3601	113	-0.52	0.10	4.85	0.73	<5	0.40	26	0.00	24	M
RKS0947+0134	3837	124	-0.12	0.17	4.70	0.71	<5	0.46	22	0.00	22	M
RKS0952+0307	3950	100	-0.14	0.09	4.71	0.71	<5	0.53	41	0.00	39	M
RKS0959-0911	4537	100	-0.36	0.11	4.61	0.69	<5	0.74	49	0.00	49	M
RKS1000+2433	0.19	96	0.00	94	A
RKS1001-1525	4845	102	0.13	0.09	4.50	0.68	<5	0.83	86	0.00	85	M
RKS1004-1143	5030	102	-0.13	0.09	4.57	0.69	<5	0.94	99	0.00	97	M
RKS1005+2629	4741	117	0.09	0.12	4.54	0.68	<5	0.87	63	0.00	61	M
RKS1006+0257	4019	101	-0.03	0.12	4.67	0.70	<5	0.55	32	0.00	30	M
RKS1008+1159	5097	101	-0.15	0.10	4.56	0.68	<5	1.00	79	0.00	78	M
RKS1011-2425	3854	101	-0.02	0.10	4.68	0.70	<5	0.46	32	0.00	30	M
RKS1020-0128	4520	100	0.02	0.09	4.62	0.69	<5	0.82	62	0.00	61	M
RKS1024-1024	4246	101	-0.26	0.10	4.68	0.70	<5	0.68	33	0.00	33	M
RKS1026+2638	5261	100	-0.10	0.09	4.57	0.69	<5	1.16	82	0.00	79	M
RKS1026-0631	4946	100	-0.56	0.09	4.55	0.68	<5	0.86	61	0.00	62	M
RKS1028+0644	4930	104	-0.16	0.12	4.54	0.68	<5	0.97	86	0.00	85	M
RKS1030-2114	4409	104	-0.11	0.10	4.65	0.70	<5	0.70	40	0.00	39	M
RKS1032+0830	3888	149	-0.22	0.20	4.70	0.71	<5	0.48	31	0.00	30	M
RKS1036-1350	5039	100	0.01	0.09	4.54	0.68	<5	1.01	80	0.00	79	M
RKS1043-2903	5269	100	0.14	0.09	4.51	0.68	<5	0.94	114	0.15	113	Y+A
RKS1046-2435	4408	105	-0.56	0.10	4.67	0.70	<5	0.65	47	0.00	47	M
RKS1053-1422	4750	112	-0.16	0.15	4.52	0.68	<5	0.87	54	0.00	53	M
RKS1054-0432	3977	108	-0.09	0.09	4.69	0.70	<5	0.50	29	0.00	27	M
RKS1056+0723	5014	107	0.06	0.10	4.53	0.68	<5	0.99	94	0.00	93	M
RKS1057+2856	4674	102	0.07	0.09	4.55	0.68	<5	0.85	61	0.00	59	M
RKS1059+2526	4724	100	-0.01	0.09	4.56	0.68	<5	0.85	61	0.00	60	M
RKS1102-0919	4902	100	-0.07	0.09	4.52	0.68	<5	0.83	71	0.00	70	M
RKS1108+1546	4290	102	-0.55	0.10	4.68	0.70	<5	0.75	45	0.00	44	M
RKS1108-2816	4221	116	-0.18	0.12	4.67	0.70	<5	0.72	88	0.00	86	M
RKS1111-1057	4360	189	-0.54	0.09	4.67	0.70	<5	0.69	70	0.00	69	M

Continued on next page

Table 10 continued from previous page

RKS ID	T_{eff} (K)	$\sigma_{T_{\text{eff}}}$ (K)	[Fe/H] (dex)	$\sigma_{[\text{Fe}/\text{H}]}$ (dex)	$\log g$ (dex)	$\sigma_{\log g}$ (dex)	$v \sin i$ (km s ⁻¹)	EW(H α) (Å)	S/N(H α)	EW(Li I) (Å)	S/N(Li I)	Status
RKS1111-1459	4302	119	-0.35	0.17	4.67	0.70	<5	0.69	38	0.00	37	M
RKS1113+0428	4389	101	0.00	0.10	4.64	0.70	<5	0.68	87	0.00	86	M
RKS1114+2542	5156	101	-0.39	0.09	4.56	0.68	<5	1.14	108	0.00	107	M
RKS1114-2306	0.79	37	0.00	37	M
RKS1115-1808	4013	102	-0.14	0.15	4.68	0.70	<5	0.62	44	0.00	43	M
RKS1116-1441	3899	120	-0.21	0.17	4.70	0.71	<5	0.51	56	0.00	54	M
RKS1117-0158	4376	102	0.10	0.09	4.64	0.70	<5	0.79	36	0.00	36	M
RKS1117-2748	3908	101	-0.20	0.11	4.70	0.71	<5	0.44	63	0.00	61	M
RKS1121+1811	5299	140	0.41	0.10	4.44	0.67	<5	1.19	99	0.00	98	M
RKS1121-2027	4138	105	-0.13	0.11	4.68	0.70	<5	0.29	103	0.00	100	A
RKS1125+2000	5292	105	0.10	0.10	4.54	0.68	<5	1.12	85	0.00	83	M
RKS1126+1517	3968	101	-0.21	0.09	4.71	0.71	<5	0.58	45	0.00	45	M
RKS1127+0358	3971	101	0.28	0.10	4.67	0.70	<5	0.49	40	0.00	37	M
RKS1128+0731	3876	100	-0.20	0.09	4.70	0.71	<5	0.63	39	0.00	37	M
RKS1134-1314	4011	107	-0.44	0.11	4.71	0.71	<5	0.64	25	0.00	25	M
RKS1135+1658	4513	100	-0.22	0.09	4.62	0.69	<5	0.90	53	0.00	52	M
RKS1139-2741	4249	103	-0.24	0.09	4.67	0.70	<5	0.75	46	0.00	45	M
RKS1141+0508	4207	102	-0.21	0.10	4.67	0.70	<5	0.63	54	0.00	52	M
RKS1147-1149	4524	103	0.10	0.09	4.58	0.69	<5	0.80	72	0.00	71	M
RKS1152+1845	5007	100	-0.25	0.09	4.57	0.69	<5	1.05	68	0.00	66	M
RKS1154+2844	3935	100	-0.11	0.09	4.70	0.71	<5	0.53	46	0.00	45	M
RKS1157+1959	5296	101	0.09	0.09	4.53	0.68	<5	1.12	98	0.00	97	M
RKS1157-2608	4720	102	-0.15	0.16	4.53	0.68	<5	0.88	75	0.00	74	M
RKS1157-2742	4513	108	0.15	0.10	4.58	0.69	<5	0.83	199	0.00	197	M
RKS1158-2355	4784	103	0.01	0.09	4.54	0.68	<5	0.97	80	0.00	79	M
RKS1159-2021	4904	101	0.10	0.09	4.50	0.68	<5	0.96	74	0.00	73	M
RKS1204+0911	4459	112	-0.55	0.10	4.65	0.70	<5	0.79	37	0.00	36	M
RKS1204-0013	4735	101	-0.24	0.10	4.52	0.68	<5	0.75	28	0.00	28	M
RKS1205-1852	3955	100	-0.08	0.12	4.70	0.71	<5	0.25	27	0.00	26	A
RKS1206-2336	5136	102	-0.08	0.09	4.55	0.68	<5	1.12	78	0.00	78	M
RKS1208-0028	3774	106	-0.10	0.13	4.74	0.71	<5	0.50	42	0.00	40	M
RKS1209-2646	3920	101	-0.04	0.11	4.68	0.70	<5	0.50	32	0.00	30	M
RKS1210-1126	3843	112	-0.14	0.14	4.70	0.71	<5	0.49	42	0.00	40	M
RKS1220-1953	4835	100	0.09	0.09	4.51	0.68	<5	0.89	72	0.00	71	M
RKS1222+2736	3954	100	0.22	0.10	4.67	0.70	<5	0.54	21	0.00	19	M
RKS1223+2754	3744	102	-0.09	0.09	4.72	0.71	<5	0.48	44	0.00	42	M
RKS1228-1654	4942	100	-0.55	0.09	4.55	0.68	<5	0.88	40	0.00	40	M
RKS1231+2013	5275	103	0.06	0.09	4.53	0.68	<5	1.08	97	0.00	94	M
RKS1233-1438	4518	117	0.07	0.09	4.60	0.69	<5	0.80	72	0.00	71	M
RKS1241+1951	4889	100	-0.09	0.09	4.51	0.68	<5	0.97	57	0.00	55	M
RKS1248-1543	5028	101	-0.08	0.09	4.56	0.68	<5	0.94	98	0.00	96	M
RKS1248-2448	4362	103	-0.40	0.10	4.66	0.70	<5	0.72	68	0.00	67	M
RKS1250-0046	3969	103	0.07	0.15	4.67	0.70	<5	0.53	53	0.00	50	M
RKS1253+0645	5222	100	-0.05	0.09	4.58	0.69	<5	1.07	91	0.00	89	M
RKS1256-2455	4248	100	-0.02	0.09	4.66	0.70	<5	0.66	32	0.00	32	M
RKS1257-1427	4504	100	-0.32	0.09	4.62	0.69	<5	0.80	71	0.00	70	M

Continued on next page

Table 10 continued from previous page

RKS ID	T_{eff} (K)	$\sigma_{T_{\text{eff}}}$ (K)	[Fe/H] (dex)	$\sigma_{[\text{Fe}/\text{H}]}$ (dex)	$\log g$ (dex)	$\sigma_{\log g}$ (dex)	$v \sin i$ (km s ⁻¹)	EW(H α) (Å)	S/N(H α)	EW(Li I) (Å)	S/N(Li I)	Status
RKS1259-0950	5237	100	-0.50	0.09	4.40	0.69	<5	1.11	58	0.00	57	M
RKS1300-0242	4241	100	-0.30	0.09	4.68	0.70	<5	0.69	49	0.00	47	M
RKS1302-2647	0.73	110	0.00	107	M
RKS1303-0509	5266	102	-0.05	0.09	4.54	0.68	<5	0.97	93	0.14	91	Y
RKS1306+2043	4105	109	-0.19	0.12	4.68	0.70	<5	0.18	55	0.00	52	A
RKS1310+0932	4642	118	-0.26	0.12	4.57	0.69	<5	0.75	47	0.00	47	M
RKS1312-0215	5082	100	0.14	0.09	4.47	0.67	<5	1.05	96	0.00	95	M
RKS1316+1701	5007	104	-0.14	0.09	4.56	0.68	<5	0.92	147	0.00	145	M
RKS1318-1446	3951	105	-0.30	0.09	4.70	0.71	<5	0.53	31	0.00	31	M
RKS1320+0407	4981	100	0.12	0.09	4.50	0.68	<5	1.01	80	0.00	79	M
RKS1323+0243	5204	102	-0.49	0.10	4.54	0.68	<5	1.15	158	0.00	156	M
RKS1327-2417	5006	100	-0.16	0.09	4.56	0.68	<5	1.02	78	0.00	77	M
RKS1331-0219	5280	101	-0.47	0.09	4.43	0.68	<5	1.11	128	0.00	126	M
RKS1333+0835	4765	102	0.13	0.10	4.52	0.68	<5	0.88	98	0.00	97	M
RKS1334+0440	3931	102	0.03	0.10	4.68	0.70	<5	0.54	48	0.00	46	M
RKS1334-0018	5109	103	0.31	0.10	4.46	0.67	<5	1.03	111	0.00	108	M
RKS1334-0820	4335	109	-0.10	0.15	4.65	0.70	8.1	-0.32	62	0.02	61	Y+A
RKS1335+0650	4805	101	0.17	0.09	4.50	0.68	<5	0.90	63	0.00	62	M
RKS1335-0023	3814	116	-0.07	0.13	4.70	0.71	<5	0.52	45	0.00	42	M
RKS1336+0746	4316	114	-0.58	0.09	4.68	0.70	<5	0.68	36	0.00	35	M
RKS1340-0411	3867	120	-0.16	0.16	4.70	0.71	<5	0.51	65	0.00	62	M
RKS1341-0007	4079	100	0.12	0.09	4.66	0.70	<5	0.68	46	0.00	44	M
RKS1342-0141	4377	101	0.00	0.12	4.65	0.70	<5	0.76	25	0.00	24	M
RKS1345+0850	4739	104	0.06	0.09	4.53	0.68	<5	0.77	25	0.00	25	M
RKS1345+1747	3762	105	-0.44	0.10	4.85	0.73	<5	0.42	51	0.00	49	M
RKS1345-0437	4018	111	-0.17	0.11	4.68	0.70	<5	0.56	37	0.00	36	M
RKS1347+0618	4252	101	-0.20	0.10	4.66	0.70	<5	0.73	39	0.00	38	M
RKS1349-2206	4302	102	0.15	0.10	4.64	0.70	<5	0.71	121	0.00	119	M
RKS1353+1256	3957	100	0.12	0.10	4.68	0.70	<5	0.57	30	0.00	28	M
RKS1353+2748	5138	100	-0.44	0.09	4.55	0.68	<5	1.11	71	0.00	69	M
RKS1359+2252	4386	100	0.09	0.09	4.64	0.70	<5	0.70	69	0.00	68	M
RKS1411-1236	5119	101	-0.11	0.09	4.55	0.68	<5	1.05	81	0.00	80	M
RKS1412+2348	4924	100	0.15	0.10	4.52	0.68	<5	0.76	67	0.00	65	M
RKS1413-0657	3857	109	-0.11	0.17	4.70	0.71	<5	0.47	48	0.00	46	M
RKS1414-1521	0.00	36	0.00	33	A
RKS1418-0636	4097	103	-0.17	0.17	4.69	0.70	<5	0.59	30	0.00	28	M
RKS1419-0509	5195	124	-0.13	0.09	4.57	0.69	<5	1.07	121	0.00	120	M
RKS1421+2937	4193	102	-0.04	0.09	4.67	0.70	<5	0.60	82	0.00	78	M
RKS1430-0838	3931	105	-0.06	0.13	4.69	0.70	<5	0.54	69	0.00	65	M
RKS1432+1121	4193	101	-0.19	0.09	4.68	0.70	<5	0.69	32	0.00	31	M
RKS1433+0920	4977	100	-0.02	0.09	4.51	0.68	<5	0.98	69	0.00	68	M
RKS1436+0944	4915	105	0.16	0.09	4.52	0.68	<5	0.87	131	0.00	129	M
RKS1437-2548	4906	148	0.22	0.13	4.50	0.68	<5	0.97	83	0.00	83	M
RKS1442+1930	4043	104	-0.10	0.09	4.68	0.70	<5	0.50	38	0.00	36	M
RKS1444+2211	4233	100	-0.29	0.09	4.67	0.70	<5	0.65	47	0.00	45	M
RKS1444-2215	4450	100	0.24	0.09	4.59	0.69	<5	0.78	51	0.00	50	M

Continued on next page

Table 10 continued from previous page

RKS ID	T_{eff} (K)	$\sigma_{T_{\text{eff}}}$ (K)	[Fe/H] (dex)	$\sigma_{[\text{Fe}/\text{H}]}$ (dex)	$\log g$ (dex)	$\sigma_{\log g}$ (dex)	$v \sin i$ (km s ⁻¹)	EW(H α) (Å)	S/N(H α)	EW(Li I) (Å)	S/N(Li I)	Status
RKS1445+1350	4932	102	-0.30	0.09	4.56	0.68	<5	0.87	93	0.00	92	M
RKS1446+1629	4187	141	-0.33	0.11	4.68	0.70	<5	0.62	68	0.00	66	M
RKS1446+2730	5181	100	0.16	0.09	4.48	0.67	<5	1.11	83	0.00	80	M
RKS1447+0242	4994	103	-0.19	0.09	4.55	0.68	<5	1.01	88	0.00	87	M
RKS1450+0648	4837	100	-0.20	0.09	4.50	0.68	<5	0.90	59	0.00	58	M
RKS1451-2418	4735	105	-0.05	0.09	4.54	0.68	<5	0.90	97	0.00	96	M
RKS1453+2320	4810	100	-0.38	0.09	4.53	0.68	<5	0.88	34	0.00	34	M
RKS1455-2707	4765	100	-0.05	0.09	4.50	0.68	<5	0.76	71	0.00	70	M
RKS1457-2124	4596	149	0.06	0.13	4.57	0.70	...	0.82	197	0.00	195	M
RKS1500-1108	4009	107	0.00	0.11	4.67	0.70	<5	0.56	66	0.00	62	M
RKS1500-2427	4170	100	-0.10	0.10	4.67	0.70	<5	0.59	48	0.00	47	M
RKS1500-2905	3790	102	-0.03	0.09	4.71	0.71	<5	0.17	34	0.00	33	A
RKS1501+1341	3953	100	-0.11	0.09	4.70	0.71	<5	0.38	29	0.00	28	M
RKS1501+1552	4712	103	0.04	0.09	4.55	0.68	<5	0.83	66	0.00	66	M
RKS1504+0538	3901	108	-0.32	0.17	4.73	0.71	<5	0.53	56	0.00	54	M
RKS1504-1835	4311	209	-0.17	0.09	4.66	0.70	<5	0.72	46	0.00	45	M
RKS1507+2456	3848	127	-0.14	0.13	4.70	0.71	6.7	0.44	42	0.00	40	M
RKS1509+2400	4653	100	0.05	0.10	4.57	0.69	<5	0.81	47	0.00	46	M
RKS1510-1622	1.23	46	0.00	46	M
RKS1515+0047	5226	124	-0.04	0.11	4.54	0.68	<5	1.06	145	0.00	142	M
RKS1515+0735	4049	141	-0.26	0.09	4.68	0.70	<5	0.57	35	0.00	34	M
RKS1519+1155	4291	100	-0.07	0.12	4.66	0.70	<5	0.71	35	0.00	34	M
RKS1519+2912	4176	126	-0.44	0.13	4.69	0.70	<5	0.58	38	0.00	38	M
RKS1520+1522	4934	100	-0.51	0.09	4.55	0.68	<5	0.86	75	0.00	73	M
RKS1522+0125	4950	119	0.22	0.10	4.50	0.68	<5	0.97	63	0.00	62	M
RKS1522-0446	4150	102	-0.17	0.10	4.67	0.70	<5	0.58	61	0.00	59	M
RKS1522-1039	4991	100	0.25	0.09	4.49	0.67	<5	0.97	82	0.00	81	M
RKS1525-2642	4563	104	-0.26	0.10	4.59	0.69	<5	0.80	57	0.00	56	M
RKS1527+0235	4116	100	0.02	0.10	4.66	0.70	<5	0.61	39	0.00	38	M
RKS1527+1035	4119	100	0.16	0.09	4.66	0.70	<5	0.69	45	0.00	43	M
RKS1528-0920	5451	141	0.18	0.10	4.36	0.66	<5	0.98	133	0.00	132	M
RKS1540-1802	4143	100	-0.05	0.11	4.67	0.70	<5	0.59	84	0.00	81	M
RKS1552+1052	3939	101	-0.16	0.09	4.71	0.71	<5	0.54	35	0.00	33	M
RKS1554-2600	4349	100	0.22	0.09	4.63	0.69	<5	0.79	37	0.00	36	M
RKS1555+1602	5143	149	-0.28	0.13	4.54	0.69	...	0.95	65	0.00	64	M
RKS1600-0147	4207	102	-0.22	0.10	4.67	0.70	<5	0.67	31	0.00	30	M
RKS1601-2625	3801	113	0.08	0.11	4.68	0.70	<5	0.42	32	0.00	30	M
RKS1604-1126	5276	102	0.09	0.09	4.52	0.68	<5	1.10	78	0.00	77	M
RKS1607-0542	4094	100	0.19	0.09	4.66	0.70	<5	0.68	30	0.00	29	M
RKS1608+1713	4859	100	0.02	0.09	4.50	0.68	<5	0.91	53	0.00	51	M
RKS1608-1308	4862	102	-0.03	0.12	4.47	0.67	<5	0.95	79	0.00	77	M
RKS1613+1331	5449	105	-0.08	0.09	4.47	0.67	<5	1.19	37	0.00	36	M
RKS1615+0721	4316	100	-0.17	0.11	4.66	0.70	<5	0.71	51	0.00	50	M
RKS1621+1713	3977	101	-0.26	0.09	4.71	0.71	<5	0.55	23	0.00	22	M
RKS1624-1338	4819	100	-0.37	0.09	4.53	0.68	<5	0.95	70	0.00	69	M
RKS1625-2156	3794	107	-0.19	0.11	4.75	0.71	<5	0.39	27	0.00	26	M

Continued on next page

Table 10 continued from previous page

RKS ID	T_{eff} (K)	$\sigma_{T_{\text{eff}}}$ (K)	[Fe/H] (dex)	$\sigma_{[\text{Fe}/\text{H}]}$ (dex)	$\log g$ (dex)	$\sigma_{\log g}$ (dex)	$v \sin i$ (km s ⁻¹)	EW(H α) (Å)	S/N(H α)	EW(Li I) (Å)	S/N(Li I)	Status
RKS1626+1539	3958	105	-0.23	0.15	4.71	0.71	<5	0.48	31	0.00	29	M
RKS1627+0055	4088	101	0.16	0.11	4.66	0.70	<5	0.65	42	0.00	40	M
RKS1627+0718	4227	103	-0.15	0.10	4.67	0.70	<5	0.72	71	0.00	69	M
RKS1629+2346	4297	100	0.04	0.11	4.65	0.70	<5	0.75	31	0.00	31	M
RKS1630-0359	4306	102	0.18	0.10	4.64	0.70	<5	0.71	51	0.00	50	M
RKS1632-1235	4000	100	-0.11	0.09	4.69	0.70	<5	0.56	32	0.00	31	M
RKS1633-0933	3909	116	0.20	0.13	4.67	0.70	<5	-0.80	21	0.00	19	A
RKS1647-0111	3931	146	-0.24	0.25	4.70	0.71	<5	0.50	27	0.00	26	M
RKS1649-2426	4579	100	0.10	0.09	4.56	0.68	<5	0.84	47	0.00	46	M
RKS1650+1854	4685	102	-0.06	0.09	4.55	0.68	<5	0.86	47	0.00	46	M
RKS1654+1154	3692	101	-0.43	0.09	4.82	0.72	<5	0.44	27	0.00	25	M
RKS1659-2616	4015	101	0.07	0.14	4.67	0.70	<5	0.58	46	0.00	44	M
RKS1701+2256	4763	101	0.08	0.10	4.56	0.68	<5	0.90	77	0.00	76	M
RKS1705-0147	4835	124	0.01	0.11	4.50	0.68	6.2	0.30	65	0.24	65	Y+A
RKS1705-0503	4273	109	-0.52	0.10	4.69	0.70	<5	0.68	86	0.00	85	M
RKS1706-0610	4846	137	0.16	0.10	4.52	0.68	<5	0.92	63	0.00	62	M
RKS1712+1821	4955	100	-0.11	0.09	4.54	0.68	<5	0.97	51	0.00	49	M
RKS1714-0824	5072	108	-0.09	0.09	4.57	0.69	<5	0.89	110	0.00	110	M
RKS1716-1210	4002	100	-0.02	0.09	4.68	0.70	<5	0.45	39	0.05	37	Y
RKS1717+2913	4778	111	0.00	0.11	4.52	0.68	<5	0.89	38	0.00	37	M
RKS1725+0206	4049	104	0.06	0.12	4.66	0.70	<5	0.56	146	0.00	140	M
RKS1729-2350	4041	115	-0.45	0.11	4.71	0.71	<5	0.55	59	0.00	58	M
RKS1733+0914	4515	102	0.03	0.09	4.62	0.69	<5	0.71	46	0.00	45	M
RKS1737+2257	4021	114	-0.14	0.09	4.69	0.70	<5	0.49	28	0.00	27	M
RKS1737-1314	0.00	46	0.00	45	A
RKS1739+0333	4904	102	0.01	0.09	4.50	0.68	<5	0.96	188	0.00	183	M
RKS1750-0603	3951	101	0.27	0.09	4.66	0.70	<5	0.57	37	0.00	34	M
RKS1752-0733	4292	102	-0.36	0.11	4.67	0.70	<5	0.73	46	0.00	45	M
RKS1753+2119	4901	110	-0.13	0.12	4.52	0.68	<5	0.87	42	0.00	42	M
RKS1754-2649	4249	182	-0.32	0.21	4.68	0.70	...	-2.51	44	0.05	42	Y+A
RKS1755+0345	4085	101	-0.11	0.09	4.68	0.70	<5	0.54	39	0.00	37	M
RKS1755+1830	4310	108	-0.14	0.15	4.66	0.70	<5	0.66	31	0.00	31	M
RKS1757-2143	4113	107	0.13	0.09	4.66	0.70	<5	0.66	54	0.00	52	M
RKS1803+2545	3939	101	0.24	0.09	4.66	0.70	<5	0.54	30	0.00	28	M
RKS1804+0149	5316	102	-0.40	0.09	4.53	0.68	<5	1.09	65	0.00	65	M
RKS1809-0019	4832	101	0.12	0.09	4.51	0.68	<5	0.81	69	0.00	67	M
RKS1809-1202	3970	104	0.04	0.09	4.68	0.70	<5	0.55	38	0.00	35	M
RKS1815+1829	4137	104	0.20	0.09	4.66	0.70	<5	0.68	57	0.00	56	M
RKS1816+1354	3812	104	-0.05	0.11	4.70	0.71	<5	0.43	47	0.00	44	M
RKS1817+2640	4591	118	-0.54	0.09	4.62	0.69	<5	0.83	48	0.00	47	M
RKS1818-0642	4673	100	0.02	0.09	4.58	0.69	<5	0.77	61	0.03	59	Y
RKS1819-0156	3983	108	-0.24	0.10	4.70	0.71	<5	0.53	57	0.00	55	M
RKS1822+0142	4129	101	-0.07	0.10	4.67	0.70	<5	-0.25	53	0.00	52	A
RKS1829+0903	4919	101	0.13	0.09	4.51	0.68	<5	0.94	67	0.00	67	M
RKS1829-0149	4666	126	0.14	0.09	4.53	0.68	<5	0.84	98	0.00	97	M
RKS1829-2758	4361	100	0.24	0.09	4.63	0.69	<5	0.75	66	0.00	65	M

Continued on next page

Table 10 continued from previous page

RKS ID	T_{eff} (K)	$\sigma_{T_{\text{eff}}}$ (K)	[Fe/H] (dex)	$\sigma_{[\text{Fe}/\text{H}]}$ (dex)	$\log g$ (dex)	$\sigma_{\log g}$ (dex)	$v \sin i$ (km s ⁻¹)	EW(H α) (Å)	S/N(H α)	EW(Li I) (Å)	S/N(Li I)	Status
RKS1831-1854	5045	103	-0.18	0.09	4.56	0.68	<5	1.05	171	0.00	168	M
RKS1833+2218	4452	116	-0.10	0.16	4.64	0.70	<5	0.73	26	0.00	25	M
RKS1833-1138	4162	140	-0.26	0.10	4.69	0.70	<5	0.59	27	0.00	26	M
RKS1833-1626	0.83	63	0.00	62	M
RKS1847-0338	4106	131	-0.33	0.13	4.69	0.70	<5	0.58	76	0.00	74	M
RKS1848+1044	4657	104	0.12	0.09	4.54	0.68	<5	0.83	106	0.00	103	M
RKS1848+1726	4009	118	-0.28	0.12	4.69	0.70	<5	0.59	61	0.00	58	M
RKS1848-1008	5023	104	-0.42	0.10	4.55	0.68	<5	0.86	89	0.00	88	M
RKS1850-2655	3947	100	-0.14	0.10	4.70	0.71	<5	0.52	65	0.00	62	M
RKS1854+0051	3904	108	-0.11	0.14	4.70	0.71	<5	0.44	23	0.00	21	M
RKS1854+1058	4089	102	0.33	0.12	4.65	0.70	<5	0.63	66	0.00	63	M
RKS1854+2844	3839	101	-0.07	0.09	4.69	0.70	<5	0.43	33	0.00	32	M
RKS1855+2333	5123	138	0.01	0.11	4.54	0.68	14.8	0.02	56	0.00	54	A
RKS1858-0030	5248	100	-0.05	0.09	4.56	0.68	<5	1.12	87	0.00	85	M
RKS1858-1014	4402	100	0.04	0.09	4.64	0.70	<5	0.70	49	0.00	48	M
RKS1859+0759	4341	108	0.05	0.14	4.63	0.69	<5	0.46	34	0.00	32	M
RKS1859+1107	4663	126	0.09	0.10	4.55	0.68	<5	0.83	55	0.00	54	M
RKS1901+0328	4426	100	0.05	0.09	4.64	0.70	<5	0.68	35	0.00	34	M
RKS1903-1102	4992	127	0.13	0.14	4.50	0.68	<5	1.01	26	0.00	25	M
RKS1907+0736	4358	205	-0.56	0.10	4.67	0.70	<5	0.72	40	0.00	40	M
RKS1908+1627	4187	101	-0.06	0.10	4.67	0.70	<5	0.61	22	0.00	21	M
RKS1908-1640	3958	106	-0.34	0.10	4.69	0.70	<5	0.54	30	0.00	29	M
RKS1910+2145	3931	100	0.07	0.10	4.67	0.70	<5	-0.41	33	0.03	31	Y+A
RKS1915+1133	5133	101	0.31	0.09	4.48	0.67	<5	1.02	90	0.00	88	M
RKS1915+2453	3953	103	-0.28	0.09	4.71	0.71	6.5	0.58	56	0.00	54	M
RKS1923-0635	4521	101	-0.35	0.09	4.62	0.69	<5	0.78	53	0.00	52	M
RKS1924+2525	3954	101	-0.20	0.13	4.70	0.71	<5	0.51	26	0.00	25	M
RKS1924-2203	4209	149	0.13	0.10	4.64	0.70	<5	0.43	23	0.00	23	M
RKS1928+1232	4668	100	0.01	0.09	4.58	0.69	<5	0.77	58	0.00	57	M
RKS1928+2854	3839	104	-0.03	0.10	4.69	0.70	<5	0.43	28	0.00	27	M
RKS1929+0709	4005	102	-0.36	0.14	4.70	0.71	<5	0.50	22	0.00	21	M
RKS1930+2140	4391	105	-0.50	0.09	4.67	0.70	<5	0.74	56	0.00	56	M
RKS1932+0034	3864	100	0.08	0.09	4.68	0.70	<5	0.36	24	0.00	22	M
RKS1932-1116	4997	102	-0.02	0.09	4.54	0.68	<5	0.93	124	0.00	122	M
RKS1934+0434	3960	104	-0.32	0.10	4.70	0.71	<5	0.52	62	0.00	60	M
RKS1936-1026	4889	100	-0.08	0.09	4.49	0.67	<5	0.96	81	0.00	81	M
RKS1943+1005	4175	102	-0.17	0.09	4.67	0.70	<5	0.63	39	0.00	38	M
RKS1952-2356	4384	101	-0.19	0.10	4.65	0.70	<5	0.69	61	0.00	60	M
RKS1954+2013	3901	100	-0.10	0.15	4.68	0.70	<5	0.43	30	0.00	29	M
RKS1954-2356	0.99	238	0.00	236	M
RKS1957+1313	4097	108	-0.11	0.12	4.68	0.70	<5	0.59	35	0.00	34	M
RKS2000+2242	5035	149	-0.01	0.13	4.54	0.69	...	1.02	747	0.00	747	M
RKS2002+0319	4527	106	0.13	0.09	4.58	0.69	<5	0.78	150	0.00	146	M
RKS2003+2005	4006	123	-0.15	0.09	4.70	0.71	<5	0.46	31	0.00	31	M
RKS2003+2320	5142	123	-0.55	0.10	4.54	0.68	<5	1.06	112	0.00	109	M
RKS2004+2547	5086	101	0.22	0.09	4.48	0.67	<5	0.96	25	0.00	24	M

Continued on next page

Table 10 continued from previous page

RKS ID	T_{eff} (K)	$\sigma_{T_{\text{eff}}}$ (K)	[Fe/H] (dex)	$\sigma_{[\text{Fe}/\text{H}]}$ (dex)	$\log g$ (dex)	$\sigma_{\log g}$ (dex)	$v \sin i$ (km s ⁻¹)	EW(H α) (Å)	S/N(H α)	EW(Li I) (Å)	S/N(Li I)	Status
RKS2008+0640	4310	108	-0.29	0.09	4.66	0.70	<5	0.60	47	0.00	46	M
RKS2009+1648	5307	100	-0.16	0.10	4.52	0.68	<5	1.16	56	0.00	55	M
RKS2009-0307	4370	102	0.20	0.10	4.63	0.69	<5	0.79	55	0.00	54	M
RKS2009-1417	4411	106	-0.21	0.10	4.65	0.70	<5	0.78	39	0.00	39	M
RKS2010-2029	4201	107	-0.21	0.11	4.68	0.70	<5	0.58	70	0.00	68	M
RKS2011+1611	5281	102	-0.12	0.09	4.52	0.68	<5	1.05	77	0.00	75	M
RKS2012-1253	3726	100	-0.12	0.09	4.72	0.71	<5	0.43	42	0.00	39	M
RKS2013-0052	4956	102	0.04	0.10	4.52	0.68	<5	0.95	111	0.00	109	M
RKS2014-0716	3867	114	-0.16	0.15	4.70	0.71	<5	0.48	23	0.00	22	M
RKS2015-2701	5078	105	0.03	0.09	4.49	0.67	<5	0.92	218	0.00	214	M
RKS2016-0204	3765	100	-0.16	0.09	4.76	0.71	<5	0.38	44	0.00	42	M
RKS2030+2650	3983	106	-0.33	0.11	4.71	0.71	<5	0.56	51	0.00	49	M
RKS2035+0607	4876	100	-0.09	0.09	4.50	0.68	<5	0.92	46	0.00	45	M
RKS2038+2346	5052	100	-0.02	0.09	4.56	0.68	<5	0.98	93	0.00	93	M
RKS2039+1004	5037	100	0.01	0.09	4.53	0.68	<5	1.07	78	0.00	76	M
RKS2041-0529	4108	105	-0.08	0.11	4.68	0.70	<5	0.61	35	0.00	34	M
RKS2041-2219	3953	105	-0.16	0.19	4.69	0.70	<5	-1.51	29	0.00	28	A
RKS2042+2050	5008	101	-0.15	0.10	4.55	0.68	<5	1.01	48	0.00	47	M
RKS2042-2116	5265	103	0.17	0.09	4.42	0.68	<5	1.07	51	0.00	50	M
RKS2044-2121	4108	102	-0.42	0.10	4.70	0.71	<5	0.64	46	0.00	45	M
RKS2047+1051	4493	100	-0.58	0.09	4.65	0.70	<5	0.79	40	0.00	39	M
RKS2050+2923	4716	103	0.00	0.11	4.55	0.68	<5	0.65	32	0.00	32	M
RKS2053-0245	3851	128	-0.30	0.24	4.77	0.72	<5	0.53	26	0.00	24	M
RKS2055+1310	4662	100	-0.12	0.15	4.57	0.69	<5	0.75	41	0.00	41	M
RKS2059+0333	3727	108	-0.46	0.09	4.85	0.73	<5	0.45	26	0.00	24	M
RKS2059-1042	5016	103	0.29	0.09	4.48	0.67	<5	0.98	103	0.00	103	M
RKS2105+0704	4303	103	0.08	0.09	4.65	0.70	<5	0.71	97	0.00	94	M
RKS2105-1654	3820	102	-0.05	0.09	4.70	0.71	<5	0.18	32	0.00	30	A
RKS2107-1355	5197	112	0.09	0.09	4.51	0.68	<5	1.02	39	0.00	38	M
RKS2108-0425	4566	116	-0.40	0.11	4.60	0.69	<5	0.38	27	0.00	26	A
RKS2116+0923	4732	102	-0.04	0.09	4.53	0.68	<5	0.82	106	0.00	104	M
RKS2118+0009	4732	100	-0.10	0.10	4.51	0.68	<5	0.93	53	0.00	53	M
RKS2119-2621	5582	123	-0.32	0.11	4.46	0.68	<5	1.22	177	0.00	175	M
RKS2120-1951	4076	107	-0.05	0.13	4.66	0.70	<5	0.56	73	0.00	70	M
RKS2122+1052	3961	101	0.01	0.18	4.69	0.70	<5	0.48	31	0.00	29	M
RKS2125+2712	5235	101	-0.14	0.09	4.56	0.68	<5	1.10	43	0.00	41	M
RKS2126+0344	3999	103	0.03	0.20	4.68	0.70	<5	0.61	26	0.00	25	M
RKS2130-1230	4141	107	-0.17	0.10	4.66	0.70	<5	0.64	71	0.00	69	M
RKS2132-2057	5033	100	-0.11	0.09	4.52	0.68	<5	1.04	75	0.00	74	M
RKS2141+1115	4693	100	0.05	0.09	4.54	0.68	<5	0.87	77	0.00	77	M
RKS2149+0543	4733	103	-0.19	0.09	4.53	0.68	<5	0.92	47	0.00	46	M
RKS2149-1140	3940	100	-0.21	0.10	4.70	0.71	<5	0.50	22	0.00	21	M
RKS2152+0154	5155	101	0.14	0.09	4.47	0.67	<5	1.05	100	0.00	99	M
RKS2153+2055	5033	100	-0.07	0.09	4.56	0.68	<5	0.93	89	0.03	88	Y
RKS2153+2850	3768	105	-0.35	0.15	4.81	0.72	<5	0.48	33	0.00	32	M
RKS2153-1249	3750	101	-0.11	0.09	4.73	0.71	<5	0.48	24	0.00	23	M

Continued on next page

Table 10 continued from previous page

RKS ID	T_{eff} (K)	$\sigma_{T_{\text{eff}}}$ (K)	[Fe/H] (dex)	$\sigma_{[\text{Fe}/\text{H}]}$ (dex)	$\log g$ (dex)	$\sigma_{\log g}$ (dex)	$v \sin i$ (km s ⁻¹)	EW(H α) (\AA)	S/N(H α)	EW(Li I) (\AA)	S/N(Li I)	Status
RKS2155-2942	5300	101	0.07	0.09	4.53	0.68	<5	1.07	84	0.00	83	M
RKS2210+2247	4839	105	-0.38	0.09	4.54	0.68	<5	0.92	27	0.00	27	M
RKS2214+2751	3847	120	-0.15	0.16	4.72	0.71	<5	0.51	38	0.00	35	M
RKS2224+2233	4389	107	-0.15	0.15	4.65	0.70	<5	0.79	25	0.00	24	M
RKS2226-1911	4473	100	0.04	0.10	4.62	0.69	<5	0.66	61	0.00	60	M
RKS2239+0406	4922	107	-0.30	0.11	4.55	0.68	<5	0.83	78	0.00	77	M
RKS2240-2940	4453	101	0.02	0.10	4.64	0.70	<5	0.67	113	0.00	111	M
RKS2241+1849	3993	100	0.03	0.18	4.67	0.70	<5	0.30	30	0.00	28	M
RKS2243-0624	4881	100	0.03	0.09	4.49	0.67	<5	0.96	94	0.00	94	M
RKS2247+1823	4663	103	0.01	0.09	4.58	0.69	<5	0.83	61	0.00	60	M
RKS2248+2443	3954	107	-0.16	0.12	4.70	0.71	<5	0.50	37	0.00	36	M
RKS2251+1358	5017	105	-0.57	0.09	4.54	0.68	<5	1.03	78	0.00	77	M
RKS2252+2324	4299	100	-0.03	0.09	4.66	0.70	<5	0.64	40	0.00	39	M
RKS2254+2331	3931	102	0.02	0.12	4.67	0.70	<5	0.48	25	0.00	23	M
RKS2258-1338	4220	100	-0.25	0.09	4.68	0.70	<5	0.53	35	0.00	34	M
RKS2259-1122	3932	105	-0.11	0.13	4.68	0.70	<5	0.53	35	0.00	33	M
RKS2301-0350	4996	103	0.20	0.09	4.50	0.68	<5	1.00	125	0.00	124	M
RKS2307-2309	4107	111	-0.11	0.09	4.68	0.70	<5	0.56	35	0.00	34	M
RKS2308+0633	3804	100	0.10	0.13	4.70	0.71	<5	0.08	33	0.00	31	A
RKS2309+1425	4005	100	-0.14	0.09	4.69	0.70	<5	0.55	51	0.00	50	M
RKS2309-0215	4841	101	0.18	0.09	4.51	0.68	<5	0.92	60	0.00	59	M
RKS2310-2955	4884	100	0.04	0.09	4.49	0.67	<5	0.96	75	0.00	74	M
RKS2316+0541	3920	100	-0.04	0.11	4.68	0.70	<5	0.51	33	0.00	32	M
RKS2317-2323	3776	100	-0.24	0.11	4.79	0.72	<5	0.46	31	0.00	30	M
RKS2323-1045	4956	104	-0.30	0.10	4.56	0.68	<5	0.99	94	0.00	93	M
RKS2326+0853	3855	100	0.08	0.11	4.67	0.70	<5	0.52	28	0.00	26	M
RKS2327-0117	4114	109	-0.30	0.09	4.69	0.70	<5	0.61	37	0.00	36	M
RKS2328+1604	4378	100	-0.43	0.09	4.66	0.70	<5	0.72	30	0.00	30	M
RKS2332-1650	4205	111	-0.04	0.09	4.67	0.70	<5	0.51	93	0.00	90	M
RKS2335+0136	4112	100	0.05	0.12	4.66	0.70	<5	0.24	32	0.00	31	A
RKS2340+2021	4604	121	0.15	0.09	4.55	0.68	<5	0.82	62	0.00	60	M
RKS2342-0234	3937	100	0.04	0.13	4.68	0.70	<5	0.46	31	0.00	30	M
RKS2345+2933	5109	110	-0.18	0.09	4.56	0.68	<5	1.03	98	0.00	98	M
RKS2348-1259	4179	104	-0.12	0.10	4.68	0.70	<5	-0.19	59	0.00	58	A
RKS2349+0310	4974	101	-0.21	0.09	4.56	0.68	<5	0.98	38	0.00	37	M
RKS2350-2924	5306	100	0.03	0.09	4.53	0.68	<5	1.11	147	0.00	147	M
RKS2353+2901	4029	108	-0.13	0.10	4.69	0.70	<5	0.47	47	0.00	44	M
RKS2355+2211	4805	100	0.01	0.09	4.51	0.68	<5	0.85	61	0.00	59	M
RKS2358+0949	5124	101	0.26	0.09	4.47	0.67	<5	1.06	84	0.00	83	M
RKS2359+0639	4390	100	0.12	0.09	4.63	0.69	<5	0.79	41	0.00	40	M
RKS2359-2602	4686	102	-0.05	0.09	4.55	0.68	<5	0.78	50	0.00	50	M

F. TABLE OF CHIRON OBSERVATIONS

Table 11. List of Spectra Used in the Final Analysis

RKS ID	R.A.	Decl.	V	Date & Time of Obs	Exp. Time	SNR
...	(hh mm ss)	(dd mm ss)	(mag)	(UTC)	(s)	...
RKS0000+1659	00 00 48.1	+16 59 17	8.8	2021-12-06 0:34:29	900	88
RKS0001-1656	00 01 25.8	-16 56 54	10.8	2018-12-01 0:59:52	900	31
RKS0007-2349	00 07 32.5	-23 49 07	8.7	2020-12-14 1:22:54	900	71
RKS0012+2142	00 12 33.5	+21 42 48	11.8	2021-08-13 7:17:31	1200	29
RKS0012+2705	00 12 04.0	+27 05 56	8.7	2018-11-08 2:21:41	900	63
RKS0016-1435	00 16 11.0	-14 35 27	10.0	2021-08-13 6:58:21	900	55
RKS0017+2057	00 17 59.1	+20 57 24	11.0	2021-07-27 7:42:39	1800	36
RKS0019-0303	00 19 12.3	-03 03 13	10.9	2018-12-30 1:03:13	900	31
RKS0019-0957	00 19 05.5	-09 57 53	9.9	2017-08-01 8:28:07	900	38
RKS0020+1738	00 20 57.1	+17 38 15	11.3	2021-11-18 0:48:58	1200	44
RKS0021+2531	00 21 16.0	+25 31 27	9.6	2021-11-19 1:01:54	900	70
RKS0022-2701	00 22 23.5	-27 01 57	8.3	2019-10-22 3:11:29	900	40
RKS0024-2701	00 24 25.9	-27 01 36	7.9	2017-08-05 6:55:29	900	113
RKS0036-0930	00 36 00.0	-09 30 56	11.2	2020-12-30 1:41:06	1800	35
RKS0036+2610	00 36 57.9	+26 10 54	9.0	2019-10-15 4:28:21	900	36
RKS0039+2115	00 39 21.8	+21 15 01	5.9	2017-08-21 7:12:12	900	230
RKS0042+2239	00 42 56.7	+22 39 34	11.5	2020-11-06 2:26:58	1800	33
RKS0045+0147	00 45 04.8	+01 47 07	8.0	2017-07-30 9:13:22	900	38
RKS0048+0516	00 48 22.9	+05 16 50	5.7	2017-07-02 10:56:38	900	253
RKS0051-2254	00 51 34.0	-22 54 36	9.0	2018-08-12 7:52:40	900	83
RKS0051+1844	00 51 21.7	+18 44 21	9.2	2018-08-13 7:53:46	900	32
RKS0055-2940	00 55 49.2	-29 40 33	9.4	2017-12-16 2:09:38	900	60
RKS0057+0551	00 57 44.5	+05 51 20	10.3	2018-11-06 2:44:30	900	40
RKS0102-1025	01 02 21.1	-10 25 25	10.1	2017-07-12 10:11:53	900	36
RKS0102+0503	01 02 24.5	+05 03 41	8.2	2017-08-06 9:31:01	900	102
RKS0104-2536	01 04 24.1	-25 36 18	9.8	2018-08-16 7:50:32	900	56
RKS0104+2607	01 04 32.4	+26 07 12	10.0	2019-09-20 5:19:31	900	37
RKS0105+1523	01 05 29.9	+15 23 24	8.7	2018-11-20 1:45:11	900	51
RKS0107+2257	01 07 37.8	+22 57 17	8.4	2017-07-12 10:30:30	900	52
RKS0108+1714	01 08 40.3	+17 14 33	10.5	2021-01-06 0:35:09	900	28
RKS0112-2514	01 12 46.1	-25 14 08	9.6	2017-08-03 8:42:26	900	43
RKS0113+1629	01 13 58.8	+16 29 40	9.8	2021-10-27 3:12:33	900	70
RKS0116+2519	01 16 39.3	+25 19 53	10.1	2017-07-17 9:58:20	900	32
RKS0117-1530	01 17 34.0	-15 30 11	9.8	2018-12-02 1:33:19	900	44
RKS0118-0052	01 18 41.0	-00 52 03	8.0	2021-11-30 0:51:40	900	135
RKS0121+2419	01 21 29.3	+24 19 50	10.7	2018-11-05 3:19:20	900	31
RKS0122-2653	01 22 07.6	-26 53 35	8.8	2017-07-21 10:00:54	900	69
RKS0123-1257	01 23 02.6	-12 57 57	7.9	2020-11-01 3:40:06	900	115
RKS0124+1829	01 24 53.9	+18 29 59	8.5	2021-01-10 0:37:58	900	68
RKS0125-0103	01 25 09.4	-01 03 34	9.5	2018-11-21 3:40:26	900	46
RKS0129+2143	01 29 04.8	+21 43 23	7.7	2018-09-18 7:03:32	900	52
RKS0135-2046	01 35 45.6	-20 46 13	10.2	2021-08-27 7:02:59	900	42
RKS0139+1515	01 39 56.1	+15 15 33	8.7	2019-10-20 4:53:06	900	32

Continued on next page

Table 11 — *Continued from previous page*

RKS ID	R.A.	Decl.	V	Date & Time of Obs	Exp. Time	SNR
...	(hh mm ss)	(dd mm ss)	(mag)	(UTC)	(s)	...
RKS0142+2016	01 42 29.7	+20 16 06	5.3	2017-07-18 10:20:17	900	245
RKS0146+1224	01 46 38.7	+12 24 42	8.9	2017-07-13 10:29:10	900	34
RKS0150+1817	01 50 28.0	+18 17 46	10.9	2021-08-13 8:22:23	1200	36
RKS0150+2927	01 50 07.8	+29 27 52	8.1	2018-11-18 2:51:35	900	69
RKS0200+2636	02 00 20.1	+26 36 00	11.0	2021-08-17 8:59:19	1200	29
RKS0205-2804	02 05 23.6	-28 04 11	10.9	2020-12-23 0:59:24	900	32
RKS0209-1620	02 09 10.9	-16 20 22	10.9	2020-12-05 3:11:14	900	31
RKS0213-2111	02 13 12.1	-21 11 47	9.8	2017-07-17 10:17:21	900	37
RKS0214-0338	02 14 13.5	-03 38 06	8.6	2017-07-18 10:38:38	900	66
RKS0215-1814	02 15 46.1	-18 14 17	9.1	2018-09-20 8:37:49	900	38
RKS0221-0652	02 21 44.4	-06 52 46	9.1	2019-10-02 5:19:19	900	40
RKS0229-1958	02 29 01.7	-19 58 45	8.8	2018-08-12 9:25:25	900	90
RKS0231-1516	02 31 42.4	-15 16 24	8.7	2017-12-16 2:46:43	900	81
RKS0231-2001	02 31 30.8	-20 01 41	10.2	2019-10-26 4:13:30	900	31
RKS0236-0309	02 36 41.7	-03 09 22	8.1	2017-07-15 10:43:21	900	43
RKS0236-2331	02 36 00.7	-23 31 16	8.3	2017-07-18 10:01:34	900	66
RKS0236-2710	02 36 00.7	-27 10 42	9.5	2019-10-02 5:37:32	900	38
RKS0236+0653	02 36 04.9	+06 53 12	5.8	2019-10-11 6:17:02	900	216
RKS0240+0111	02 40 42.8	+01 11 55	9.5	2021-02-17 0:12:25	900	39
RKS0242+0322	02 42 32.5	+03 22 26	10.1	2019-10-20 6:12:14	900	31
RKS0243+1925	02 43 20.8	+19 25 45	8.2	2018-10-02 6:49:04	900	81
RKS0246-2305	02 46 42.8	-23 05 11	10.3	2017-08-04 10:16:27	900	31
RKS0246+1146	02 46 17.2	+11 46 30	8.6	2019-10-02 5:55:58	900	62
RKS0246+2538	02 46 15.2	+25 38 59	7.9	2019-09-26 5:53:45	900	56
RKS0247+2842	02 47 55.8	+28 42 44	11.1	2018-11-08 4:43:00	900	31
RKS0248-1145	02 48 06.5	-11 45 47	10.8	2017-12-15 2:51:21	900	33
RKS0248+2704	02 48 09.1	+27 04 07	7.6	2019-01-03 1:13:26	900	77
RKS0250+1542	02 50 36.8	+15 42 35	8.9	2018-09-29 7:32:22	900	38
RKS0251-0816	02 51 44.4	-08 16 09	9.8	2019-10-15 6:59:33	900	33
RKS0251+1038	02 51 42.8	+10 38 42	10.0	2019-10-15 6:37:50	900	35
RKS0252-1246	02 52 32.1	-12 46 10	6.1	2019-10-02 6:14:44	900	191
RKS0255+2652	02 55 39.0	+26 52 23	7.5	2020-12-20 1:36:05	900	81
RKS0255+2807	02 55 41.2	+28 07 47	11.1	2018-10-07 5:50:56	900	30
RKS0257-2458	02 57 13.1	-24 58 30	7.8	2020-10-31 4:35:33	900	119
RKS0258+2646	02 58 52.4	+26 46 26	8.2	2019-10-01 6:22:13	900	37
RKS0300+0744	03 00 02.8	+07 44 59	8.0	2017-08-05 9:52:44	900	83
RKS0303+2006	03 03 49.0	+20 06 39	8.6	2019-11-21 4:16:57	900	52
RKS0306+0157	03 06 26.7	+01 57 54	9.1	2020-10-27 5:34:33	900	81
RKS0308-2410	03 08 25.6	-24 10 03	10.1	2021-08-18 8:26:05	900	46
RKS0310+1203	03 10 15.1	+12 03 01	9.4	2020-11-03 4:38:29	900	56
RKS0314-2626	03 14 44.6	-26 26 46	9.2	2018-10-02 8:02:24	900	68
RKS0314+0858	03 14 47.2	+08 58 50	7.8	2019-10-21 4:47:01	900	63
RKS0320+0827	03 20 29.1	+08 27 16	9.6	2019-10-08 7:06:54	900	37
RKS0322+2709	03 22 28.1	+27 09 21	11.0	2020-12-06 3:23:24	900	28
RKS0324-0521	03 24 59.7	-05 21 49	7.9	2019-09-18 7:52:13	900	88

Continued on next page

Table 11 -- *Continued from previous page*

RKS ID	R.A.	Decl.	V	Date & Time of Obs	Exp. Time	SNR
...	(hh mm ss)	(dd mm ss)	(mag)	(UTC)	(s)	...
RKS0329-1140	03 29 19.7	-11 40 42	10.0	2018-08-14 10:10:03	900	43
RKS0332-0927	03 32 55.8	-09 27 29	3.7	2017-08-02 10:24:15	404	344
RKS0341+0336	03 41 10.5	+03 36 40	9.6	2021-11-12 4:03:36	900	82
RKS0342-2427	03 42 44.6	-24 27 58	9.2	2019-10-05 6:45:05	900	51
RKS0343-1253	03 43 06.1	-12 53 39	10.9	2019-10-10 7:09:44	900	27
RKS0343-1906	03 43 55.3	-19 06 39	7.1	2019-09-18 8:10:39	900	112
RKS0343+1640	03 43 52.5	+16 40 19	10.0	2019-03-06 0:00:20	900	46
RKS0344+1155	03 44 51.1	+11 55 12	9.2	2018-10-03 6:46:19	900	42
RKS0345-2751	03 45 24.1	-27 51 44	8.2	2019-12-16 2:06:56	900	60
RKS0348+1512	03 48 32.9	+15 12 07	9.5	2020-12-02 3:48:15	900	46
RKS0348+2519	03 48 26.3	+25 19 23	8.6	2019-11-20 4:19:05	900	55
RKS0349-1329	03 49 15.9	-13 29 29	11.1	2021-11-20 3:05:47	1200	51
RKS0350-2349	03 50 19.5	-23 49 44	9.9	2019-10-10 7:45:00	900	37
RKS0354-0649	03 54 35.4	-06 49 33	9.0	2019-10-10 6:51:39	900	59
RKS0357-0109	03 57 28.6	-01 09 34	8.1	2019-09-19 8:17:34	900	61
RKS0404+2634	04 04 15.2	+26 34 24	11.2	2021-11-18 4:22:50	1200	38
RKS0406-2051	04 06 34.8	-20 51 11	9.7	2020-01-21 0:36:01	900	36
RKS0407+1413	04 07 43.9	+14 13 24	10.8	2021-11-23 4:32:57	1200	47
RKS0408+1220	04 08 30.8	+12 20 16	8.6	2020-02-09 0:23:08	900	44
RKS0417+2033	04 17 26.9	+20 33 17	9.6	2021-11-29 3:00:29	900	72
RKS0419-0408	04 19 05.7	-04 08 55	10.5	2020-02-11 0:42:20	900	33
RKS0420-1445	04 20 10.5	-14 45 39	9.8	2020-10-27 5:58:01	900	54
RKS0421-1945	04 21 31.6	-19 45 23	10.4	2018-10-03 7:25:48	900	30
RKS0427+2426	04 27 52.9	+24 26 41	9.4	2018-10-07 7:34:38	900	40
RKS0429+2155	04 29 00.1	+21 55 21	8.3	2020-02-07 0:42:09	900	66
RKS0430+0058	04 30 16.7	+00 58 47	10.5	2018-12-17 3:48:55	900	32
RKS0436+2707	04 36 48.2	+27 07 55	8.1	2020-10-30 6:01:20	900	102
RKS0441+2054	04 41 18.8	+20 54 05	8.1	2021-03-01 23:57:47	900	97
RKS0445+0938	04 45 27.2	+09 38 27	11.2	2021-11-29 2:37:47	1200	44
RKS0448-1056	04 48 01.1	-10 56 01	9.5	2020-02-02 3:06:08	900	42
RKS0449-1447	04 49 32.7	-14 47 22	10.9	2018-10-10 6:18:24	900	38
RKS0451+2837	04 51 33.3	+28 37 49	9.6	2021-12-12 3:57:24	900	61
RKS0453+2214	04 53 04.7	+22 14 06	8.8	2017-12-15 3:46:03	900	59
RKS0454+0722	04 54 16.6	+07 22 22	8.2	2021-11-30 4:05:02	900	129
RKS0455-2833	04 55 41.9	-28 33 50	8.1	2020-01-31 0:49:08	900	76
RKS0503+0322	05 03 32.1	+03 22 56	11.1	2021-12-08 3:41:03	1200	39
RKS0506-1102	05 06 30.0	-11 02 34	9.6	2021-11-30 4:40:27	900	77
RKS0512+1943	05 12 53.4	+19 43 19	9.9	2020-02-15 0:43:19	900	30
RKS0513-2158	05 13 59.1	-21 58 24	10.5	2021-01-15 4:31:46	900	30
RKS0514+0039	05 14 48.1	+00 39 43	10.0	2018-11-21 5:24:08	900	39
RKS0514+1952	05 14 17.0	+19 52 58	9.5	2021-11-27 4:31:19	900	67
RKS0518-2123	05 18 47.1	-21 23 37	9.4	2018-10-10 6:54:11	900	38
RKS0519-0304	05 19 12.6	-03 04 25	7.8	2019-03-05 0:49:27	753	104
RKS0519-1550	05 19 59.5	-15 50 22	8.7	2018-10-10 7:29:20	900	49
RKS0522+0236	05 22 37.4	+02 36 11	7.8	2020-11-28 5:49:26	900	118

Continued on next page

Table 11 — *Continued from previous page*

RKS ID	R.A.	Decl.	V	Date & Time of Obs	Exp. Time	SNR
...	(hh mm ss)	(dd mm ss)	(mag)	(UTC)	(s)	...
RKS0523+1719	05 23 38.3	+17 19 26	7.9	2020-02-01 0:46:07	900	67
RKS0533-2643	05 33 04.6	-26 43 28	9.1	2020-02-28 0:10:36	900	47
RKS0534-2328	05 34 48.6	-23 28 08	8.8	2018-11-08 8:25:57	900	74
RKS0535+2805	05 35 00.8	+28 05 54	10.1	2021-01-10 2:39:13	900	30
RKS0536+1119	05 36 30.9	+11 19 40	8.9	2020-02-29 0:00:51	900	58
RKS0542+0240	05 42 45.8	+02 40 44	8.6	2018-11-22 7:08:38	900	69
RKS0544-2225	05 44 26.5	-22 25 18	6.2	2020-10-26 8:04:39	422	181
RKS0549-1734	05 49 22.5	-17 34 44	8.5	2021-12-17 2:49:25	900	105
RKS0552-2246	05 52 31.9	-22 46 36	10.6	2021-12-18 3:48:04	1200	52
RKS0553-0559	05 53 00.2	-05 59 41	9.7	2020-03-01 23:59:13	900	40
RKS0554-1942	05 54 30.4	-19 42 05	10.6	2019-10-26 8:58:34	720	28
RKS0554+0208	05 54 28.5	+02 08 32	8.8	2020-02-29 0:19:16	900	50
RKS0600+2101	06 00 53.9	+21 01 15	10.0	2018-11-21 6:32:48	900	37
RKS0602+0848	06 02 44.2	+08 48 30	10.8	2021-01-24 2:44:54	900	32
RKS0608+2630	06 08 13.2	+26 30 08	9.4	2019-11-26 5:26:26	900	40
RKS0609+0009	06 09 46.1	+00 09 32	10.9	2019-12-03 7:09:31	900	32
RKS0609+0540	06 09 35.9	+05 40 08	8.5	2018-11-22 7:43:29	900	71
RKS0612+1023	06 12 08.4	+10 23 39	9.7	2019-12-08 6:12:33	900	39
RKS0614+0510	06 14 24.4	+05 10 05	8.4	2020-11-27 6:07:56	900	86
RKS0616+2512	06 16 39.5	+25 12 21	9.4	2020-10-30 7:23:03	900	62
RKS0617+1759	06 17 25.8	+17 59 21	10.3	2018-01-31 2:32:04	900	34
RKS0618-1352	06 18 22.1	-13 52 07	9.9	2020-03-02 0:16:55	900	34
RKS0620+0215	06 20 13.2	+02 15 32	9.8	2020-02-19 0:46:02	900	37
RKS0621-2212	06 21 33.1	-22 12 53	8.5	2020-03-02 0:34:34	900	61
RKS0626+1845	06 26 10.2	+18 45 24	6.8	2019-11-08 7:23:41	900	148
RKS0629+2700	06 29 05.5	+27 00 31	8.6	2018-11-19 6:49:22	900	62
RKS0630-1148	06 30 07.3	-11 48 32	9.1	2020-03-03 0:06:12	900	47
RKS0632-2701	06 32 08.8	-27 01 58	11.4	2020-12-27 3:36:41	1800	35
RKS0633+0527	06 33 12.6	+05 27 46	7.9	2020-02-05 2:22:59	900	76
RKS0637+1945	06 37 05.2	+19 45 10	10.2	2020-02-28 0:41:02	900	36
RKS0641+2357	06 41 15.7	+23 57 27	8.1	2020-02-15 1:43:55	900	62
RKS0647-1815	06 47 15.7	-18 15 31	10.6	2018-11-21 7:27:14	900	32
RKS0652-0510	06 52 18.0	-05 10 25	6.6	2020-03-03 0:23:39	900	150
RKS0652-2306	06 52 59.6	-23 06 27	9.0	2020-02-07 3:18:19	900	46
RKS0658-1259	06 58 26.0	-12 59 30	9.1	2018-02-28 3:20:36	900	38
RKS0700-2847	07 00 09.4	-28 47 02	10.8	2020-03-15 23:55:04	900	30
RKS0701-2556	07 01 13.7	-25 56 55	6.7	2021-01-24 3:20:56	900	179
RKS0701+0655	07 01 35.5	+06 55 36	8.2	2020-02-28 0:58:55	900	57
RKS0702-0647	07 02 42.9	-06 47 57	8.4	2020-02-19 1:05:02	900	73
RKS0706+2358	07 06 52.1	+23 58 08	10.1	2018-02-10 1:41:33	900	39
RKS0707+0326	07 07 09.3	+03 26 50	9.8	2020-10-30 7:40:51	900	54
RKS0708-0958	07 08 09.3	-09 58 07	8.9	2018-12-20 5:55:09	900	63
RKS0708+2950	07 08 04.2	+29 50 04	8.3	2018-12-16 6:07:45	900	58
RKS0710-1425	07 10 49.5	-14 25 58	10.0	2018-12-17 4:42:05	900	41
RKS0712-2453	07 12 04.8	-24 53 31	10.4	2020-03-07 3:10:36	900	29

Continued on next page

Table 11 -- *Continued from previous page*

RKS ID	R.A.	Decl.	V	Date & Time of Obs	Exp. Time	SNR
...	(hh mm ss)	(dd mm ss)	(mag)	(UTC)	(s)	...
RKS0713+2500	07 13 53.1	+25 00 40	8.4	2018-12-19 5:27:33	900	59
RKS0716-0339	07 16 10.6	-03 39 57	9.0	2020-03-05 0:34:50	900	46
RKS0723-2001	07 23 29.2	-20 01 24	9.9	2018-12-30 3:45:00	900	42
RKS0723+1257	07 23 47.0	+12 57 52	8.2	2018-12-29 4:38:01	900	59
RKS0723+2024	07 23 43.5	+20 24 58	10.0	2020-02-07 2:47:35	900	38
RKS0724-1753	07 24 34.2	-17 53 31	10.3	2020-02-18 1:29:50	900	35
RKS0725-1041	07 25 29.8	-10 41 59	11.6	2021-12-12 6:17:52	1200	37
RKS0726-1546	07 26 26.5	-15 46 13	9.2	2022-10-15 8:59:55	900	80
RKS0730-0340	07 30 17.5	-03 40 24	10.4	2020-03-16 0:12:54	900	37
RKS0732+1719	07 32 02.8	+17 19 09	11.0	2022-03-20 1:00:04	900	38
RKS0734-0653	07 34 26.1	-06 53 48	8.2	2020-03-03 0:41:07	900	68
RKS0739-0335	07 39 59.3	-03 35 51	7.2	2020-02-20 3:31:17	900	118
RKS0741-2921	07 41 17.4	-29 21 32	10.7	2020-02-19 1:48:22	900	30
RKS0745+0208	07 45 01.1	+02 08 14	10.2	2020-03-02 1:10:25	900	29
RKS0752+2555	07 52 47.4	+25 55 35	8.6	2020-03-16 0:31:00	900	47
RKS0754-2518	07 54 10.8	-25 18 11	9.8	2020-02-05 5:16:11	900	40
RKS0754+1914	07 54 54.0	+19 14 10	7.8	2020-03-01 1:46:05	900	67
RKS0757-0048	07 57 57.7	-00 48 51	8.1	2020-03-09 1:03:21	900	79
RKS0758-1501	07 58 25.5	-15 01 13	9.3	2018-11-19 6:31:22	900	54
RKS0758-2537	07 58 04.3	-25 37 35	8.4	2020-03-10 0:55:32	900	68
RKS0759+2050	07 59 33.9	+20 50 38	7.7	2020-03-03 1:49:45	900	85
RKS0808+2106	08 08 13.1	+21 06 18	9.4	2019-01-13 5:11:19	900	56
RKS0813-1355	08 13 08.4	-13 55 01	9.4	2020-01-07 6:54:28	900	43
RKS0814+1301	08 14 35.9	+13 01 22	8.8	2020-03-05 2:11:58	900	55
RKS0815-2600	08 15 40.0	-26 00 35	10.1	2020-03-10 1:13:08	900	32
RKS0817+1717	08 17 08.0	+17 17 56	9.4	2020-03-15 0:54:59	900	41
RKS0819+0120	08 19 19.0	+01 20 19	8.4	2020-03-11 0:33:04	900	55
RKS0820+1404	08 20 55.3	+14 04 16	9.8	2020-03-11 0:50:51	900	33
RKS0823+2150	08 23 30.9	+21 50 57	9.5	2020-03-11 1:08:36	900	33
RKS0827+2855	08 27 11.4	+28 55 53	9.6	2020-03-12 1:38:11	900	30
RKS0832-2323	08 32 33.3	-23 23 06	10.2	2020-03-12 3:24:58	900	33
RKS0838-0415	08 38 19.2	-04 15 29	11.3	2021-01-27 5:29:16	1800	36
RKS0838-1315	08 38 45.2	-13 15 24	9.7	2020-03-13 2:26:36	900	36
RKS0839+0657	08 39 00.2	+06 57 19	7.9	2020-03-13 2:44:26	900	81
RKS0839+1131	08 39 50.7	+11 31 21	7.6	2020-11-28 8:14:25	900	126
RKS0840-0628	08 40 00.2	-06 28 33	9.9	2021-11-01 8:12:41	900	64
RKS0848+0628	08 48 26.1	+06 28 06	10.4	2017-12-15 7:31:57	900	32
RKS0850+0751	08 50 42.2	+07 51 52	9.8	2021-03-01 2:41:10	900	74
RKS0852+2819	08 52 35.8	+28 19 50	6.0	2021-01-20 5:14:32	900	230
RKS0855+0132	08 55 07.6	+01 32 47	10.0	2021-01-29 3:58:50	900	52
RKS0901+1515	09 01 17.4	+15 15 56	9.3	2020-12-11 6:39:14	900	69
RKS0904-1554	09 04 20.6	-15 54 51	8.8	2018-03-25 1:21:12	900	81
RKS0905+2517	09 05 18.4	+25 17 52	10.4	2021-01-12 5:55:35	900	35
RKS0907+2252	09 07 18.0	+22 52 21	8.0	2021-03-24 2:28:12	900	105
RKS0909+0512	09 09 54.1	+05 12 12	8.4	2021-01-12 6:13:22	900	97

Continued on next page

Table 11 — *Continued from previous page*

RKS ID	R.A.	Decl.	V	Date & Time of Obs	Exp. Time	SNR
...	(hh mm ss)	(dd mm ss)	(mag)	(UTC)	(s)	...
RKS0914+0426	09 14 53.6	+04 26 34	7.9	2018-01-31 5:32:52	900	113
RKS0918+2718	09 18 21.5	+27 18 41	9.5	2021-02-23 3:25:22	900	36
RKS0919+0053	09 19 28.3	+00 53 49	8.2	2021-01-03 7:05:29	900	80
RKS0920-0545	09 20 44.3	-05 45 14	9.1	2021-01-26 5:31:03	900	69
RKS0929-0522	09 29 35.0	-05 22 21	9.7	2018-12-17 6:34:39	900	41
RKS0929+0539	09 29 54.8	+05 39 18	7.2	2020-03-14 2:41:45	900	36
RKS0932-1111	09 32 25.5	-11 11 04	7.8	2020-03-02 4:12:42	900	89
RKS0932+2909	09 32 11.1	+29 09 25	11.4	2020-12-05 8:25:14	900	28
RKS0937+2231	09 37 58.3	+22 31 23	9.9	2018-03-26 1:23:09	900	44
RKS0937+2241	09 37 11.3	+22 41 38	9.5	2019-01-31 5:09:42	900	39
RKS0938+0240	09 38 23.9	+02 40 36	11.9	2021-01-17 5:57:26	1800	32
RKS0947+0134	09 47 16.6	+01 34 36	11.0	2019-02-17 4:24:35	900	32
RKS0952+0307	09 52 39.1	+03 07 48	10.6	2018-02-12 4:00:32	900	40
RKS0959-0911	09 59 11.3	-09 11 00	9.9	2020-12-16 7:18:24	900	49
RKS1000+2433	10 00 01.7	+24 33 10	7.9
RKS1001-1525	10 01 37.2	-15 25 29	8.7	2018-02-12 4:38:50	900	86
RKS1004-1143	10 04 37.6	-11 43 46	8.2	2021-01-05 7:55:34	900	98
RKS1005+2629	10 05 26.5	+26 29 16	9.1	2018-02-11 5:02:18	900	62
RKS1006+0257	10 06 56.8	+02 57 51	10.0	2019-03-03 4:12:52	900	31
RKS1008+1159	10 08 12.7	+11 59 49	8.1	2021-02-17 5:26:58	900	78
RKS1011-2425	10 11 45.0	-24 25 33	11.0	2021-01-12 8:17:05	900	31
RKS1020-0128	10 20 43.4	-01 28 11	9.4	2018-03-11 3:14:34	900	61
RKS1024-1024	10 24 14.9	-10 24 21	10.0	2020-02-05 6:23:19	900	33
RKS1026-0631	10 26 41.2	-06 31 34	9.8	2022-03-01 4:18:08	900	62
RKS1026+2638	10 26 59.5	+26 38 29	8.2	2018-03-11 3:32:22	894	81
RKS1028+0644	10 28 10.4	+06 44 06	8.5	2018-03-11 3:49:53	900	86
RKS1030-2114	10 30 21.9	-21 14 12	9.6	2020-03-12 5:58:34	900	40
RKS1032+0830	10 32 00.6	+08 30 38	10.8	2021-01-20 6:54:24	900	31
RKS1036-1350	10 36 30.7	-13 50 35	8.7	2018-03-13 4:11:25	900	80
RKS1043-2903	10 43 28.2	-29 03 51	7.7	2020-12-28 8:02:13	900	114
RKS1046-2435	10 46 36.9	-24 35 07	9.4	2019-01-29 6:46:05	900	47
RKS1053-1422	10 53 22.5	-14 22 28	9.3	2021-01-16 8:22:41	900	54
RKS1054-0432	10 54 49.1	-04 32 30	10.4	2020-02-20 7:01:58	900	37
RKS1056+0723	10 56 30.7	+07 23 18	7.4	2019-03-05 4:08:17	570	94
RKS1057+2856	10 57 11.4	+28 56 16	8.9	2019-04-11 2:05:02	900	60
RKS1059+2526	10 59 38.3	+25 26 15	8.5	2021-03-03 4:42:49	900	61
RKS1102-0919	11 02 50.1	-09 19 49	9.0	2018-02-27 4:37:26	900	71
RKS1108-2816	11 08 06.3	-28 16 04	9.3	2021-11-20 8:13:14	900	87
RKS1108+1546	11 08 31.7	+15 46 03	9.8	2021-04-01 3:05:01	900	45
RKS1111-1057	11 11 10.7	-10 57 03	9.2	2018-03-12 3:51:56	900	70
RKS1111-1459	11 11 33.1	-14 59 28	9.1	2018-07-01 23:10:50	900	37
RKS1113+0428	11 13 13.2	+04 28 56	8.7	2018-02-26 5:40:12	900	87
RKS1114-2306	11 14 48.1	-23 06 17	9.0
RKS1114+2542	11 14 33.1	+25 42 37	7.8	2021-02-03 5:51:50	1800	108
RKS1115-1808	11 15 20.7	-18 08 37	10.2	2021-01-07 8:05:18	900	48

Continued on next page

Table 11 -- *Continued from previous page*

RKS ID	R.A.	Decl.	V	Date & Time of Obs	Exp. Time	SNR
...	(hh mm ss)	(dd mm ss)	(mag)	(UTC)	(s)	...
RKS1116-1441	11 16 22.1	-14 41 36	10.0	2018-03-13 5:22:10	900	55
RKS1117-0158	11 17 13.6	-01 58 54	9.7	2020-02-29 5:57:50	900	36
RKS1117-2748	11 17 07.5	-27 48 48	9.8	2018-03-13 5:40:16	900	63
RKS1121-2027	11 21 26.6	-20 27 13	8.6	2018-02-26 6:20:21	900	103
RKS1121+1811	11 21 49.3	+18 11 24	7.9	2021-03-14 4:36:16	900	99
RKS1125+2000	11 25 39.9	+20 00 07	8.3	2018-03-29 2:51:50	900	85
RKS1126+1517	11 26 49.9	+15 17 38	10.5	2022-04-03 3:26:47	900	45
RKS1127+0358	11 27 38.5	+03 58 35	10.6	2021-07-08 22:43:40	900	39
RKS1128+0731	11 28 27.7	+07 31 02	10.2	2018-06-19 23:40:18	900	38
RKS1134-1314	11 34 50.4	-13 14 31	10.4	2020-12-18 8:21:25	900	33
RKS1135+1658	11 35 59.1	+16 58 05	9.5	2019-04-07 3:27:11	900	52
RKS1139-2741	11 39 08.1	-27 41 46	10.0	2019-02-18 3:18:19	900	45
RKS1141+0508	11 41 49.5	+05 08 26	9.6	2019-07-05 23:30:28	900	53
RKS1147-1149	11 47 03.8	-11 49 26	9.0	2021-01-10 8:17:24	900	71
RKS1152+1845	11 52 08.3	+18 45 18	8.4	2018-06-19 23:02:16	900	67
RKS1154+2844	11 54 57.4	+28 44 15	10.5	2022-03-13 4:35:11	900	46
RKS1157-2608	11 57 16.2	-26 08 29	8.9	2019-04-21 5:00:51	900	75
RKS1157-2742	11 57 56.2	-27 42 25	7.0	2021-03-04 3:17:50	900	199
RKS1157+1959	11 57 28.9	+19 59 02	8.1	2021-03-10 5:17:11	900	98
RKS1158-2355	11 58 11.7	-23 55 25	8.7	2019-05-05 4:15:09	900	80
RKS1159-2021	11 59 10.0	-20 21 13	7.9	2020-03-06 6:56:56	900	74
RKS1204-0013	12 04 47.8	-00 13 36	10.8	2021-02-08 7:29:38	900	35
RKS1204+0911	12 04 17.4	+09 11 35	9.9	2019-02-18 5:06:34	900	36
RKS1205-1852	12 05 50.6	-18 52 30	10.0	2017-07-05 1:14:00	900	36
RKS1206-2336	12 06 09.0	-23 36 08	8.6	2021-01-18 8:05:10	900	78
RKS1208-0028	12 08 22.2	-00 28 57	11.3	2023-03-07 4:20:11	1800	41
RKS1209-2646	12 09 23.4	-26 46 46	11.0	2021-01-11 7:24:16	900	31
RKS1210-1126	12 10 33.6	-11 26 59	11.3	2023-03-12 4:29:26	1800	41
RKS1220-1953	12 20 46.8	-19 53 45	9.0	2018-03-28 3:18:27	900	72
RKS1222+2736	12 22 34.0	+27 36 16	10.9	2019-02-18 6:54:13	900	30
RKS1223+2754	12 23 34.7	+27 54 47	11.3	2022-03-02 5:54:55	1800	43
RKS1228-1654	12 28 19.1	-16 54 39	9.5	2020-03-06 7:14:19	900	40
RKS1231+2013	12 31 18.2	+20 13 04	7.9	2021-06-27 0:40:33	900	96
RKS1233-1438	12 33 59.7	-14 38 19	9.1	2018-03-26 3:55:21	900	72
RKS1241+1951	12 41 37.0	+19 51 05	9.1	2019-07-05 23:49:11	900	56
RKS1248-1543	12 48 32.2	-15 43 09	7.9	2017-07-14 0:54:08	900	98
RKS1248-2448	12 48 10.7	-24 48 23	8.9	2017-07-14 0:34:39	900	67
RKS1250-0046	12 50 43.5	-00 46 05	8.5	2020-03-14 5:26:16	900	52
RKS1253+0645	12 53 54.4	+06 45 46	8.2	2018-03-26 4:44:59	838	90
RKS1256-2455	12 56 30.0	-24 55 31	10.0	2020-01-23 8:38:50	900	32
RKS1257-1427	12 57 43.9	-14 27 48	9.1	2018-03-23 6:28:11	900	71
RKS1259-0950	12 59 01.5	-09 50 02	7.5	2017-07-08 23:54:29	900	57
RKS1300-0242	13 00 16.9	-02 42 17	9.8	2019-03-07 6:44:36	900	48
RKS1302-2647	13 02 20.6	-26 47 13	8.4
RKS1303-0509	13 03 49.7	-05 09 42	7.7	2018-04-12 2:59:09	707	93

Continued on next page

Table 11 -- *Continued from previous page*

RKS ID	R.A.	Decl.	V	Date & Time of Obs	Exp. Time	SNR
...	(hh mm ss)	(dd mm ss)	(mag)	(UTC)	(s)	...
RKS1306+2043	13 06 15.3	+20 43 45	9.4	2018-03-28 5:12:45	900	54
RKS1310+0932	13 10 16.9	+09 32 09	9.3	2021-02-18 7:30:12	900	47
RKS1312-0215	13 12 43.7	-02 15 54	7.6	2020-03-15 5:14:46	900	96
RKS1316+1701	13 16 51.0	+17 01 01	6.5	2020-03-15 5:33:28	900	147
RKS1318-1446	13 18 05.8	-14 46 48	10.9	2021-02-22 5:59:56	900	31
RKS1320+0407	13 20 43.7	+04 07 58	8.6	2021-02-25 9:02:24	900	80
RKS1323+0243	13 23 39.1	+02 43 23	7.1	2021-02-07 7:37:05	900	157
RKS1327-2417	13 27 02.9	-24 17 25	8.7	2021-02-11 7:12:32	900	77
RKS1331-0219	13 31 39.9	-02 19 02	7.3	2019-07-10 0:27:53	900	128
RKS1333+0835	13 33 32.4	+08 35 12	8.0	2021-02-18 7:47:43	900	98
RKS1334-0018	13 34 16.2	-00 18 49	7.4	2019-07-05 1:29:23	900	110
RKS1334-0820	13 34 43.2	-08 20 31	9.2	2021-02-20 7:26:25	900	62
RKS1334+0440	13 34 21.5	+04 40 02	10.0	2021-03-08 7:50:48	900	47
RKS1335-0023	13 35 24.7	-00 23 20	10.3	2019-03-15 8:51:23	900	44
RKS1335+0650	13 35 06.3	+06 50 27	8.9	2021-02-19 7:31:22	900	62
RKS1336+0746	13 36 56.6	+07 46 01	10.0	2021-03-08 6:03:03	900	36
RKS1340-0411	13 40 07.1	-04 11 09	9.6	2018-03-29 4:25:57	900	64
RKS1341-0007	13 41 55.6	-00 07 44	9.8	2021-02-26 6:59:33	900	45
RKS1342-0141	13 42 26.0	-01 41 10	9.2	2021-02-26 6:38:59	900	30
RKS1345-0437	13 45 05.3	-04 37 13	10.5	2019-04-11 5:48:26	900	37
RKS1345+0850	13 45 14.7	+08 50 09	8.5	2019-05-08 5:57:52	900	34
RKS1345+1747	13 45 05.0	+17 47 07	9.8	2019-03-16 6:27:16	900	50
RKS1347+0618	13 47 28.7	+06 18 56	10.0	2019-06-01 4:25:25	900	39
RKS1349-2206	13 49 44.8	-22 06 39	8.2	2021-02-08 8:25:04	900	121
RKS1353+1256	13 53 27.5	+12 56 32	9.8	2017-06-25 0:07:53	900	29
RKS1353+2748	13 53 05.2	+27 48 24	8.4	2019-04-07 5:23:17	900	70
RKS1359+2252	13 59 19.4	+22 52 11	9.1	2021-02-11 9:00:01	900	69
RKS1411-1236	14 11 46.1	-12 36 42	7.9	2020-03-15 5:52:00	900	80
RKS1412+2348	14 12 41.5	+23 48 51	8.9	2018-02-26 8:10:45	900	66
RKS1413-0657	14 13 31.1	-06 57 32	10.1	2019-04-11 6:06:03	900	47
RKS1414-1521	14 14 21.3	-15 21 22	10.2
RKS1418-0636	14 18 58.2	-06 36 12	9.1	2018-04-24 5:32:51	900	29
RKS1419-0509	14 19 34.8	-05 09 04	7.6	2021-01-05 8:38:10	900	121
RKS1421+2937	14 21 57.2	+29 37 46	8.6	2019-06-02 2:18:44	900	81
RKS1430-0838	14 30 47.7	-08 38 46	9.4	2018-05-04 4:01:42	900	68
RKS1432+1121	14 32 13.1	+11 21 11	9.7	2019-09-01 23:06:08	900	31
RKS1433+0920	14 33 34.9	+09 20 03	8.8	2021-06-14 2:27:03	900	69
RKS1436+0944	14 36 00.5	+09 44 47	7.5	2021-02-10 8:54:54	900	130
RKS1437-2548	14 37 04.8	-25 48 09	8.3	2021-02-02 7:44:04	900	83
RKS1442+1930	14 42 26.2	+19 30 12	10.1	2019-03-22 6:53:48	900	38
RKS1444-2215	14 44 35.5	-22 15 11	9.3	2019-05-21 6:05:04	900	51
RKS1444+2211	14 44 11.9	+22 11 07	9.9	2019-04-21 5:42:06	900	46
RKS1445+1350	14 45 24.1	+13 50 46	7.9	2021-02-04 9:10:21	900	92
RKS1446+1629	14 46 23.2	+16 29 48	9.3	2018-03-28 6:06:14	900	67
RKS1446+2730	14 46 03.0	+27 30 44	8.0	2019-04-07 6:25:28	900	82

Continued on next page

Table 11 -- *Continued from previous page*

RKS ID	R.A.	Decl.	V	Date & Time of Obs	Exp. Time	SNR
...	(hh mm ss)	(dd mm ss)	(mag)	(UTC)	(s)	...
RKS1447+0242	14 47 16.1	+02 42 11	7.8	2020-03-15 6:27:11	900	88
RKS1450+0648	14 50 20.9	+06 48 53	9.1	2021-02-17 9:07:27	900	59
RKS1451-2418	14 51 40.4	-24 18 14	7.8	2017-08-07 0:39:09	900	97
RKS1453+2320	14 53 41.5	+23 20 42	8.7	2017-07-07 0:43:04	900	34
RKS1455-2707	14 55 55.0	-27 07 38	9.0	2017-07-02 2:35:28	900	70
RKS1457-2124	14 57 28.0	-21 24 55	5.7	2021-05-01 4:47:50	385	171
RKS1500-1108	15 00 43.4	-11 08 06	9.5	2018-05-23 4:56:52	900	64
RKS1500-2427	15 00 19.3	-24 27 14	9.9	2021-02-10 9:13:00	900	48
RKS1500-2905	15 00 09.5	-29 05 27	11.5	2022-08-03 23:56:44	1200	34
RKS1501+1341	15 01 06.5	+13 41 39	11.0	2021-02-24 8:25:10	900	36
RKS1501+1552	15 01 29.9	+15 52 07	9.1	2021-07-17 0:43:36	900	66
RKS1504-1835	15 04 53.9	-18 35 27	9.5	2020-03-15 6:44:59	900	45
RKS1504+0538	15 04 53.5	+05 38 17	9.8	2018-03-26 6:10:10	900	55
RKS1507+2456	15 07 23.5	+24 56 07	10.2	2019-07-18 1:10:39	900	41
RKS1509+2400	15 09 04.2	+24 00 57	9.3	2019-06-06 3:08:12	900	46
RKS1510-1622	15 10 13.0	-16 22 45	9.1	2020-03-15 7:04:28	900	46
RKS1515+0047	15 15 59.1	+00 47 46	6.9	2017-08-07 0:20:08	900	144
RKS1515+0735	15 15 45.4	+07 35 52	10.7	2021-02-24 8:58:11	900	34
RKS1519+1155	15 19 35.3	+11 55 19	9.9	2019-08-11 23:19:48	900	34
RKS1519+2912	15 19 21.1	+29 12 22	10.3	2021-06-13 2:51:04	900	38
RKS1520+1522	15 20 38.9	+15 22 48	8.8	2021-06-13 3:28:07	900	74
RKS1522-0446	15 22 04.1	-04 46 38	9.5	2018-04-07 9:30:19	900	61
RKS1522-1039	15 22 36.6	-10 39 40	8.0	2017-07-05 2:51:45	900	81
RKS1522+0125	15 22 42.5	+01 25 07	8.3	2017-07-14 2:18:23	900	63
RKS1525-2642	15 25 58.5	-26 42 20	8.8	2017-08-07 1:53:14	900	56
RKS1527+0235	15 27 42.6	+02 35 51	10.2	2018-04-21 5:35:19	900	39
RKS1527+1035	15 27 38.0	+10 35 39	9.9	2018-05-23 4:22:00	900	44
RKS1528-0920	15 28 09.6	-09 20 52	6.9	2019-06-20 4:39:56	900	117
RKS1540-1802	15 40 34.5	-18 02 56	8.9	2018-03-23 8:10:23	900	83
RKS1552+1052	15 52 08.2	+10 52 28	9.4	2018-05-15 4:12:41	900	34
RKS1554-2600	15 54 38.4	-26 00 15	9.2	2017-06-25 1:57:44	900	37
RKS1555+1602	15 55 19.0	+16 02 39	8.7	2021-03-14 7:41:00	900	65
RKS1600-0147	16 00 16.4	-01 47 55	10.3	2021-03-14 8:10:03	900	30
RKS1601-2625	16 01 39.7	-26 25 15	10.8	2019-03-20 9:44:38	900	31
RKS1604-1126	16 04 26.7	-11 26 59	8.0	2021-05-07 5:08:03	900	78
RKS1607-0542	16 07 34.3	-05 42 25	10.3	2021-03-16 9:05:18	900	29
RKS1608-1308	16 08 24.4	-13 08 07	8.7	2018-05-24 5:35:13	900	78
RKS1608+1713	16 08 05.3	+17 13 44	9.1	2019-07-10 2:19:30	900	52
RKS1613+1331	16 13 18.4	+13 31 36	6.7	2019-08-05 1:20:40	900	36
RKS1615+0721	16 15 57.0	+07 21 25	8.7	2018-04-12 7:45:18	900	51
RKS1621+1713	16 21 38.0	+17 13 33	10.8	2019-08-12 0:45:19	900	29
RKS1624-1338	16 24 19.8	-13 38 29	8.4	2018-05-13 6:51:58	900	70
RKS1625-2156	16 25 13.0	-21 56 14	10.3	2021-02-11 8:46:46	900	34
RKS1626+1539	16 26 33.4	+15 39 53	10.5	2018-04-21 6:19:28	900	30
RKS1627+0055	16 27 20.3	+00 55 29	10.0	2018-04-21 6:01:35	900	42

Continued on next page

Table 11 — *Continued from previous page*

RKS ID	R.A.	Decl.	V	Date & Time of Obs	Exp. Time	SNR
...	(hh mm ss)	(dd mm ss)	(mag)	(UTC)	(s)	...
RKS1627+0718	16 27 56.9	+07 18 19	8.8	2017-07-03 3:03:36	900	71
RKS1629+2346	16 29 14.3	+23 46 34	10.1	2020-03-16 8:22:33	900	31
RKS1630-0359	16 30 43.0	-03 59 21	9.6	2019-07-06 3:08:15	900	51
RKS1632-1235	16 32 57.8	-12 35 30	10.6	2019-08-06 0:44:08	900	32
RKS1633-0933	16 33 41.6	-09 33 11	11.3	2020-02-29 8:57:48	1500	25
RKS1647-0111	16 47 17.5	-01 11 20	10.8	2019-08-07 2:38:19	900	35
RKS1649-2426	16 49 53.1	-24 26 48	9.6	2017-06-29 3:05:30	900	46
RKS1650+1854	16 50 05.2	+18 54 01	8.9	2017-07-10 2:14:54	900	46
RKS1654+1154	16 54 12.0	+11 54 52	10.7	2019-09-20 23:45:42	900	32
RKS1659-2616	16 59 33.2	-26 16 04	10.4	2018-08-15 1:48:27	900	45
RKS1701+2256	17 01 59.8	+22 56 09	8.8	2021-07-09 1:47:55	900	77
RKS1705-0147	17 05 08.5	-01 47 09	9.5	2022-08-16 0:25:28	900	65
RKS1705-0503	17 05 03.3	-05 03 59	7.7	2019-09-19 23:55:29	900	86
RKS1706-0610	17 06 08.2	-06 10 02	8.8	2018-06-02 4:01:07	900	62
RKS1712+1821	17 12 37.6	+18 21 04	8.0	2017-07-30 1:22:35	900	50
RKS1714-0824	17 14 08.0	-08 24 13	8.5	2022-03-17 8:30:26	900	110
RKS1716-1210	17 16 20.2	-12 10 41	10.5	2018-06-29 3:00:30	900	39
RKS1717+2913	17 17 40.4	+29 13 38	8.4	2017-07-07 2:46:21	900	37
RKS1725+0206	17 25 45.2	+02 06 41	7.5	2017-08-17 23:58:47	900	144
RKS1729-2350	17 29 06.5	-23 50 10	9.6	2018-05-23 7:52:01	900	59
RKS1733+0914	17 33 07.2	+09 14 37	9.6	2019-07-10 3:37:30	900	45
RKS1737-1314	17 37 46.4	-13 14 46	10.1
RKS1737+2257	17 37 48.7	+22 57 20	9.9	2017-07-05 3:12:27	900	38
RKS1739+0333	17 39 16.9	+03 33 18	6.5	2017-08-05 1:36:56	900	186
RKS1750-0603	17 50 34.0	-06 03 01	10.1	2017-08-01 1:27:36	900	36
RKS1752-0733	17 52 16.6	-07 33 37	9.9	2021-06-11 3:53:25	900	46
RKS1753+2119	17 53 29.9	+21 19 31	8.5	2017-07-27 2:16:23	900	42
RKS1754-2649	17 54 54.1	-26 49 41	10.3	2022-08-17 2:26:38	920	43
RKS1755+0345	17 55 24.7	+03 45 16	10.1	2018-06-19 6:12:34	900	38
RKS1755+1830	17 55 44.8	+18 30 01	9.2	2019-09-30 23:29:43	900	31
RKS1757-2143	17 57 40.9	-21 43 10	10.0	2018-04-08 9:30:29	900	53
RKS1803+2545	18 03 47.7	+25 45 20	10.8	2021-03-22 9:08:50	900	30
RKS1804+0149	18 04 01.8	+01 49 56	8.1	2019-09-08 0:41:10	900	65
RKS1809-0019	18 09 32.2	-00 19 37	8.9	2019-05-03 5:41:32	900	68
RKS1809-1202	18 09 33.2	-12 02 19	10.5	2018-06-20 6:20:22	900	37
RKS1815+1829	18 15 18.2	+18 29 59	10.1	2022-03-13 9:25:24	900	57
RKS1816+1354	18 16 02.2	+13 54 48	10.2	2018-04-08 9:48:19	900	46
RKS1817+2640	18 17 49.8	+26 40 16	9.6	2021-06-11 5:05:17	900	48
RKS1818-0642	18 18 40.6	-06 42 03	9.3	2019-04-11 8:11:40	900	60
RKS1819-0156	18 19 50.8	-01 56 19	9.7	2018-04-09 9:20:08	900	57
RKS1822+0142	18 22 17.2	+01 42 25	10.1	2021-03-28 8:46:03	1200	53
RKS1829-0149	18 29 52.4	-01 49 05	8.0	2017-07-02 4:38:34	900	98
RKS1829-2758	18 29 22.3	-27 58 19	9.4	2021-06-11 5:59:48	900	65
RKS1829+0903	18 29 31.9	+09 03 43	8.7	2019-09-15 23:31:29	900	67
RKS1831-1854	18 31 18.9	-18 54 31	6.8	2017-08-06 4:16:43	900	170

Continued on next page

Table 11 — *Continued from previous page*

RKS ID	R.A.	Decl.	V	Date & Time of Obs	Exp. Time	SNR
...	(hh mm ss)	(dd mm ss)	(mag)	(UTC)	(s)	...
RKS1833-1138	18 33 28.8	-11 38 09	10.0	2019-10-25 23:45:11	900	32
RKS1833-1626	18 33 24.8	-16 26 39	9.1	2019-07-10 3:18:32	900	62
RKS1833+2218	18 33 17.7	+22 18 51	8.9	2017-07-13 3:43:52	900	30
RKS1847-0338	18 47 27.2	-03 38 23	8.8	2017-08-07 4:07:32	900	76
RKS1848-1008	18 48 01.4	-10 08 46	8.5	2021-06-11 6:17:26	900	89
RKS1848+1044	18 48 29.2	+10 44 43	8.0	2017-08-07 3:27:42	900	105
RKS1848+1726	18 48 51.8	+17 26 20	9.2	2018-06-19 6:48:30	900	60
RKS1850-2655	18 50 21.1	-26 55 25	9.7	2018-08-12 1:59:09	900	64
RKS1854+0051	18 54 53.2	+00 51 46	10.7	2019-11-05 23:54:32	900	31
RKS1854+1058	18 54 53.6	+10 58 40	9.6	2018-09-10 23:57:11	900	65
RKS1854+2844	18 54 43.7	+28 44 55	11.6	2022-04-23 9:16:57	1200	33
RKS1855+2333	18 55 53.2	+23 33 23	8.2	2018-06-30 4:26:13	900	55
RKS1858-0030	18 58 56.4	-00 30 14	8.4	2019-05-03 10:08:10	900	86
RKS1858-1014	18 58 03.3	-10 14 37	9.8	2019-07-05 5:46:59	900	49
RKS1859+0759	18 59 38.6	+07 59 14	10.8	2020-11-03 23:56:35	1200	33
RKS1859+1107	18 59 39.2	+11 07 04	9.2	2019-07-10 4:34:24	900	55
RKS1901+0328	19 01 51.0	+03 28 14	9.7	2019-07-06 6:42:35	900	35
RKS1903-1102	19 03 05.8	-11 02 38	8.4	2017-06-24 7:17:28	900	32
RKS1907+0736	19 07 02.0	+07 36 57	9.2	2017-08-19 1:58:20	900	40
RKS1908-1640	19 08 10.7	-16 40 41	10.6	2019-05-17 8:51:25	900	30
RKS1908+1627	19 08 02.6	+16 27 37	10.2	2019-07-11 5:30:39	900	33
RKS1910+2145	19 10 32.1	+21 45 46	11.4	2021-06-01 6:07:36	1800	32
RKS1915+1133	19 15 35.0	+11 33 16	8.1	2019-07-10 6:02:39	900	89
RKS1915+2453	19 15 18.8	+24 53 49	9.7	2021-04-11 9:39:07	900	55
RKS1923-0635	19 23 16.4	-06 35 07	9.7	2019-07-05 6:48:51	900	52
RKS1924-2203	19 24 34.2	-22 03 43	10.9	2019-11-06 0:50:23	900	31
RKS1924+2525	19 24 26.5	+25 25 50	10.9	2021-05-05 8:44:51	900	36
RKS1928+1232	19 28 15.3	+12 32 09	9.2	2019-06-01 8:43:02	900	58
RKS1928+2854	19 28 25.5	+28 54 10	10.9	2021-04-27 9:40:59	900	33
RKS1929+0709	19 29 05.1	+07 09 35	10.5	2019-07-06 7:10:32	900	29
RKS1930+2140	19 30 05.4	+21 40 34	10.0	2022-04-09 9:42:59	900	56
RKS1932-1116	19 32 06.7	-11 16 29	7.5	2017-08-19 1:40:18	900	123
RKS1932+0034	19 32 37.9	+00 34 39	10.4	2017-08-03 4:01:41	900	32
RKS1934+0434	19 34 39.8	+04 34 57	9.4	2018-05-16 9:31:30	900	61
RKS1936-1026	19 36 45.6	-10 26 36	8.4	2021-04-07 9:33:55	900	81
RKS1943+1005	19 43 25.3	+10 05 22	10.0	2017-07-19 4:26:42	900	38
RKS1952-2356	19 52 29.9	-23 56 57	9.5	2018-06-19 7:25:58	900	60
RKS1954-2356	19 54 17.7	-23 56 27	6.2
RKS1954+2013	19 54 37.5	+20 13 06	11.1	2021-04-25 8:55:50	900	30
RKS1957+1313	19 57 25.4	+13 13 24	10.1	2019-07-05 8:13:33	900	34
RKS2000+2242	20 00 43.7	+22 42 39	7.7	2017-08-05 3:22:08	900	102
RKS2002+0319	20 02 47.0	+03 19 34	7.5	2017-08-18 2:36:59	900	148
RKS2003+2005	20 03 00.9	+20 05 49	10.9	2021-04-25 9:28:47	900	31
RKS2003+2320	20 03 52.1	+23 20 26	7.3	2017-07-19 5:04:20	900	111
RKS2004+2547	20 04 10.0	+25 47 24	7.8	2017-07-15 5:19:05	900	33

Continued on next page

Table 11 — *Continued from previous page*

RKS ID	R.A.	Decl.	V	Date & Time of Obs	Exp. Time	SNR
...	(hh mm ss)	(dd mm ss)	(mag)	(UTC)	(s)	...
RKS2008+0640	20 08 24.3	+06 40 43	9.8	2019-04-21 9:50:39	900	47
RKS2009-0307	20 09 41.0	-03 07 44	9.6	2019-07-05 7:33:04	900	55
RKS2009-1417	20 09 36.4	-14 17 12	9.8	2019-09-08 3:24:02	900	39
RKS2009+1648	20 09 34.3	+16 48 20	7.6	2017-07-07 6:22:34	900	56
RKS2010-2029	20 10 19.5	-20 29 36	8.9	2017-08-05 4:00:04	900	69
RKS2011+1611	20 11 06.0	+16 11 16	7.4	2017-08-08 5:18:09	900	76
RKS2012-1253	20 12 09.4	-12 53 35	11.3	2021-05-26 7:16:24	1800	41
RKS2013-0052	20 13 59.8	-00 52 00	7.8	2017-07-02 6:51:03	900	110
RKS2014-0716	20 14 28.1	-07 16 55	10.2	2017-07-20 5:58:36	900	28
RKS2015-2701	20 15 17.3	-27 01 58	5.7	2017-07-19 6:52:53	900	217
RKS2016-0204	20 16 22.0	-02 04 08	11.2	2021-06-07 7:15:18	1800	43
RKS2030+2650	20 30 10.6	+26 50 34	9.7	2021-04-29 9:53:55	900	50
RKS2035+0607	20 35 12.7	+06 07 37	8.9	2017-07-23 5:06:25	900	46
RKS2038+2346	20 38 26.2	+23 46 41	8.7	2022-06-11 7:40:51	900	93
RKS2039+1004	20 39 22.0	+10 04 32	8.5	2019-09-02 4:24:34	900	77
RKS2041-0529	20 41 40.6	-05 29 34	10.5	2019-07-16 5:18:38	900	34
RKS2041-2219	20 41 42.2	-22 19 20	9.8	2017-07-23 4:28:59	900	29
RKS2042-2116	20 42 05.8	-21 16 37	9.3	2020-11-06 0:55:31	900	51
RKS2042+2050	20 42 49.3	+20 50 40	8.3	2018-09-29 1:40:48	900	47
RKS2044-2121	20 44 00.6	-21 21 20	9.8	2017-07-03 6:49:23	900	46
RKS2047+1051	20 47 16.8	+10 51 36	9.7	2018-06-19 9:37:05	900	39
RKS2050+2923	20 50 10.5	+29 23 02	8.3	2019-09-18 1:43:57	900	32
RKS2053-0245	20 53 56.9	-02 45 57	11.1	2021-04-28 9:22:31	900	30
RKS2055+1310	20 55 06.8	+13 10 36	8.8	2017-08-19 4:17:27	900	41
RKS2059-1042	20 59 14.4	-10 42 49	8.5	2021-11-25 0:12:40	900	103
RKS2059+0333	20 59 08.5	+03 33 09	12.0	2021-06-20 7:14:08	1800	36
RKS2105-1654	21 05 43.4	-16 54 49	10.5	2019-11-04 1:40:02	900	31
RKS2105+0704	21 05 19.7	+07 04 09	8.3	2017-08-21 4:57:08	900	96
RKS2107-1355	21 07 10.3	-13 55 22	7.1	2017-07-20 8:31:30	900	38
RKS2108-0425	21 08 45.4	-04 25 36	9.5	2019-09-18 2:22:03	900	37
RKS2116+0923	21 16 32.4	+09 23 37	8.0	2017-08-20 5:03:26	900	105
RKS2118+0009	21 18 02.9	+00 09 41	8.2	2019-11-12 1:15:26	900	53
RKS2119-2621	21 19 45.6	-26 21 10	6.6	2020-11-28 0:17:19	900	177
RKS2120-1951	21 20 13.8	-19 51 08	9.1	2018-11-16 0:29:42	900	72
RKS2122+1052	21 22 26.6	+10 52 25	9.9	2017-07-17 7:45:02	900	30
RKS2125+2712	21 25 29.0	+27 12 38	8.3	2018-09-29 2:26:22	900	42
RKS2126+0344	21 26 42.4	+03 44 13	10.5	2021-04-25 10:12:05	900	32
RKS2130-1230	21 30 02.7	-12 30 36	9.1	2018-08-28 4:34:51	900	70
RKS2132-2057	21 32 23.5	-20 57 26	8.5	2017-07-19 7:32:19	900	75
RKS2141+1115	21 41 01.3	+11 15 46	9.2	2022-05-16 9:00:19	900	77
RKS2149-1140	21 49 45.9	-11 40 57	10.9	2020-11-17 1:27:25	900	28
RKS2149+0543	21 49 12.2	+05 43 22	8.7	2018-09-29 3:37:49	900	47
RKS2152+0154	21 52 06.5	+01 54 23	8.2	2021-05-22 9:10:17	900	100
RKS2153-1249	21 53 07.5	-12 49 40	11.0	2019-07-10 7:20:20	900	30
RKS2153+2055	21 53 05.3	+20 55 49	8.2	2021-04-29 10:11:31	900	89

Continued on next page

Table 11 -- *Continued from previous page*

RKS ID	R.A.	Decl.	V	Date & Time of Obs	Exp. Time	SNR
...	(hh mm ss)	(dd mm ss)	(mag)	(UTC)	(s)	...
RKS2153+2850	21 53 07.2	+28 50 15	11.4	2021-05-23 9:38:31	1800	33
RKS2155-2942	21 55 41.9	-29 42 22	8.5	2020-10-29 0:21:11	900	84
RKS2210+2247	22 10 31.4	+22 47 49	9.2	2017-06-25 8:58:36	900	38
RKS2214+2751	22 14 31.4	+27 51 18	10.3	2018-08-15 4:48:05	900	37
RKS2224+2233	22 24 45.5	+22 33 04	8.8	2019-11-22 0:08:57	900	35
RKS2226-1911	22 26 13.5	-19 11 18	9.3	2020-11-04 0:58:48	900	61
RKS2239+0406	22 39 50.7	+04 06 58	8.5	2020-11-02 0:38:35	900	77
RKS2240-2940	22 40 43.3	-29 40 28	7.8	2018-10-01 4:31:37	900	112
RKS2241+1849	22 41 35.0	+18 49 27	10.7	2018-11-03 0:59:03	900	29
RKS2243-0624	22 43 21.3	-06 24 02	8.1	2020-10-29 1:02:57	900	94
RKS2247+1823	22 47 13.6	+18 23 04	9.0	2020-12-13 0:29:06	900	60
RKS2248+2443	22 48 35.5	+24 43 26	11.0	2020-10-26 1:01:18	1500	36
RKS2251+1358	22 51 26.3	+13 58 11	8.3	2020-11-01 1:02:32	900	78
RKS2252+2324	22 52 02.5	+23 24 47	9.8	2018-06-05 9:59:32	900	39
RKS2254+2331	22 54 30.8	+23 31 06	11.1	2021-07-04 8:41:32	1850	29
RKS2258-1338	22 58 06.2	-13 38 33	10.1	2020-11-10 3:01:16	900	35
RKS2259-1122	22 59 53.6	-11 22 54	10.6	2020-11-11 3:24:39	900	34
RKS2301-0350	23 01 51.5	-03 50 55	7.5	2020-11-01 1:20:25	900	125
RKS2307-2309	23 07 07.0	-23 09 34	9.6	2018-12-19 1:05:01	900	34
RKS2308+0633	23 08 52.4	+06 33 39	10.9	2020-12-17 0:26:52	900	32
RKS2309-0215	23 09 10.7	-02 15 38	8.6	2017-07-14 7:16:48	900	59
RKS2309+1425	23 09 54.9	+14 25 35	10.3	2021-08-18 6:00:22	1200	51
RKS2310-2955	23 10 48.8	-29 55 03	8.7	2020-11-06 1:13:22	900	75
RKS2316+0541	23 16 51.8	+05 41 45	10.5	2017-12-15 0:59:34	900	33
RKS2317-2323	23 17 00.2	-23 23 46	10.8	2020-11-10 3:57:41	900	31
RKS2323-1045	23 23 04.8	-10 45 51	7.8	2018-11-08 2:57:00	716	94
RKS2326+0853	23 26 12.3	+08 53 37	10.5	2020-12-12 0:28:20	900	35
RKS2327-0117	23 27 04.8	-01 17 10	10.4	2017-12-15 1:17:01	900	36
RKS2328+1604	23 28 26.1	+16 04 00	9.8	2017-06-25 9:39:11	900	30
RKS2332-1650	23 32 49.3	-16 50 44	8.6	2017-08-18 5:11:39	900	92
RKS2335+0136	23 35 00.2	+01 36 19	9.6	2017-07-27 8:02:42	900	31
RKS2340+2021	23 40 51.4	+20 21 57	8.3	2021-07-08 7:47:20	900	61
RKS2342-0234	23 42 10.6	-02 34 36	10.3	2019-09-17 3:26:25	900	29
RKS2345+2933	23 45 09.9	+29 33 42	8.4	2021-11-03 1:31:00	900	98
RKS2348-1259	23 48 25.6	-12 59 14	9.6	2021-12-07 0:20:16	900	59
RKS2349+0310	23 49 01.1	+03 10 52	8.4	2018-09-29 4:41:28	900	37
RKS2350-2924	23 50 14.9	-29 24 06	7.9	2021-10-28 1:16:33	900	147
RKS2353+2901	23 53 08.5	+29 01 05	9.8	2018-08-16 6:25:28	900	45
RKS2355+2211	23 55 26.5	+22 11 35	8.8	2017-07-11 9:41:29	900	60
RKS2358+0949	23 58 19.8	+09 49 50	8.3	2021-08-17 6:37:07	900	84
RKS2359-2602	23 59 13.6	-26 02 55	8.7	2017-06-29 10:25:57	900	50
RKS2359+0639	23 59 47.7	+06 39 50	8.9	2018-09-29 5:01:24	900	41

REFERENCES

- Adibekyan, V. Z., Figueira, P., Santos, N. C., et al. 2013, *A&A*, 554, A44. doi:10.1051/0004-6361/201321520
- Airapetian, V. S., Barnes, R., Cohen, O., et al. 2020, *International Journal of Astrobiology*, 19, 2, 136. doi:10.1017/S1473550419000132
- Arney, G. N. 2019, *ApJL*, 873, L7. doi:10.3847/2041-8213/ab0651
- Astropy Collaboration, Robitaille, T. P., Tollerud, E. J., et al. 2013, *A&A*, 558, A33. doi:10.1051/0004-6361/201322068
- Astropy Collaboration, Price-Whelan, A. M., Sipőcz, B. M., et al. 2018, *AJ*, 156, 123. doi:10.3847/1538-3881/aabc4f
- Bahcall, J. N., Pinsonneault, M. H., & Wasserburg, G. J. 1995, *Reviews of Modern Physics*, 67, 781. doi:10.1103/RevModPhys.67.781
- Bailer-Jones, C. A. L. 2022, *ApJL*, 935, L9. doi:10.3847/2041-8213/ac816a
- Barnes, S. A. 2003, *ApJ*, 586, 464. doi:10.1086/367639
- Barnes, S. A. 2007, *ApJ*, 669, 1167. doi:10.1086/519295
- Bell, C. P. M., Mamajek, E. E., & Naylor, T. 2015, *MNRAS*, 454, 593. doi:10.1093/mnras/stv1981
- Bensby, T., Feltzing, S., & Lundström, I. 2003, *A&A*, 410, 527. doi:10.1051/0004-6361:20031213
- Binks, A. S. & Jeffries, R. D. 2014, *MNRAS*, 438, L11. doi:10.1093/mnrasl/slt141
- Blanco-Cuaresma, S., Soubiran, C., Jofré, P., et al. 2014, *A&A*, 566, A98. doi:10.1051/0004-6361/201323153
- Bland-Hawthorn, J. & Gerhard, O. 2016, *ARA&A*, 54, 529. doi:10.1146/annurev-astro-081915-023441
- Boley, K. M., Wang, J., Zinn, J. C., et al. 2021, *AJ*, 162, 85. doi:10.3847/1538-3881/ac0e2d
- Buchhave, L. A., Latham, D. W., Johansen, A., et al. 2012, *Nature*, 486, 375. doi:10.1038/nature11121
- Buchhave, L. A., Bizzarro, M., Latham, D. W., et al. 2014, *Nature*, 509, 593. doi:10.1038/nature13254
- Butler, R. P., Marcy, G. W., Williams, E., et al. 1997, *ApJL*, 474, L115. doi:10.1086/310444
- Casagrande, L., Schönrich, R., Asplund, M., et al. 2011, *A&A*, 530, A138. doi:10.1051/0004-6361/201016276
- Cayrel de Strobel, G. & Cayrel, R. 1989, *A&A*, 218, L9
- Cram, L. E. & Mullan, D. J. 1985, *ApJ*, 294, 626. doi:10.1086/163330
- Cuntz, M. & Guinan, E. F. 2016, *ApJ*, 827, 79. doi:10.3847/0004-637X/827/1/79
- Davenport, J. R. A., Covey, K. R., Clarke, R. W., et al. 2019, *ApJ*, 871, 241. doi:10.3847/1538-4357/aaf76
- de la Fuente Marcos, R. & de la Fuente Marcos, C. 2018, *Research Notes of the American Astronomical Society*, 2, 30. doi:10.3847/2515-5172/aac2d0
- De Gennaro, S., von Hippel, T., Winget, D. E., et al. 2009, *ApJ*, 696, 12. doi:10.1088/0004-637X/696/1/12
- Douglas, S. T., Agueros, M. A., Covey, K. R., et al. 2017, *ApJ*, 842, 83. doi:10.3847/1538-4357/aa6e52
- Dressing, C. D. & Charbonneau, D. 2015, *ApJ*, 807, 45. doi:10.1088/0004-637X/807/1/45
- Earl, N., Tollerud, E., Jones, C., et al. 2020, Zenodo
- Edwards, B., Rice, M., Zingales, T., et al. 2019, *Experimental Astronomy*, 47, 29. doi:10.1007/s10686-018-9611-4
- Ehrenfreund, P., Irvine, W., Becker, L., et al. 2002, *Exo-Astrobiology*, 518, 9
- Erkaev, N. V., Lammer, H., Odert, P., et al. 2013, *Astrobiology*, 13, 1011. doi:10.1089/ast.2012.0957
- Edvardsson, B., Andersen, J., Gustafsson, B., et al. 1993, *A&A*, 275, 101.
- Faherty, J. K., Bochanski, J. J., Gagne, J., et al. 2018, *ApJ*, 863, 91. doi:10.3847/1538-4357/aac76e
- Fekel, F. C., Bopp, B. W., Africano, J. L., et al. 1986, *AJ*, 92, 1150. doi:10.1086/114246
- Feltzing, S., Bensby, T., & Lundström, I. 2003, *A&A*, 397, L1. doi:10.1051/0004-6361:20021661
- Feng, F., Anglada-Escude, G., Tuomi, M., et al. 2019, *MNRAS*, 490, 5002. doi:10.1093/mnras/stz2912
- Fischer, D. A. & Valenti, J. 2005, *ApJ*, 622, 1102. doi:10.1086/428383
- Fischer, D. A., Marcy, G. W., Butler, R. P., et al. 2008, *ApJ*, 675, 790. doi:10.1086/525512
- France, K., Arulanantham, N., Fossati, L., et al. 2018, *ApJS*, 239, 16. doi:10.3847/1538-4365/aae1a3
- Freeman, K. & Bland-Hawthorn, J. 2002, *ARA&A*, 40, 487. doi:10.1146/annurev.astro.40.060401.093840
- Freund, S., Czesla, S., Robrade, J., et al. 2022, *A&A*, 664, A105. doi:10.1051/0004-6361/202142573
- Gagne, J., Mamajek, E. E., Malo, L., et al. 2018, *ApJ*, 856, 23. doi:10.3847/1538-4357/aaae09
- Gaia Collaboration, Brown, A. G. A., Vallenari, A., et al. 2016, *A&A*, 595, A2. doi:10.1051/0004-6361/201629512
- Gaia Collaboration, Brown, A. G. A., Vallenari, A., et al. 2018, *A&A*, 616, A1. doi:10.1051/0004-6361/201833051
- Gaia Collaboration, Vallenari, A., Brown, A. G. A., et al. 2022, arXiv:2208.00211. doi:10.48550/arXiv.2208.00211
- Gaidos, E., Fischer, D. A., Mann, A. W., et al. 2013, *ApJ*, 771, 18. doi:10.1088/0004-637X/771/1/18
- Gaidos, E., Mann, A. W., Kraus, A. L., et al. 2016, *MNRAS*, 457, 3, 2877. doi:10.1093/mnras/stw097
- García-Álvarez, D., Lanza, A. F., Messina, S., et al. 2011, *A&A*, 533, A30. doi:10.1051/0004-6361/201116646

- Gomes, J. I., Pinfield, D. J., Marocco, F., et al. 2013, *MNRAS*, 431, 2745. doi:10.1093/mnras/stt371
- Gossage, S., Conroy, C., Dotter, A., et al. 2018, *ApJ*, 863, 67. doi:10.3847/1538-4357/aad0a0
- Gray, R. O. & Corbally, C. 2009, *Stellar Spectral Classification by Richard O. Gray and Christopher J. Corbally*. Princeton University Press, 2009. ISBN: 978-0-691-12511-4
- Gray, R. O., Corbally, C. J., Garrison, R. F., et al. 2003, *AJ*, 126, 2048. doi:10.1086/378365
- Gray, R. O., Corbally, C. J., Garrison, R. F., et al. 2006, *AJ*, 132, 161. doi:10.1086/504637
- Gray, D. F. 2008, *The Observation and Analysis of Stellar Photospheres*, by David F. Gray, Cambridge, UK: Cambridge University Press, 2008
- Griffin, R. F. 1994, *The Observatory*, 114, 294
- Griffin, R. F. 2009, *The Observatory*, 129, 317
- Griffin, R. F. 2016, *The Observatory*, 136, 179
- Halbwachs, J.-L., Mayor, M., & Udry, S. 2018, *A&A*, 619, A81. doi:10.1051/0004-6361/201833377
- Hall, J. C. 2008, *Living Reviews in Solar Physics*, 5, 2. doi:10.12942/lrsp-2008-2
- Harman, C. E., Schwieterman, E. W., Schottelkotte, J. C., et al. 2015, *ApJ*, 812, 137. doi:10.1088/0004-637X/812/2/137
- Hartmann, L., Bopp, B. W., Dussault, M., et al. 1981, *ApJ*, 249, 662. doi:10.1086/159326
- Helminiak, K. G., Brahm, R., Ratajczak, M., et al. 2014, *A&A*, 567, A64. doi:10.1051/0004-6361/201220985
- Henry, T. J. & Jao, W.-C. 2024, *ARA&A*, 62, 593. doi:10.1146/annurev-astro-052722-102740
- Henry, T. J. & McCarthy, D. W. 1993, *AJ*, 106, 773. doi:10.1086/116685
- Henry, T. J., Soderblom, D. R., Donahue, R. A., et al. 1996, *AJ*, 111, 439. doi:10.1086/117796
- Henry, T. J., Jao, W.-C., Subasavage, J. P., et al. 2006, *AJ*, 132, 2360. doi:10.1086/508233
- Henry, T. J., Jao, W.-C., Winters, J. G., et al. 2018, *AJ*, 155, 265. doi:10.3847/1538-3881/aac262
- Henry, T., Casetti-Dinescu, D., Horch, E., et al. 2022, *AAS Meeting Abstracts*
- Herbig, G. H. 1985, *ApJ*, 289, 269. doi:10.1086/162887
- Hinkel, N. R., Timmes, F. X., Young, P. A., et al. 2014, *AJ*, 148, 54. doi:10.1088/0004-6256/148/3/54
- Horch, E. P., Veillette, D. R., Baena Gallé, R., et al. 2009, *AJ*, 137, 5057. doi:10.1088/0004-6256/137/6/5057
- Horch, E. P., Broderick, K. G., Casetti-Dinescu, D. I., et al. 2021, *AJ*, 161, 295. doi:10.3847/1538-3881/abf9a8
- Hubbard-James, H.-S., Lesley, D. X., Henry, T. J., et al. 2022, *AJ*, 164, 174. doi:10.3847/1538-3881/ac8d6a
- Hunter, J. D. 2007, *Computing in Science & Engineering*, 9, 90. doi:10.1109/MCSE.2007.55
- Isaacson, H. & Fischer, D. 2010, *ApJ*, 725, 875. doi:10.1088/0004-637X/725/1/875
- Ivezić, Ž., Sesar, B., Jurić, M., et al. 2008, *ApJ*, 684, 287. doi:10.1086/589678
- Jeffries, R. D., Byrne, P. B., Doyle, J. G., et al. 1994, *MNRAS*, 270, 153. doi:10.1093/mnras/270.1.153
- Johns, T., Paredes, L., Henry, T., et al. 2024, *AAS Meeting Abstracts*, 243, 463.04.
- Johnson, D. R. H. & Soderblom, D. R. 1987, *AJ*, 93, 864. doi:10.1086/114370
- Johnstone, C. P., Bartel, M., & Gudel, M. 2021, *A&A*, 649, A96. doi:10.1051/0004-6361/202038407
- Kanodia, S. & Wright, J. 2018, *Research Notes of the American Astronomical Society*, 2, 4. doi:10.3847/2515-5172/aaa4b7
- Kasting, J. F., Whitmire, D. P., & Reynolds, R. T. 1993, *Icarus*, 101, 108. doi:10.1006/icar.1993.1010
- Kasting, J. F., Whittet, D. C. B., & Sheldon, W. R. 1996, *Lunar and Planetary Science Conference*
- Kasting, J. F., Kopparapu, R., Ramirez, R. M., et al. 2014, *Proceedings of the National Academy of Science*, 111, 35, 12641. doi:10.1073/pnas.1309107110
- Kopparapu, R. K., Ramirez, R., Kasting, J. F., et al. 2013, *ApJ*, 765, 131. doi:10.1088/0004-637X/765/2/131
- Kunimoto, M. & Matthews, J. M. 2020, *AJ*, 159, 248. doi:10.3847/1538-3881/ab88b0
- Lammer, H., Selsis, F., Ribas, I., et al. 2003, *ApJL*, 598, L121. doi:10.1086/380815
- Lammer, H., Lichtenegger, H. I. M., Kulikov, Y. N., et al. 2007, *Astrobiology*, 7, 185. doi:10.1089/ast.2006.0128
- Lammer, H., Bredehoft, J. H., Coustenis, A., et al. 2009, *A&A Rv*, 17, 181. doi:10.1007/s00159-009-0019-z
- Lebreton, Y., Fernandes, J., & Lejeune, T. 2001, *A&A*, 374, 540. doi:10.1051/0004-6361:20010757
- Lehtinen, J., Jetsu, L., Hackman, T., et al. 2016, *A&A*, 588, A38. doi:10.1051/0004-6361/201527420
- Lillo-Box, J., Santos, N. C., Santerne, A., et al. 2022, *A&A*, 667, A102. doi:10.1051/0004-6361/202243898
- Lim, D., Koch-Hansen, A. J., Hansen, C. J., et al. 2021, *A&A*, 655, A26. doi:10.1051/0004-6361/202141728
- Lindgren, L., Hernandez, J., Bombrun, A., et al. 2018, *A&A*, 616, A2. doi:10.1051/0004-6361/201832727
- Lopez-Santiago, J., Montes, D., Galvez-Ortiz, M. C., et al. 2010, *A&A*, 514, A97. doi:10.1051/0004-6361/200913437
- Lu, Y. L., Angus, R., Curtis, J. L., et al. 2021, *AJ*, 161, 189. doi:10.3847/1538-3881/abe4d6
- Luck, R. E. & Heiter, U. 2006, *AJ*, 131, 3069. doi:10.1086/504080

- Luck, R. E. 2017, *AJ*, 153, 21.
doi:10.3847/1538-3881/153/1/21
- Luck, R. E. 2018, *AJ*, 155, 111.
doi:10.3847/1538-3881/aaa9b5
- Luger, R. & Barnes, R. 2015, *Astrobiology*, 15, 119.
doi:10.1089/ast.2014.1231
- Mamajek, E. E. & Bell, C. P. M. 2014, *MNRAS*, 445, 2169.
doi:10.1093/mnras/stu1894
- Mamajek, E. E. & Hillenbrand, L. A. 2008, *ApJ*, 687, 1264.
doi:10.1086/591785
- Mann, A. W., Gaidos, E., Lépine, S., & Hilton, E. J. 2012, *ApJ*, 753, 90. doi:10.1088/0004-637X/753/1/90
- Martinez-Arnaiz, R., Maldonado, J., Montes, D., et al. 2010, *A&A*, 520, A79. doi:10.1051/0004-6361/200913725
- Mason, B. D., Wycoff, G. L., Hartkopf, W. I., et al. 2001, *AJ*, 122, 3466. doi:10.1086/323920
- Mason, B. D., Hartkopf, W. I., Wycoff, G. L., et al. 2006, *AJ*, 132, 2219. doi:10.1086/508231
- Meadows, V. S., Reinhard, C. T., Arney, G. N., et al. 2018, *Astrobiology*, 18, 6, 630. doi:10.1089/ast.2017.1727
- Medina, A. A., Winters, J. G., Irwin, J. M., et al. 2022, *ApJ*, 935, 104. doi:10.3847/1538-4357/ac77f9
- Melbourne, K., Youngblood, A., France, K., et al. 2020, *AJ*, 160, 269. doi:10.3847/1538-3881/abbf5c
- Messina, S., Desidera, S., Turatto, M., et al. 2010, *A&A*, 520, A15. doi:10.1051/0004-6361/200913644
- Miguel, Y., Kaltenegger, L., Linsky, J. L., et al. 2015, *MNRAS*, 446, 345. doi:10.1093/mnras/stu2107
- Mishenina, T. V., Soubiran, C., Kovtyukh, V. V., et al. 2012, *A&A*, 547, A106. doi:10.1051/0004-6361/201118412
- Molliere, P., van Boekel, R., Bouwman, J., et al. 2017, *A&A*, 600, A10. doi:10.1051/0004-6361/201629800
- Montes, D. & Martin, E. L. 1998, *A&AS*, 128, 485.
doi:10.1051/aas:1998159
- Montes, D., Fernández-Figueroa, M. J., De Castro, E., et al. 1997, *A&AS*, 125, 263. doi:10.1051/aas:1997374
- Montes, D., López-Santiago, J., Gálvez, M. C., et al. 2001, *MNRAS*, 328, 45. doi:10.1046/j.1365-8711.2001.04781.x
- Montes, D. 2013, *Highlights of Spanish Astrophysics VII*, 661
- Morris, B. M., Curtis, J. L., Sakari, C., et al. 2019, *AJ*, 158, 101. doi:10.3847/1538-3881/ab2e04
- NASA Exoplanet Science Institute 2020, *Planetary Systems Composite Table*, doi:10.26133/NEA13
- Newville, M., Stensitzki, T., Allen, D. B., et al. 2014, *Zenodo*
- Niraula, P., Redfield, S., Dai, F., et al. 2017, *AJ*, 154, 266.
doi:10.3847/1538-3881/aa957c
- Nisak, A. H., White, R. J., Yep, A., et al. 2022, *AJ*, 163, 278. doi:10.3847/1538-3881/ac63c3
- Nordström, B., Mayor, M., Andersen, J., et al. 2004, *A&A*, 418, 989. doi:10.1051/0004-6361:20035959
- Núñez, A., Agüeros, M. A., Covey, K. R., et al. 2022, *ApJ*, 931, 45. doi:10.3847/1538-4357/ac6517
- Paredes, L. A., Henry, T. J., Quinn, S. N., et al. 2021, *AJ*, 162, 176. doi:10.3847/1538-3881/ac082a
- Paredes, L. A., Dissertation, Georgia State University, 2022.
- Pecaut, M. J. & Mamajek, E. E. 2013, *ApJS*, 208, 9.
doi:10.1088/0067-0049/208/1/9
- Pedregosa, F. and 18 colleagues 2011. *Scikit-learn: Machine Learning in Python*. *Journal of Machine Learning Research* 12, 2825–2830. doi:10.48550/arXiv.1201.0490
- Perryman, M. A. C., Brown, A. G. A., Lebreton, Y., et al. 1998, *A&A*, 331, 81.
doi:10.48550/arXiv.astro-ph/9707253
- Piskunov, N. E. & Valenti, J. A. 2002, *A&A*, 385, 1095.
doi:10.1051/0004-6361:20020175
- Plavchan, P., Werner, M. W., Chen, C. H., et al. 2009, *ApJ*, 698, 1068. doi:10.1088/0004-637X/698/2/1068
- Quanz, S. P., Ottiger, M., Fontanet, E., et al. 2022, *A&A*, 664, A21. doi:10.1051/0004-6361/202140366
- Quintana, E. V., Colon, K. D., Mosby, G., et al. 2021, *arXiv:2108.06438*. doi:10.48550/arXiv.2108.06438
- Reddy, B. E., Lambert, D. L., & Allende Prieto, C. 2006, *MNRAS*, 367, 1329. doi:10.1111/j.1365-2966.2006.10148.x
- Ribas, I., Guinan, E. F., Güdel, M., et al. 2005, *ApJ*, 622, 1, 680. doi:10.1086/427977
- Richey-Yowell, T., Shkolnik, E. L., Schneider, A. C., et al. 2019, *ApJ*, 872, 17. doi:10.3847/1538-4357/aafa74
- Richey-Yowell, T., Shkolnik, E. L., Loyd, R. O. P., et al. 2022, *ApJ*, 929, 169. doi:10.3847/1538-4357/ac5f48
- Riedel, A. R., Finch, C. T., Henry, T. J., et al. 2014, *AJ*, 147, 85. doi:10.1088/0004-6256/147/4/85
- Riedel, A. R., Alam, M. K., Rice, E. L., et al. 2017, *ApJ*, 840, 87. doi:10.3847/1538-4357/840/2/87
- Rugheimer, S., Kaltenegger, L., Segura, A., et al. 2015, *ApJ*, 809, 57. doi:10.1088/0004-637X/809/1/57
- Schaefer, G. H., White, R. J., Baines, E. K., et al. 2018, *ApJ*, 858, 71. doi:10.3847/1538-4357/aaba71
- Virtanen, P., Gommers, R., Oliphant, T. E., et al. 2020, *Nature Methods*, 17, 261. doi:10.1038/s41592-019-0686-2
- Seager, S. 2010, *Exoplanet Atmospheres: Physical Processes*. By Sara Seager. Princeton University Press, 2010. ISBN: 978-1-4008-3530-0
- Segura, A., Walkowicz, L. M., Meadows, V., et al. 2010, *Astrobiology*, 10, 751. doi:10.1089/ast.2009.0376
- Shea, M., Hansen, C., Horch, E., et al. 2023, *AAS Meeting Abstracts*

- Siess, L., Dufour, E., & Forestini, M. 2000, *A&A*, 358, 593.
doi:10.48550/arXiv.astro-ph/0003477
- Skoda, P., Draper, P. W., Neves, M. C., et al. 2014, *Astronomy and Computing*, 7, 108.
doi:10.1016/j.ascom.2014.06.001
- Skrutskie, M. F., Cutri, R. M., Stiening, R., et al. 2006, *AJ*, 131, 1163. doi:10.1086/498708
- Skumanich, A. 1972, *ApJ*, 171, 565. doi:10.1086/151310
- Soderblom, D. R., Jones, B. F., Balachandran, S., et al. 1993, *AJ*, 106, 1059. doi:10.1086/116704
- Soderblom, D. R., Hillenbrand, L. A., Jeffries, R. D., et al. 2014, *Protostars and Planets VI*, 219.
doi:10.2458/azu_uapress_9780816531240-ch010
- Soderblom, D. R. 2010, *ARA&A*, 48, 581.
doi:10.1146/annurev-astro-081309-130806
- Soubiran, C., Le Campion, J.-F., Brouillet, N., et al. 2020, *VizieR Online Data Catalog*, B/pastel
- Spada, F. & Lanzafame, A. C. 2020, *A&A*, 636, A76.
doi:10.1051/0004-6361/201936384
- Sperauskas, J., Deveikis, V., & Tokovinin, A. 2019, *A&A*, 626, A31. doi:10.1051/0004-6361/201935346
- Spitzer, L. & Schwarzschild, M. 1951, *ApJ*, 114, 385.
doi:10.1086/145478
- Sreejith, A. G., Fossati, L., Youngblood, A., et al. 2020, *A&A*, 644, A67. doi:10.1051/0004-6361/202039167
- Stanford-Moore, S. A., Nielsen, E. L., De Rosa, R. J., et al. 2020, *ApJ*, 898, 27. doi:10.3847/1538-4357/ab9a35
- Strassmeier, K., Washuettl, A., Granzer, T., et al. 2000, *A&AS*, 142, 275. doi:10.1051/aas:2000328
- Strassmeier, K. G., Fekel, F. C., Bopp, B. W., Dempsey, R. C., & Henry, G. W. 1993, *ApJS*, 72, 191.
doi:10.1086/191414
- Tarter, J. C., Backus, P. R., Mancinelli, R. L., et al. 2007, *Astrobiology*, 7, 30. doi:10.1089/ast.2006.0124
- Taylor, M. B. 2005, in *Astronomical Society of the Pacific Conference Series*, Vol. 347, *Astronomical Data Analysis Software and Systems XIV*, ed. P. Shopbell, M. Britton, & R. Ebert, 29
- Tian, F. 2009, *ApJ*, 703, 905.
doi:10.1088/0004-637X/703/1/905
- Tian, F. 2015, *Annual Review of Earth and Planetary Sciences*, 43, 459.
doi:10.1146/annurev-earth-060313-054834
- Tokovinin, A., Fischer, D. A., Bonati, M., et al. 2013, *PASP*, 125, 1336. doi:10.1086/674012
- Tokovinin, A., Mason, B. D., Mendez, R. A., et al. 2019, *AJ*, 158, 48. doi:10.3847/1538-3881/ab24e4
- Torres, C. A. O., Quast, G. R., da Silva, L., et al. 2006, *A&A*, 460, 695. doi:10.1051/0004-6361:20065602
- Ujjwal, K., Kartha, S. S., Mathew, B., et al. 2020, *AJ*, 159, 166. doi:10.3847/1538-3881/ab76d6
- Viana Almeida, P., Santos, N. C., Melo, C., et al. 2009, *A&A*, 501, 965. doi:10.1051/0004-6361/200811194
- Walkowicz, L. M. & Hawley, S. L. 2009, *AJ*, 137, 3297.
doi:10.1088/0004-6256/137/2/3297
- Wang, H.-J. & Wei, J.-Y. 2009, *Research in Astronomy and Astrophysics*, 9, 315. doi:10.1088/1674-4527/9/3/006
- West, A. A., Hawley, S. L., Bochanski, J. J., et al. 2008, *AJ*, 135, 785. doi:10.1088/0004-6256/135/3/785
- White, R. J., Gabor, J. M., & Hillenbrand, L. A. 2007, *AJ*, 133, 2524. doi:10.1086/514336
- Wright, J. T. & Eastman, J. D. 2014, *PASP*, 126, 838.
doi:10.1086/678541
- Yee, S. W., Petigura, E. A., & von Braun, K. 2017, *ApJ*, 836, 77. doi:10.3847/1538-4357/836/1/77
- Youngblood, A., France, K., Loyd, R. O. P., et al. 2017, *ApJ*, 843, 31. doi:10.3847/1538-4357/aa76dd
- Youngblood, A., Pineda, J. S., Ayres, T., et al. 2022, *ApJ*, 926, 129. doi:10.3847/1538-4357/ac4711
- Zuckerman, B., Song, I., & Bessell, M. S. 2004, *ApJL*, 613, L65. doi:10.1086/425036
- Zúñiga-Fernández, S., Bayo, A., Elliott, P., et al. 2021, *A&A*, 645, A30. doi:10.1051/0004-6361/202037830